Technical Report 530

Millstone Hill Thomson Scatter Results for 1972

J. V. Evans

J. M. Holt

18 September 1978

Prepared for the National Science Foundation
under NSF Grant No. ATM 75-22193

Lincoln Laboratory

MASSACHUSETTS INSTITUTE OF TECHNOLOGY

LEXINGTON, MASSACHUSETTS

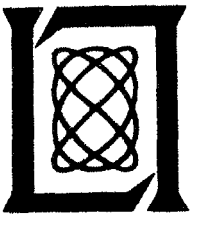

ABSTRACT

During 1972, the vertically directed incoherent scatter radar at Millstone Hill (42.6°N, 71.5°W) was employed to measure electron density, electron and ion temperatures, and vertical ion velocity in the F-region over periods of 24 hours, one or two times per month. The observations spanned the height interval 200 to 900 km, approximately, and achieved a time resolution of about 30 minutes. This report presents the results of these measurements in a set of contour diagrams.

For a number of the days, the spectra of the signals gathered at altitudes between 450 and 1125 km have been the subject of further analysis in an effort to determine the percentage of H^+ ions present over Millstone. The results suggest that H^+ ions are escaping from the F-region to the magnetosphere at a value close to the theoretical limiting flux during the daytime in all seasons. At night the flux becomes downward commencing near midnight in winter, but may remain upward throughout the night in summer.

CONTENTS

MILLSTONE HILL THOMSON SCATTER RESULTS FOR 1972

I. INTRODUCTION

Since 1963, incoherent (Thomson) scatter radar measurements of F-region electron densities, and electron and ion temperatures have been conducted at Millstone Hill, Westford, Massachusetts (42.6°N, 71.5°W) (Refs. 1 to 9). This paper is the tenth in a series of annual reports, and presents the results gathered in this program during the calendar year 1972. The observations reported were made for periods of 24 hours, once or twice a month. The results obtained in earlier years have been published in the articles listed in Table I, and have been transmitted to the World Data Center A, Boulder, Colorado.

TABLE I

PUBLICATIONS CONCERNING THE MILLSTONE HILL UHF (68-cm Wavelength) THOMSON SCATTER RESULTS

Year	Months Covered	Publication
1963	February 1963 to January 1964	Ref.1
	March, July, August, September	Ref.10
	April, July, November	Ref.11
1964	January through December	Ref.2
	April, July, November	Ref.12
1965	January through December	Ref.3
	January, April, August	Ref.13
	June	Ref.14
	June, August, September	Ref.15
1966	January through December	Ref.4
	January, March, July, September	Ref.16
1967	January through December	Ref.5
	February, June, October, December	Ref.16
1968	January through December	Ref.6
	October	Ref.17
1969	January through December	Ref.7
	February, April, July	Ref.18
	September, October	Ref.19
1970	January through December	Ref.8
1971	January through December	Ref.9

The results reported in this paper are of F-region electron density N_e, electron and ion temperatures T_e and T_i, and vertical velocity V_z and span the altitude interval 200 to 900 km, approximately. The measurements were made by transmitting single long pulses on each sweep of the radar time base and integrating the returns in a digital computer. Spectral information (from which T_e and T_i are determined) was obtained by examining the outputs from a bank of filters matched to the length of the pulse (0.5 or 1.0 msec).[20] Additional measurements were made of the E- and F-regions by transmitting pairs of pulses, whose spacing could be varied allowing the echo autocorrelation function to be determined in the computer. This approach also allowed for the digital subtraction of unwanted returns from distant hills,[21] and has been described in detail elsewhere.[22] Results gathered for E-region ion temperature using this pulse-pair method in 1972 have been employed in the study of tides in the lower thermosphere and reported in a number of papers (e.g., Ref. 23).

Other observations conducted in 1972 that are not reported here include short observing periods chosen to coincide with the overhead pass of a satellite (ISIS II) or with the launch of a rocket from Wallops Island. In addition, some data gathered over short periods (less than 12 hours) as part of a program of propagation studies have been omitted as contributing little to the report.

Section II describes the equipment, data gathering, and reduction procedures. During 1972, these were changed little from those employed the previous year and described in Ref. 9. Results for electron density, electron and ion temperatures, and vertical velocity are presented in Sec. III. In Sec. IV, we present results for the abundance of H^+ ions over Millstone in the upper part of the F2-region and discuss these results in light of present understanding of the fluxes linking the ionosphere and magnetosphere.

II. EQUIPMENT, OBSERVING, AND DATA-ANALYSIS PROCEDURES

A. Equipment

1. General

The UHF (68-cm wavelength) incoherent scatter radar equipment has been described.[1] This system employs a fixed vertically directed 220-foot-diameter antenna and hence can measure only the vertical component of the ion drift. Extensive modifications to the data-taking procedures were made in 1968 (Ref. 6) which allowed the echo power spectra to be measured for many heights simultaneously. This scheme made use of banks of matched filters for each of the pulse lengths (0.5, 1.0 or 2.0 msec) employed, and has been described in detail in Ref. 20. Owing to an imperfect match between the filters and the spectra of the pulses (especially for the 0.5-msec pulses), some systematic errors were introduced in the measurements of T_e and T_i over some altitudes and empirical correction procedures were developed in an effort to remedy these.[7,9] In 1976, the filter bank system was replaced by a digital correlator which obviated this problem.

During 1972, some incoherent scatter observations were conducted using the smaller 84-foot-diameter steerable antenna and associated L-band (23-cm wavelength) radar. This system is described in Ref. 24. When used for incoherent scatter studies, control of the radar timing was assumed by the incoherent scatter timing unit (located in the Ionosphere Laboratory) and the 30-MHz IF output of the L-band receiver was connected to the 30-MHz IF input to the UHF receiver, so that the data-taking and sampling procedure remained unchanged. (Actually, it was necessary to rearrange the elements of the filter bank to span a wider frequency range as described in Ref. 20.)

2. New Ionosonde

The principal change in 1972 to the apparatus employed at Millstone for ionospheric research was the introduction of a new HF ionospheric sweep sounder. In February, the C-4 ionosonde was replaced by a "Digisonde 128" ionospheric sounder manufactured by Lowell Technological Institute Research Foundation (Lowell, Massachusetts).[25] Since this instrument provides only about 80 mW of RF power, it was necessary to construct a transmitter power amplifier to be used with it. This was accomplished using portions of a spare C-4 sounder that was on hand. The original C-4 sounder was left intact and available as a standby system until June 1973, when it finally was shut down. Standby operation of the C-4 was accomplished by employing the same transmitter amplifier for both systems and switching it between the two.

The Digisonde 128 sounder is shown in Fig. 1. Unlike the C-4, it is located at the main radar site and supplies the exciter signal to the transmitter power amplifier via coaxial cable. This transmitter unit, constructed from the spare C-4 components, is shown in Fig. 2. The transmitter unit is located in the building near the antenna. The received signal (at RF) is sent over coaxial cable from the antenna to the receiver just over 1 km away. To overcome the attenuation in the coaxial cables, broadband preamplifiers are employed together with matching filters to compensate for the attenuation vs frequency response of the cables.

With the exception of the tape recorder and the printer, there are no moving parts in the new system (Fig. 1). Together with complete solid-state construction (except for the transmitter

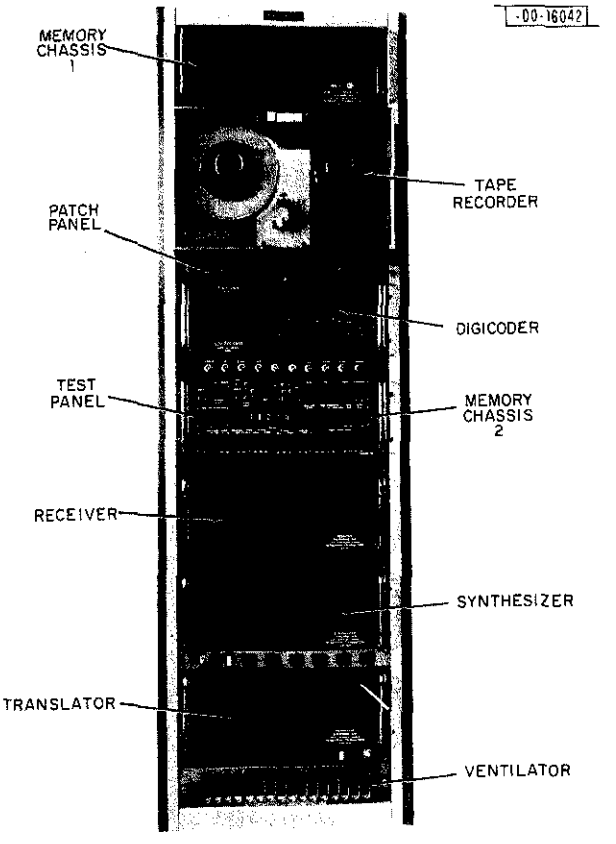

Fig. 1. Photograph of the Digisonde 128 system showing the main components.

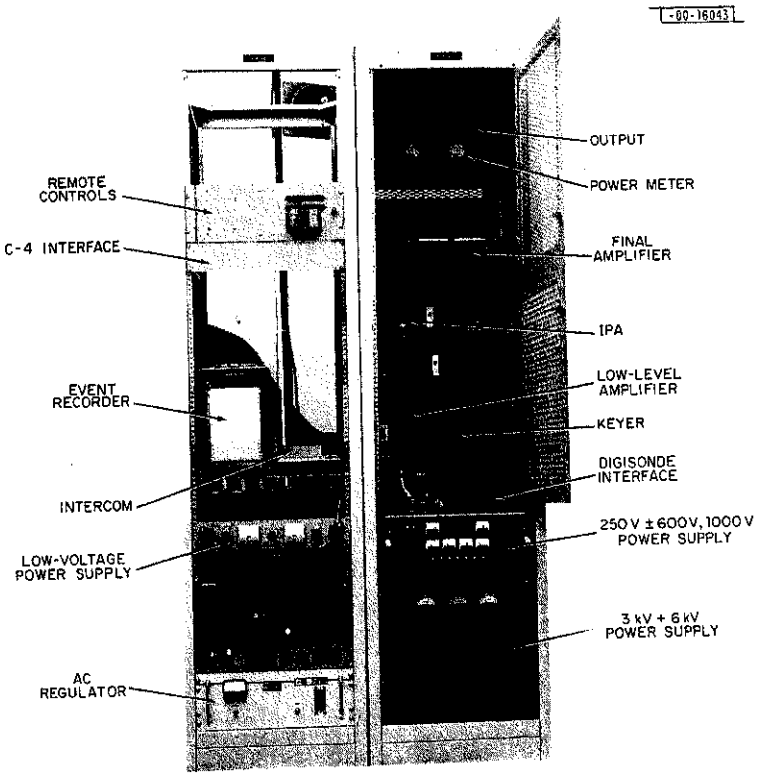

Fig.2. Photograph of the transmitter power amplifier constructed for the Digisonde 128 system using surplus C-4 components.

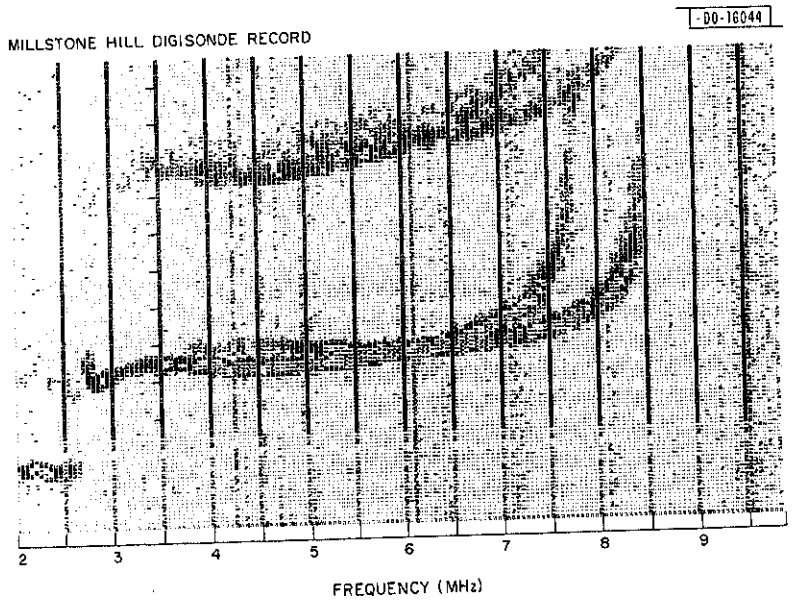

Fig.3. Example of a record printed by the Digisonde 128 sounder.

power amplifier), this insures greater reliability. A second desirable feature of the new instrument is that it provides hard-copy records in real time, from which f_oF2 can be read off easily. Figure 3 provides an example of one of these records.

A block diagram of the Digisonde system is given in Fig. 4. Unlike the C-4, there are no free-running oscillators. All the required frequencies (and time) are generated from an internal stable quartz oscillator. Thus, the desired transmitter and receiver frequencies are selected by internal digital control of a frequency synthesizer. The control of the synthesizer can be transferred to a local computer, but this has not been done at Millstone. The smallest frequency interval between soundings is 25 kHz. This option is employed for E-region soundings, which may be made over the frequency range 1 to 4 MHz once per hour. A complete sounding from 2 to 16 MHz (or 2 to 10 MHz) usually is made twice per hour, on the half hour, with 50-kHz resolution. The ionogram shown in Fig. 3 covers the range 2 to 10 MHz, and was made using 50-kHz frequency steps. The vertical dark lines denote frequency intervals of 0.5 MHz.

The most novel feature of the new ionosonde is its integration capability. At each frequency, a train of $2^N \times 80$ pulses (N = 1, 2, 3, 4, 5...) is transmitted before the next frequency is selected. At Millstone, N = 2 usually is employed; i.e., 320 pulses are transmitted on each frequency. The phase of the pulses in each subgroup of 80 pulses is made to change from pulse to pulse by 0° or 180°, according to a pseudorandom code generated by a shift register. The phase of the receiver local oscillator is changed likewise, so that the instrument remains phase coherent, but at the output, the phase of an unwanted interfering signal is being changed continuously. The receiver signals are converted in a multiple-conversion superheterodyne receiver to an intermediate frequency of 100 kHz, where they are amplified by a logarithmic amplifier.

The correctly phase-decoded 100-kHz IF is sampled in 128 height ranges. Two samples are taken in each height range, providing sin and cos components of one cycle of the 100-kHz signal. Selectable sample periods are provided so that either every cycle of the 100-kHz IF, or every second, or third, or fourth one can be sampled. This corresponds to sampling on 1.5-, 3-, 4.5- or 6-km radar height increments.

The median value of signal amplitude and phase is determined for each height range; to do this, the samples are compared with the respective values already stored in a digital memory. This comparison determines whether the value stored must be increased, decreased or left the same. A changing weight function allows fast and optimal convergence of the digitally measured values after decoding phase-coherent amplitudes. The improvement of signal-to-interference ratio by this integration process is proportional to the square root of the number of samples, which for N = 1 is $\sqrt{80}$, or approximately 20 dB.

The sin and cos samples of the amplitude are measured in 256 increments. These samples are converted after integration into a complex amplitude (phase in 8 increments and amplitude in 64 increments). Using binary code, the amplitude is expressed as one character of six bits (or 64 levels). Two adjacent amplitude samples are separated by one phase character containing the preceding phase measurement on the lower three octal bits (8 portions) and the following phase measurement of three octal bits. Thus, the 128 height ranges produce, after one integration period (one frequency), a set of 192 characters. These are preceded by a block of information containing: year, date, hour, minutes, seconds, frequency transmitted, receiver gain, gain range setting, and information on range sample delay and density (Fig. 5). Means are provided to introduce information into characters, which are part of the previously mentioned information block. All information is provided in binary form and when combined with 192 characters

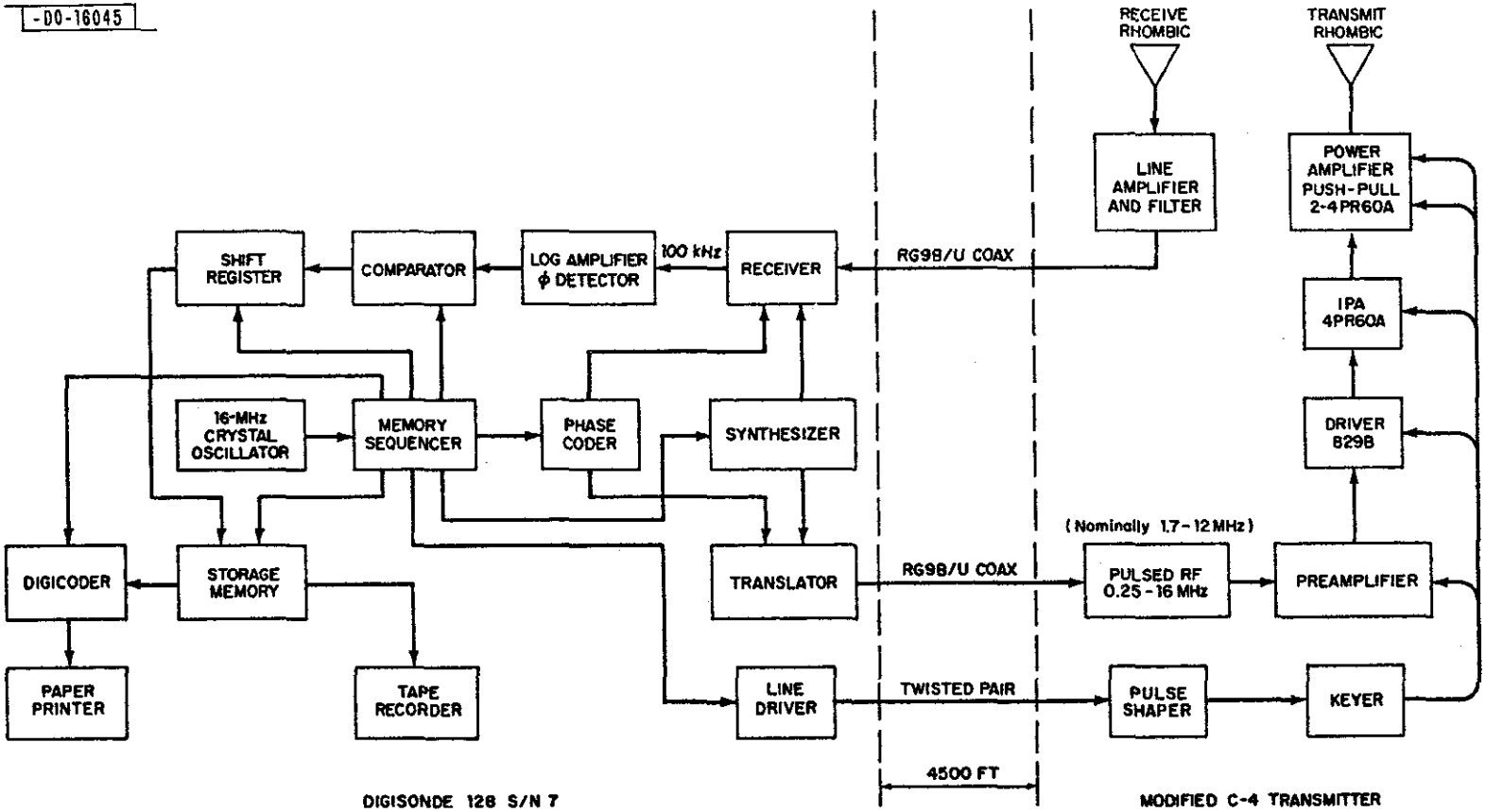

Fig.4. Simplified block diagram of the Digisonde 128 sounder.

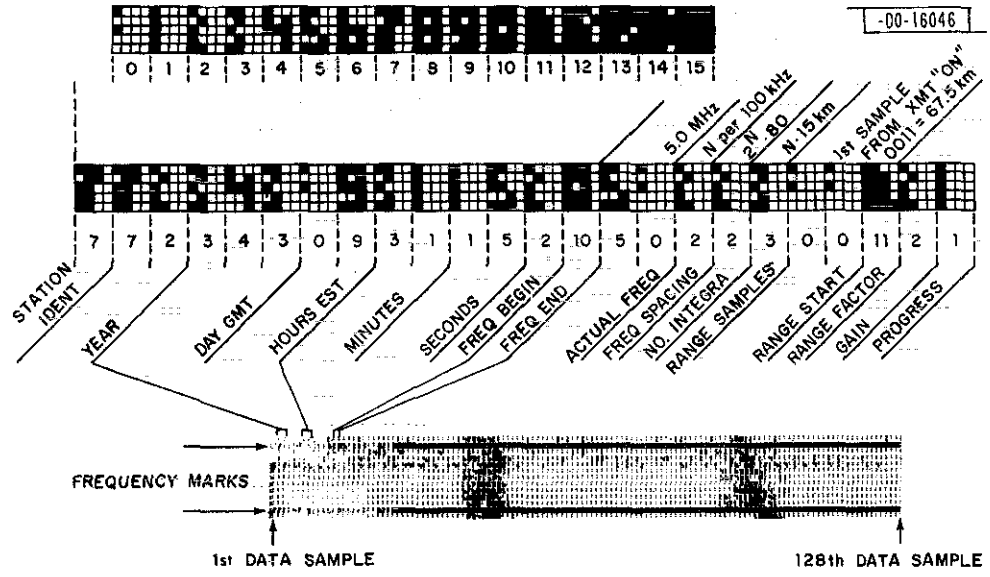

Fig.5. Key to the intensity level code (top) employed in the ionosonde records (cf. Fig.3), preface information (center), sample record strip (bottom) showing location of the preface.

of data, will form one-tenth of one record. During the integration time, the contents of the memory, generated in the preceding sampling process, plus the peripheral information mentioned above are transferred through a storage memory onto tape.

The data are read out of the memory at a rate of 500 characters per second, compatible with the fastest integration time of 0.4 second for each frequency. Preface and record gaps reduce the maximum frequency stepping rate to two per second.

At Millstone, magnetic tape recordings have not been made routinely thus far, and the printer output is employed instead. Owing to the slower speed of the printer, the memory cannot be read out at 500 characters per second and hence it is necessary to slow down the sweep speed. This is accomplished by integrating over 320 pulses (4 × 80) before changing frequency. The preface information appears on the printed record (Fig. 3) in the manner shown in Fig. 5.

The printed records provide ionograms plotted using a numeric technique developed at Lowell Technological Institute Foundation. The picture elements consist of numerals, using a special type font, having the property that the apparent blackness is proportional to the numeric value. Thus, large numbers like 7 or 8 appear much darker than, say, 3 or 4 (Fig. 5). The picture, made on a standard Magnafax telecopier, results from coding standard BCD data from any digital device into a form suitable for the telecopier.

In Fig. 3, the heavy, black, vertical lines mark each tenth sounding frequency. The station identification data have been printed automatically at the low-altitude end of each frequency marker. The axes are standard: vertical axis represents time delay (virtual height), horizontal axis represents frequency, while the intensity (z-axis) represents echo amplitude.

Since the printer records give the log of the median intensity at each height and frequency (in order to achieve enough dynamic range) some of the "contrast" between echoes and interference tends to be lost. This can be recovered, in part, by printing as "zero" all numbers below an adjustable threshold.

Provision to operate the C-4 sounder was maintained initially as this allowed an observer the capability of finding f_oF2 by sweeping the frequency manually. In addition, the C-4 provided 35-mm film copies of the ionograms that were sent routinely to the World Data Center. Using a storage tube display and camera system, a means was developed of photographing the ionograms produced by the Digisonde (e.g., Fig. 3), so that we could continue to send film records to the World Data Center. (The paper records tend to be bulky and cannot be reproduced readily.) At this point, operation of the C-4 was discontinued.

B. Observing Procedures

During 1972, we attempted to make observations using the single long-pulse method and the newer pulse-pair scheme at least once per month for 24 hours. Table II lists the operating modes employed for the single long-pulse measurements and the altitudes over which these provided data. In normal or "regular" operations, the cycle A, B, C was repeated every 30 minutes with 8 minutes of data being collected in each mode.

TABLE II

THE NORMAL "ONE-PULSE" EXPERIMENT MODE SEQUENCE

Mode	Pulse Length (μsec)	Height Resolution (km)	Sample Spacing (km)	Altitude Coverage (km)	Measured Parameters	
					Direct	Deduced
A	100	15	7.5	100-1000	Power	N_e
B	500	75	30	150-1500	Power	N_e
			75	225- 675	Power spectrum	T_e, T_i, V_z
C	1000	150	30	300-2000	Power	N_e
			75	450-1125	Power spectrum	T_e, T_i, V_z
D*	1000	50	30	150- 500	Power	–
			75	150- 350	Power spectrum	V_d

*Employed with the L-band steerable radar during 2-D experiments.

As described in Ref. 9, provision was made in 1971 to switch rapidly between the L-band and UHF radar transmitters and reload the computer with a new data-taking program which established automatically the proper condition for the interface equipment that transfers data from the radar to the computer.[24] During 1972, advantage was taken of this capability to switch rapidly between operation of the L-band radar employed to track the Navy Navigation Satellites (in a program of propagation studies) and incoherent scatter operation of the UHF radar. (The two radars cannot be employed simultaneously as the transmitter cooling and power supply, the radar interface equipment, and the computer all are shared.) These mixed operations (termed

STATS for Satellite Tracking and Thomson Scatter) permitted a cycle A, B, C to be completed once per hour and hence afforded less time resolution than regular runs. Only the results from the longer STATS runs that were completed successfully are included here.

A second application of this rapid switching capability was in observations that attempted to resolve the drift motions of the ions in the magnetic meridian plane into components parallel to the magnetic field (caused by neutral winds and diffusion under the influence of pressure variations) and normal to the magnetic field (caused by the E-W component of the F-region electric field). These measurements are termed here "2-D" and were a precursor for later attempts to measure all three components of the drift (termed "3-D"). Since the UHF radar measures the vertical component (V_z) of the drift, it was necessary only to employ the L-band radar to measure one component of the drift in the magnetic meridian to secure a second independent measurement from which the two wanted components could be recovered. For most 2-D measurements, the L-band antenna was directed in the magnetic meridian at 15° elevation (Table III). In this direction, the beam is almost normal to the field lines at F-region heights. However, on two occasions (Table III) the beam was directed in the magnetic E-W direction. Table III lists all the observing periods for which useful data were gathered and are presented in this report.

The 2-D sequence was A-mode (4 minutes), B-mode (4 minutes), C-mode (8 minutes), and D-mode (16 minutes); this could be repeated approximately every 40 minutes.

C. Data Reduction

As described previously,[20] no attempt is made to analyze the data in real time (i.e., as it is gathered) as this would be too time consuming. Instead, the samples of echo power collected as functions of range and frequency are stored on magnetic tape at the end of each integration period along with other pertinent information such as the mode type, start time, and duration of the run. A profile of echo power vs height (i.e., corrected for the R^{-2} dependence where R is the range) is computed and printed out by a high-speed printer. Together with a printout of the signal-to-noise ratio at each point within each frequency spectrum, this allows the data quality to be monitored while they are being gathered.

While alert operators usually could detect malfunctions of the equipment from the printout, subtle effects such as the failure of any (of three) frequency synthesizers employed in the receiver to remain phase locked to the site master frequency standard would not be evident. Accordingly, a frequency counter was provided to monitor each synthesizer in turn. Despite this, data for the vertical velocity on some days appear so scattered as to lead one to suspect that the receiver was not operating properly. This appears to be the case for 12-13 July and the vertical drift velocity data for these days have been discarded.

The first step in analyzing the data is to construct a plot of the F-region critical frequency f_oF2 vs time for the days of observation. For this, the values are scaled from the Millstone ionograms. Also included in the plots are values obtained at Ottawa (45°N) and Wallops Island (38°N), which are the two stations in routine operation closest to Millstone. Including values from these stations usually reveals any errors in scaling the local ionograms, and can serve to guide the interpolation that is necessary if any half-hourly values from Millstone are missing for any reason. Examples of these plots have been included in a number of previous reports.[4,5]

Values for f_oF2 are scaled from the smooth curves drawn through the points on the plots at half-hour intervals and entered into the computer via punched cards. These are stored and used

TABLE III

INCOHERENT SCATTER OBSERVATIONS – 1972

Begin			End			Mean		
Date	C*	EST	Date	C*	EST	Kp	Obs†	Comment
25 January		1220	26 January	D	1240	4–	Reg	
26 January	D	1350	27 January		1500	3_o	2-D	Az = 252°, El = 15°
23 February	Q	0950	24 February	D	1150	3+	Reg	
9 March		1000	10 March	QQ	1000	1_o	Reg	
23 March		1620	24 March	D	1510	3+	2-D	Az = 345°, El = 15°
26 April	QQ	1600	27 April		1700	1+	Reg	
9 May		1230	10 May		1330	2+	Reg	
25 May	Q	1130	26 May		1300	2–	STATS	Gap 1600-2030
30 May		0920	31 May		1010	3+	2-D	Az = 345°, El = 15°
8 June	Q	1020	9 June	QQ	1710	1+	STATS	
13 June	Q	0920	14 June		1100	2–	Reg	
28 June		1030	29 June		0500	2+	2-D	Az = 345°, El = 15°
30 June	QQ	1150	1 July	Q	1200	1_o	2-D	Az = 345°, El = 15°
12 July		0850	13 July	QQ	1020	1_o	Reg	No vertical drift data
26 July	D	1020	27 July		1420	2+	2-D	Az = 255°, El = 30°
7 August		0920	8 August	Q	1110	2–	Reg	
6 September		1010	7 September		1300	2–	2-D	Az = 345°, El = 18°
12 September	Q	0820	13 September		1100	2–	Reg	
3 October	QQ	0810	4 October	Q	1010	1+	Reg	
15 November	D	0930	16 November	D	1630	4_o	2-D	Gaps 1530-1900, 0300-0500
6 December	QQ	0930	7 December		1600	2	2-D	Az = 345°, El = 15°

*Condition:

QQ One of five quietest days in month
Q One of ten quietest days in month
D One of five most disturbed days in month.

†Observations:

Reg = Regular, 2-D = L-band and UHF radar measurements, STATS = Satellite Tracking and Thomson Scatter.

to obtain the value of f_oF2 at the midpoint of each A-mode run by linear interpolation.* The program combines measurements of echo power made with the all A-, B-, and C-mode runs in each cycle of observation into a single "power profile." This is converted to an absolute profile of electron density vs altitude by allowing for the effects on the backscatter power of altitude variations in the ratio T_e/T_i and normalizing the resultant curve to have the correct value of electron density (N_{max})† at the peak of the layer.

Values for electron and ion temperatures are recovered from the spectra assuming that O^+ is the only ion present. This assumption is a good one except at night near sunspot minimum when sufficient H^+ ions may be present at altitudes below 900 km to render the temperature estimates unreliable. More accurate values can be obtained using a program due to J. L. Massa (private communication, 1976) which attempts to recover T_e, T_i, and the H^+/N_e ratio at each altitude (Sec. IV). Unfortunately this program consumes a considerable amount of computer time and hence is not run routinely.

It has been found[20] that estimates of T_e/T_i obtained from the B- and C-mode data tend to differ at night in summer when $T_e/T_i \rightarrow 1.0$. This leads to differences in the estimates for T_i. It is believed that the discrepancy stems from the large amount of smearing of the frequency spectra of the signals introduced using 0.5-msec pulses (B-mode) particularly at night when the spectra are narrow. In principle, attempts are made to compensate for this by the method employed in the data analysis,[20] but the measurement accuracy must suffer at such times. Since it also was evident that the filters employed in the receiver spectrum analyzer in the B-mode are less perfectly matched to the transmitter pulse than those in the C-mode, it is believed that the systematic errors are primarily in the B-mode estimates. Assuming the C-mode is correct, J. E. Salah derived an empirical correction scheme by comparing the data in the two modes gathered at 525-km nominal height on four days,[7] and this was employed to correct the B-mode temperatures gathered in 1969 and 1970.[7,8] Subsequently, B. A. Emery performed a more detailed comparison employing several heights (to allow for differences in the effective center height of the pulse for the two modes) using two years' data.[9] Emery found that the corrections to be applied to the T_i and T_e/T_i values obtained in the B-mode depend not only on the prevailing value of T_e/T_i (taken to be that observed in the C-mode) but to a lesser extent also on T_i (again assumed to be the C-mode value). A smooth continuous correction scheme was derived from this comparison and employed to correct the results reported for 1971.[9] The same scheme was employed for the results reported here. Finally, the values for electron temperature were corrected for the effect of the changing Debye length with altitude.[8]

Beginning in 1976, the analog filter bank spectrum analyzer was replaced by a digital correlator that is believed to be less susceptible as a source of systematic error. The data gathered with this device cannot be analyzed with the ANALYSIS program and a new program (INSCAL) has been written which attempts to recover N_e, T_e, and T_i as functions of height, allowing for the influence on the N_e profile of height variations of T_e/T_i and on the T_e profile of variations in N_e (via the Debye length correction), in a truly self-consistent fashion. That employed in ANALYSIS[20] represents only a first-order correction, but in view of the possible bias errors in the B-mode results at some times, a more elaborate approach seems unwarranted.

---

*Actually, the time chosen = start time + 4 minutes.

† $N_{max} = 1.24 \times 10^4 \, (f_oF2)^2$ el/cm^3 when f_oF2 is expressed in megahertz.

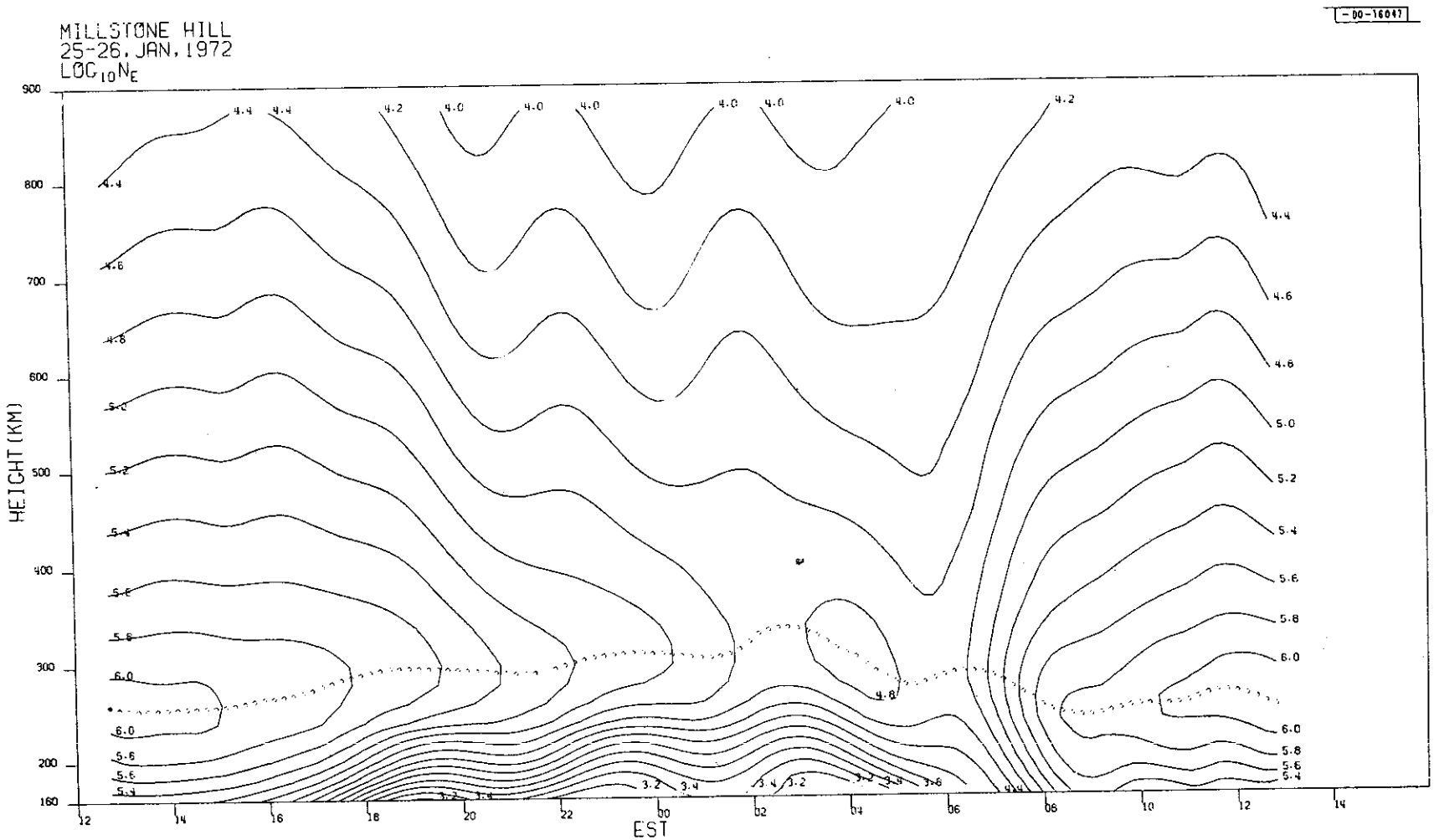

(a) $Log_{10} N_e$.

Fig.6(a-d). Results for 25-26 January 1972.

The next part of the analysis involves smoothing the electron density, electron and ion temperatures, and vertical velocity estimates as functions of height and time. This operation is performed by fitting, in a least-mean-squares sense, a two-dimensional polynomial surface that best represents the data. The program that performs this is known as INSCON, and has been described in Ref. 8. The INSCON program can compensate for distortion in the profiles of T_e and T_i vs altitude introduced by the fact that the effective center height for the pulse is not given simply by the time at which the echoes are sampled (i.e., the so-called "nominal" height), but is shifted owing to the variation of echo power with delay within the pulse. This effect automatically is taken into account in constructing the electron density profiles, but was not included routinely for the plots of T_e and T_i. The results published for 1970 and subsequently (including those presented here) have been corrected for this effect.

A subroutine of the INSCON program produces a plotting tape to drive a Calcomp plotter which is used to obtain contour diagrams of N_e, T_e, T_i, and V_z. These are given in the next section. In addition, INSCON provides the coefficients of the polynomial fit from which the variation of any parameter as a function of height or time (within the period fitted) can be recovered. The sets of coefficients for each day are combined on a single tape which is transmitted to the World Data Center (in Boulder) together with a listing given here as Appendix A. These, together with a simple FORTRAN recovery program (RCVR) allow numerical values to be obtained in machine-readable form by other users.[8]

III. RESULTS FOR ELECTRON DENSITY, ELECTRON AND ION TEMPERATURES, AND VERTICAL VELOCITY

A. General

Computer-drawn contour plots of N_e, T_e, T_i, and V_z as functions of altitude and time have been generated in the manner outlined above (and described in detail in Ref. 8); these are presented for the days listed in Table III in Figs. 6 through 26. Contours of N_e are labeled in units of $\log_{10} N_e$ (el/cm^3) and are drawn in steps of $\log_{10} N_e = 0.2$ wherever $\log_{10} N_e \geq 3.0$. Regions well above $h_{max}F2$ sometimes are encountered where, owing to experimental error, the density appears to be increasing with altitude. These usually have been edited from the plots, but in any case are not considered real. The accuracy of these plots is greatest in the vicinity of $h_{max}F2$ (shown as broken line) where the experimental uncertainty is set chiefly by the uncertainty in determining f_oF2 (typically ±0.2 MHz). At higher altitudes, however, the uncertainty in the incoherent scatter measurements contributes to the overall uncertainty – especially at night when the echoes are weakest.

It is believed that the 30-minute time resolution provided by the "regular" measurement scheme allows the normal diurnal variations to be followed adequately, but fluctuations caused, for example, by Traveling Ionospheric Disturbances (TIDs) with periods of less than about 2 hours, are effectively smoothed out.

The results for electron and ion temperatures are presented as isotherms at 200°K and 100°K intervals, respectively. The electron temperature exhibits a large diurnal variation and increases very rapidly at sunrise. It is possible that this rapid increase is not properly represented in the plots gathered for the STATS observations (Table III) where the time resolution afforded by the measurements was reduced to ~1 hour.

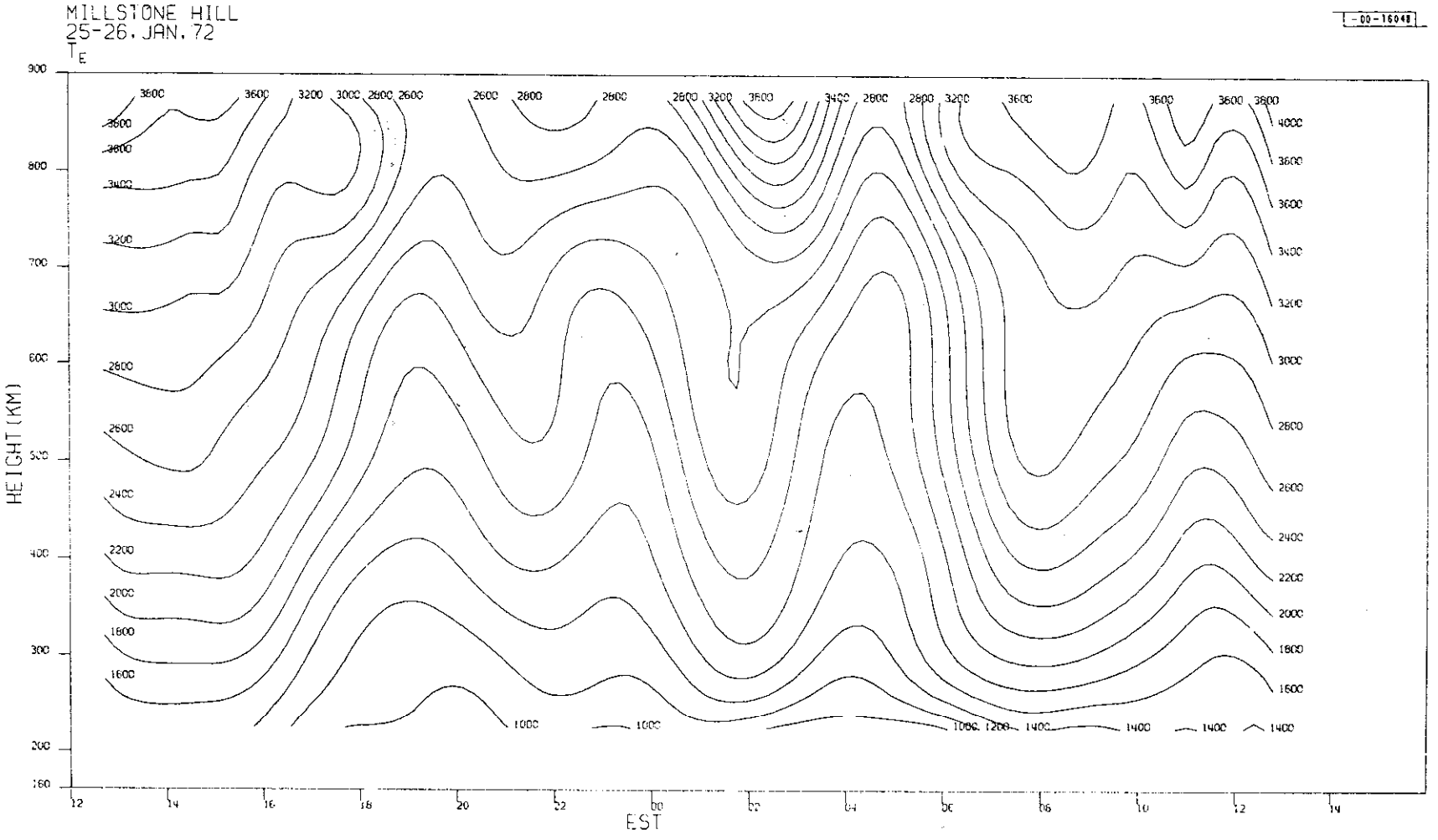

(b) T_e.

Fig.6(a-d). Continued.

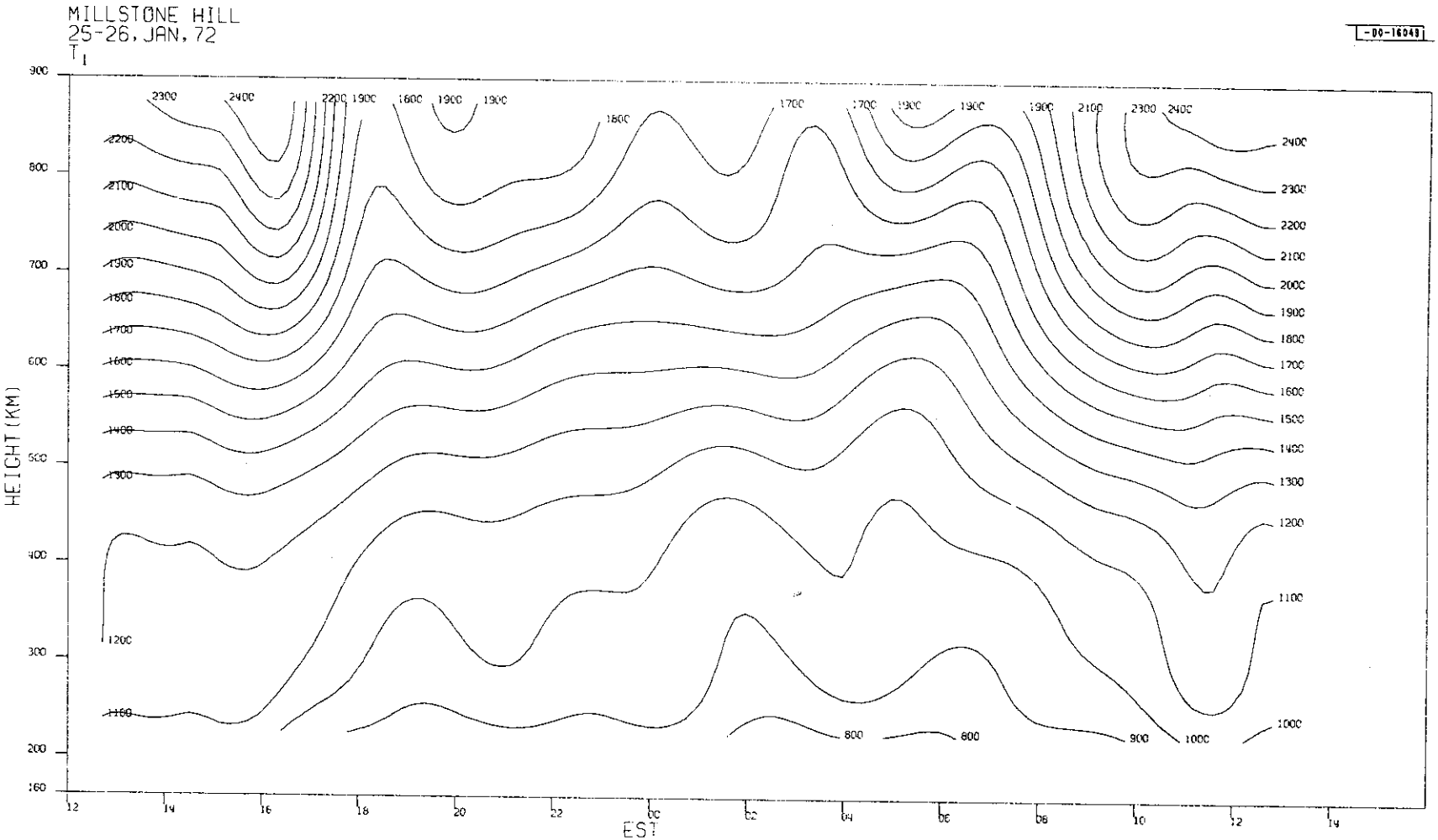

(c) T_i.

Fig.6(a-d). Continued.

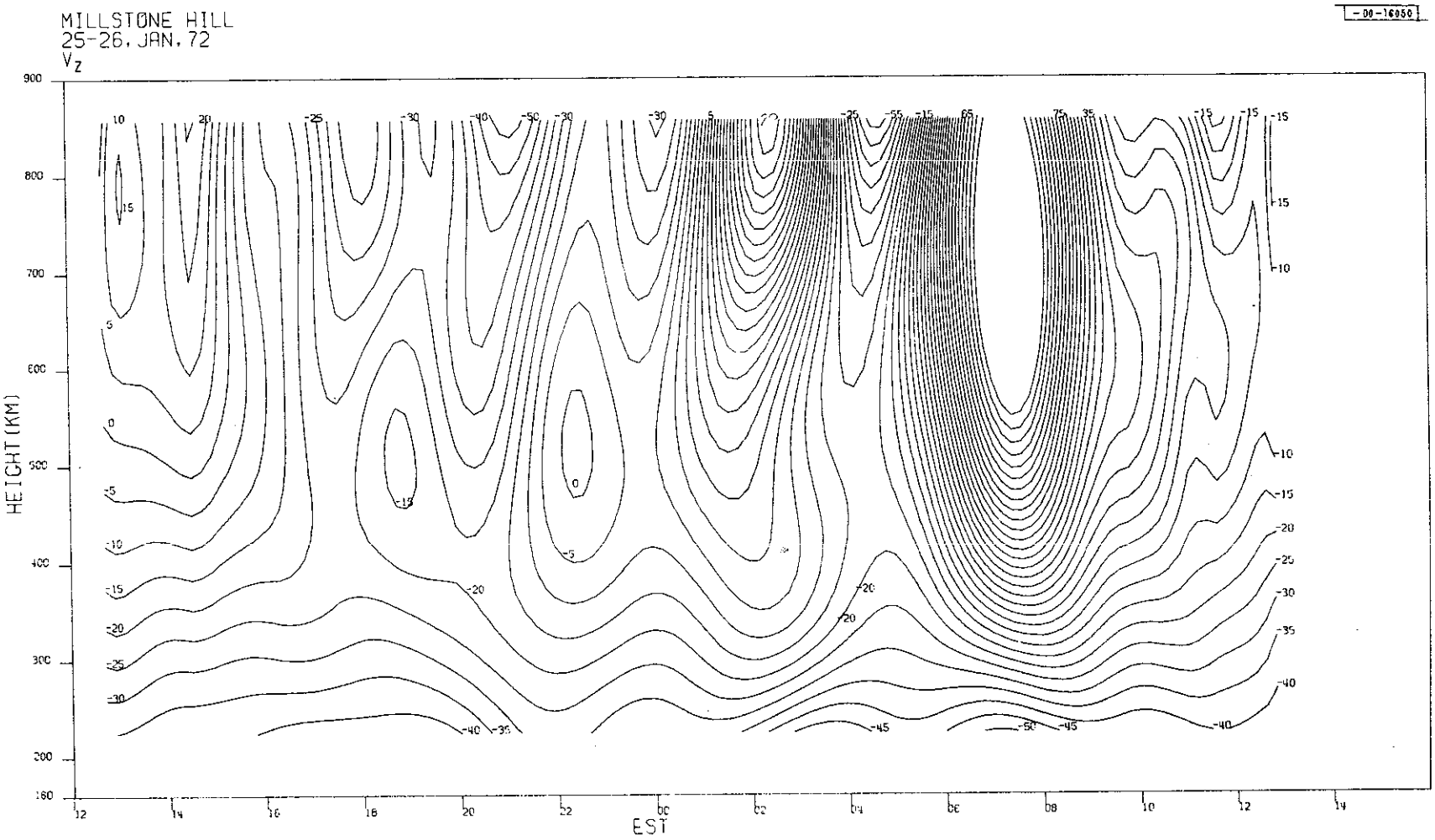

(d) V_z.

Fig. 6(a-d). Continued.

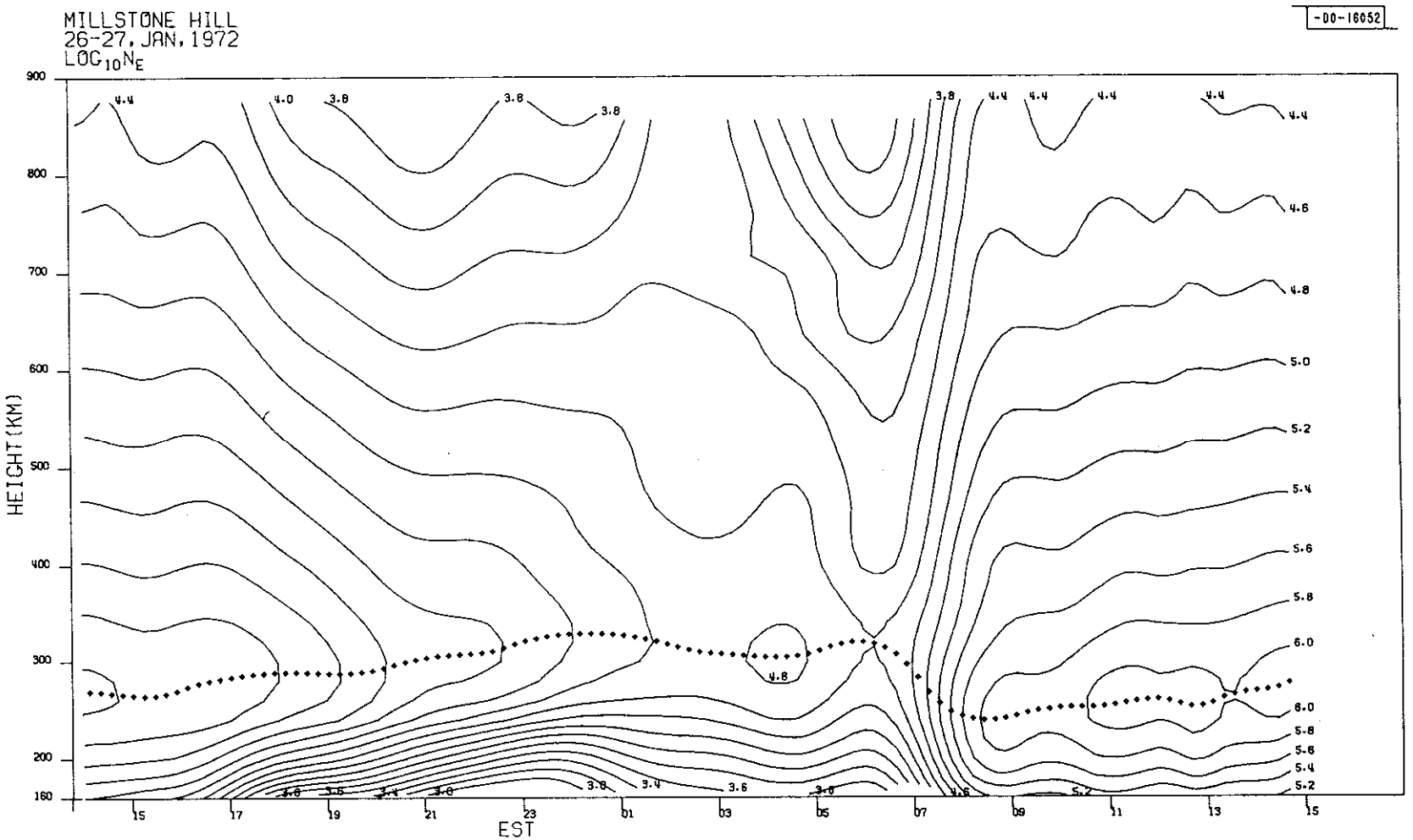

(a) $Log_{10} N_e$.

Fig.7(a-d). Results for 26-27 January 1972.

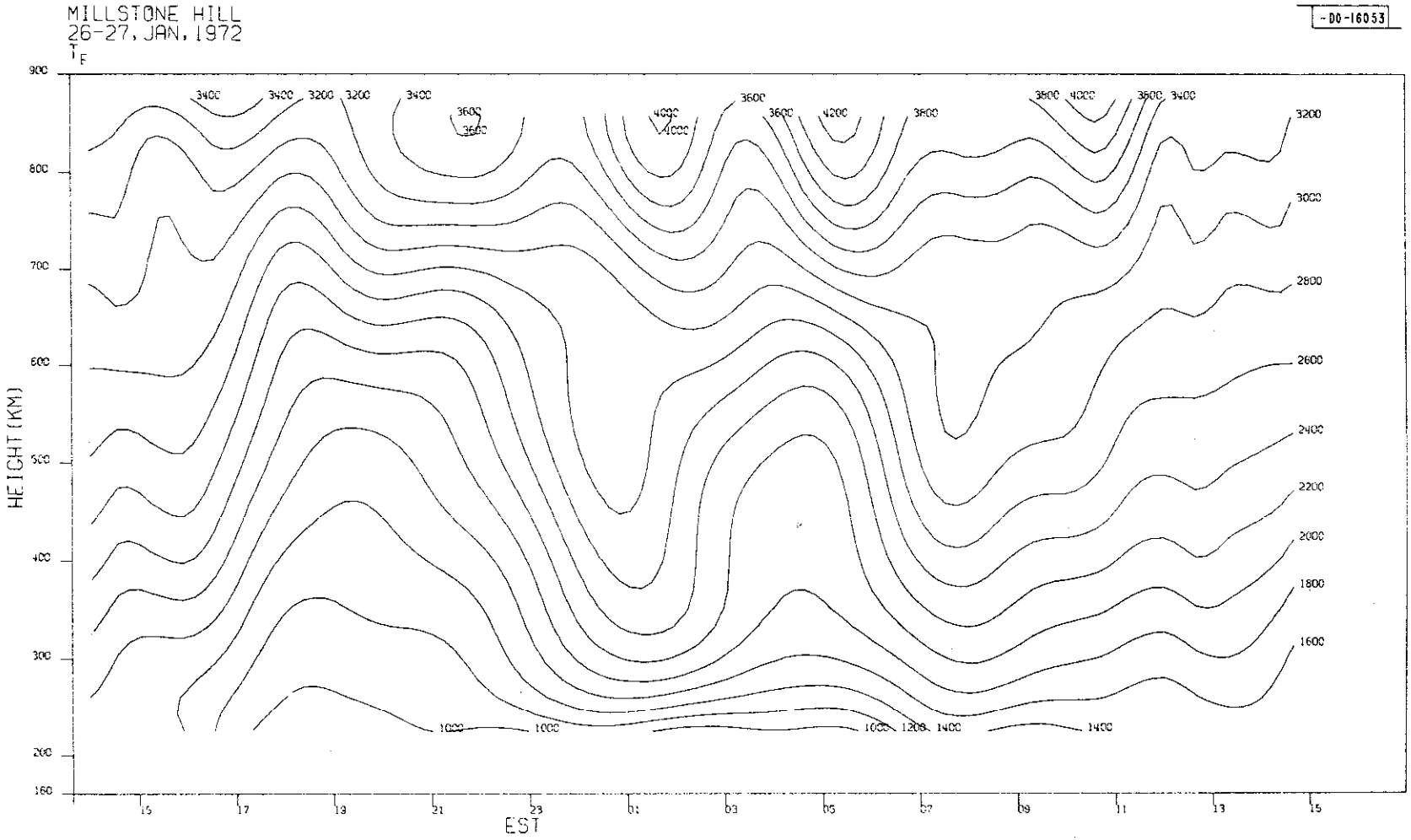

(b) T_e.

Fig.7(a-d). Continued.

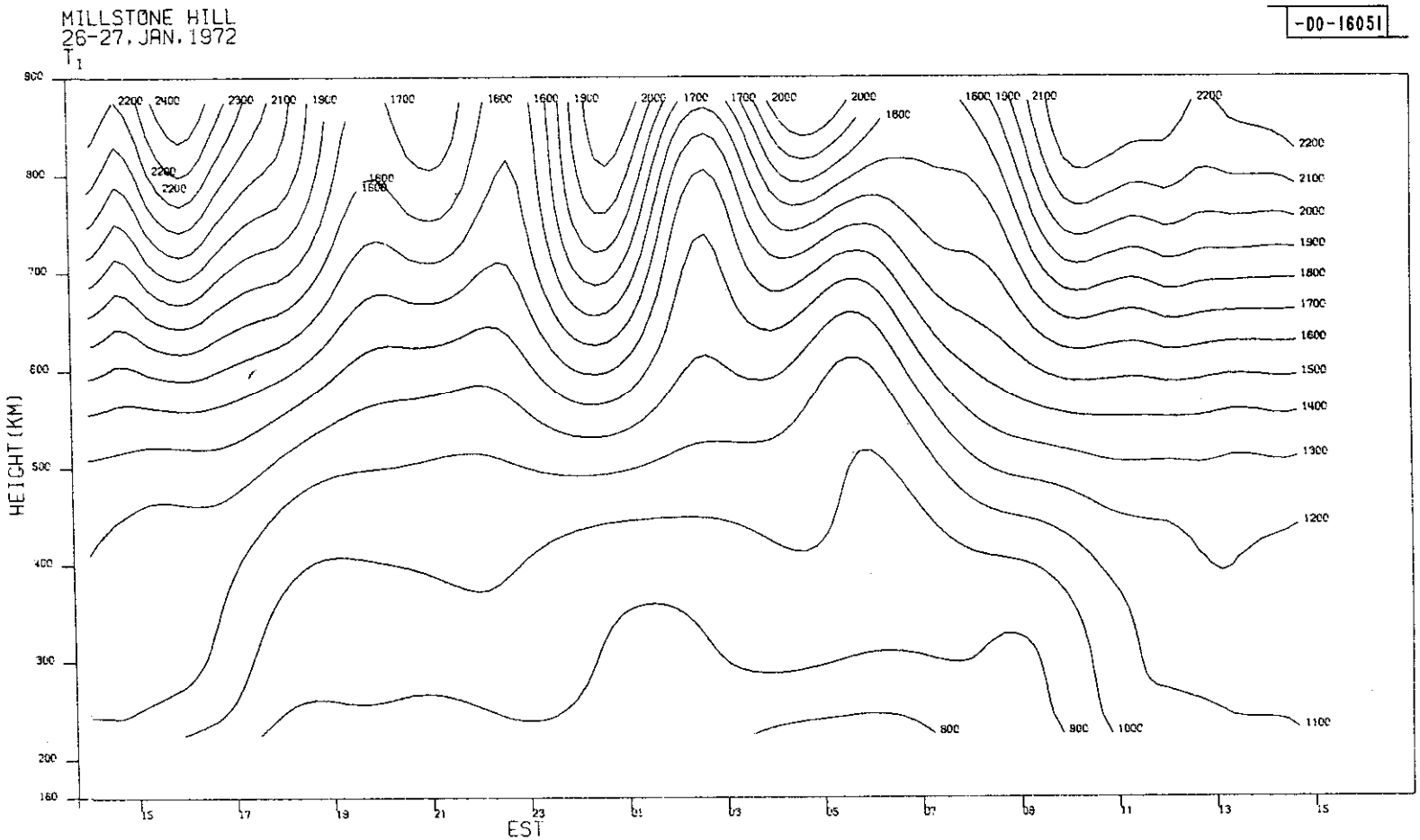

(c) T_i.

Fig.7(a-d). Continued.

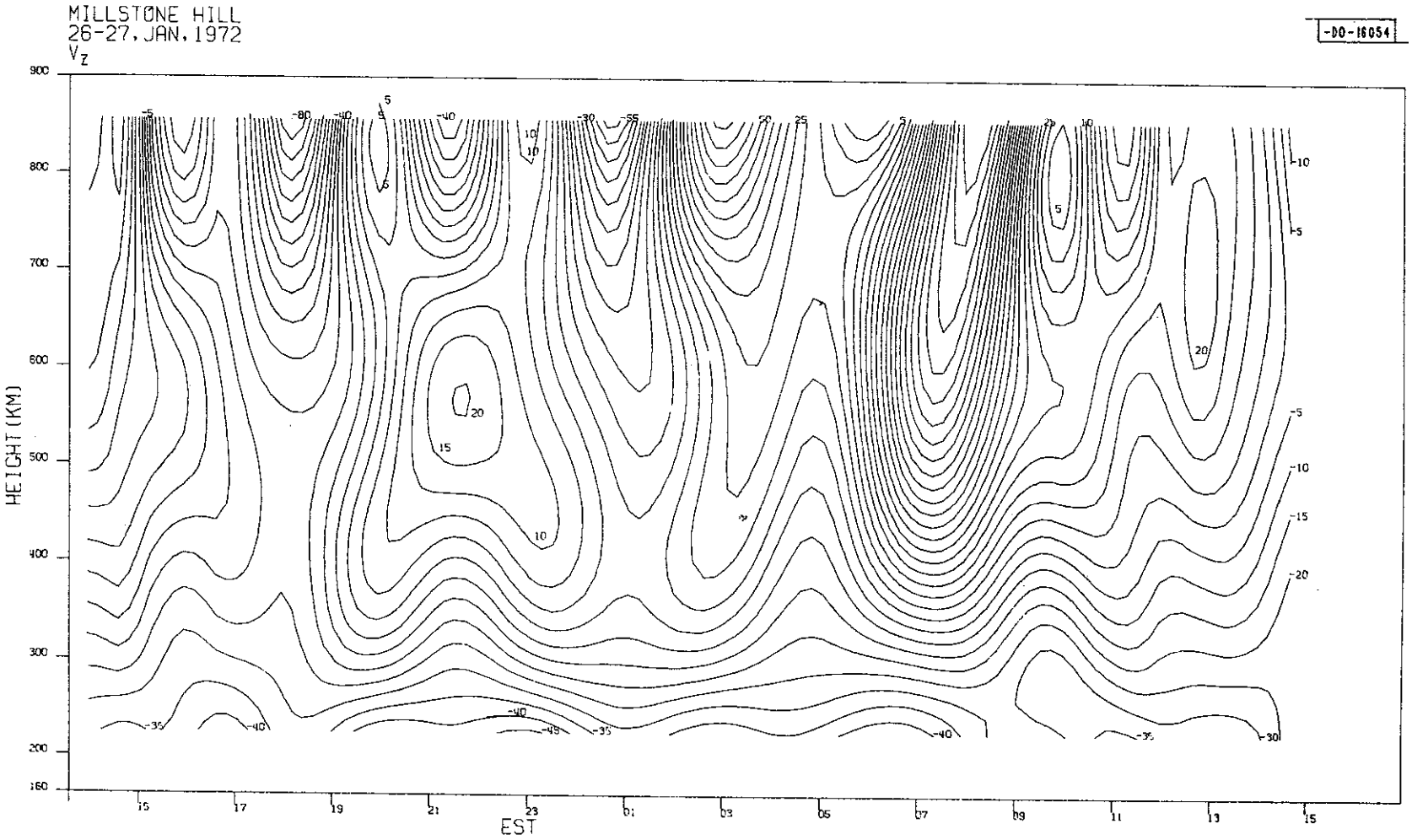

(d) V_z.

Fig.7(a-d). Continued.

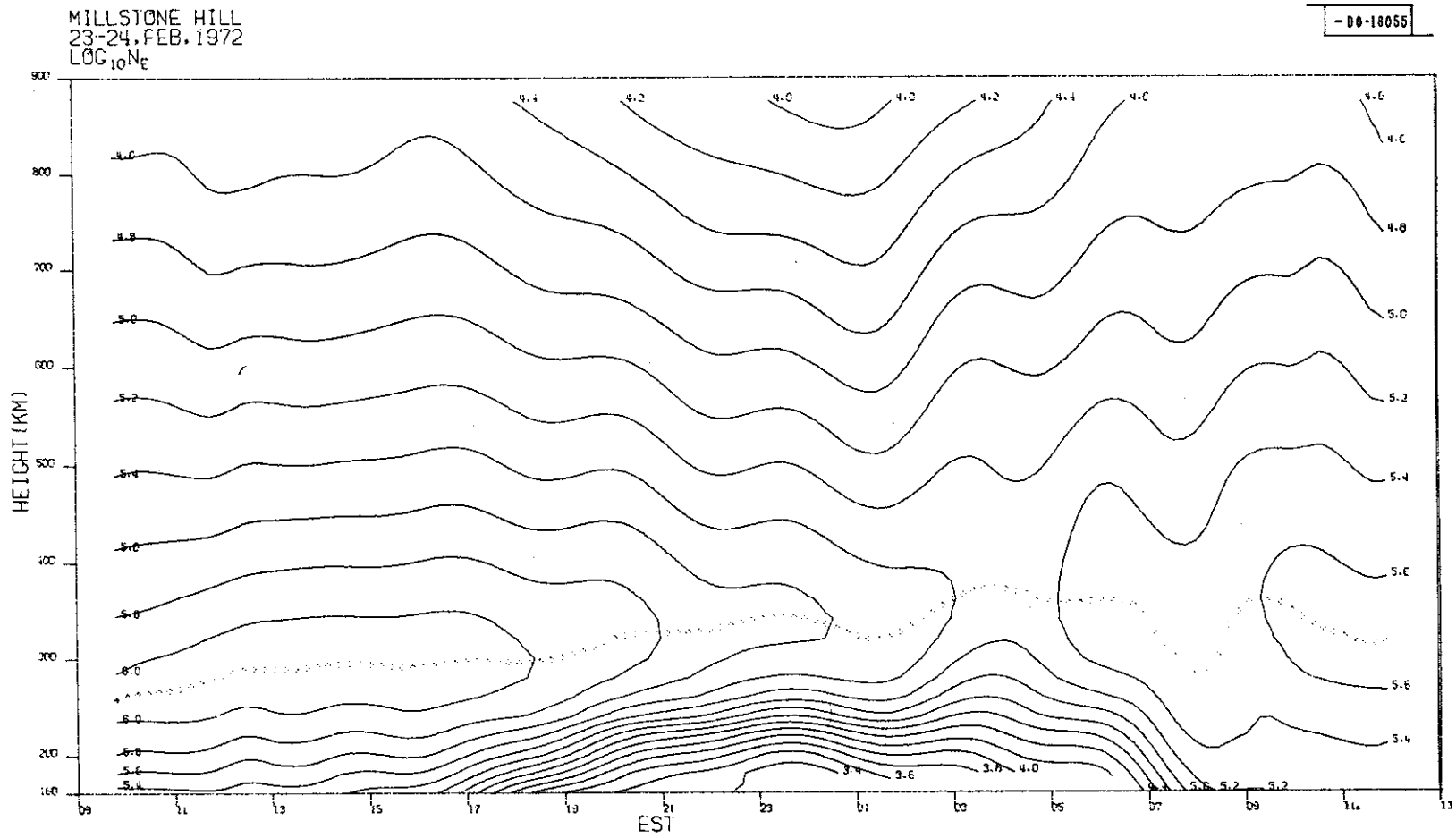

(a) $Log_{10} N_e$.

Fig.8(a-d). Results for 23-24 February 1972.

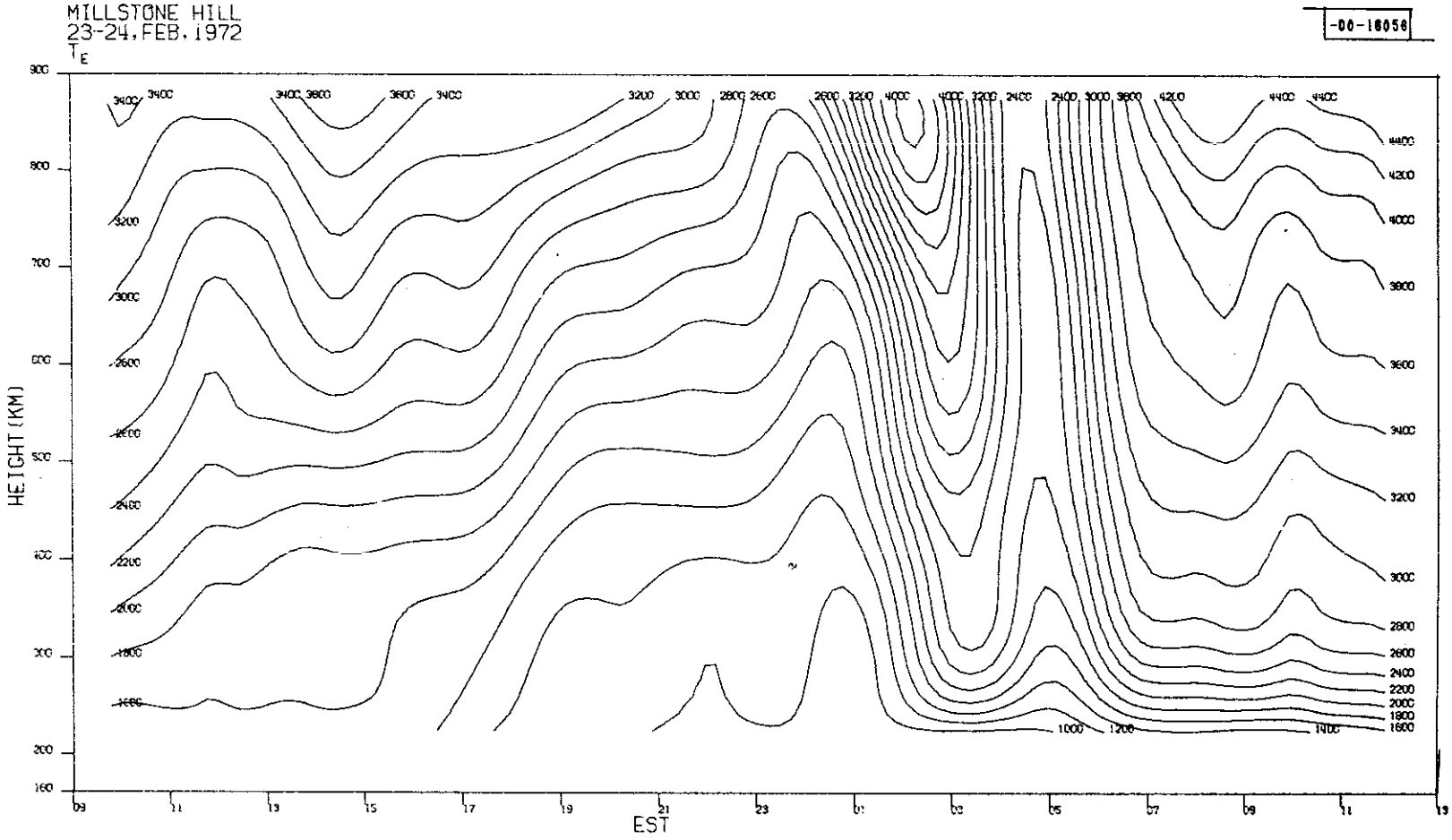

(b) T_e.

Fig.8(a-d). Continued.

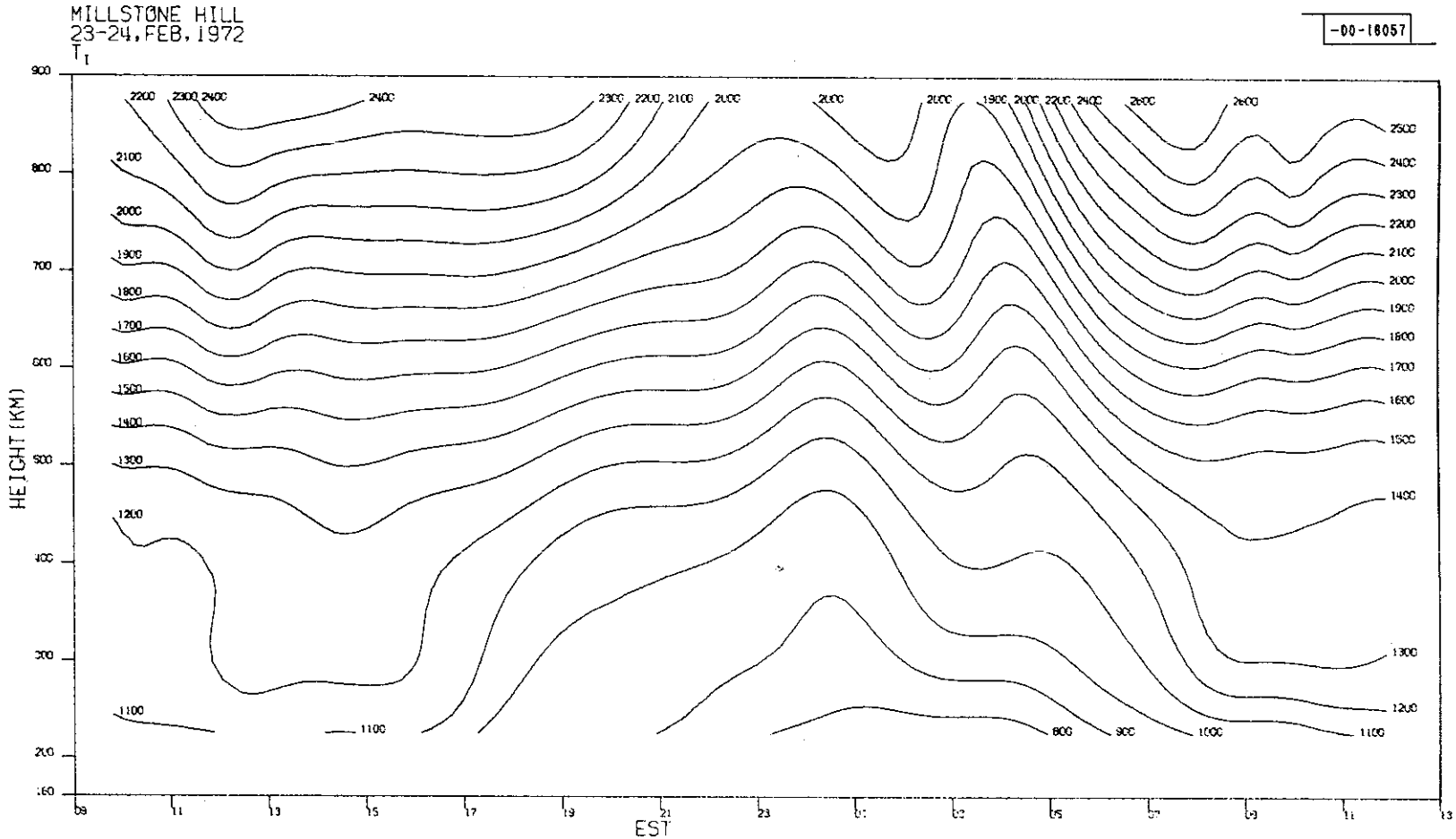

(c) T_i.

Fig.8(a-d). Continued.

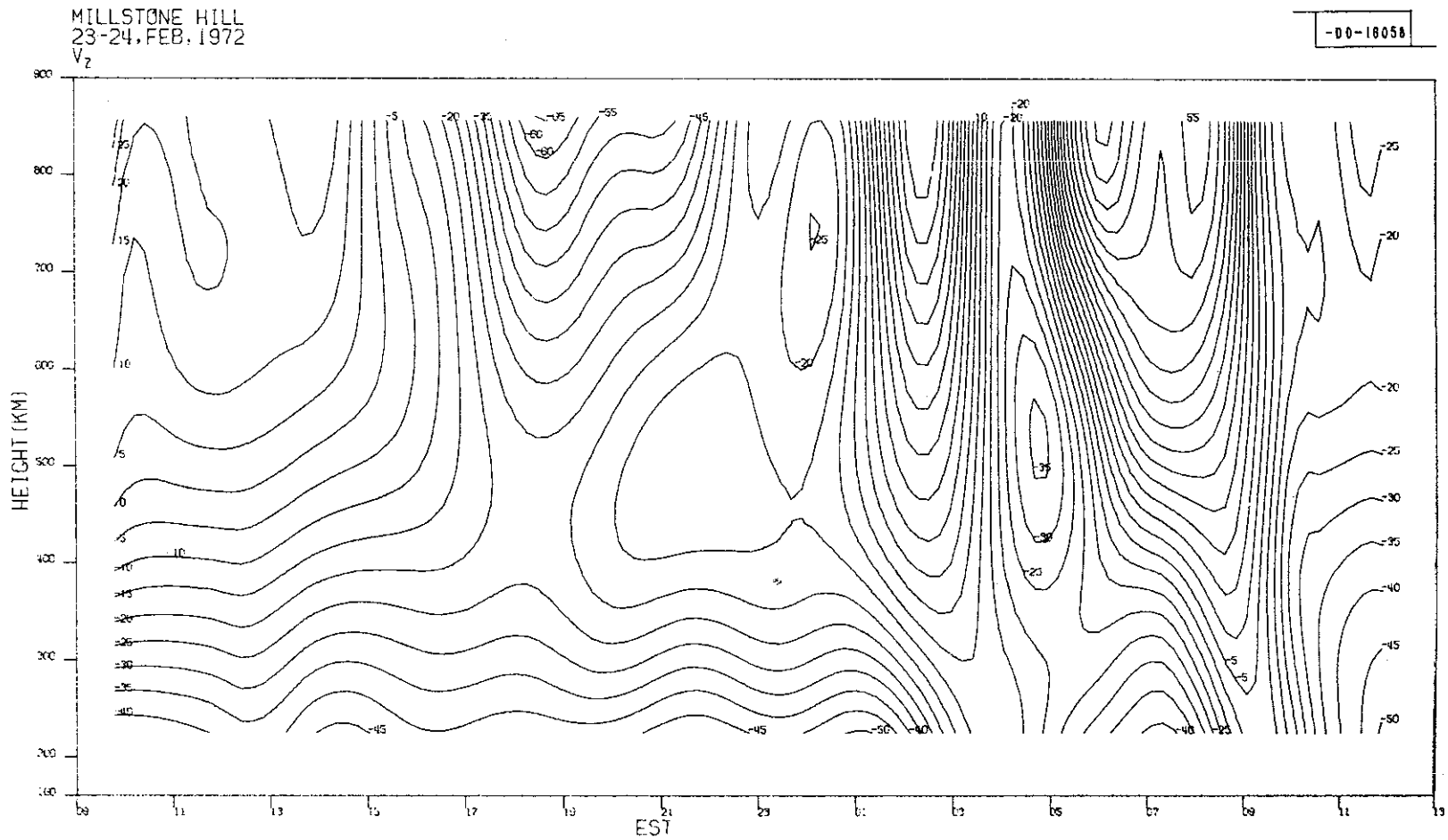

(d) V_z.

Fig.8(a-d). Continued.

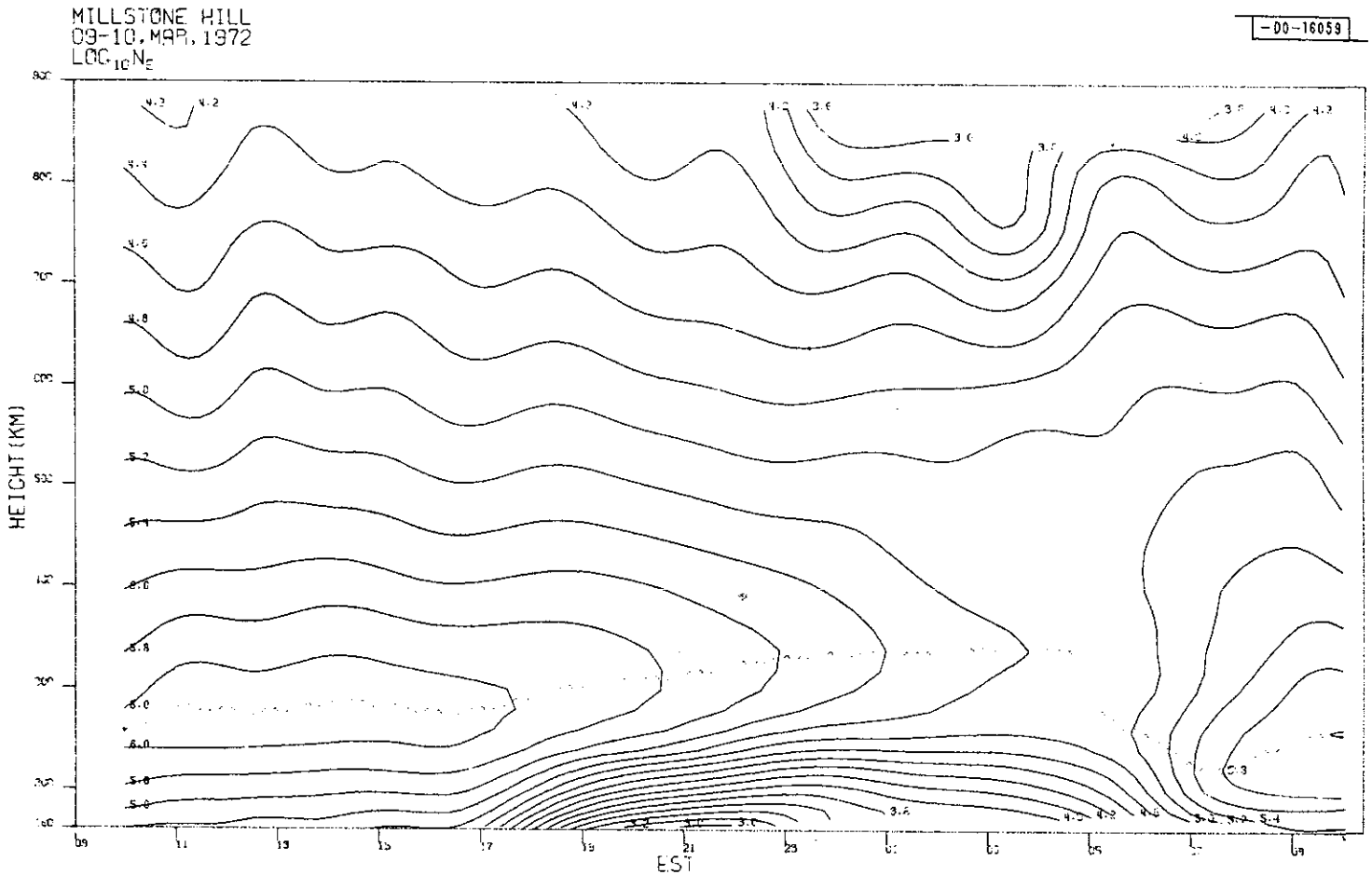

(a) $Log_{10} N_e$.

Fig.9(a-d). Results for 9-10 March 1972.

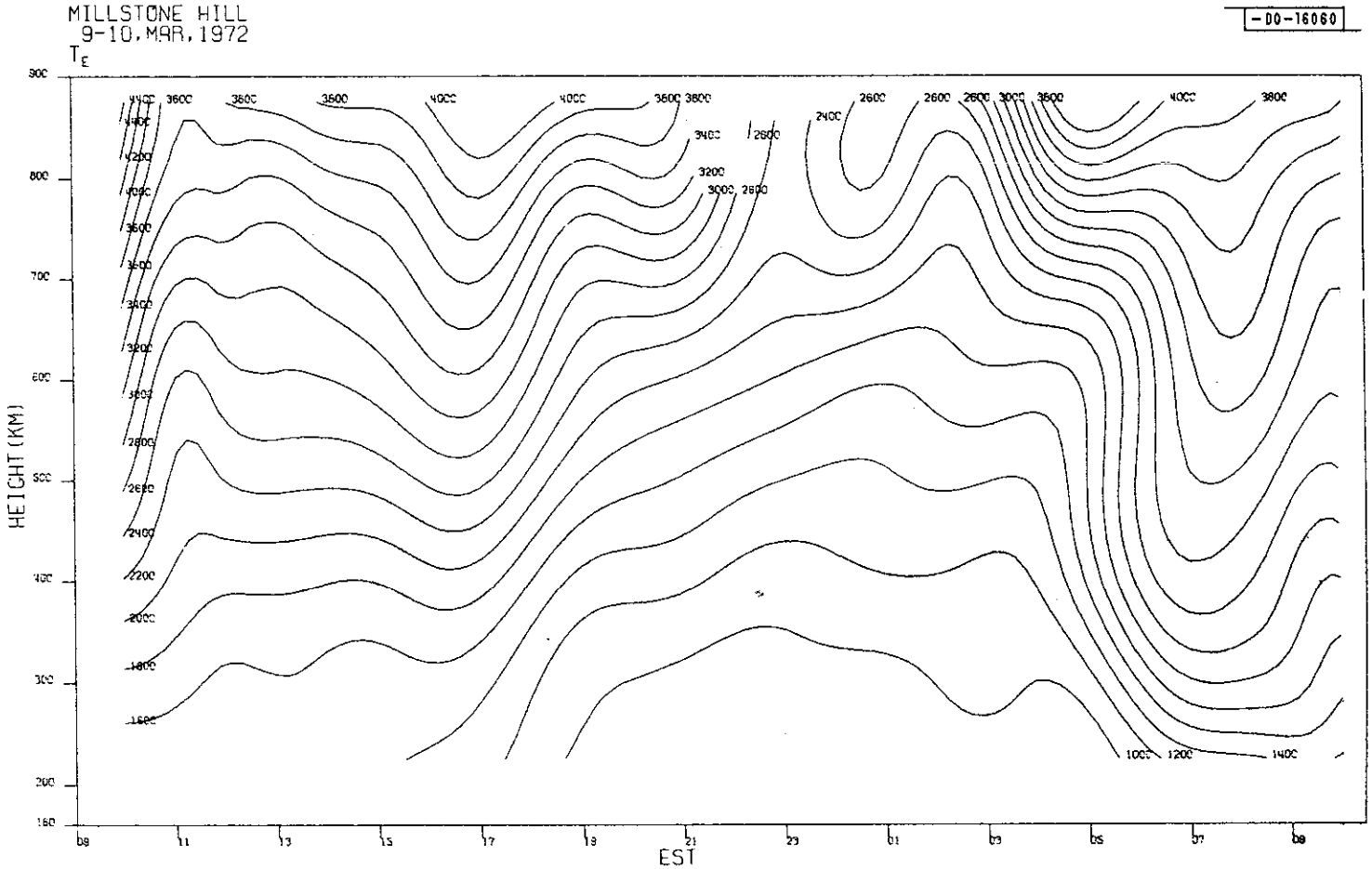

(b) T_e.

Fig.9(a-d). Continued.

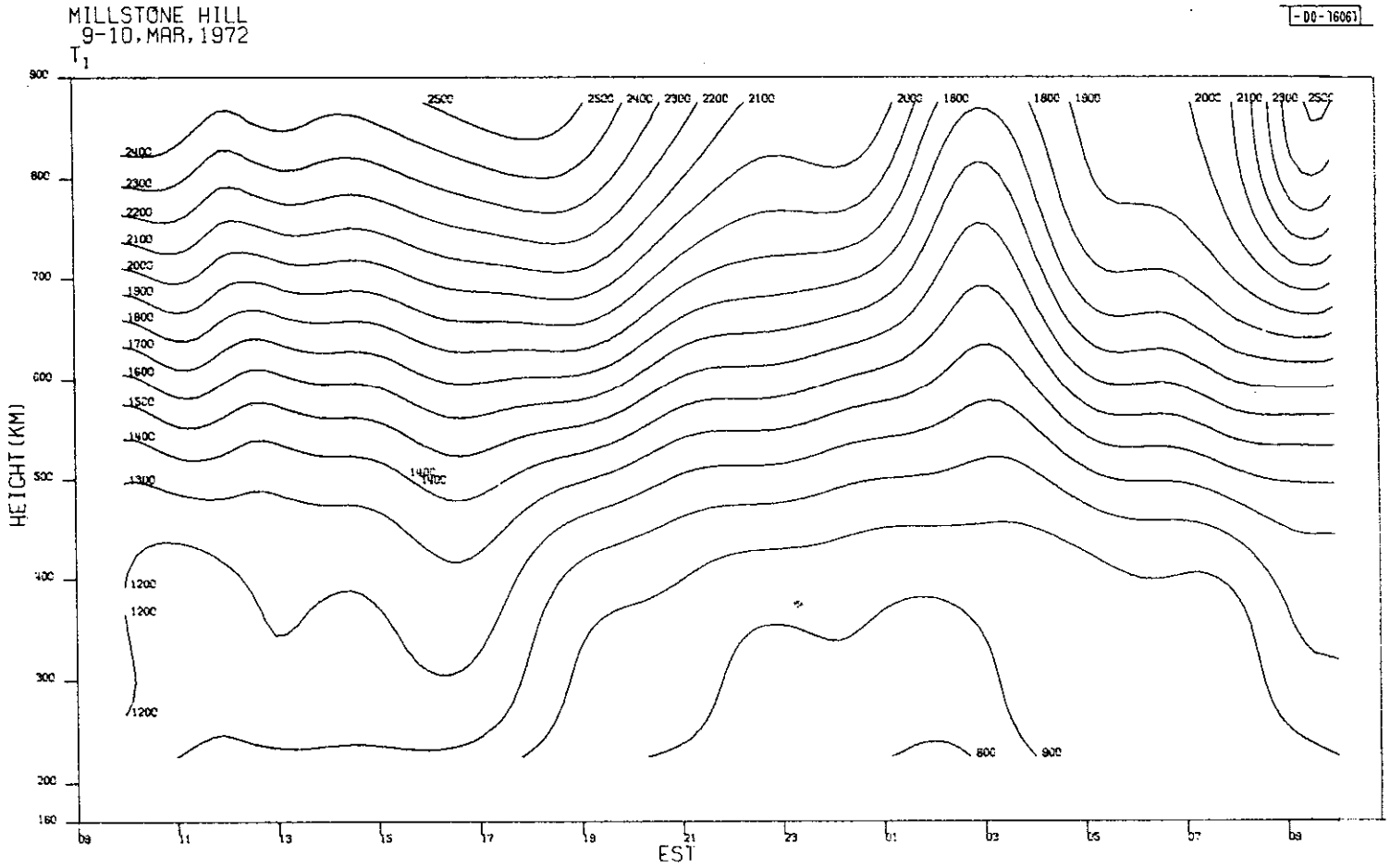

(c) T_i.

Fig. 9(a-d). Continued.

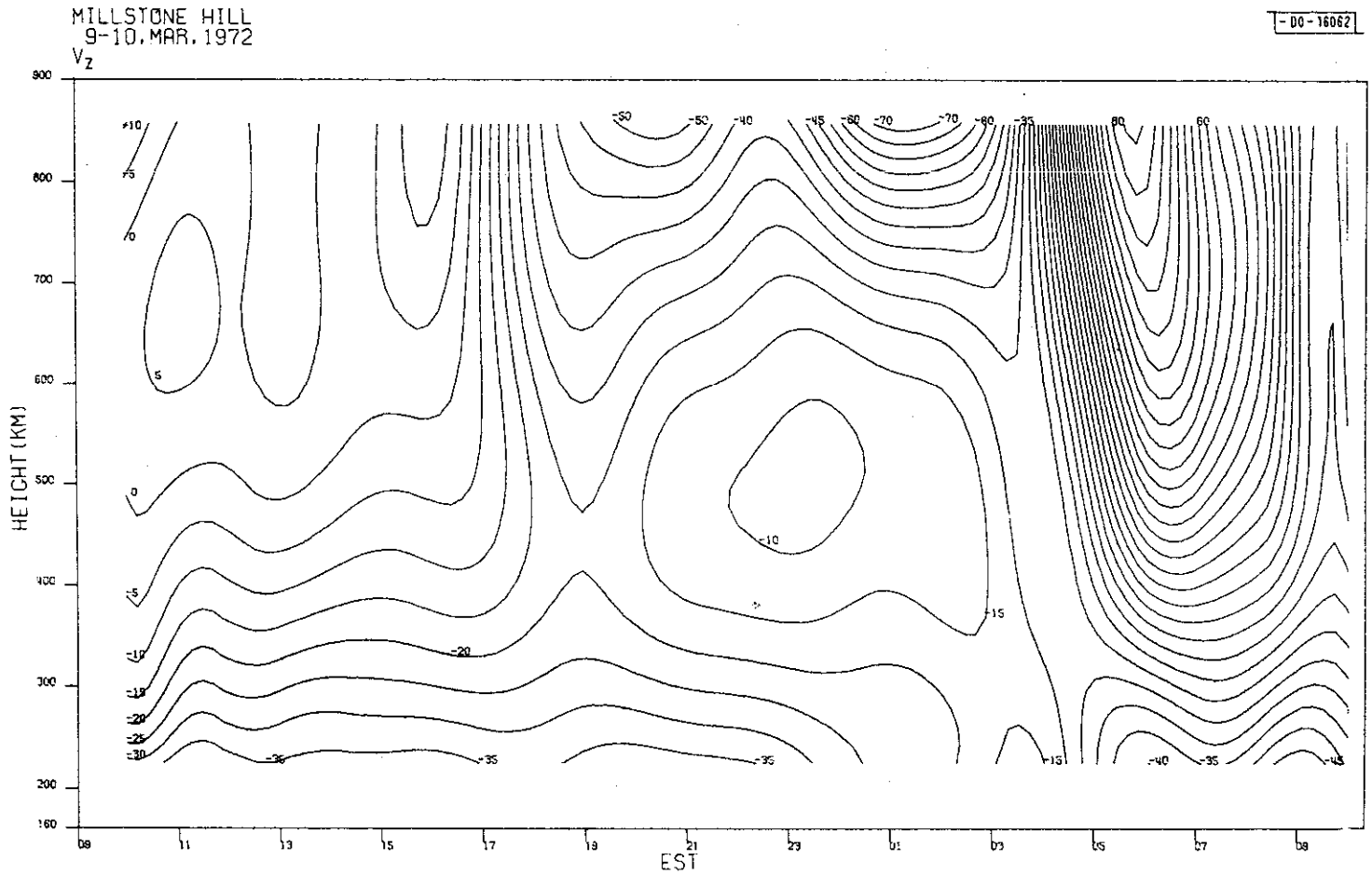

(d) V_z.

Fig.9(a-d). Continued.

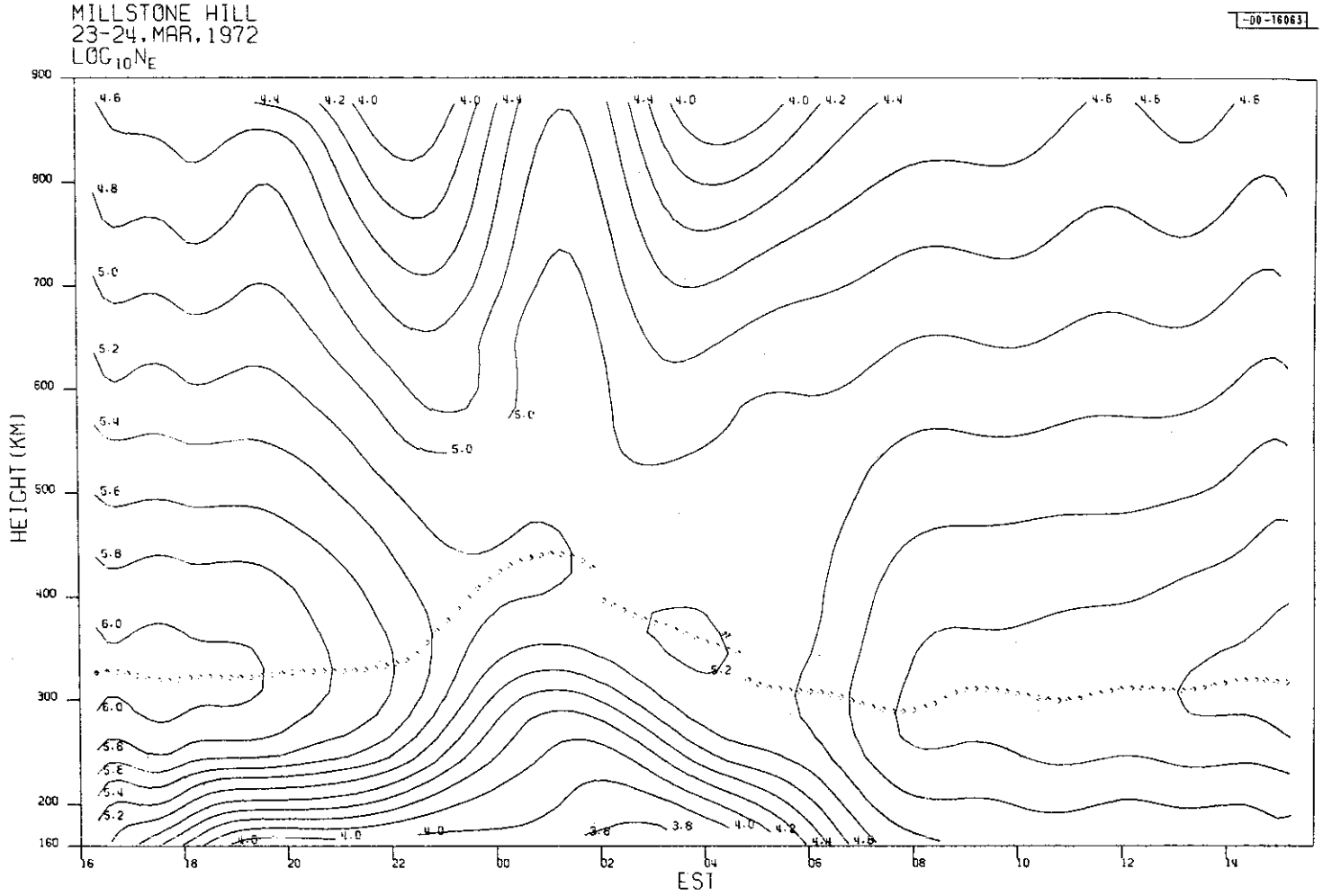

(a) $Log_{10} N_e$.

Fig. 10(a-d). Results for 23-24 March 1972.

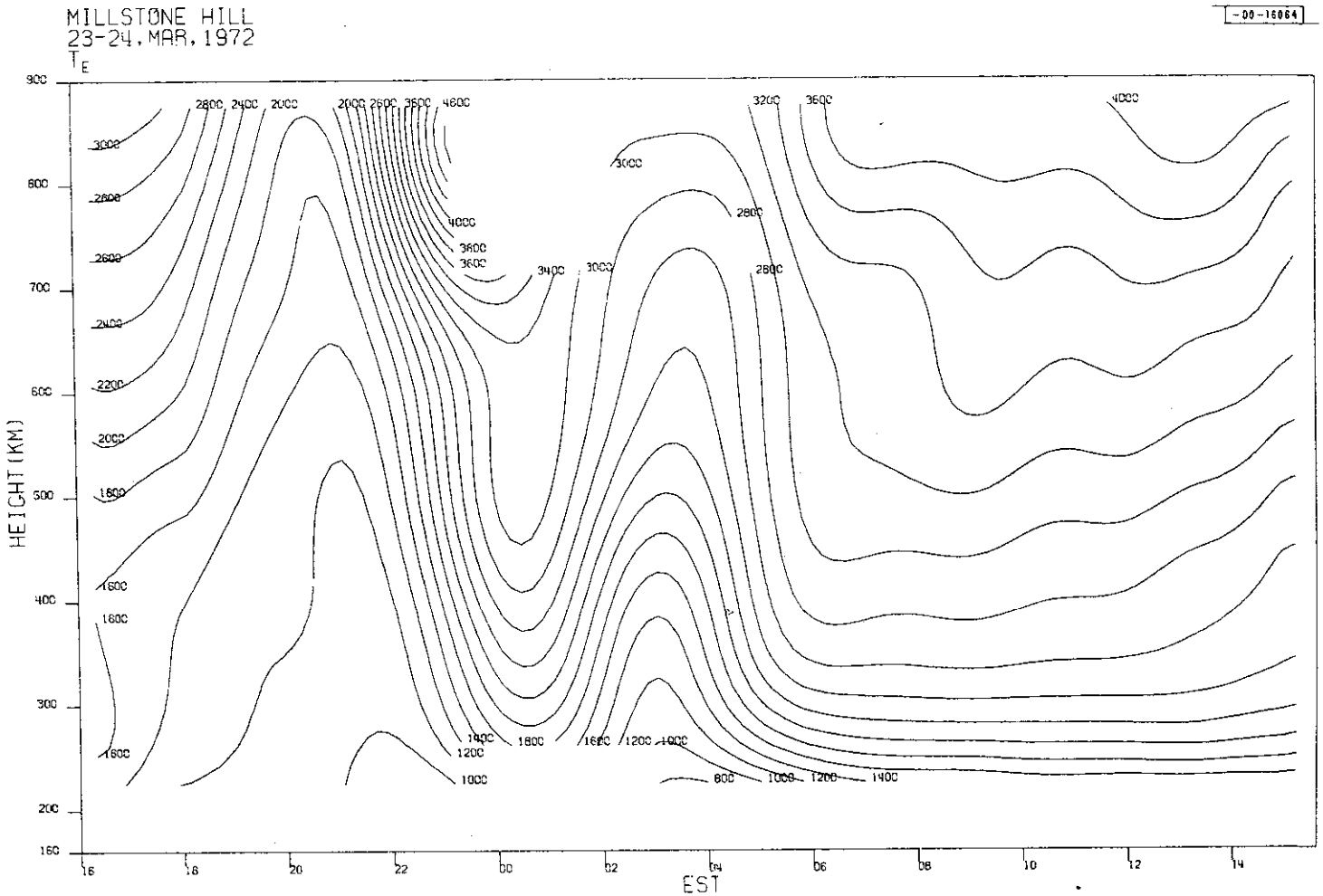

(b) T_e.

Fig.10(a-d). Continued.

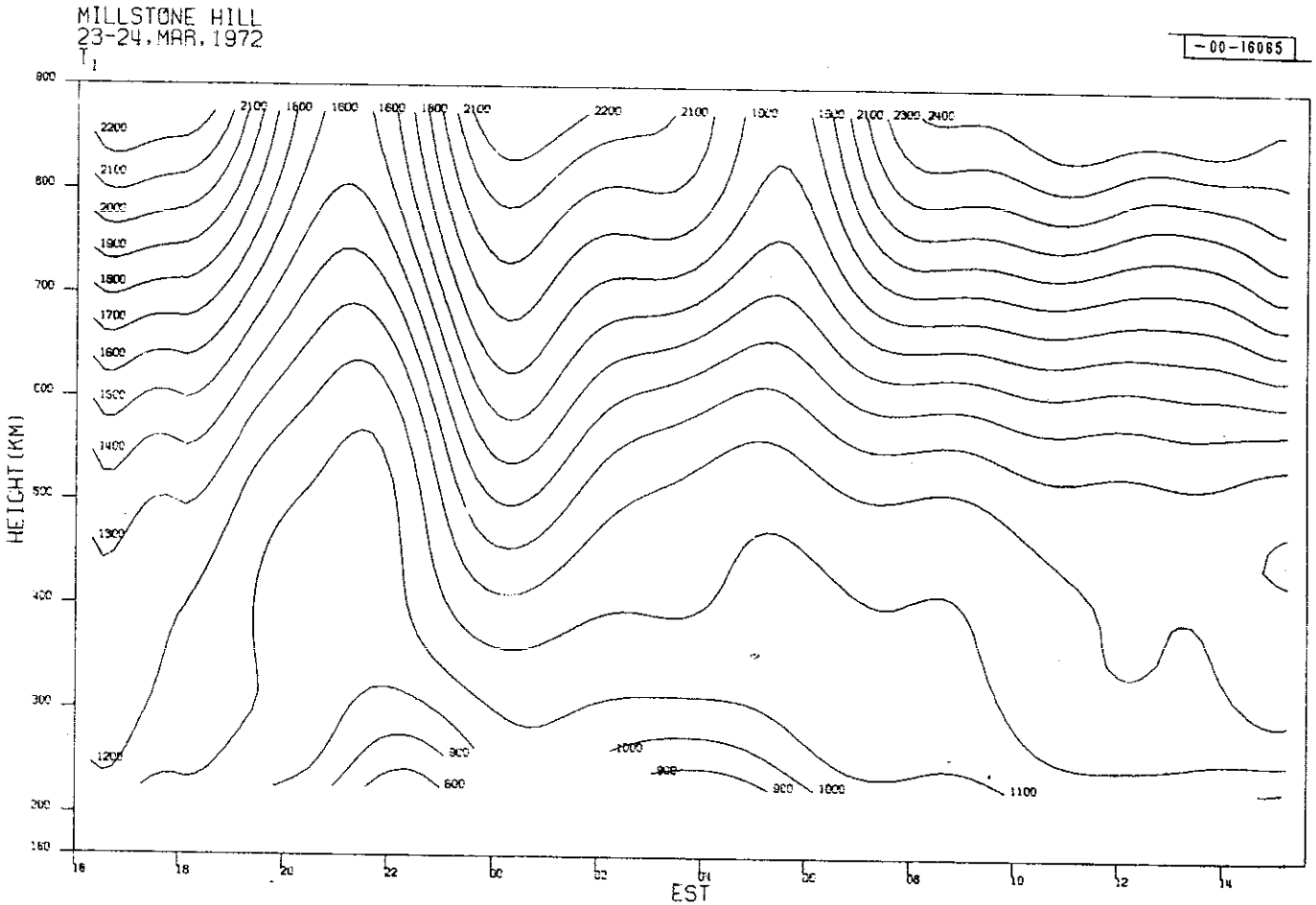

(c) T_i.

Fig. 10(a-d). Continued.

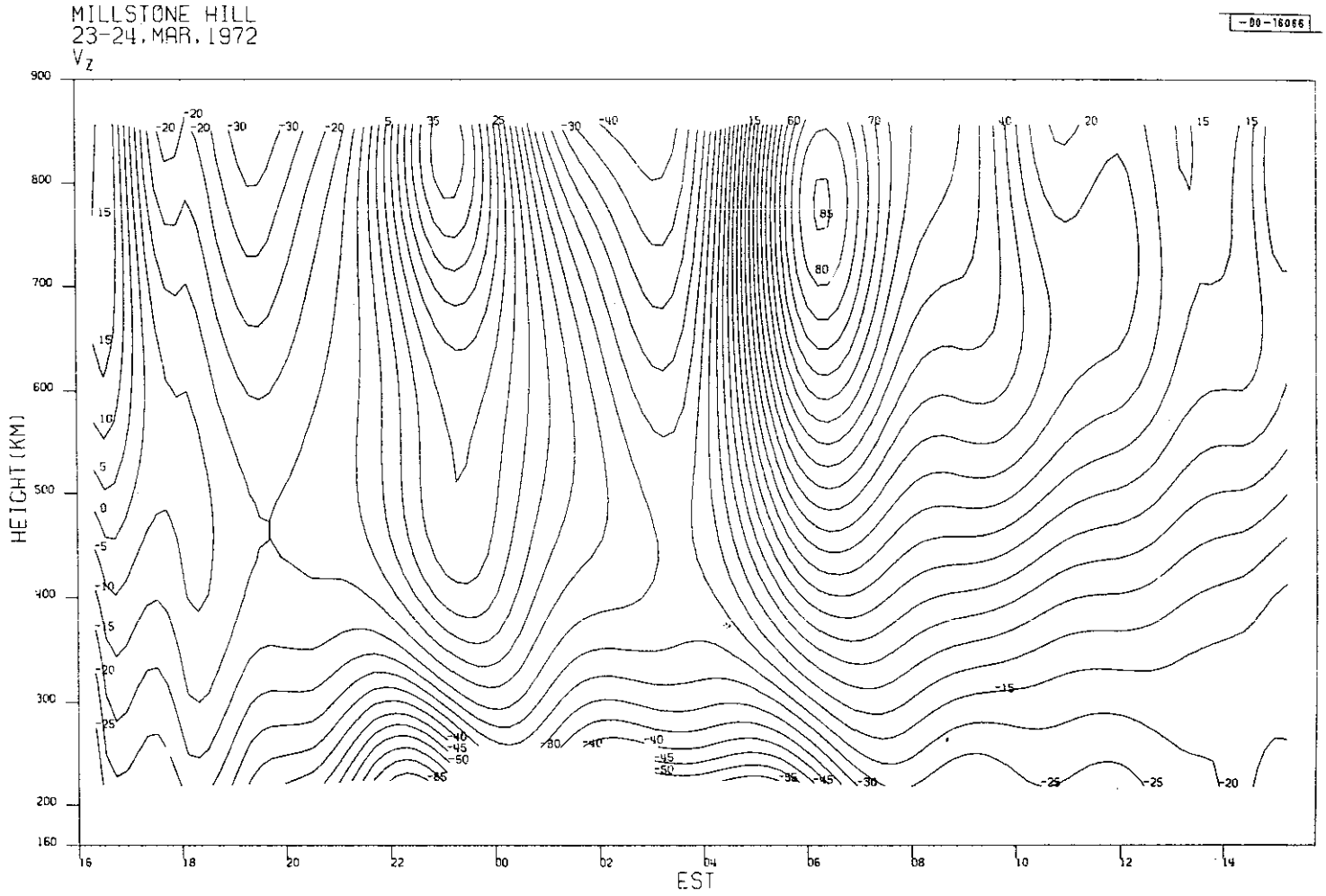

(d) V_z.

Fig. 10(a-d). Continued.

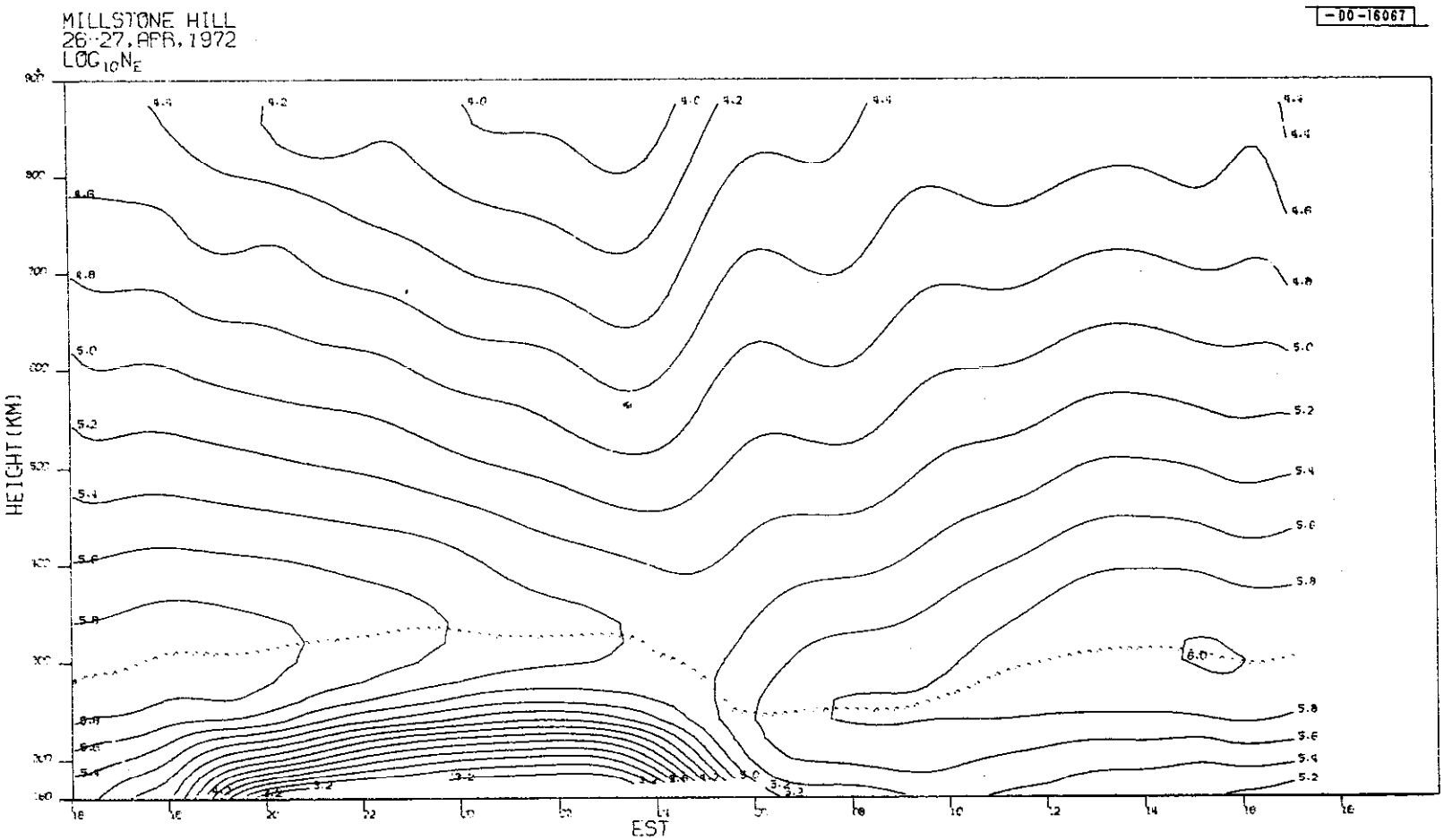

(a) $Log_{10} N_e$.

Fig. 11(a-d). Results for 26-27 April 1972.

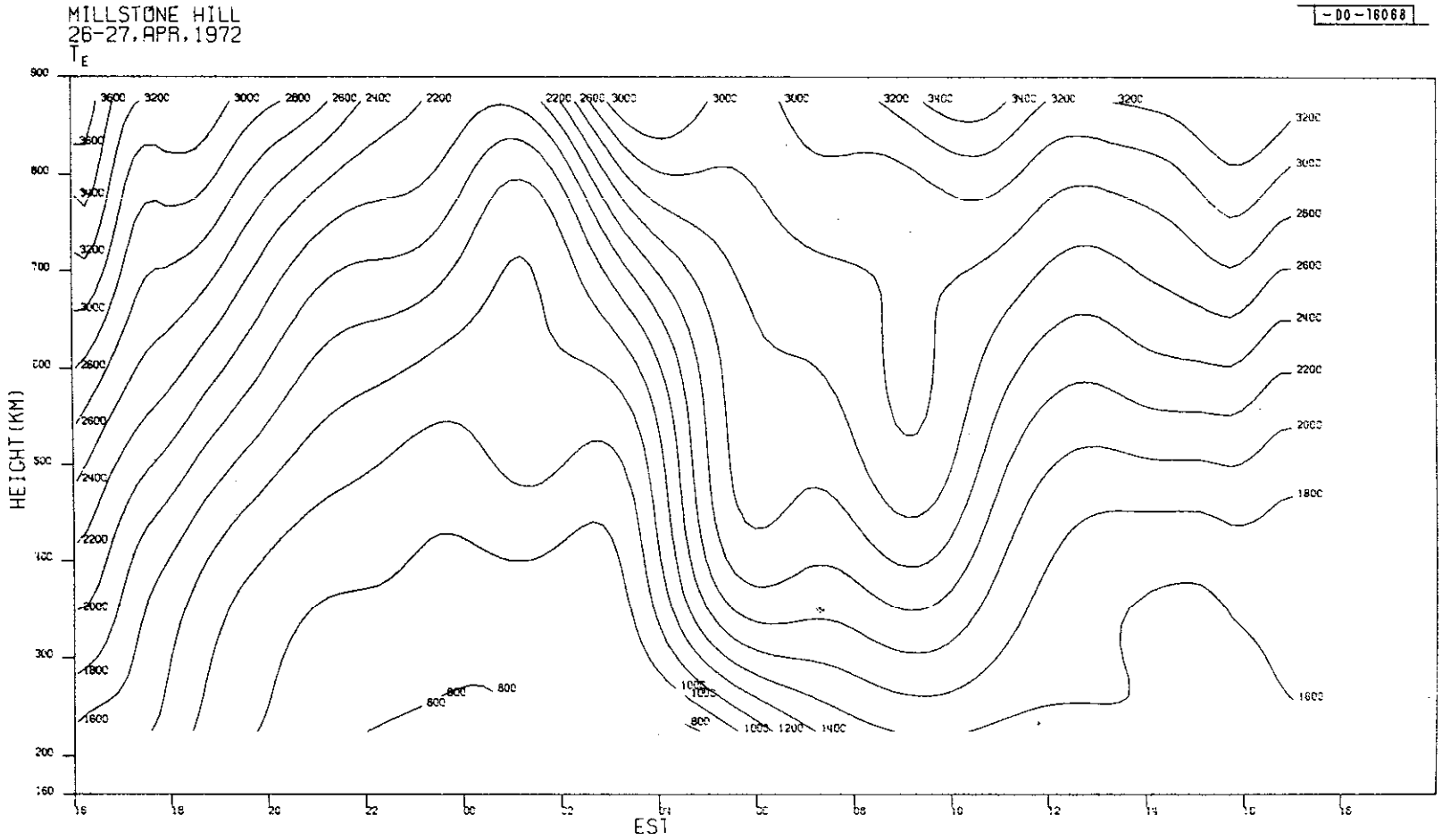

(b) T_e.

Fig. 11(a-d). Continued.

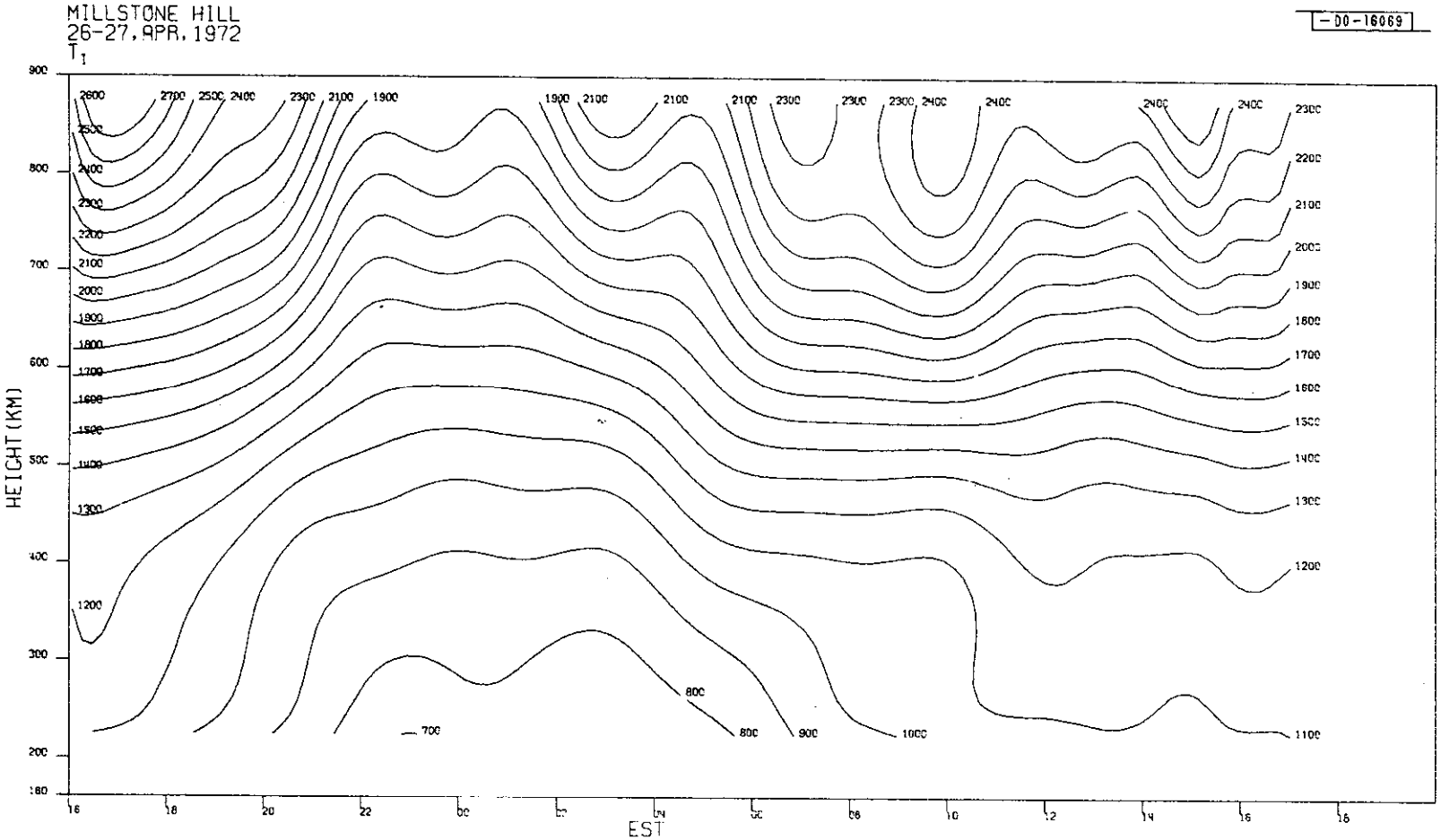

(c) T_i.

Fig.11(a-d). Continued.

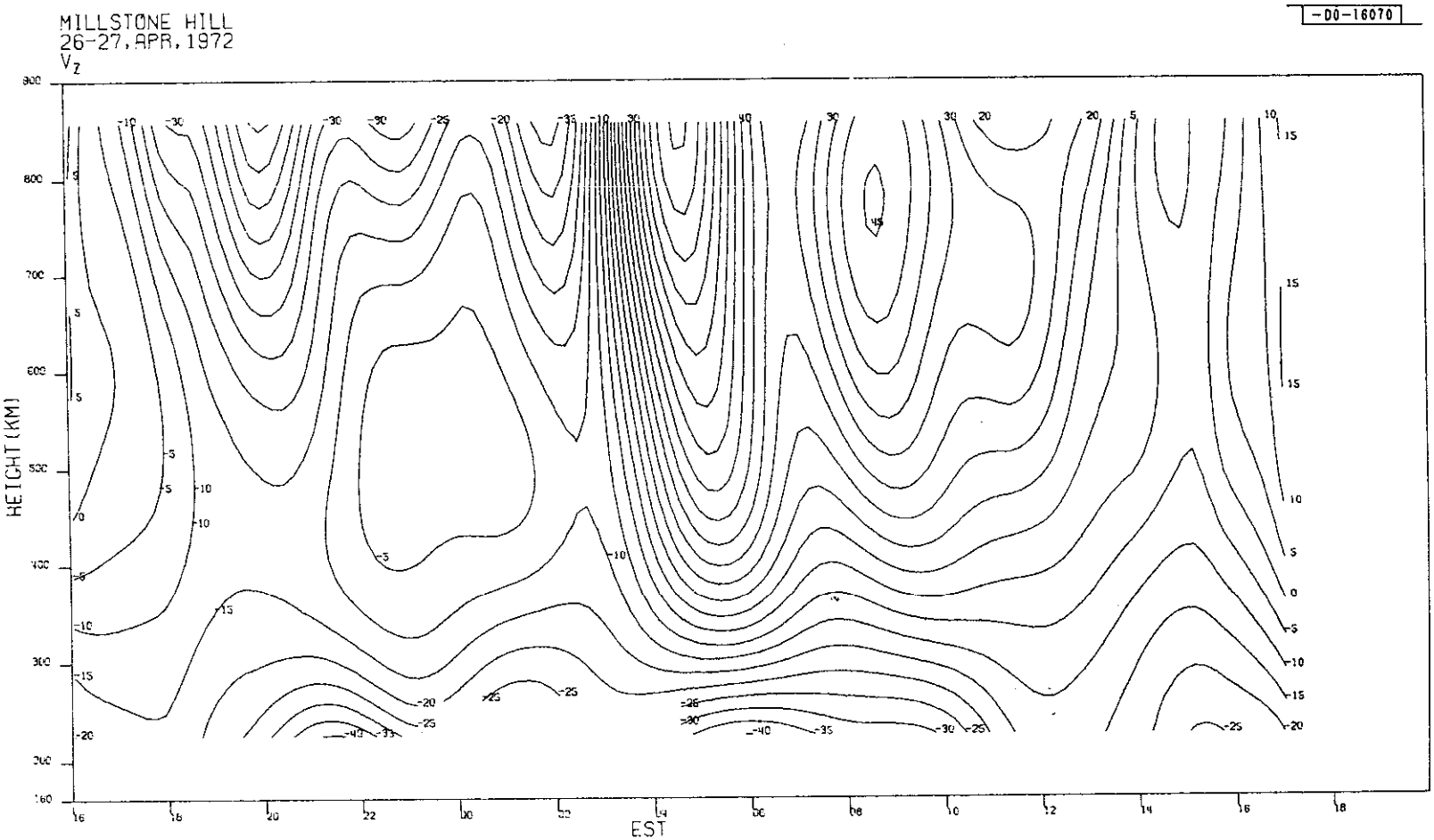

(d) V_z.

Fig. 11(a-d). Continued.

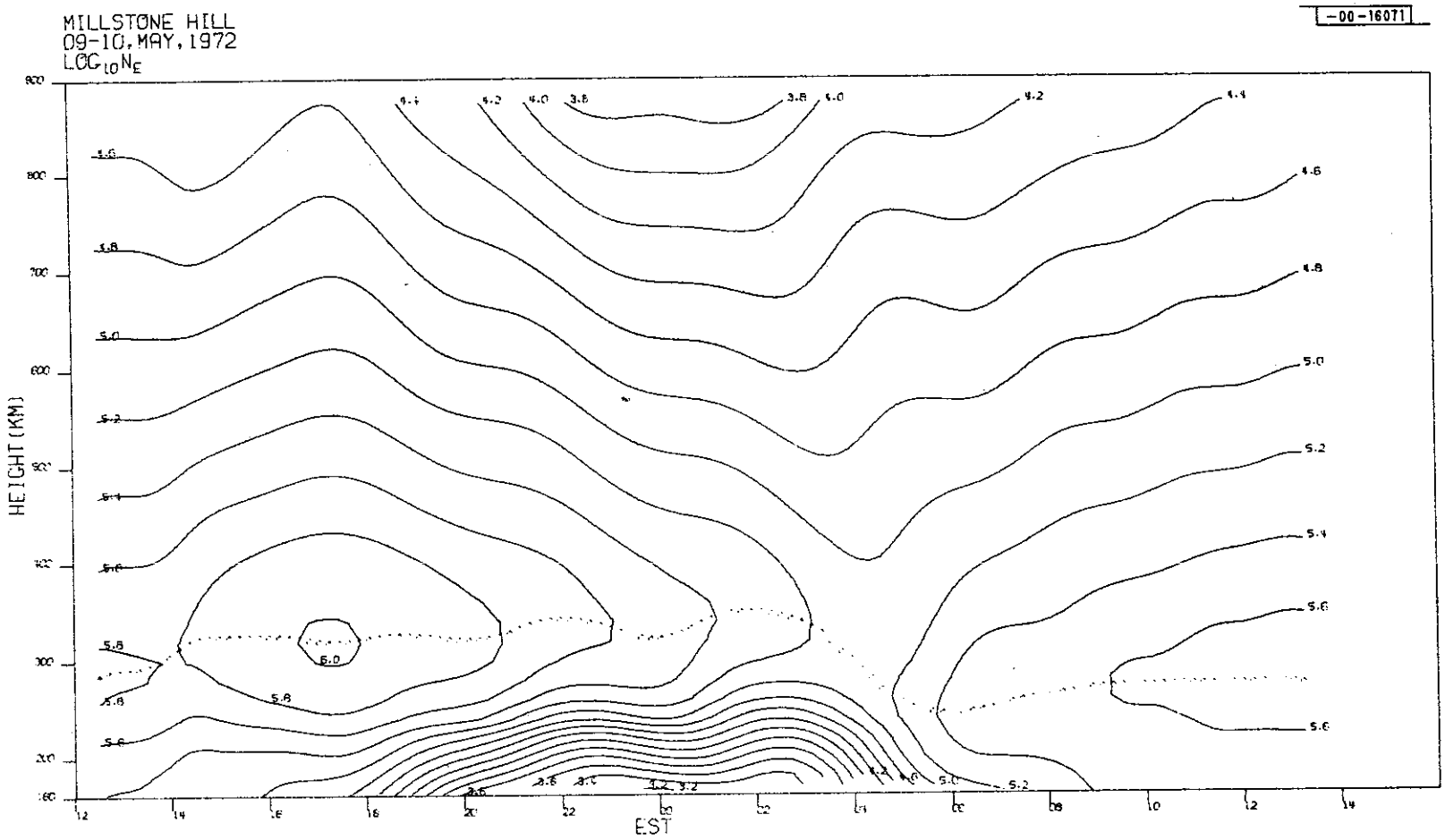

(a) $\text{Log}_{10} N_e$.

Fig.12(a-d). Results for 9-10 May 1972.

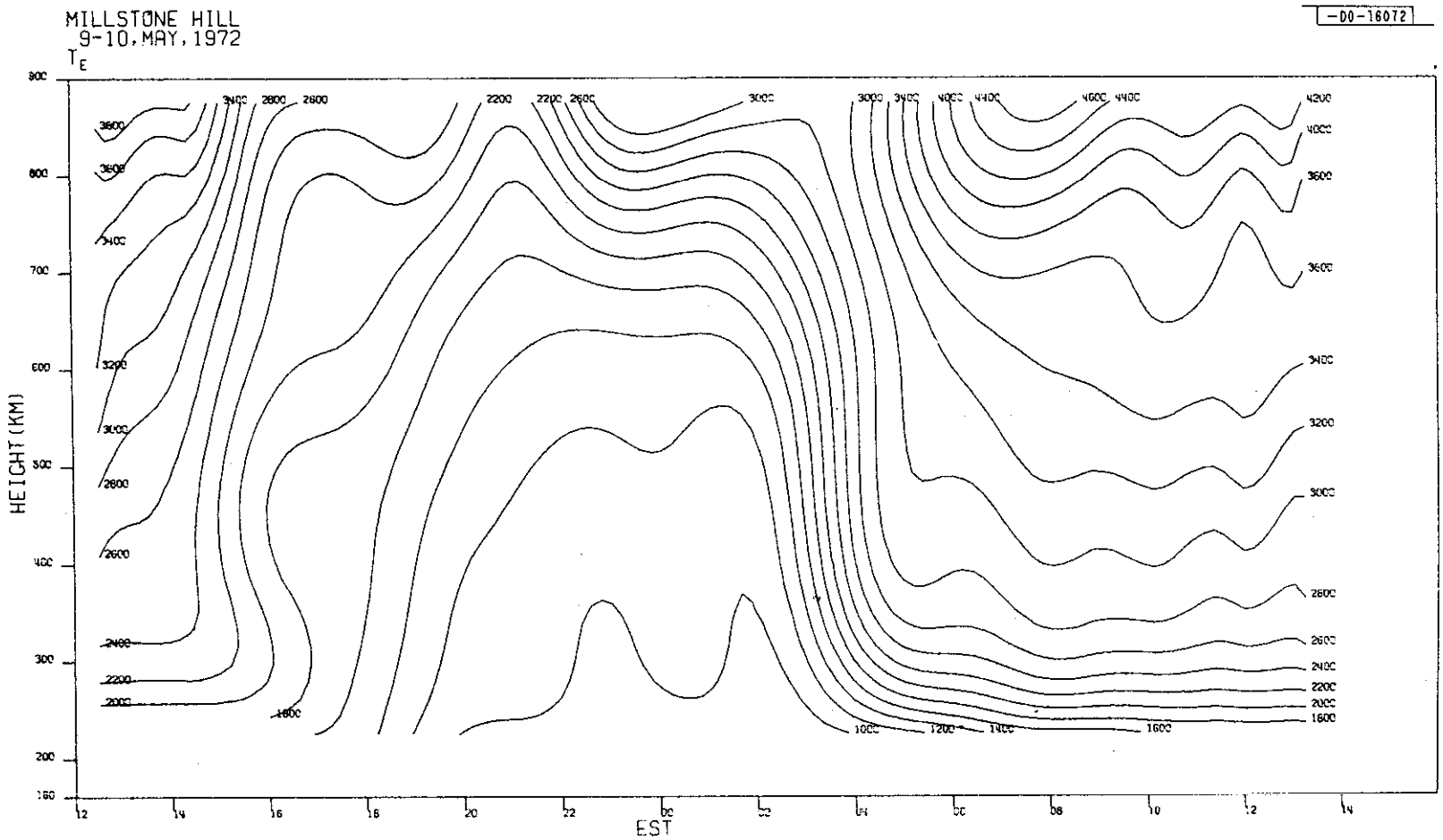

(b) T_e.

Fig. 12(a-d). Continued.

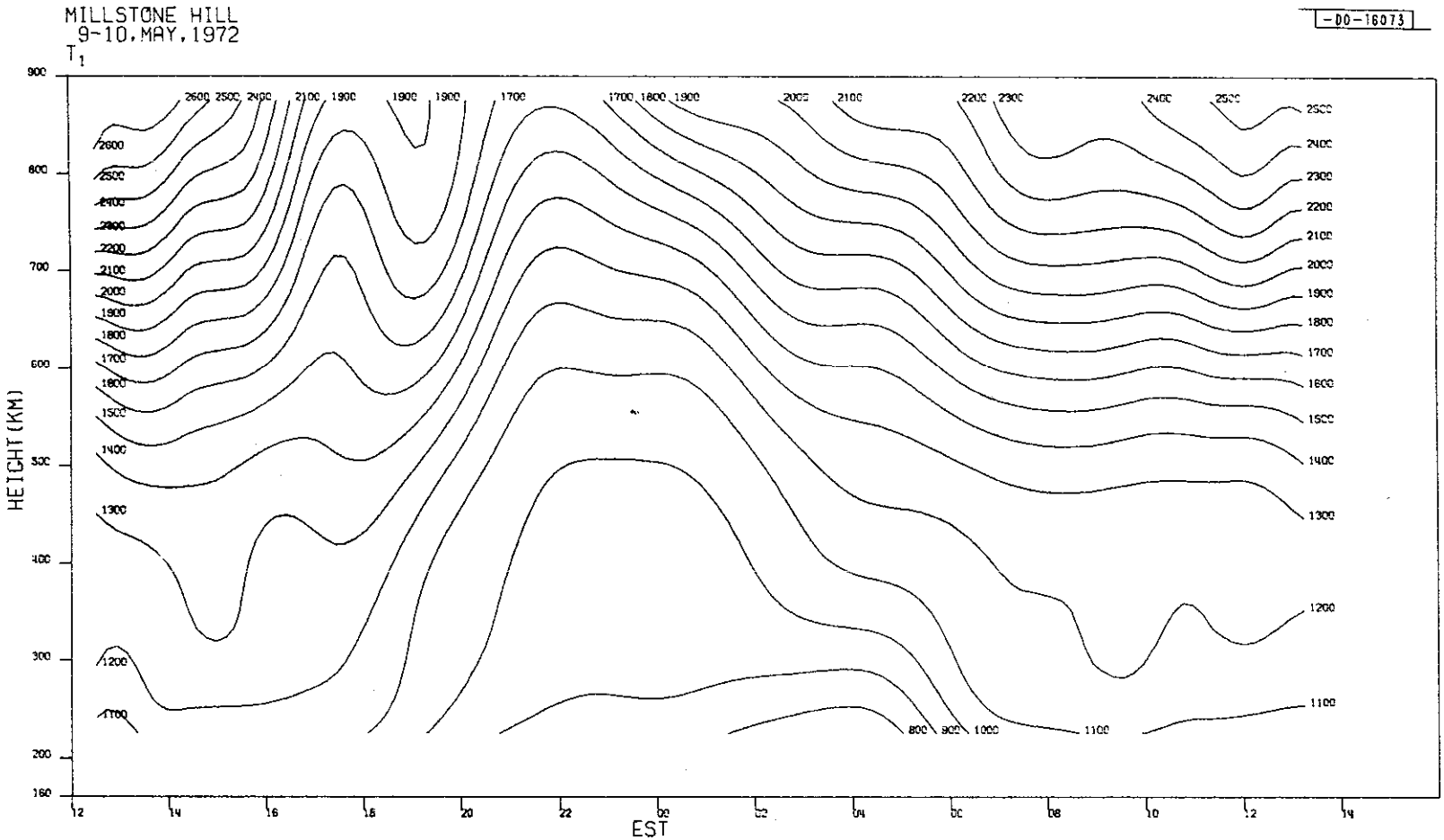

(c) T_i.

Fig. 12(a-d). Continued.

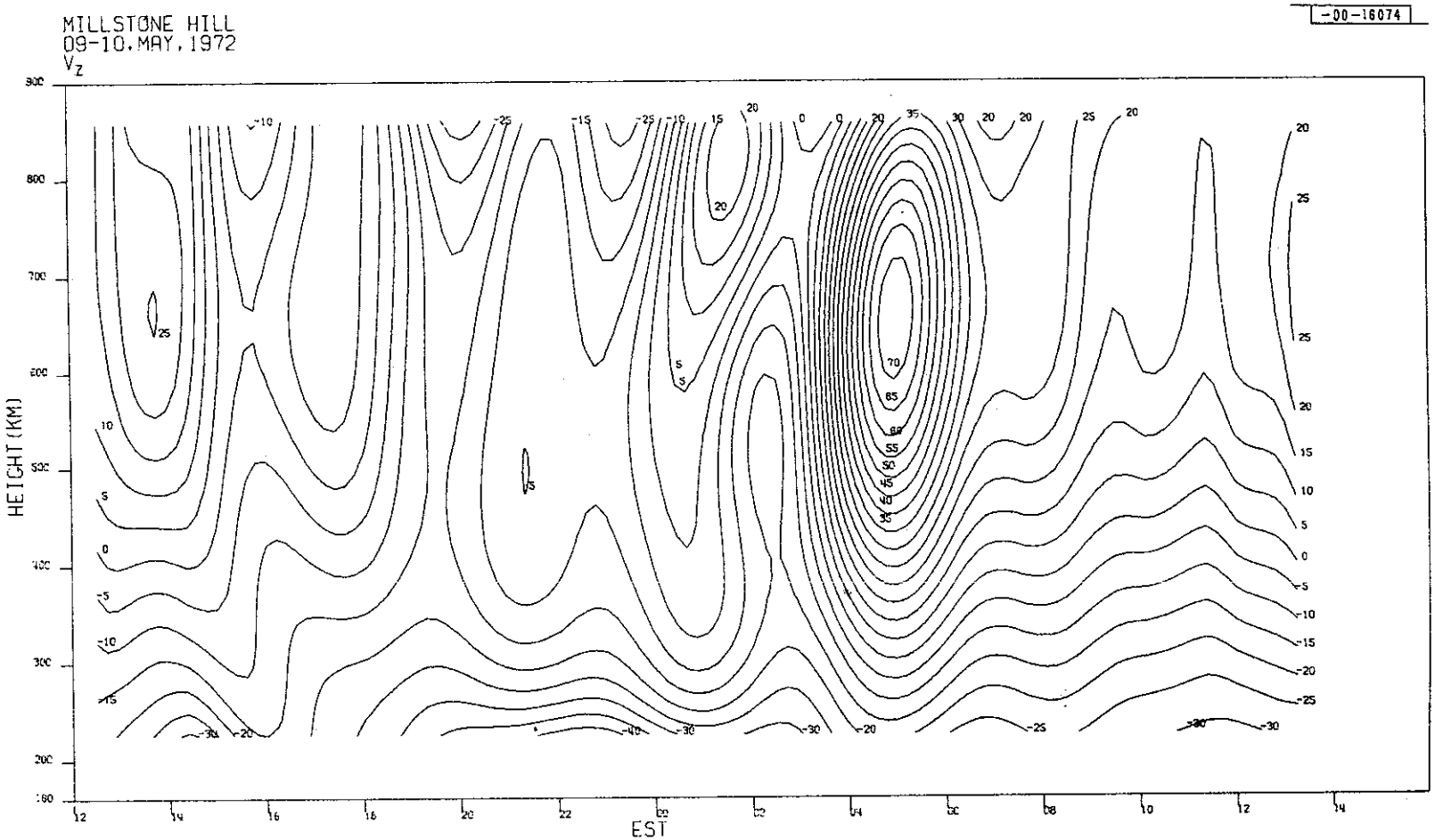

(d) V_z.

Fig.12(a-d). Continued.

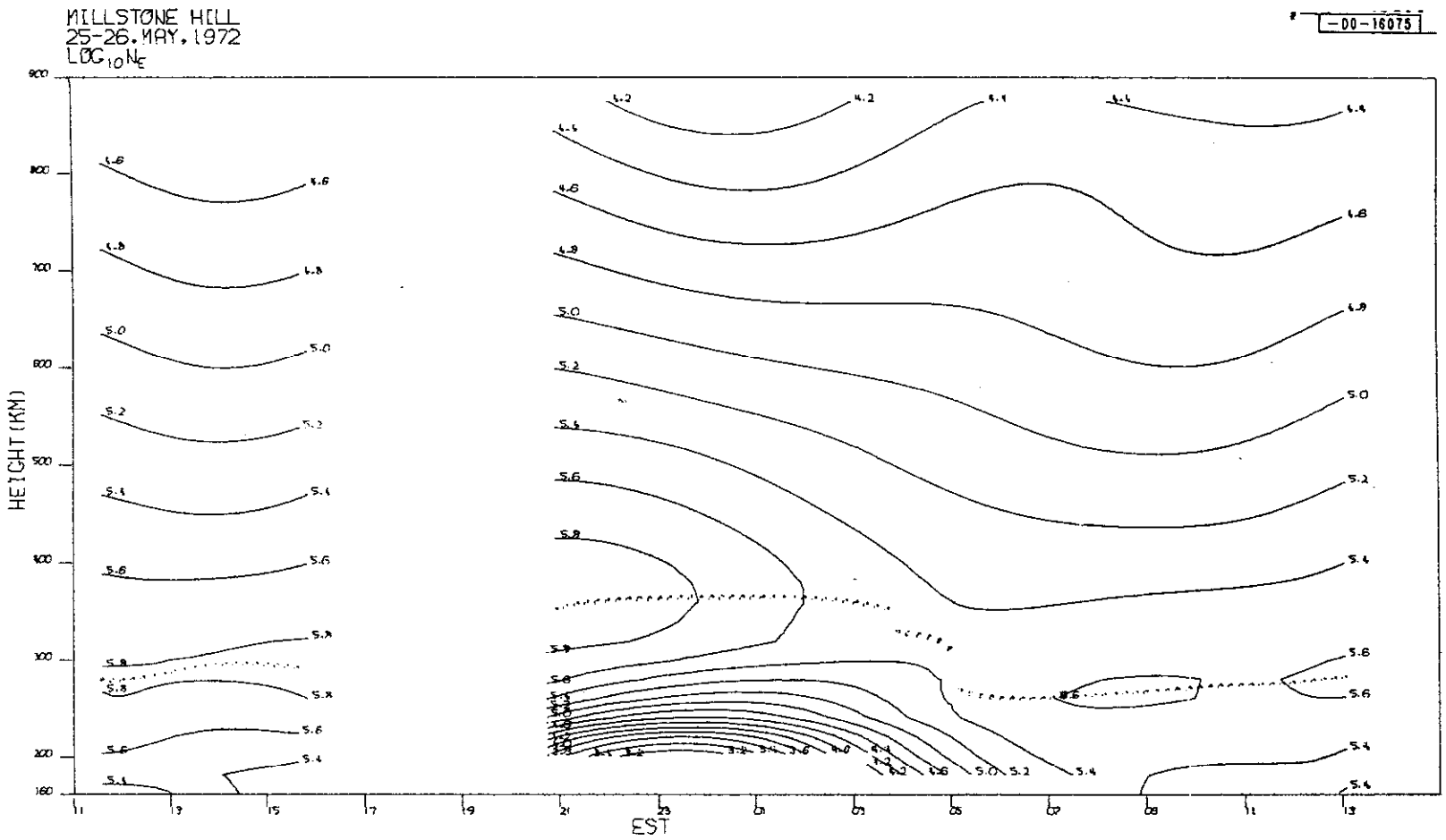

(a) $\text{Log}_{10} N_e$.

Fig.13(a-d). Results for 25-26 May 1972.

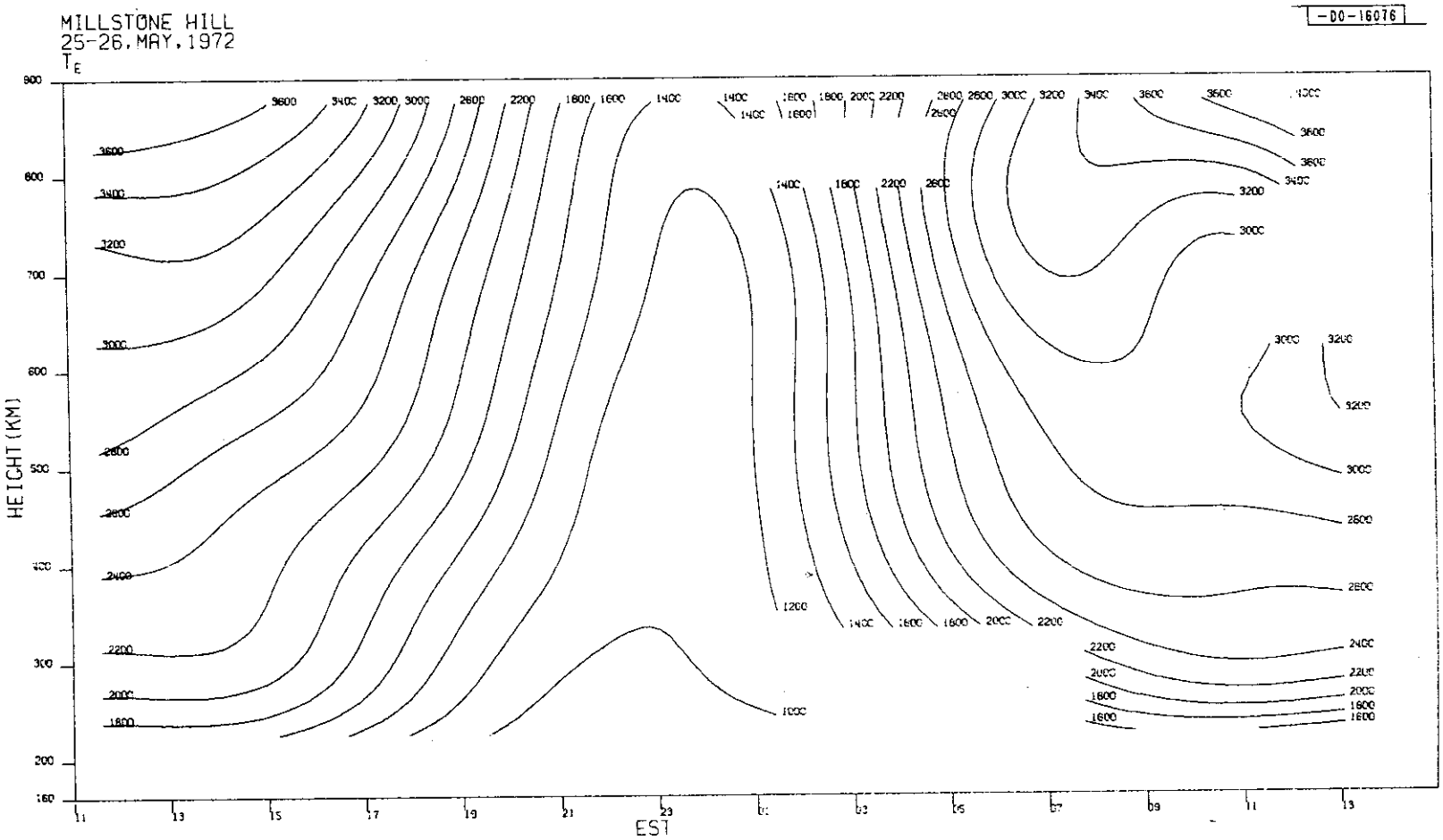

(b) T_e.

Fig. 13(a-d). Continued.

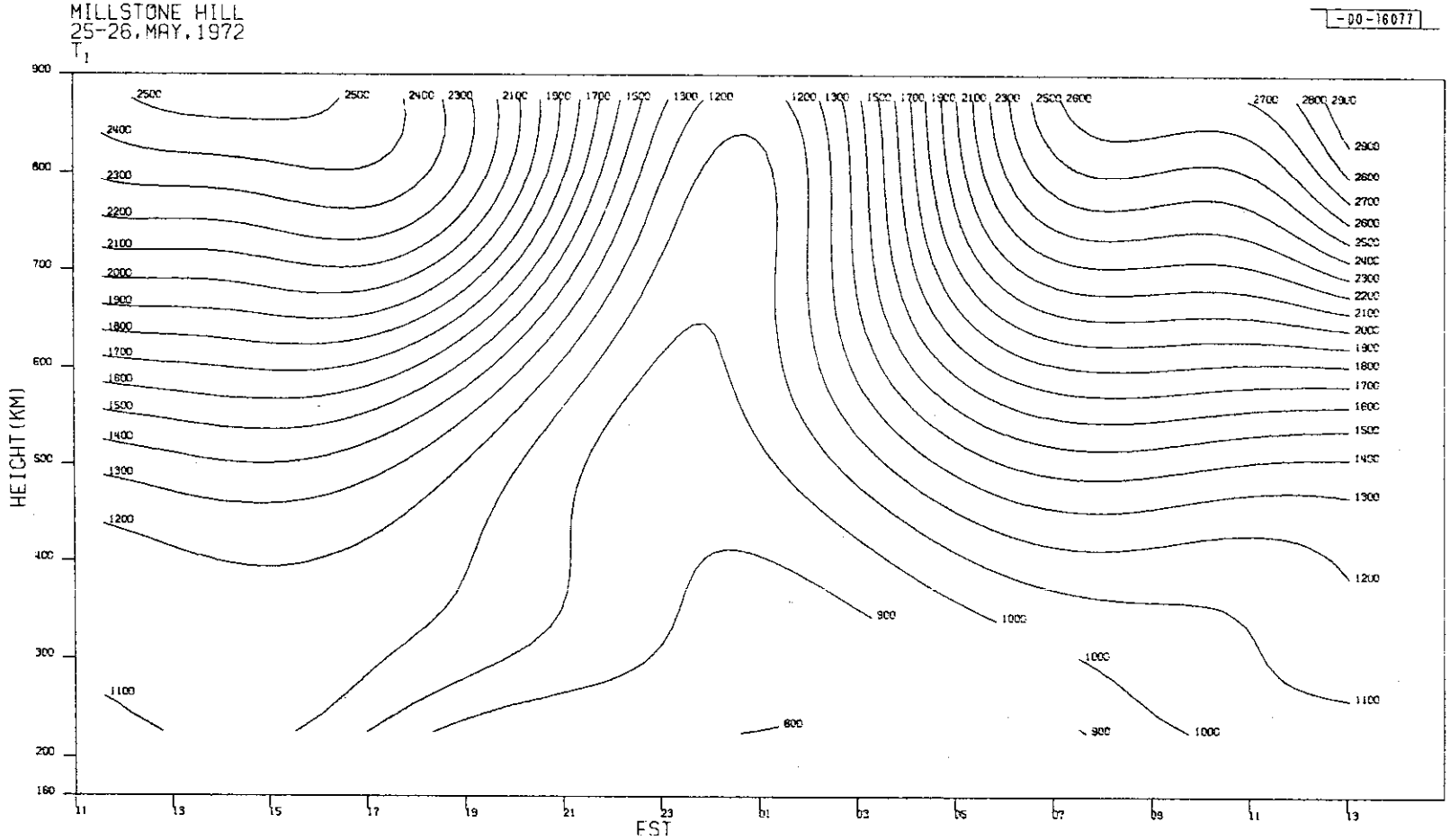

(c) T_i.

Fig. 13(a-d). Continued.

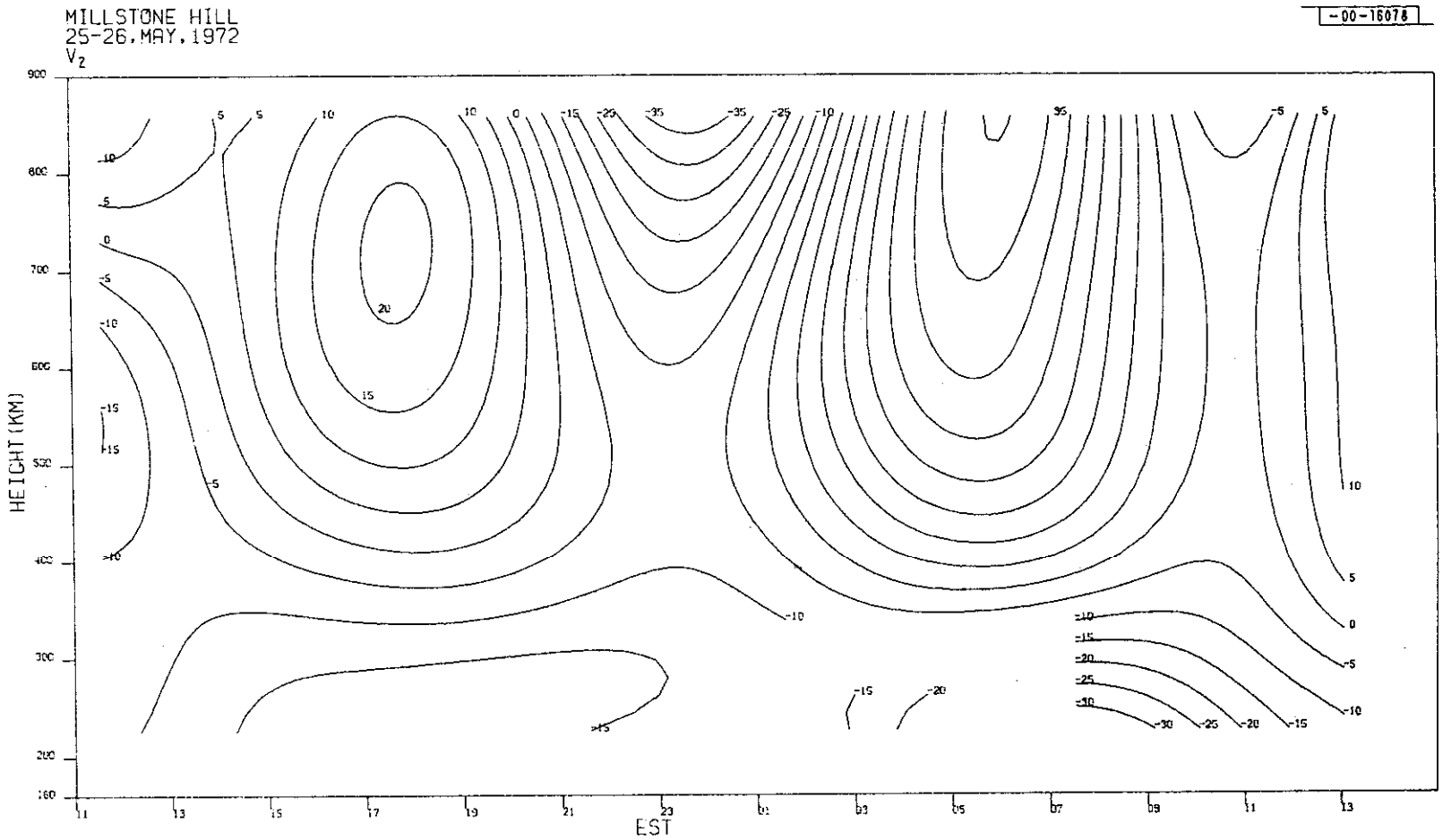

(d) V_z.

Fig. 13(a-d). Continued.

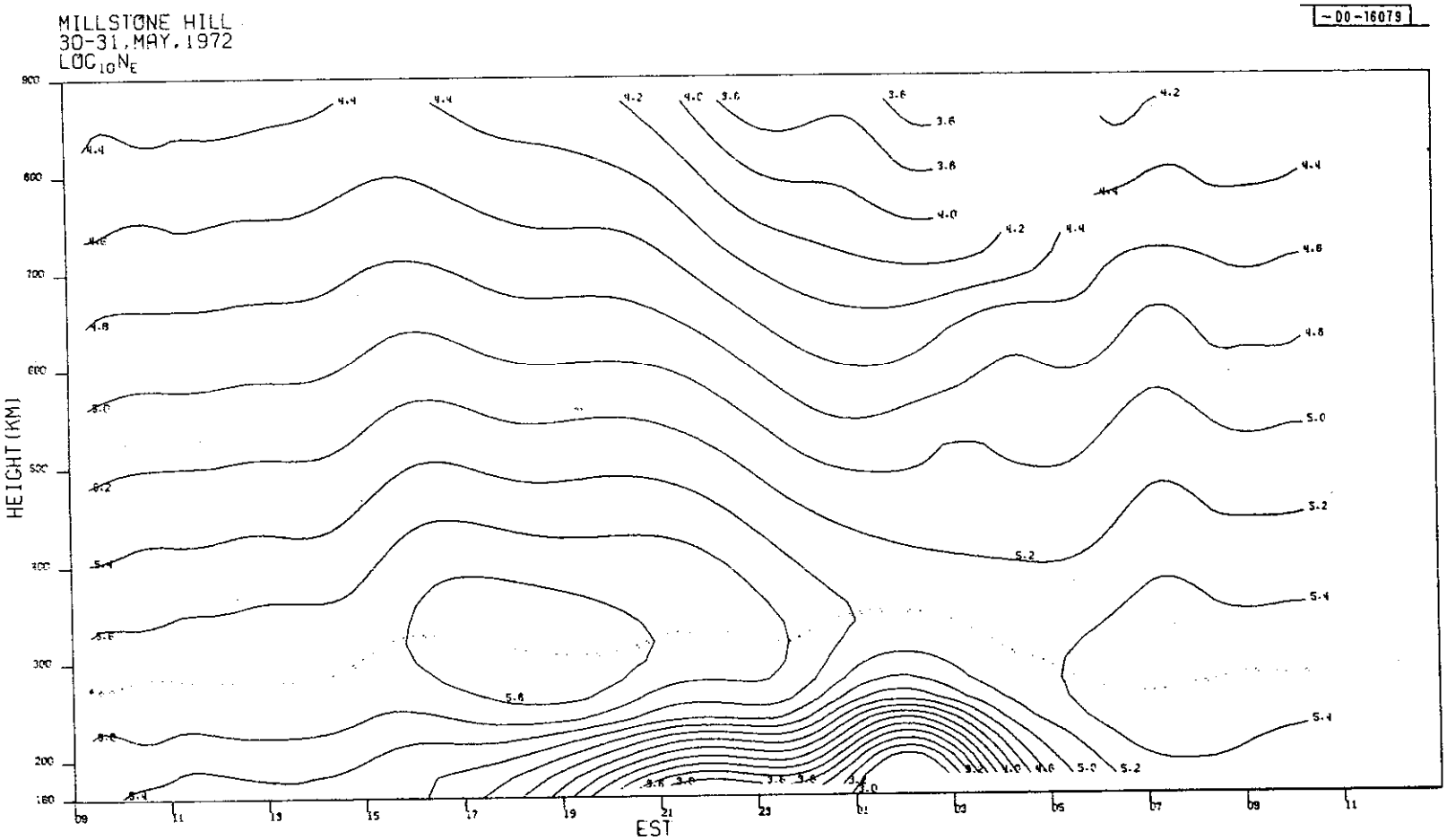

(a) $Log_{10} N_e$.

Fig.14(a-d). Results for 30-31 May 1972.

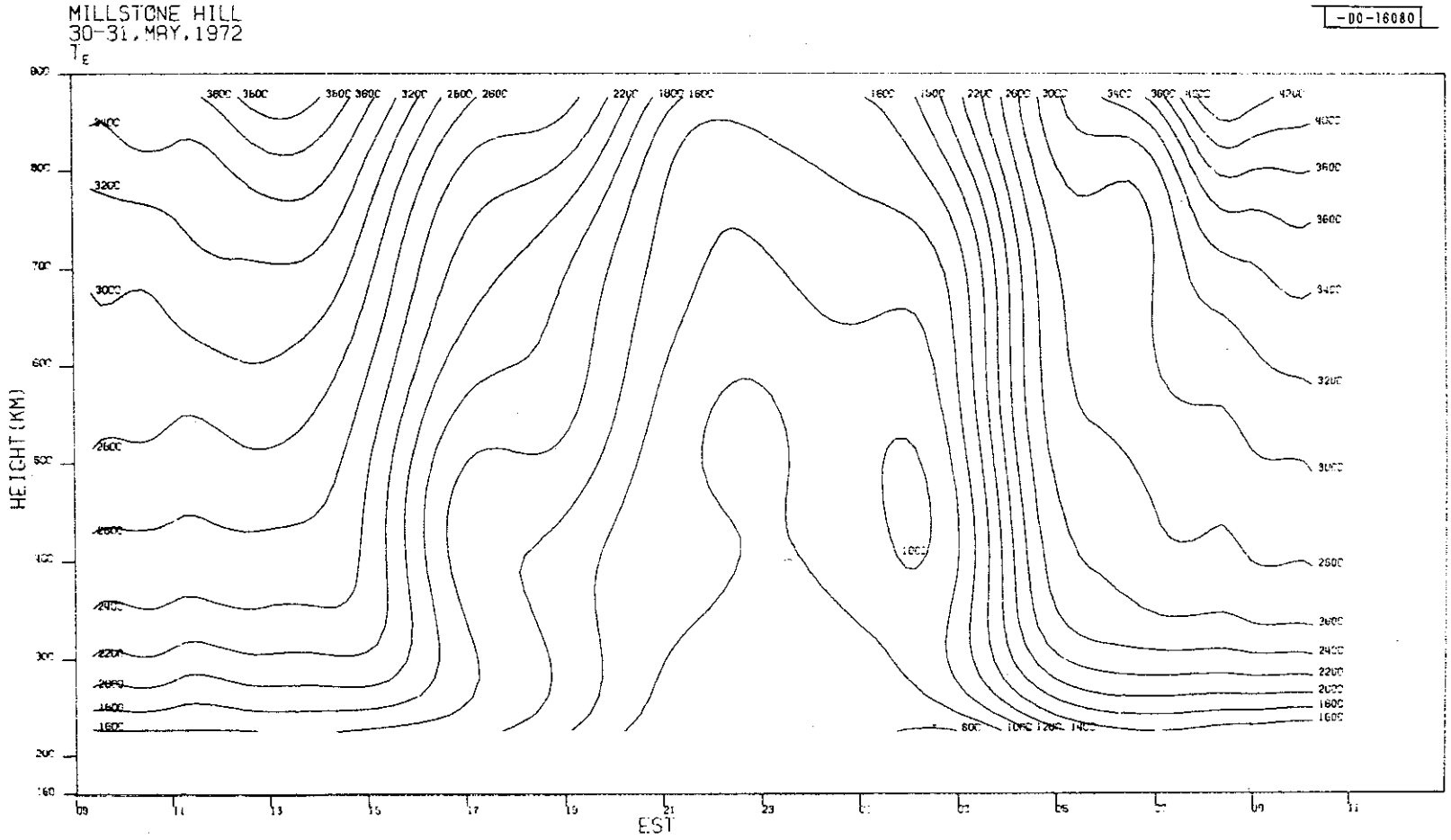

(b) T_e.

Fig.14(a-d). Continued.

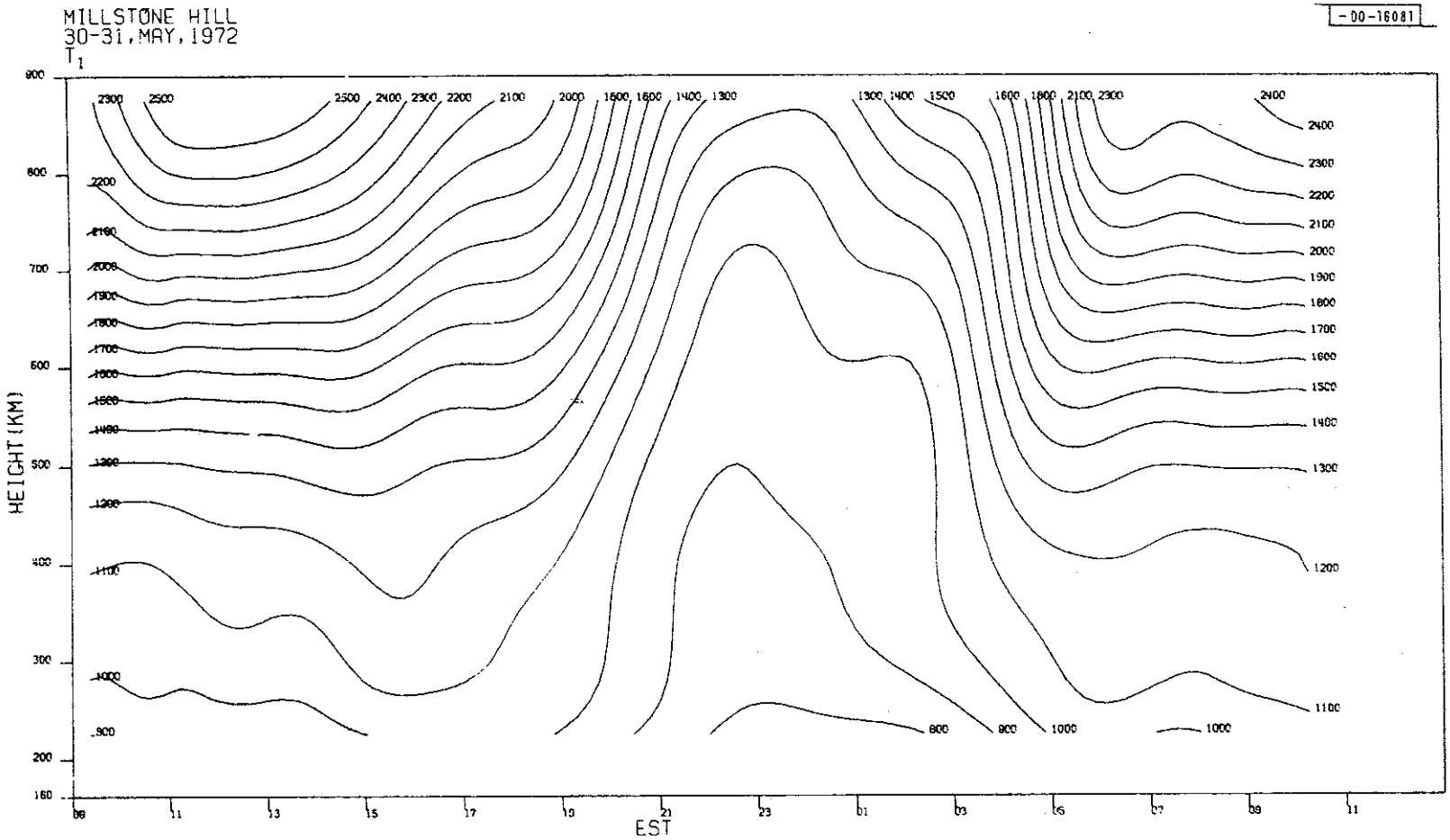

(c) T_i.

Fig.14(a-d). Continued.

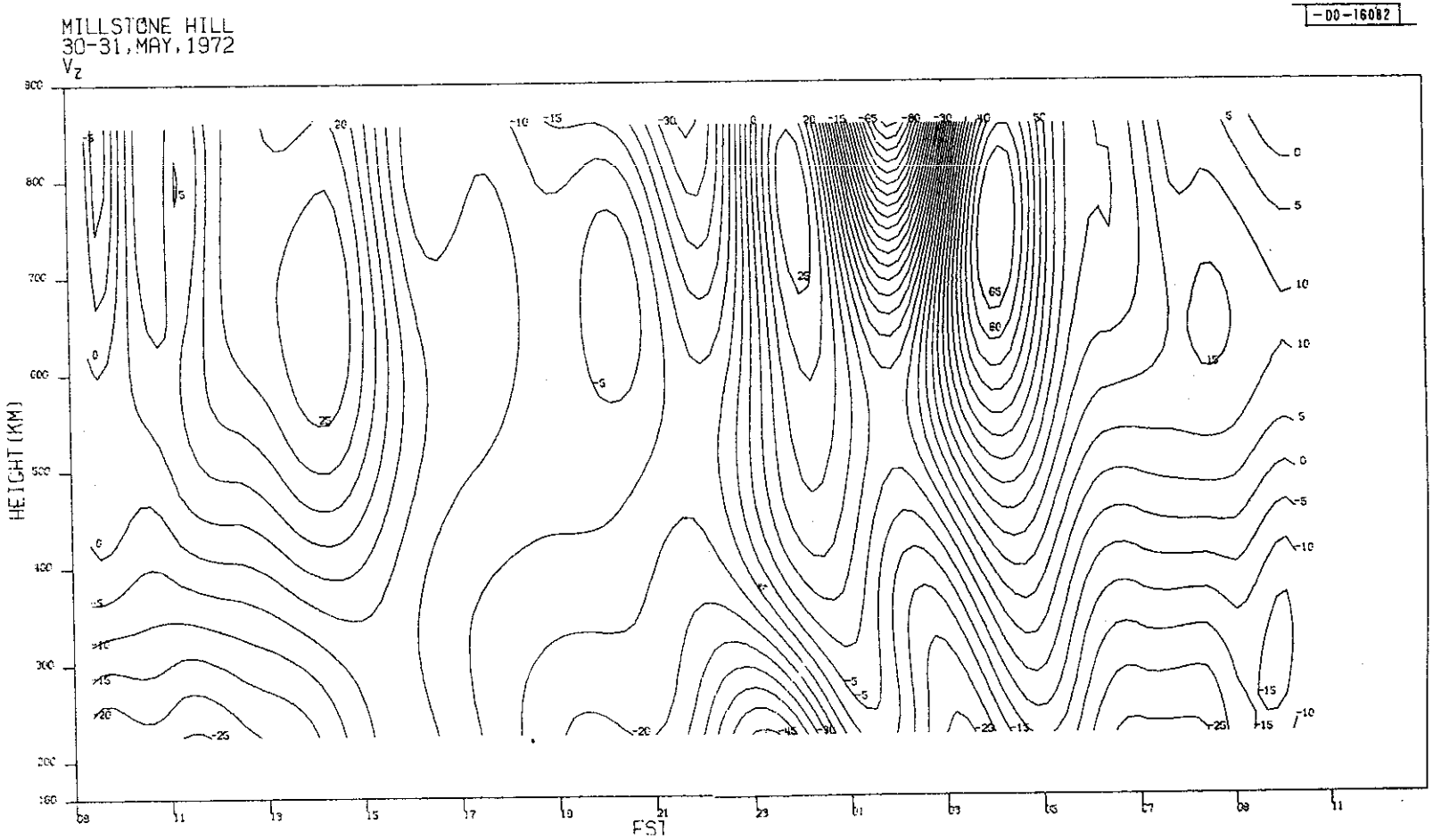

(d) V_z.

Fig.14(a-d). Continued.

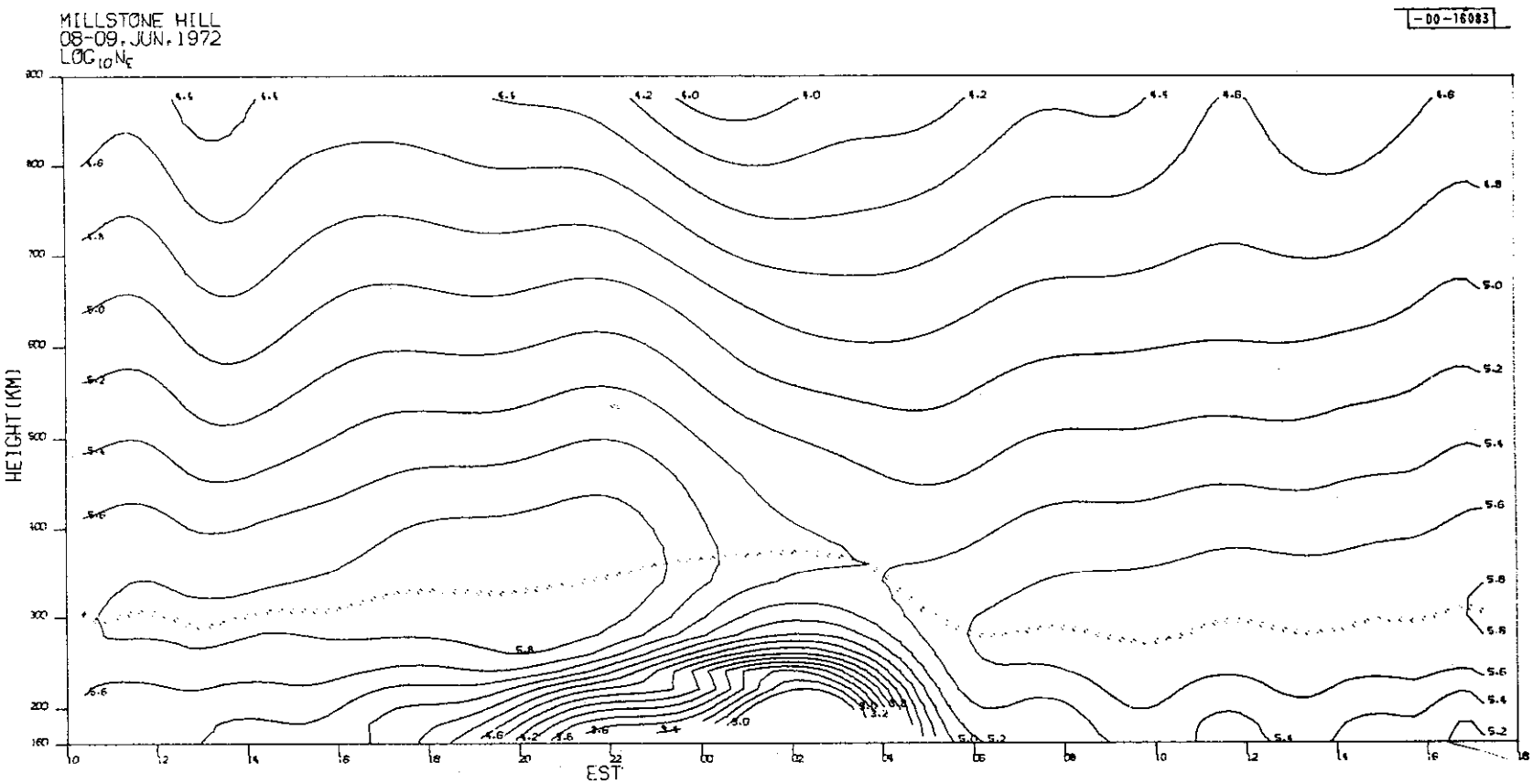

(a) $\text{Log}_{10} N_e$.

Fig. 15(a-d). Results for 8-9 June 1972.

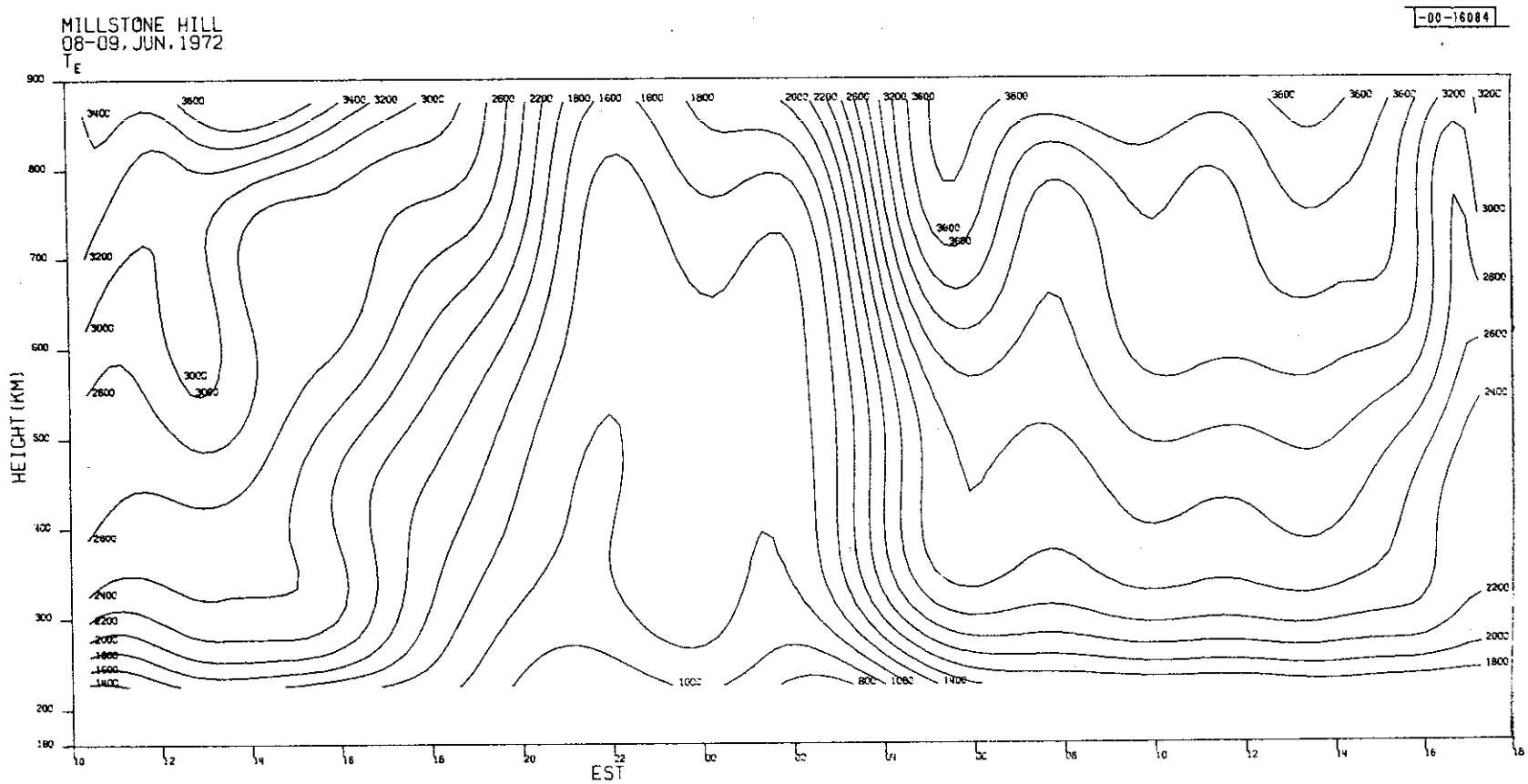

(b) T_e.

Fig. 15(a-d). Continued.

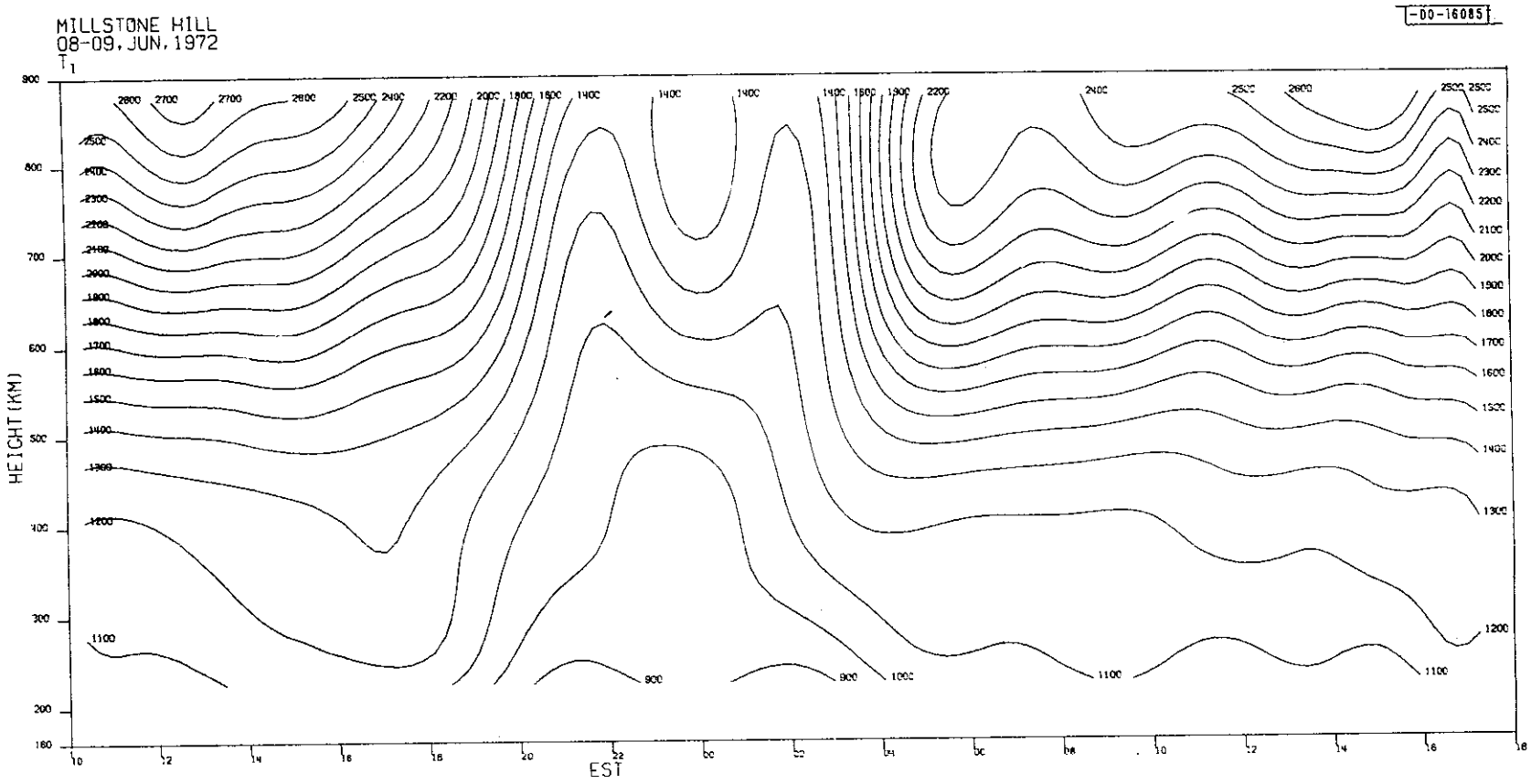

(c) T_i.

Fig. 15(a-d). Continued.

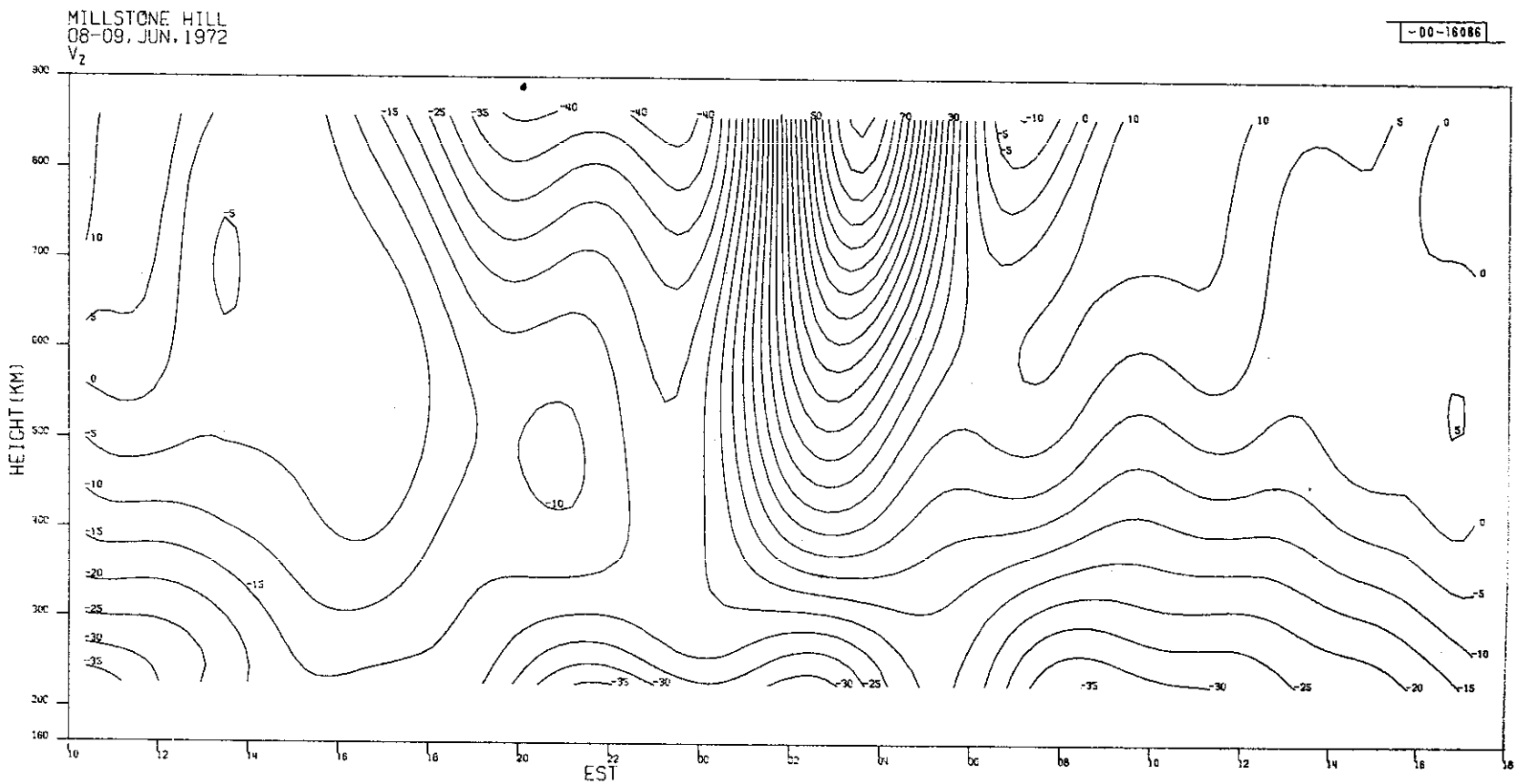

(d) V_z.

Fig. 15(a-d). Continued.

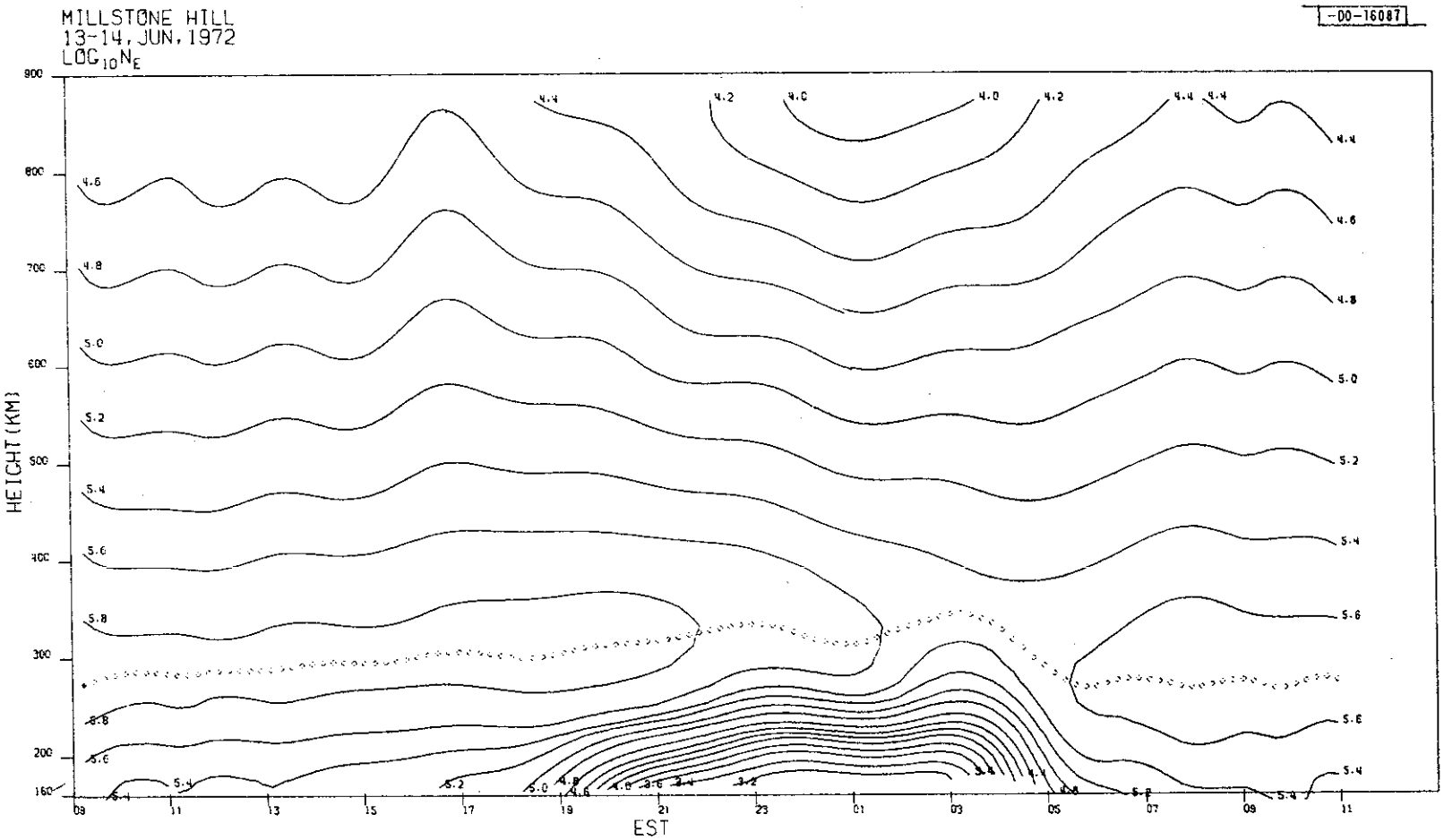

(a) $Log_{10} N_e$.

Fig. 16(a-d). Results for 13-14 June 1972.

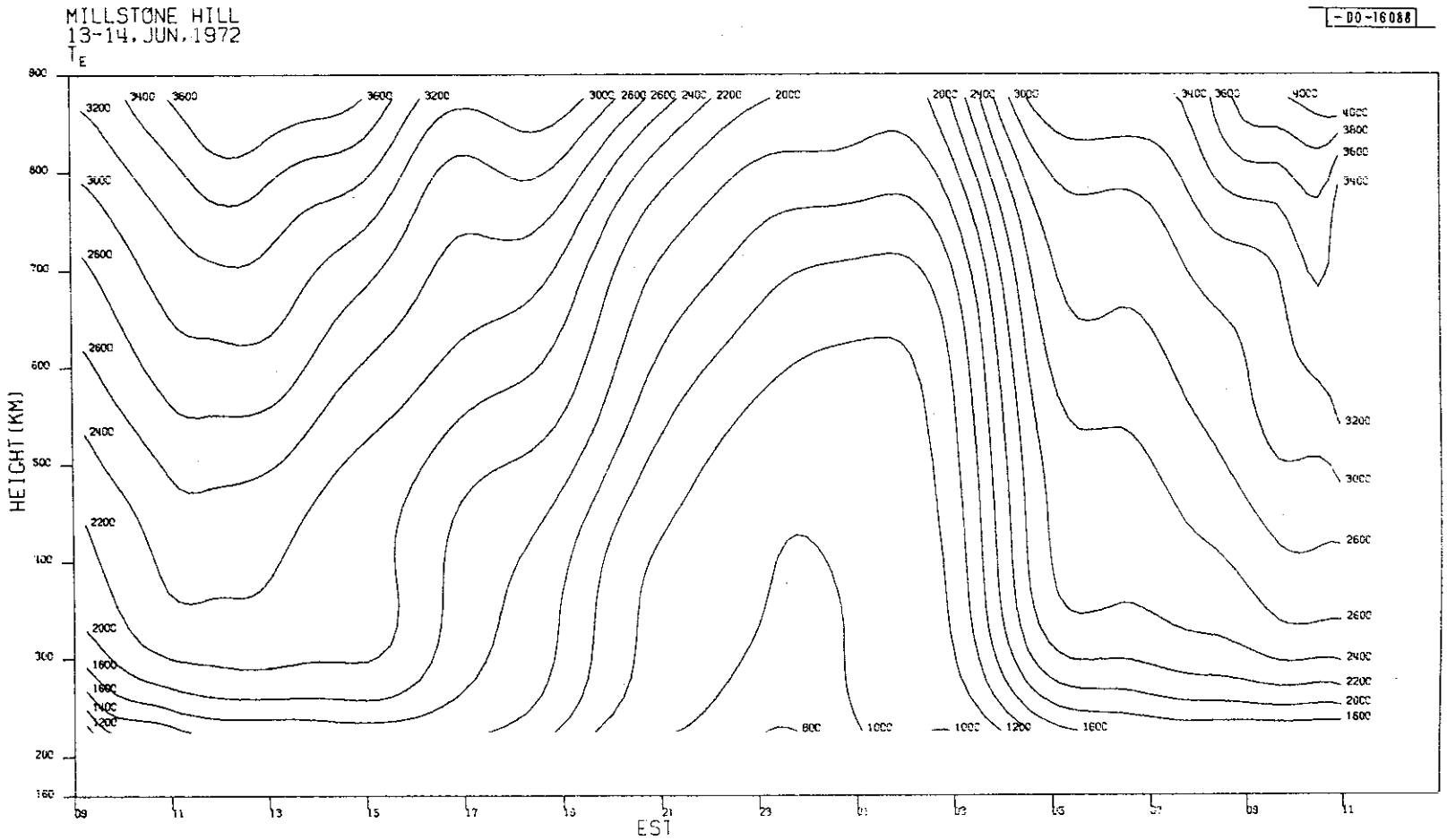

(b) T_e.

Fig.16(a-d). Continued.

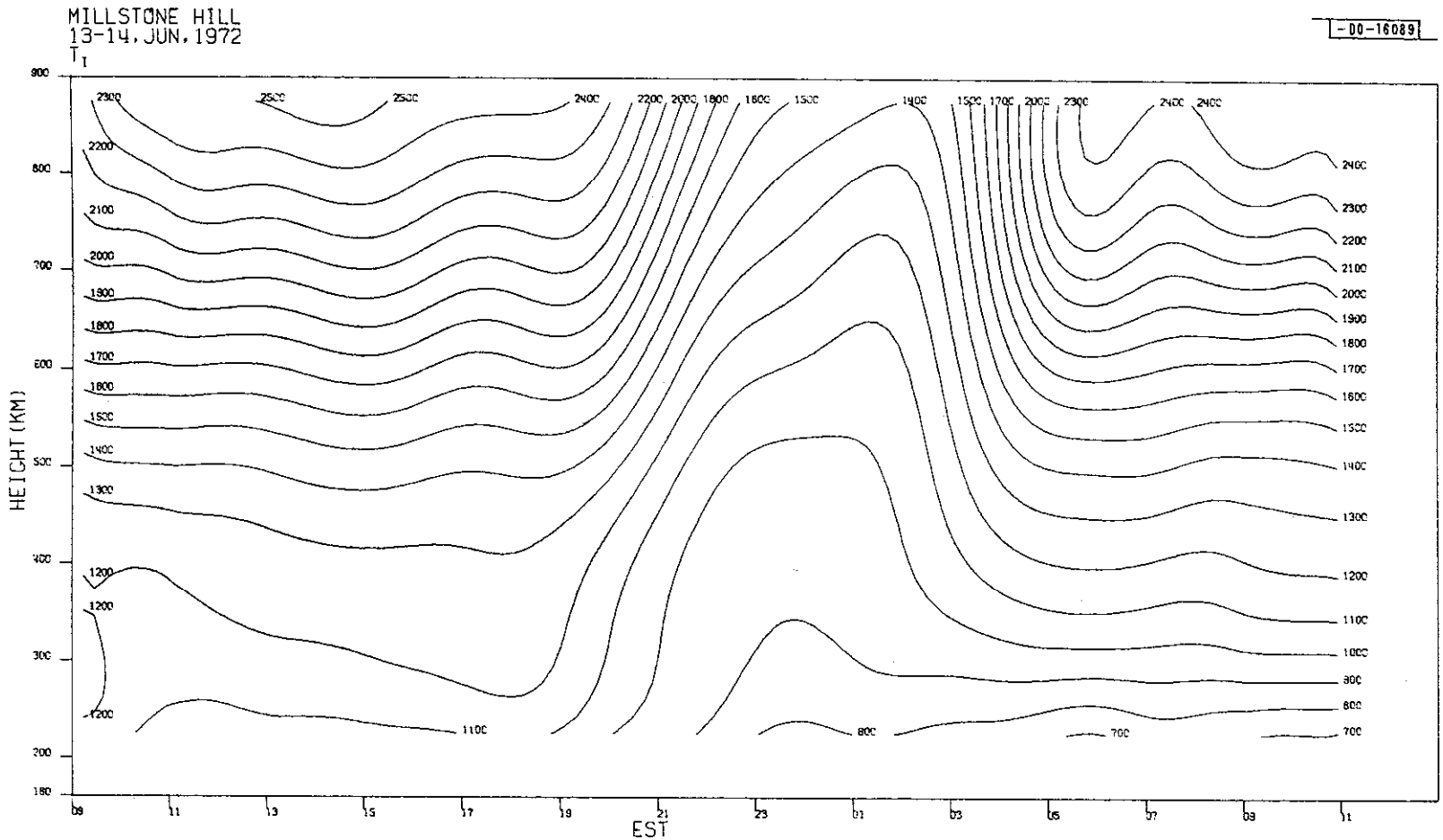

(c) T_i.

Fig. 16(a-d). Continued.

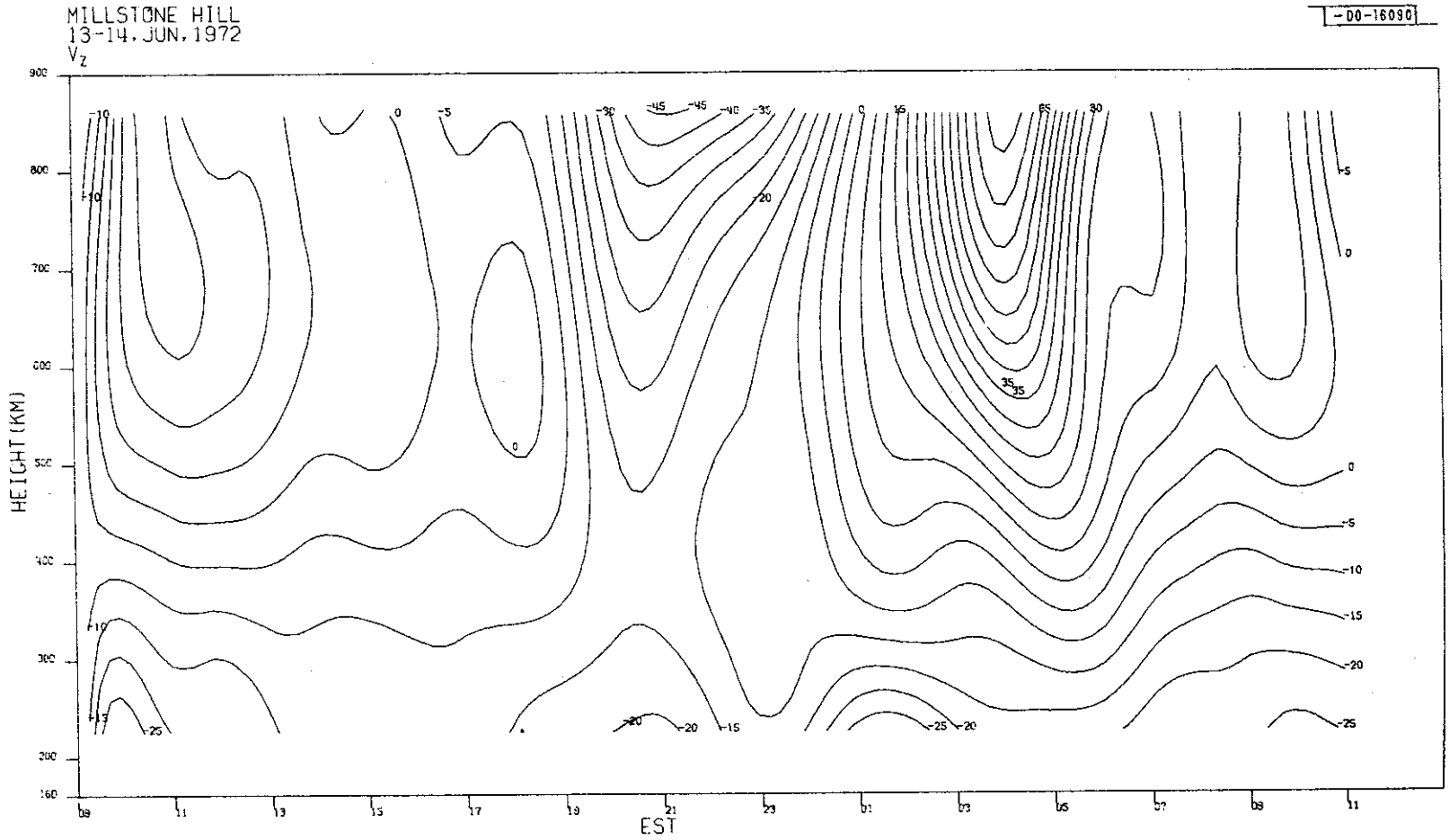

(d) V_z.

Fig.16(a-d). Continued.

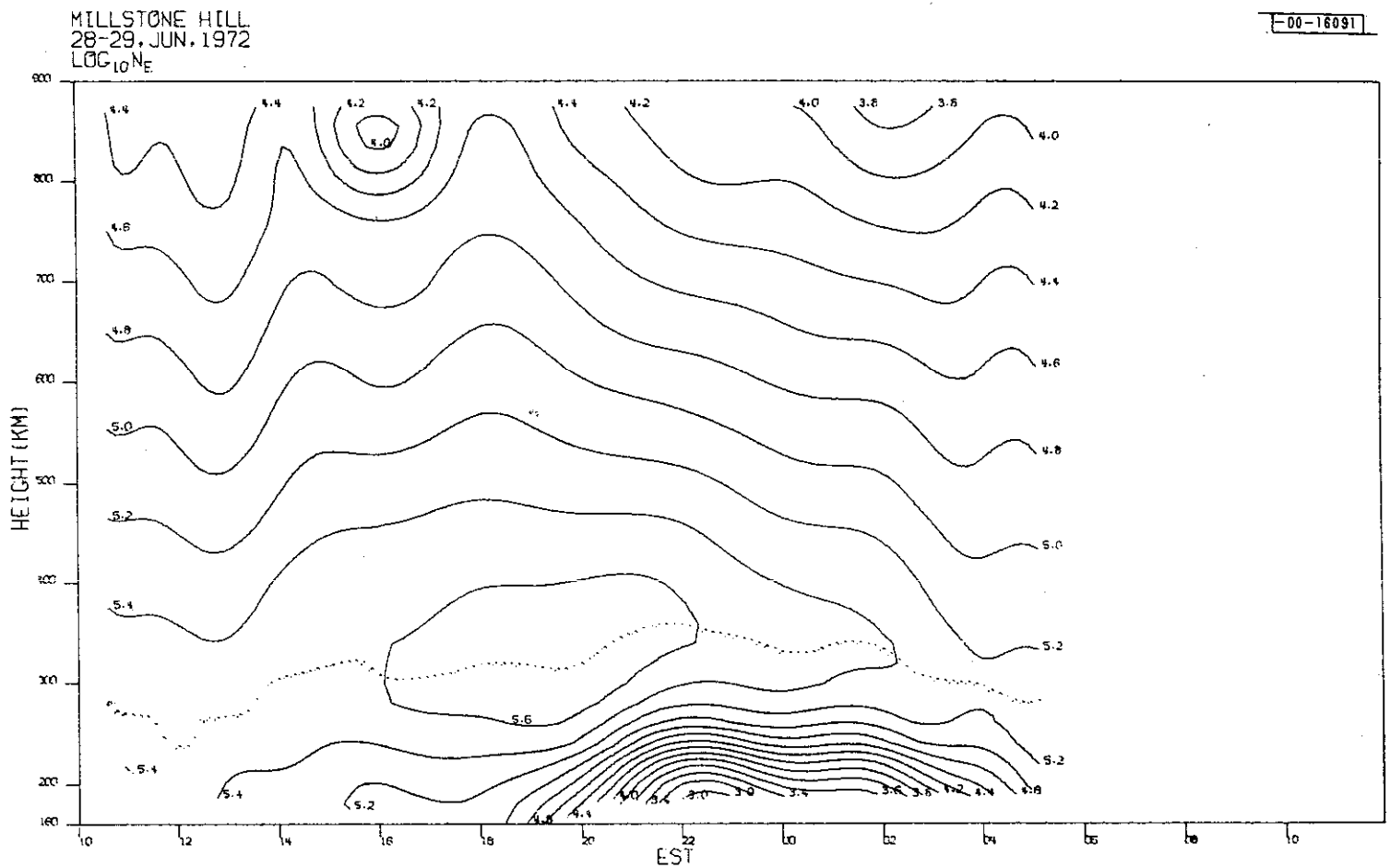

(a) $Log_{10} N_e$.

Fig. 17(a-d). Results for 28-29 June 1972.

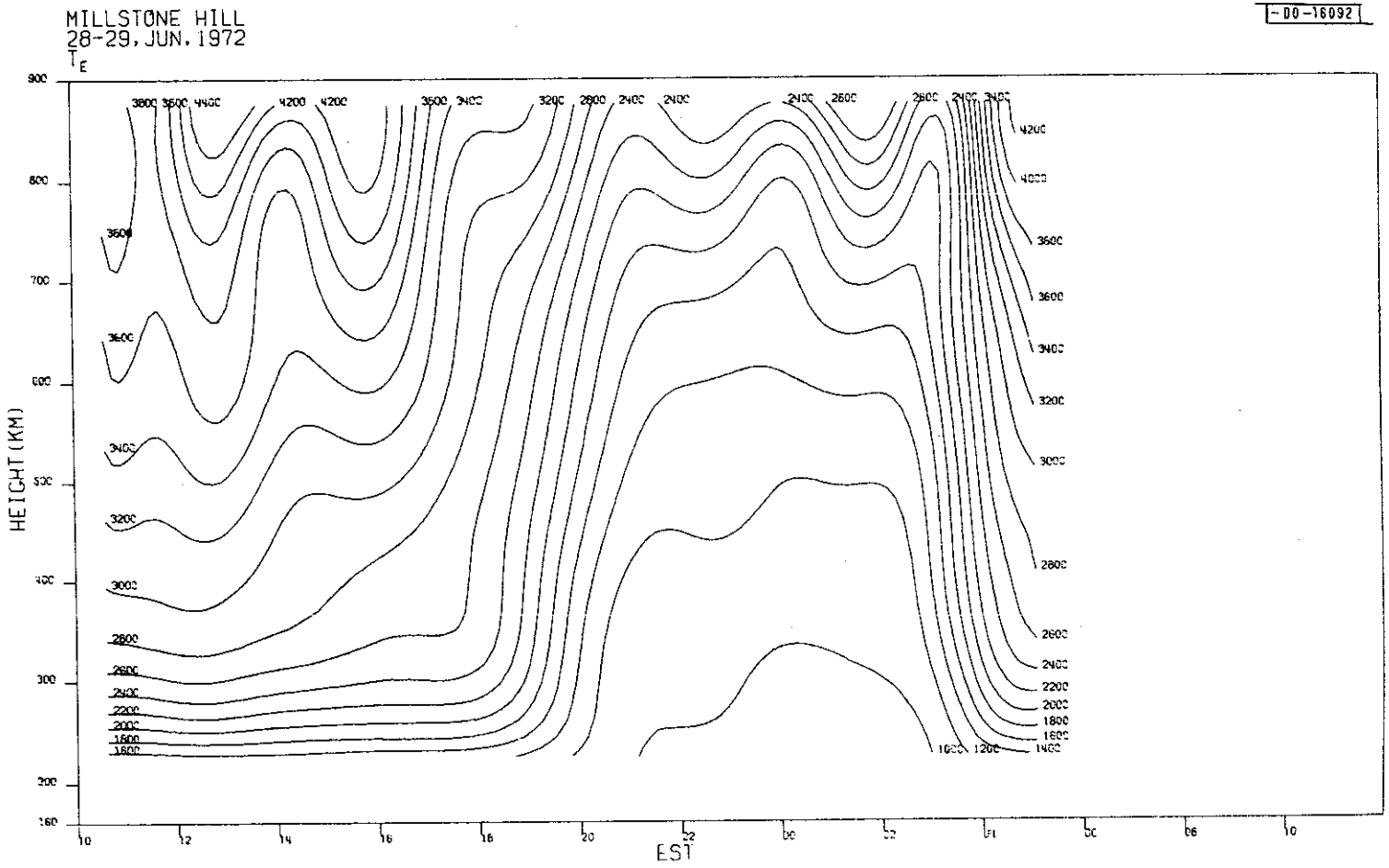

(b) T_e.

Fig. 17(a-d). Continued.

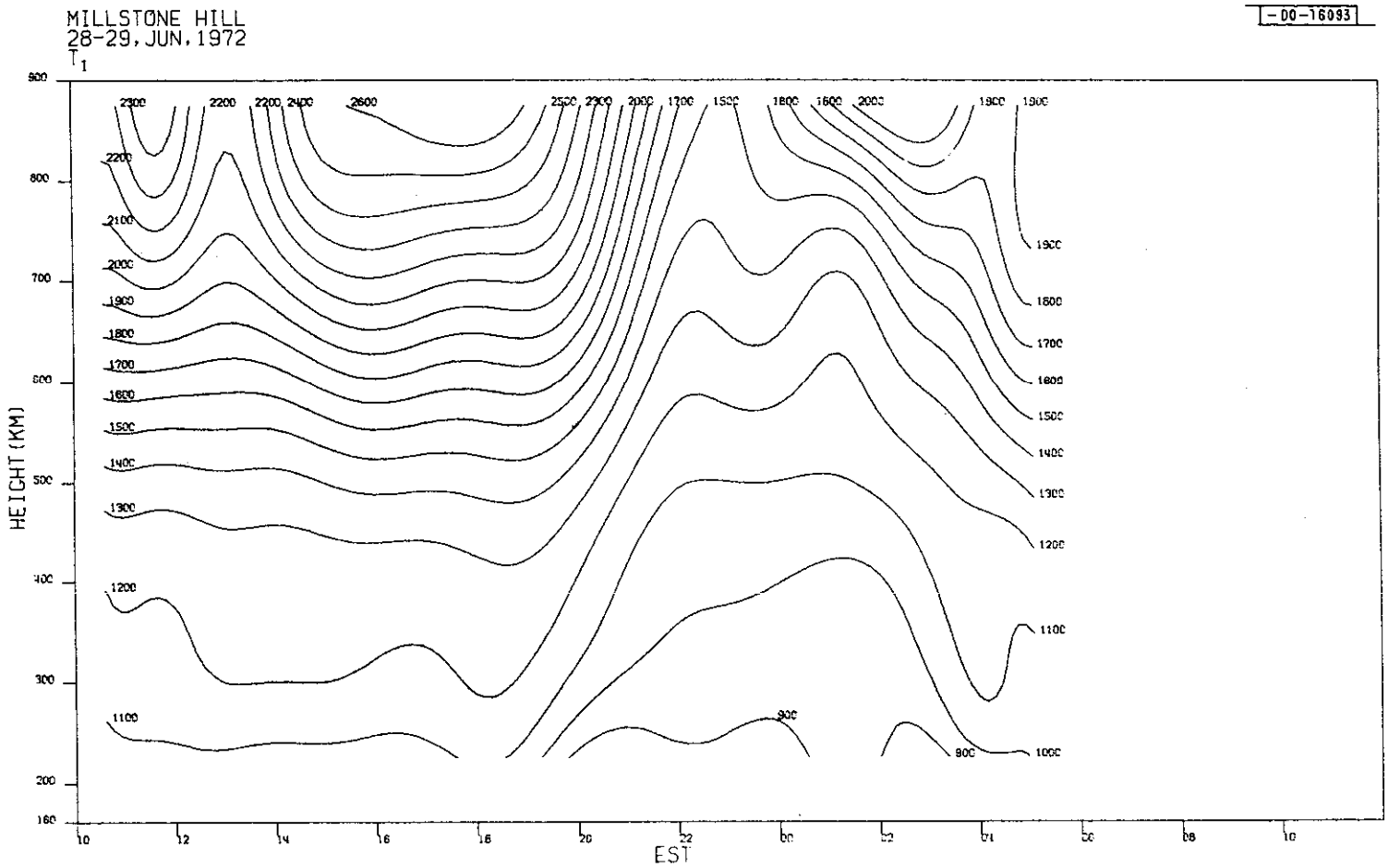

(c) T_i.

Fig. 17(a-d). Continued.

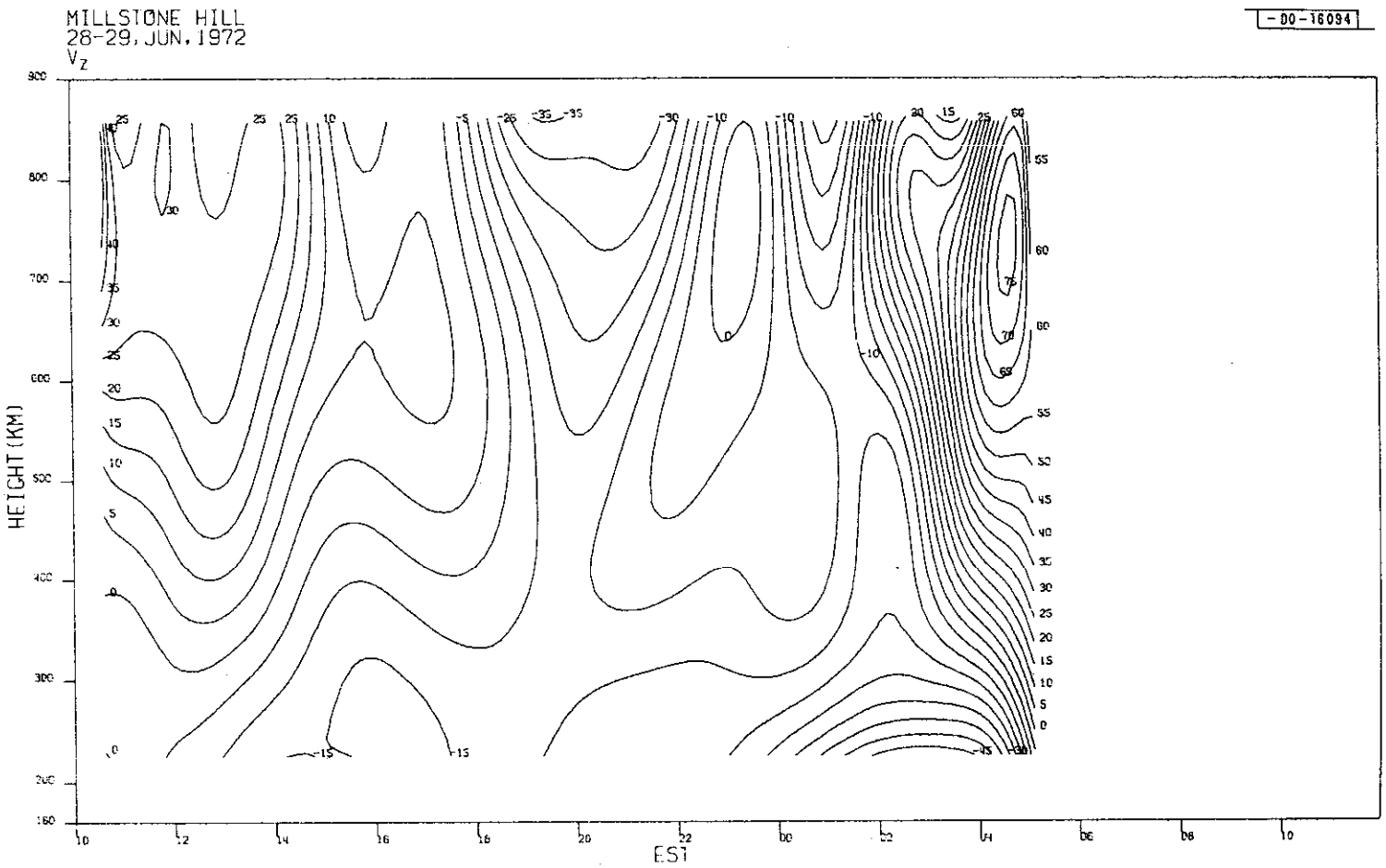

(d) V_z.

Fig. 17(a-d). Continued.

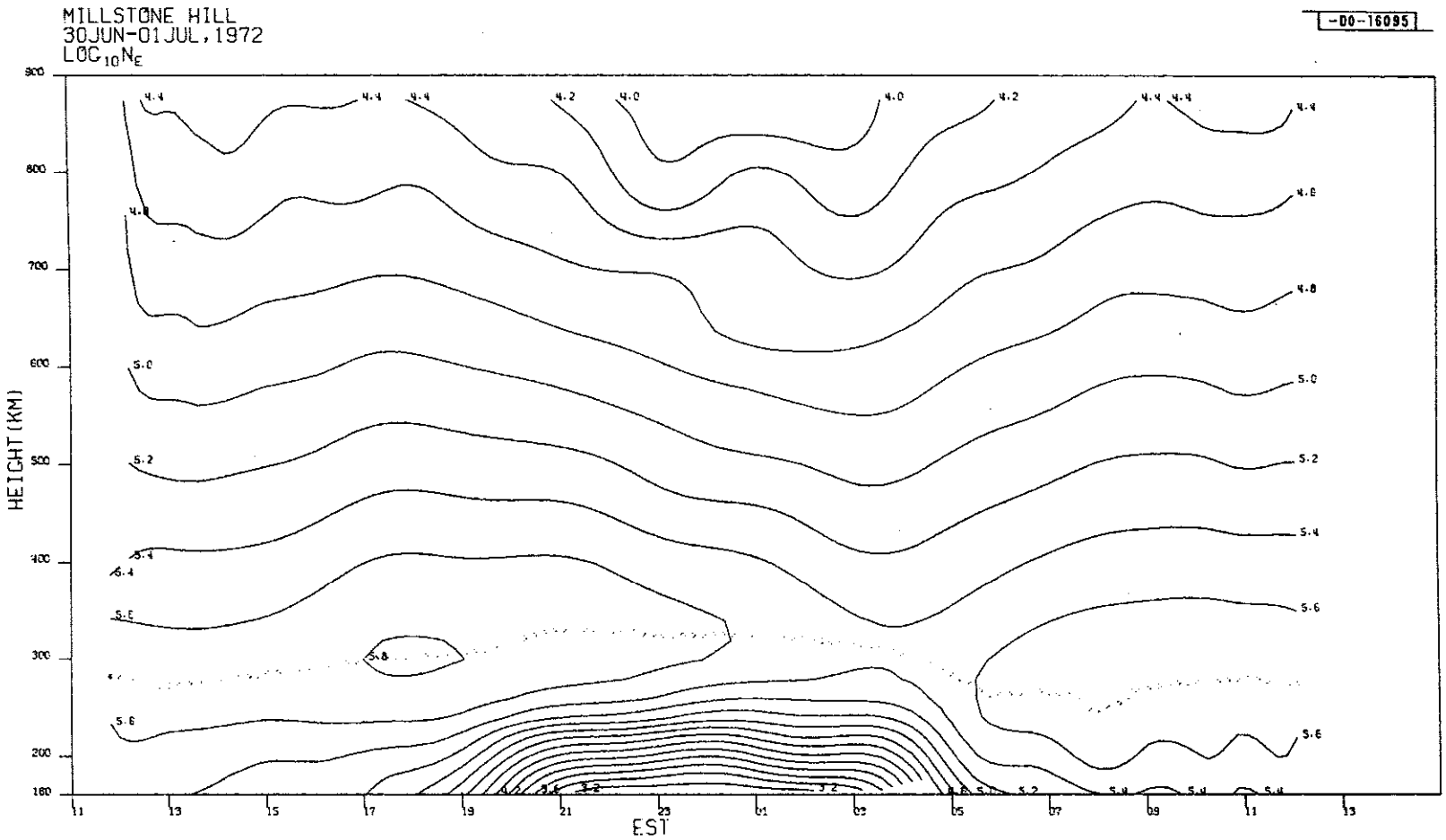

(a) $\text{Log}_{10} N_e$.

Fig.18(a-d). Results for 30 June – 1 July 1972.

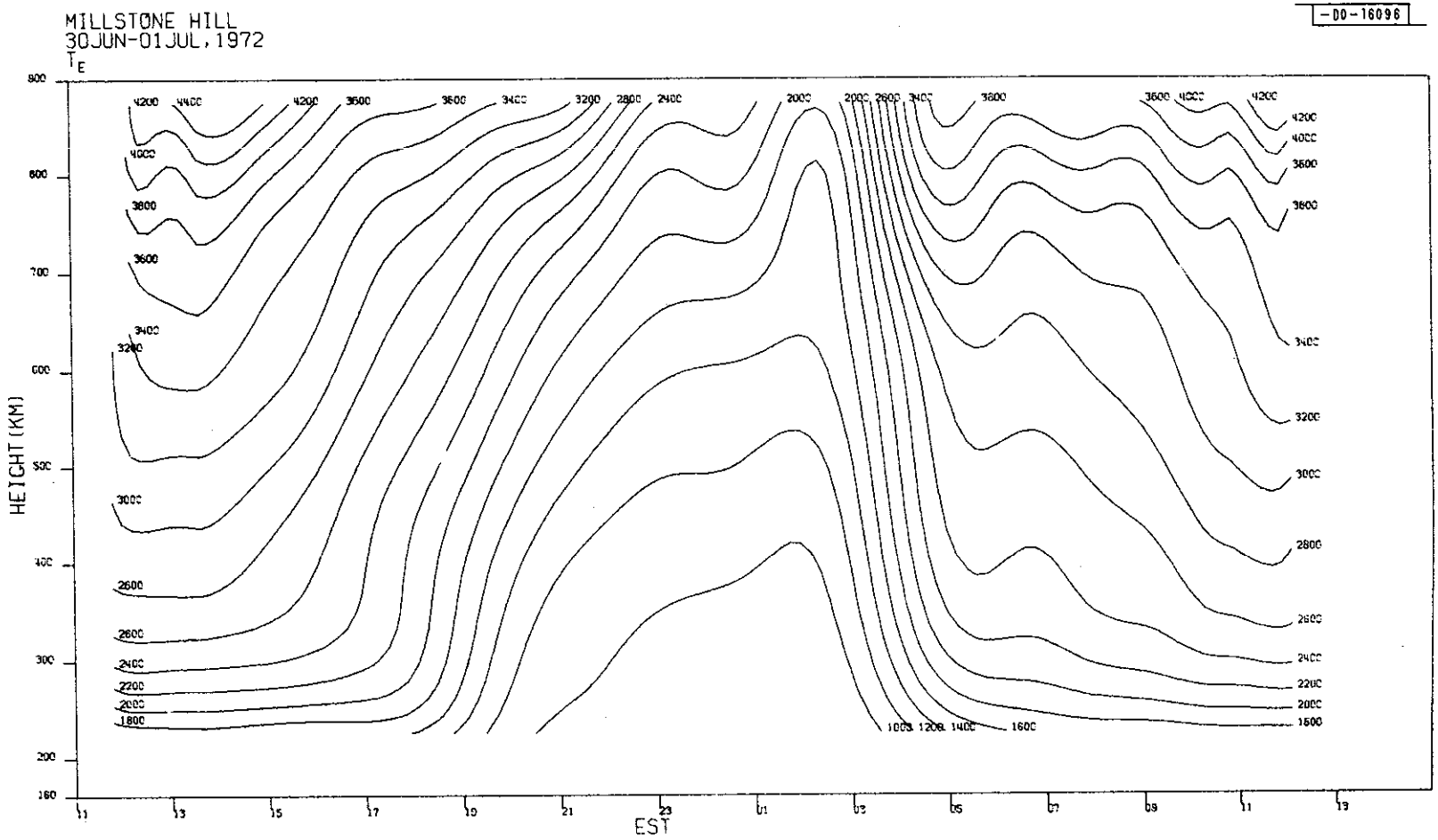

(b) T_e.

Fig. 18(a-d). Continued.

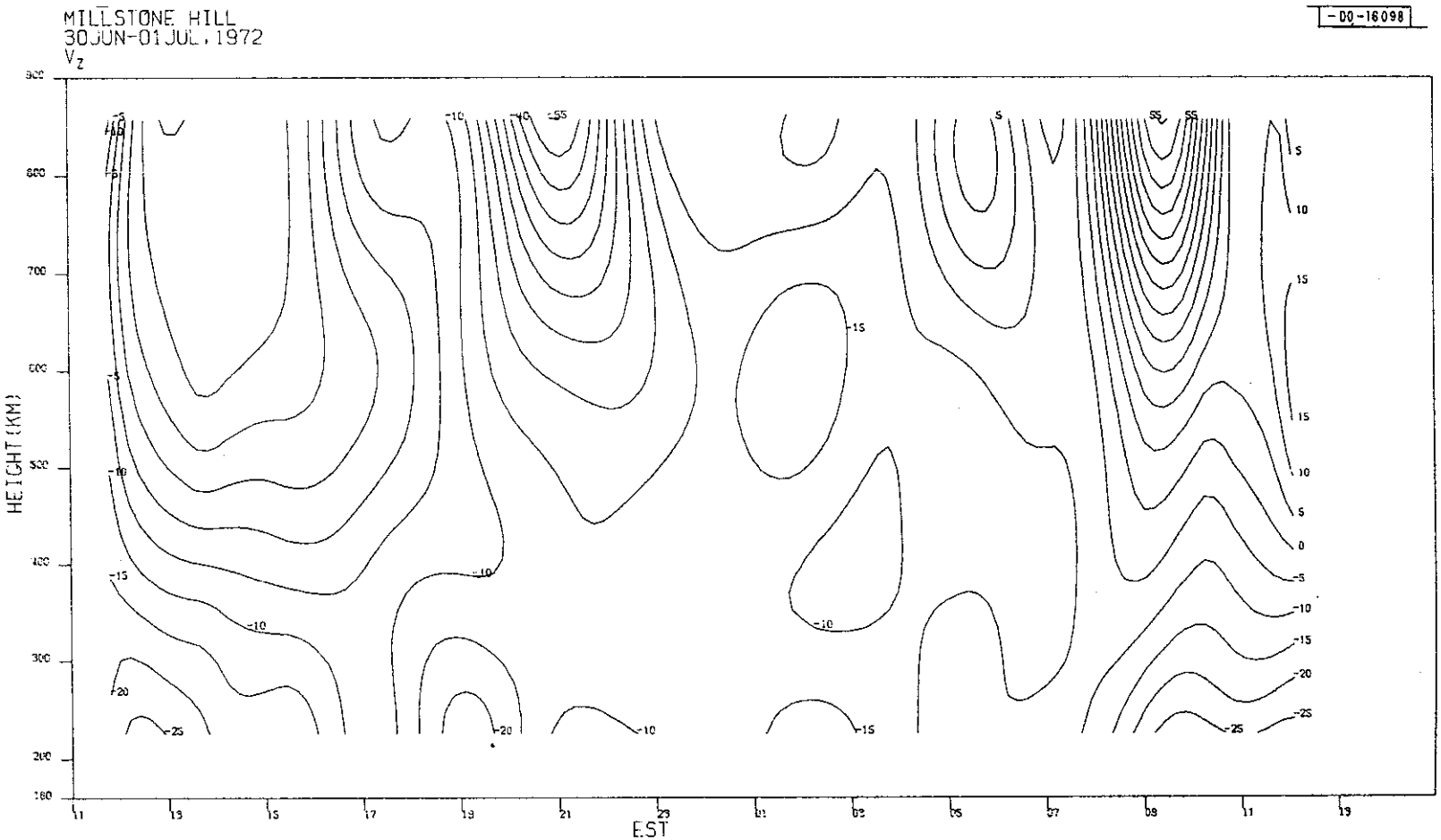

(d) V_z.

Fig.18(a-d). Continued.

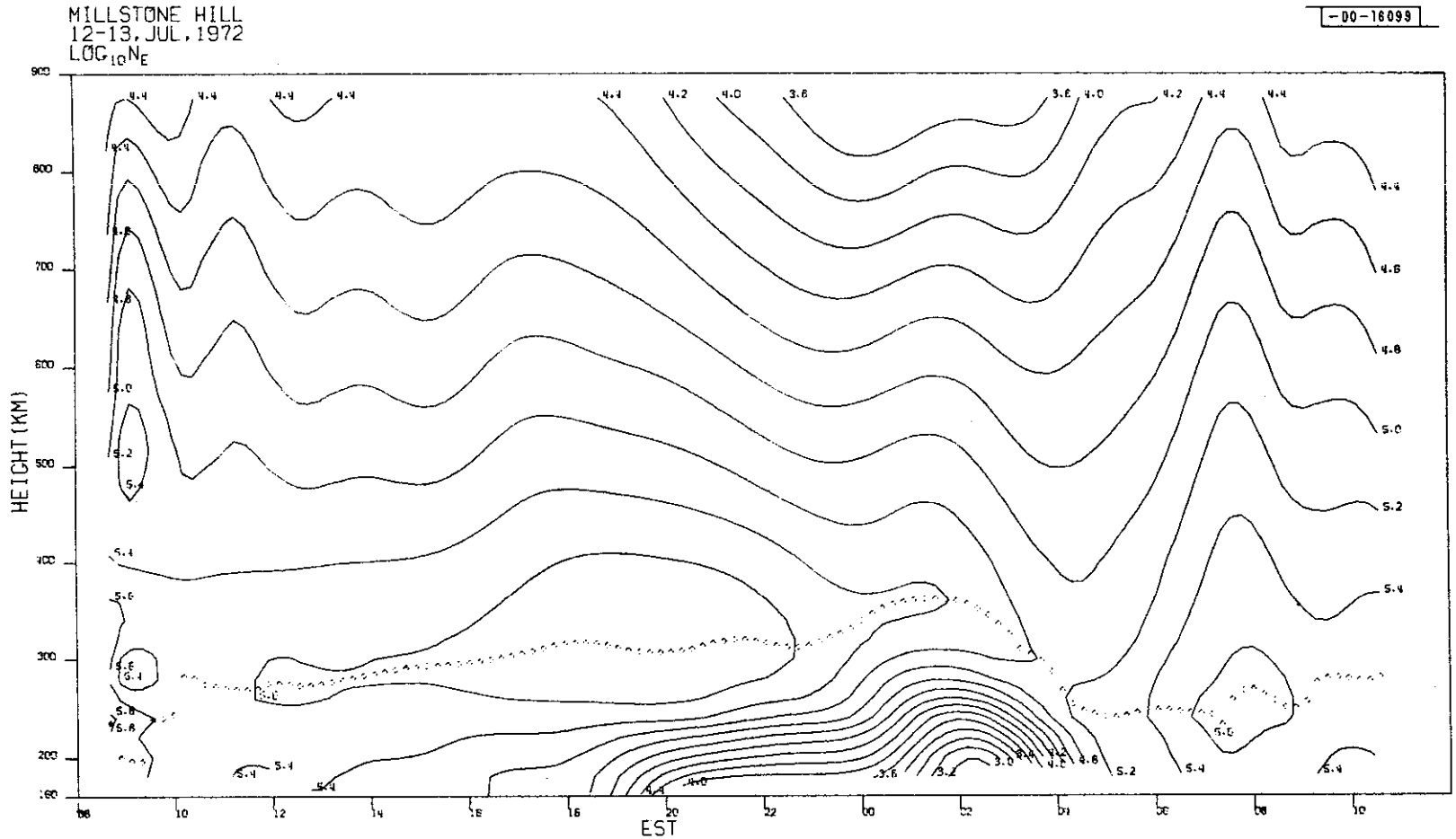

(a) $Log_{10} N_e$.

Fig. 19(a-c). Results for 12-13 July 1972.

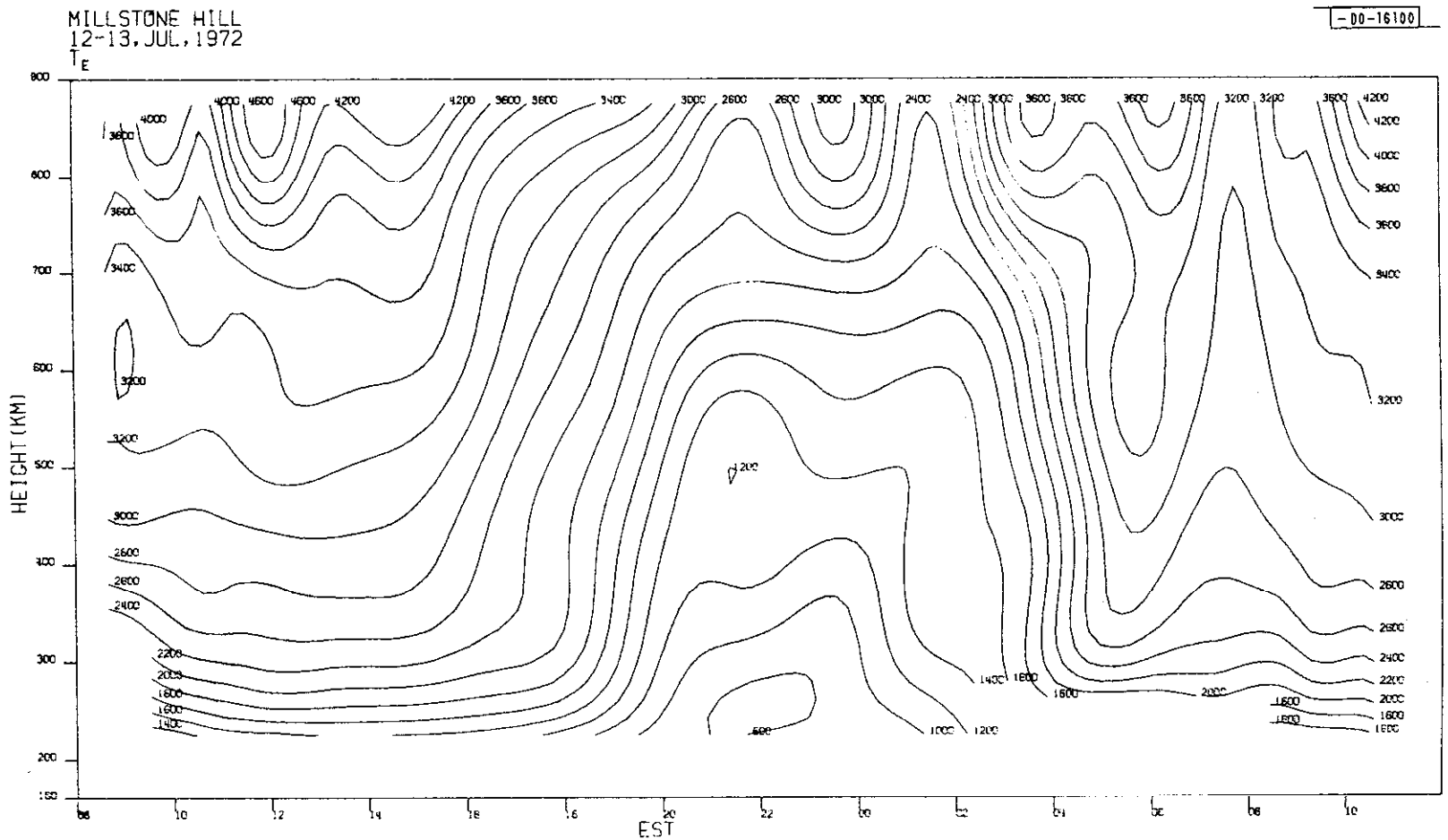

(b) T_e.

Fig. 19(a-c). Continued.

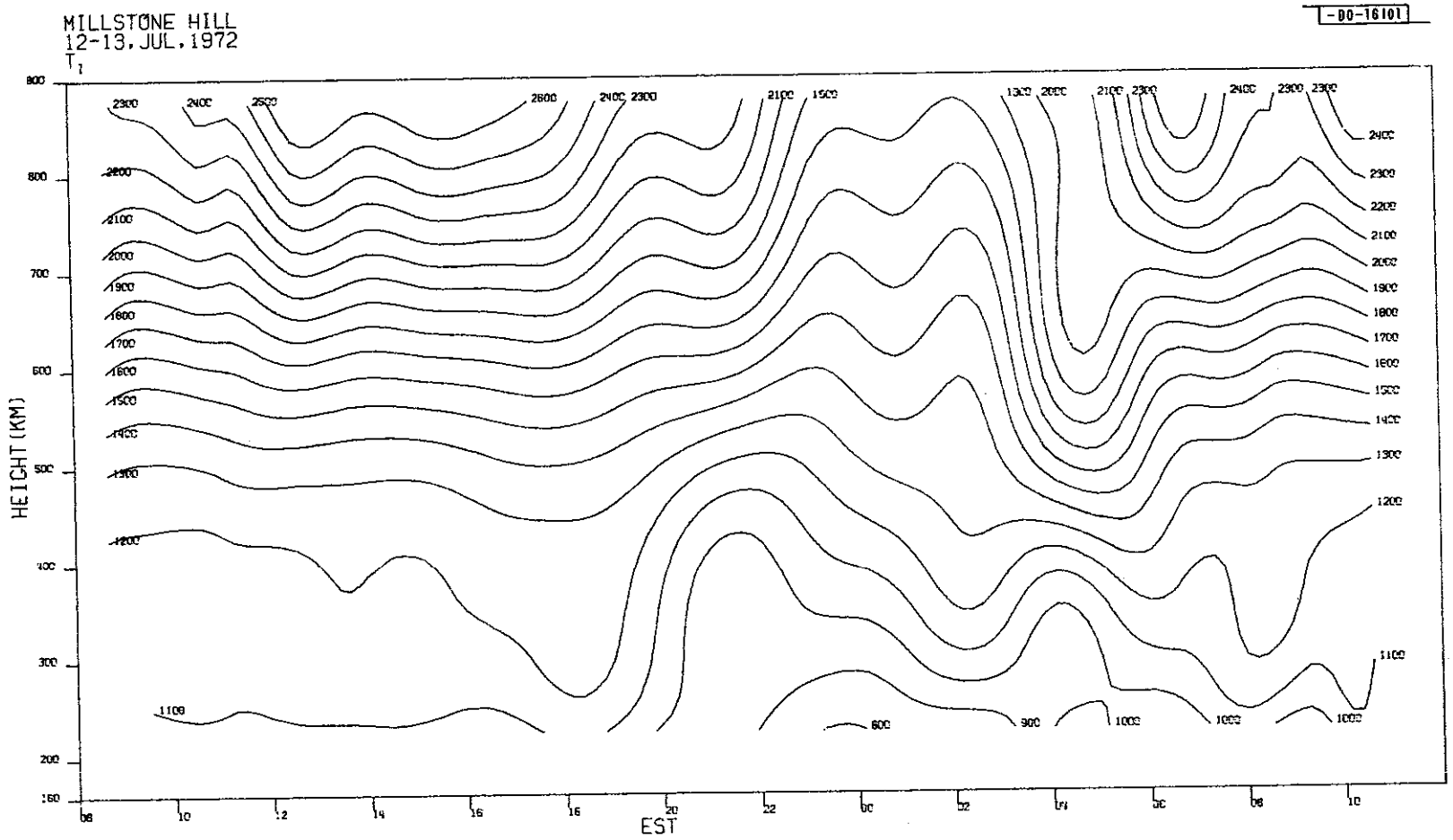

(c) T_i.

Fig.19(a-c). Continued.

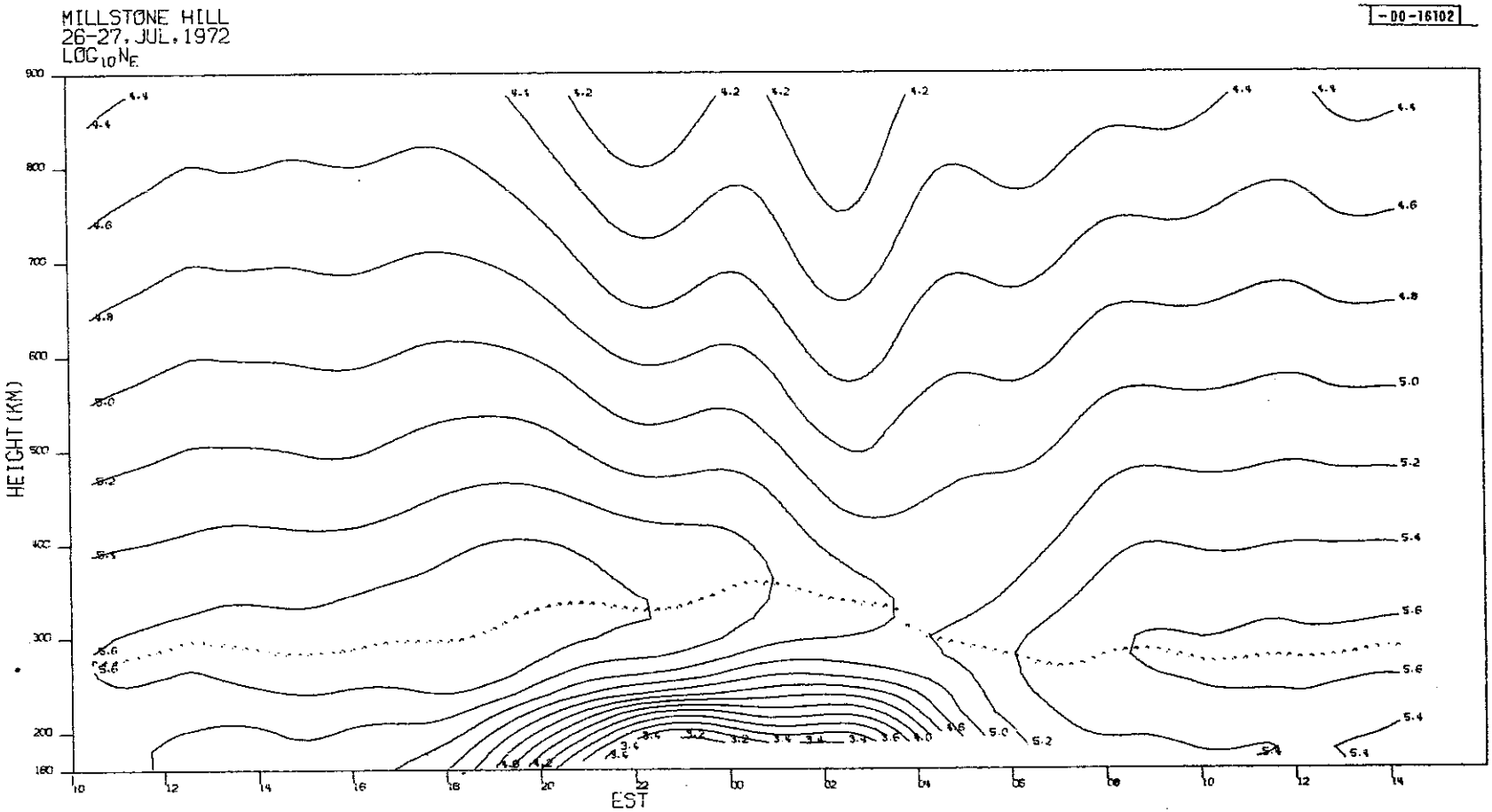

(a) $\text{Log}_{10} N_e$.

Fig.20(a-d). Results for 26-27 July 1972.

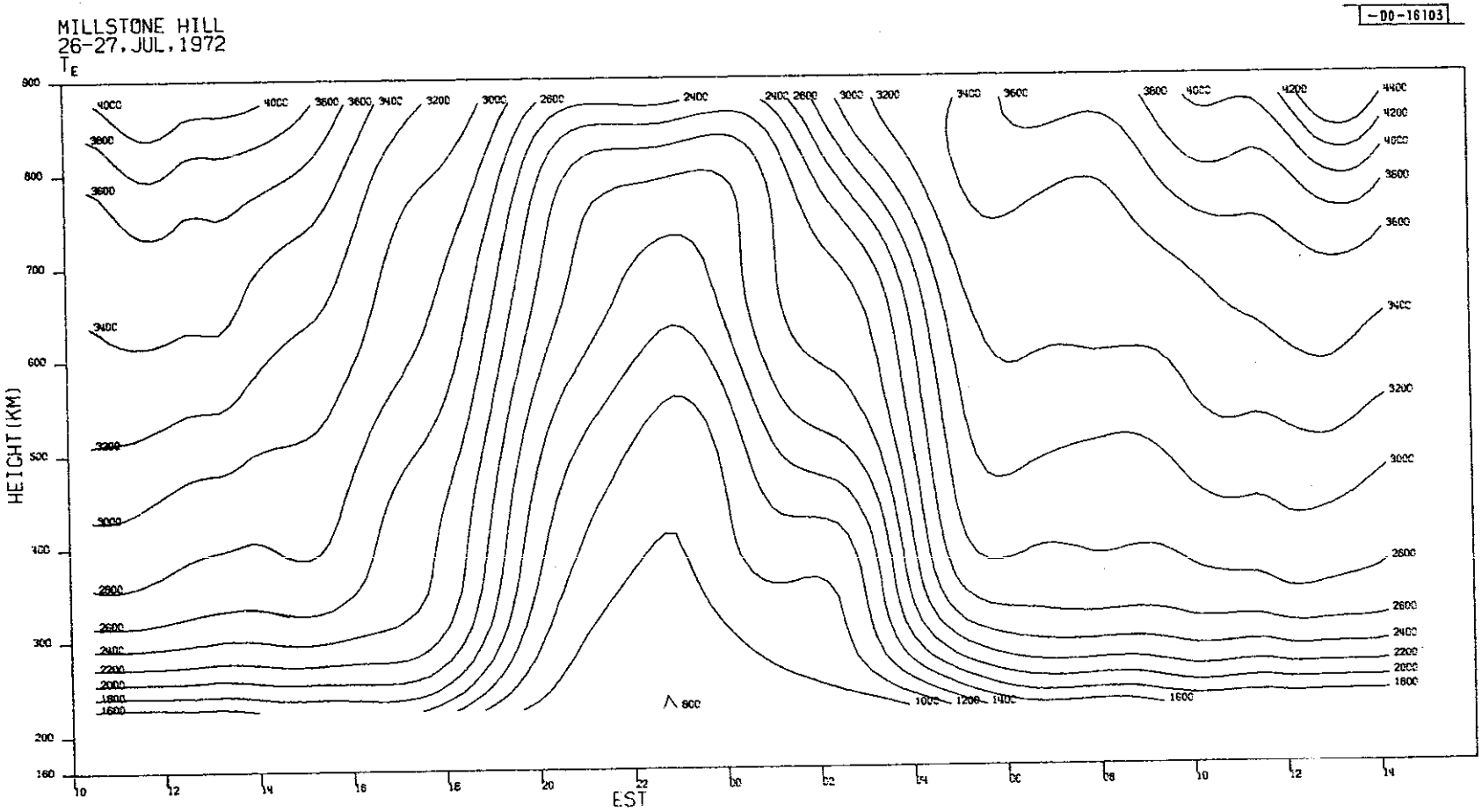

(b) T_e.

Fig. 20(a-d). Continued.

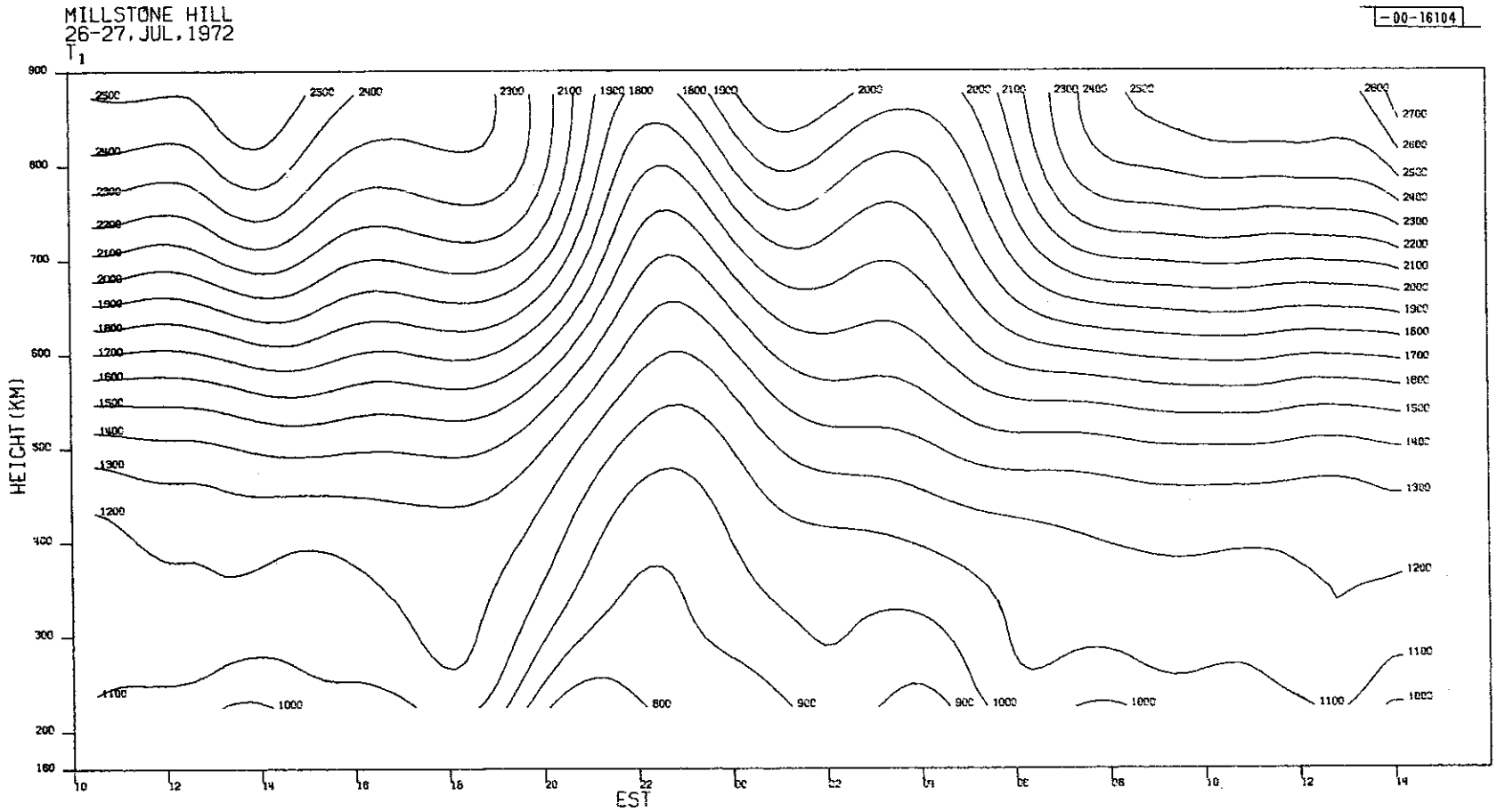

(c) T_i.

Fig.20(a-d). Continued.

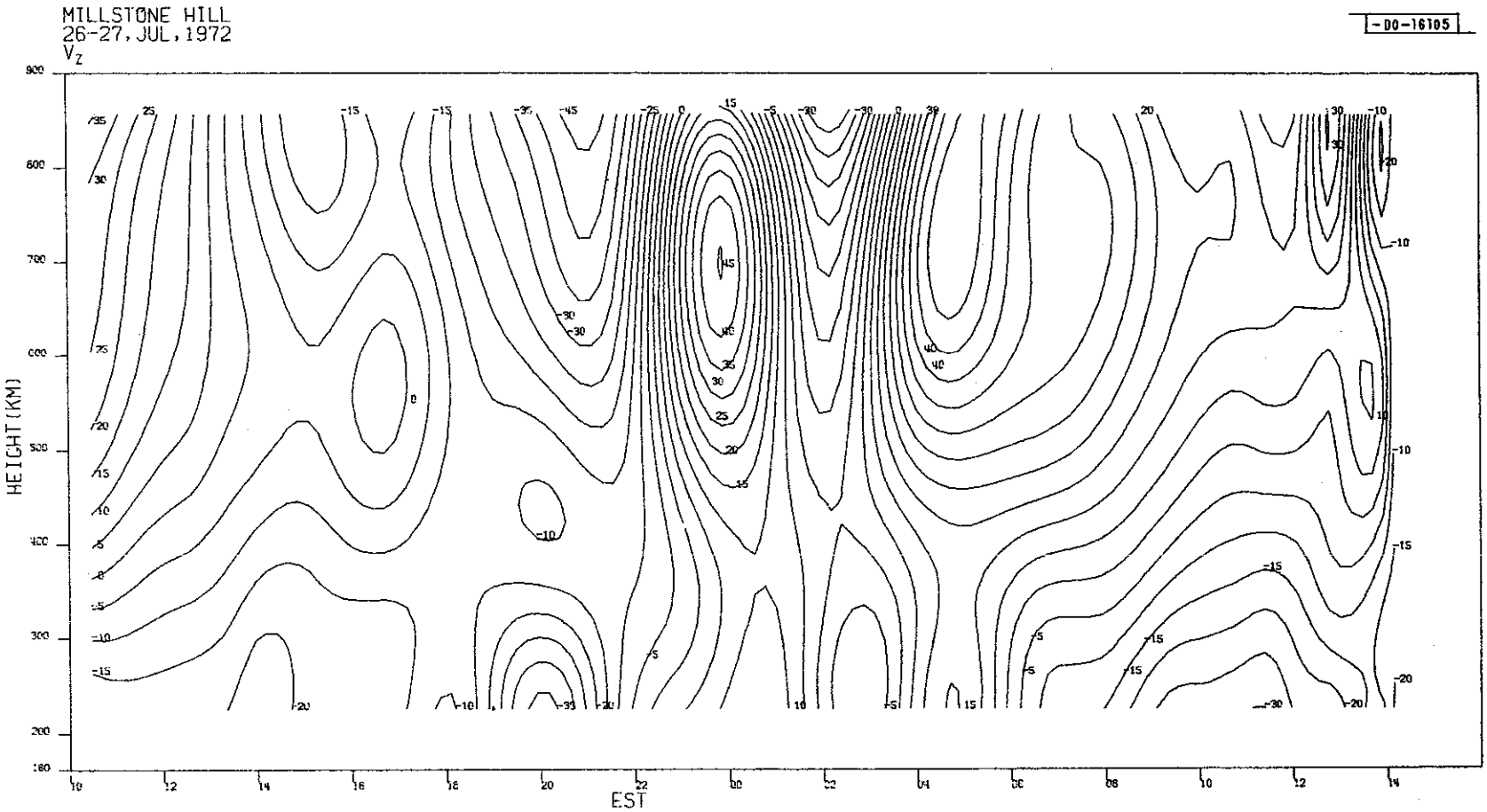

(d) V_z.

Fig. 20(a-d). Continued.

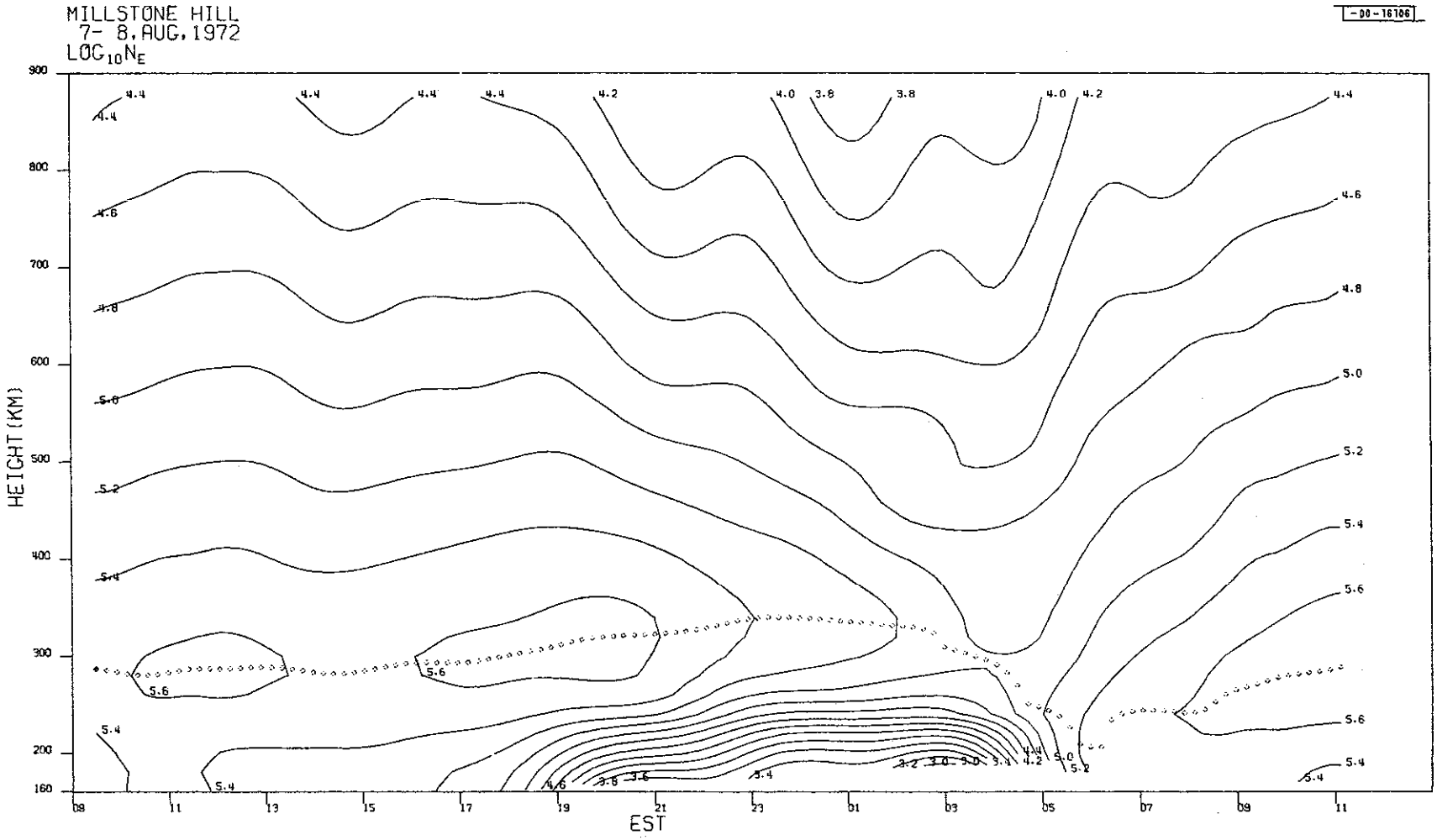

(a) $Log_{10} N_e$.

Fig.21(a–d). Results for 7–8 August 1972.

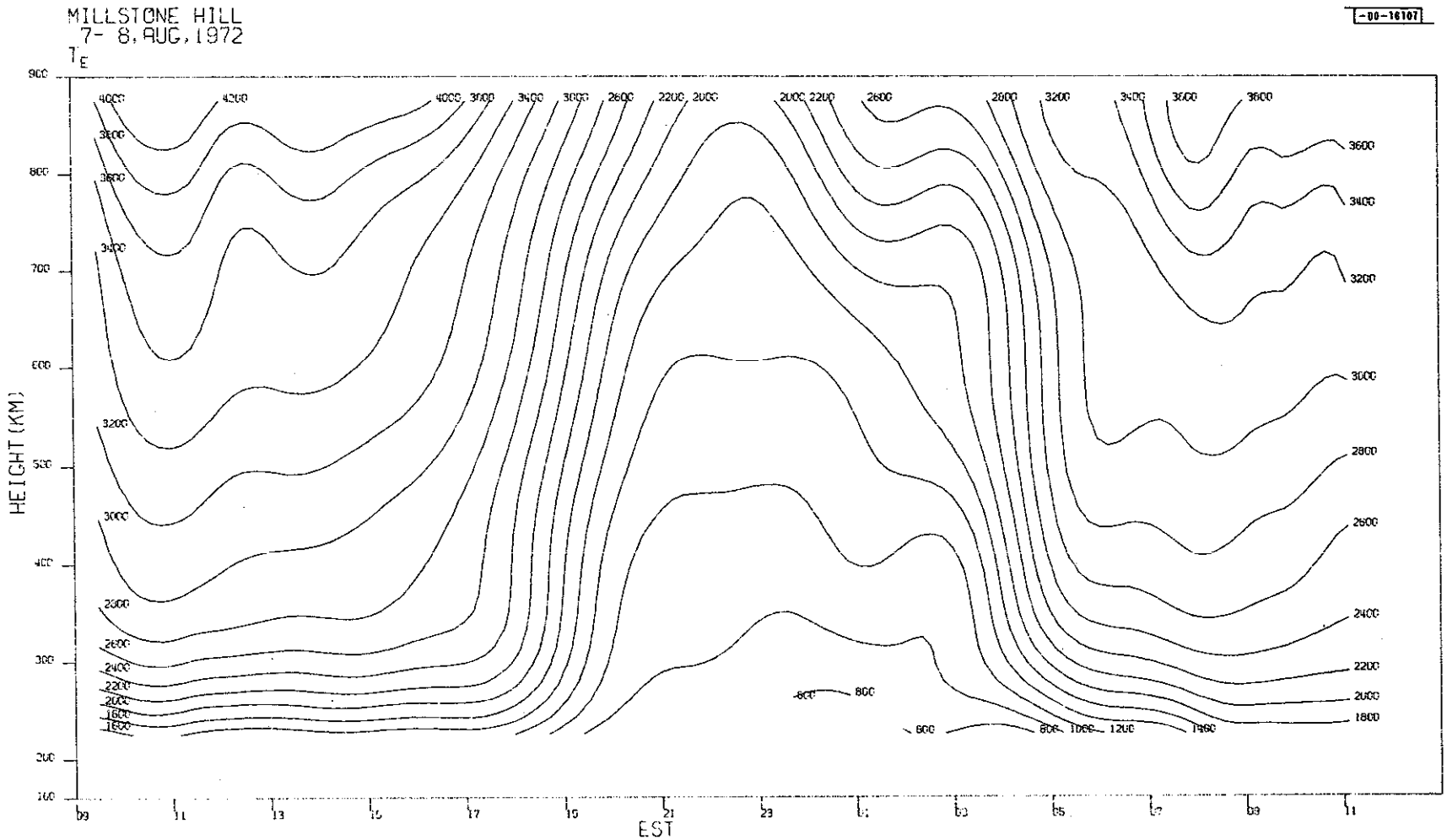

(b) T_e.

Fig.21(a-d). Continued.

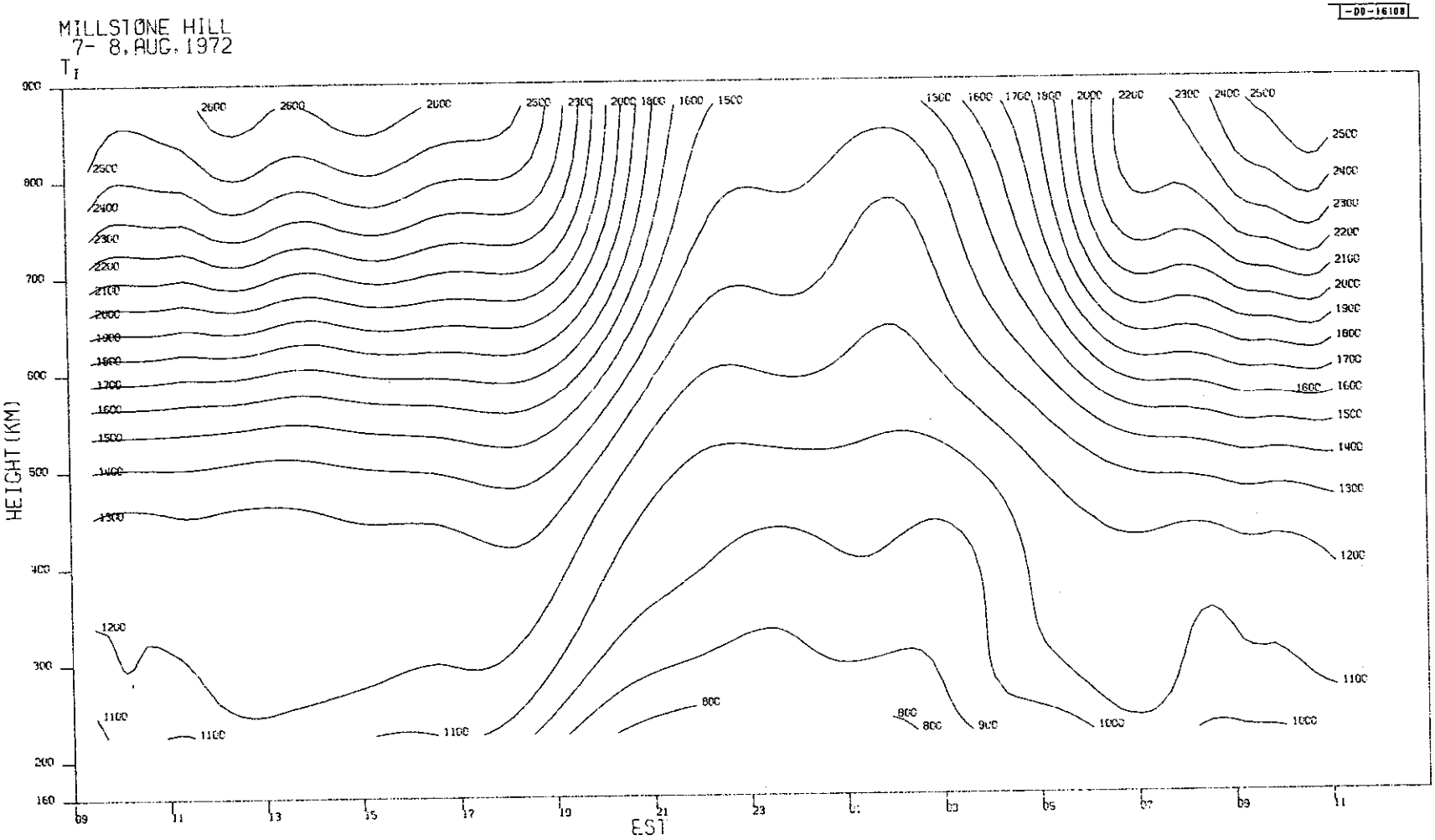

(c) T_i.

Fig.21(a-d). Continued.

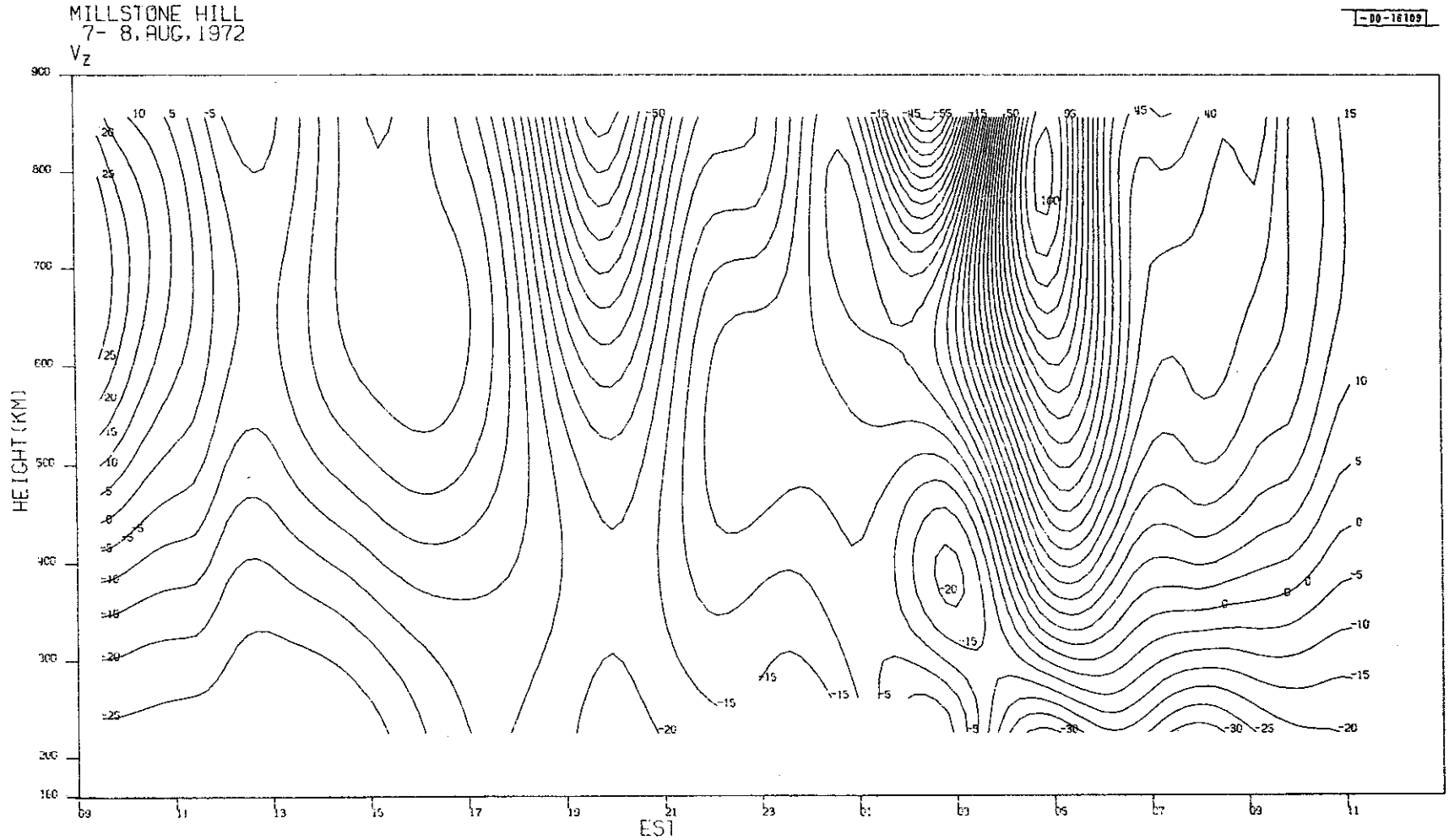

(d) V_z.

Fig.21(a-d). Continued.

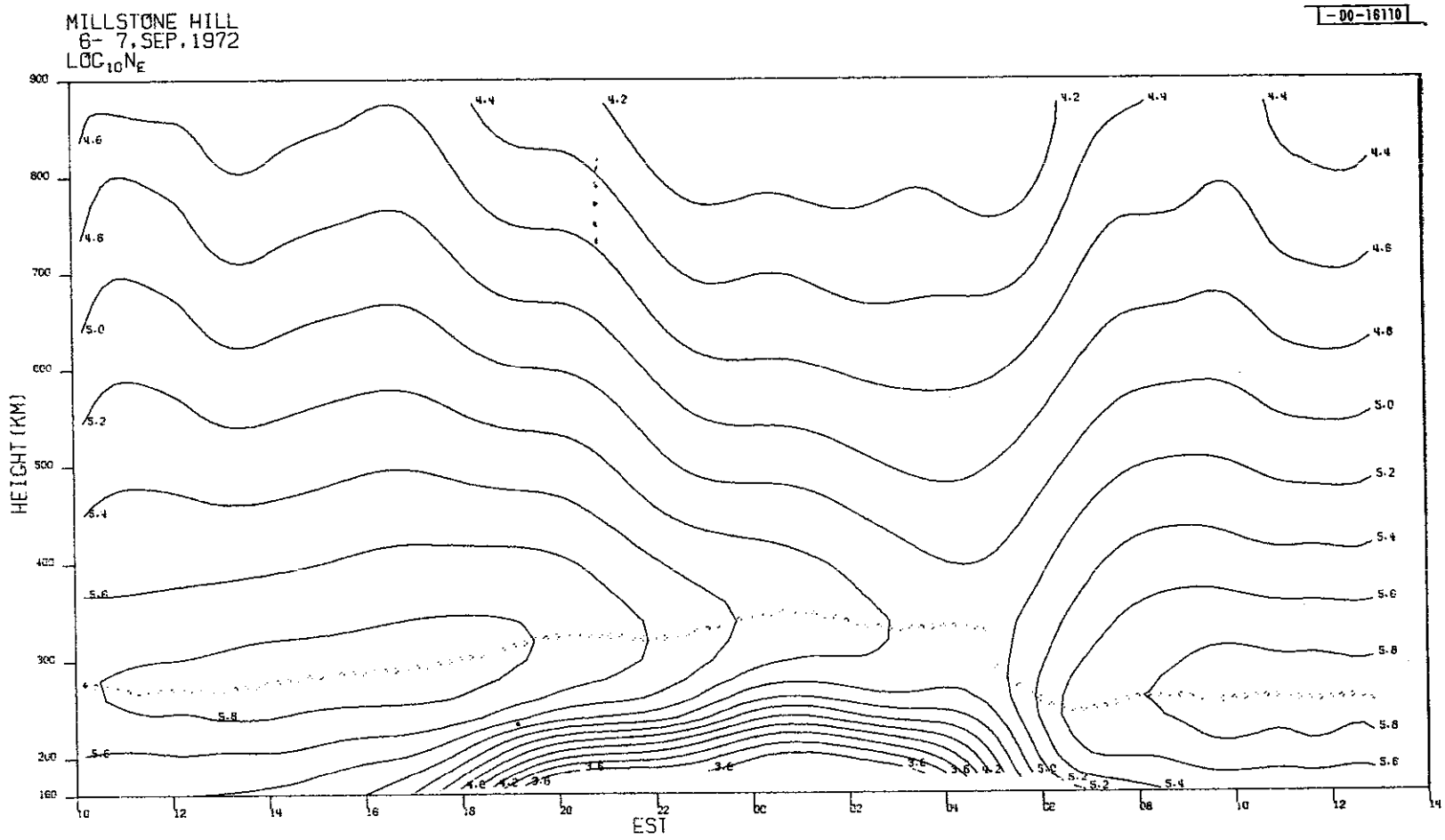

(a) $Log_{10} N_e$.

Fig.22(a-d). Results for 6-7 September 1972.

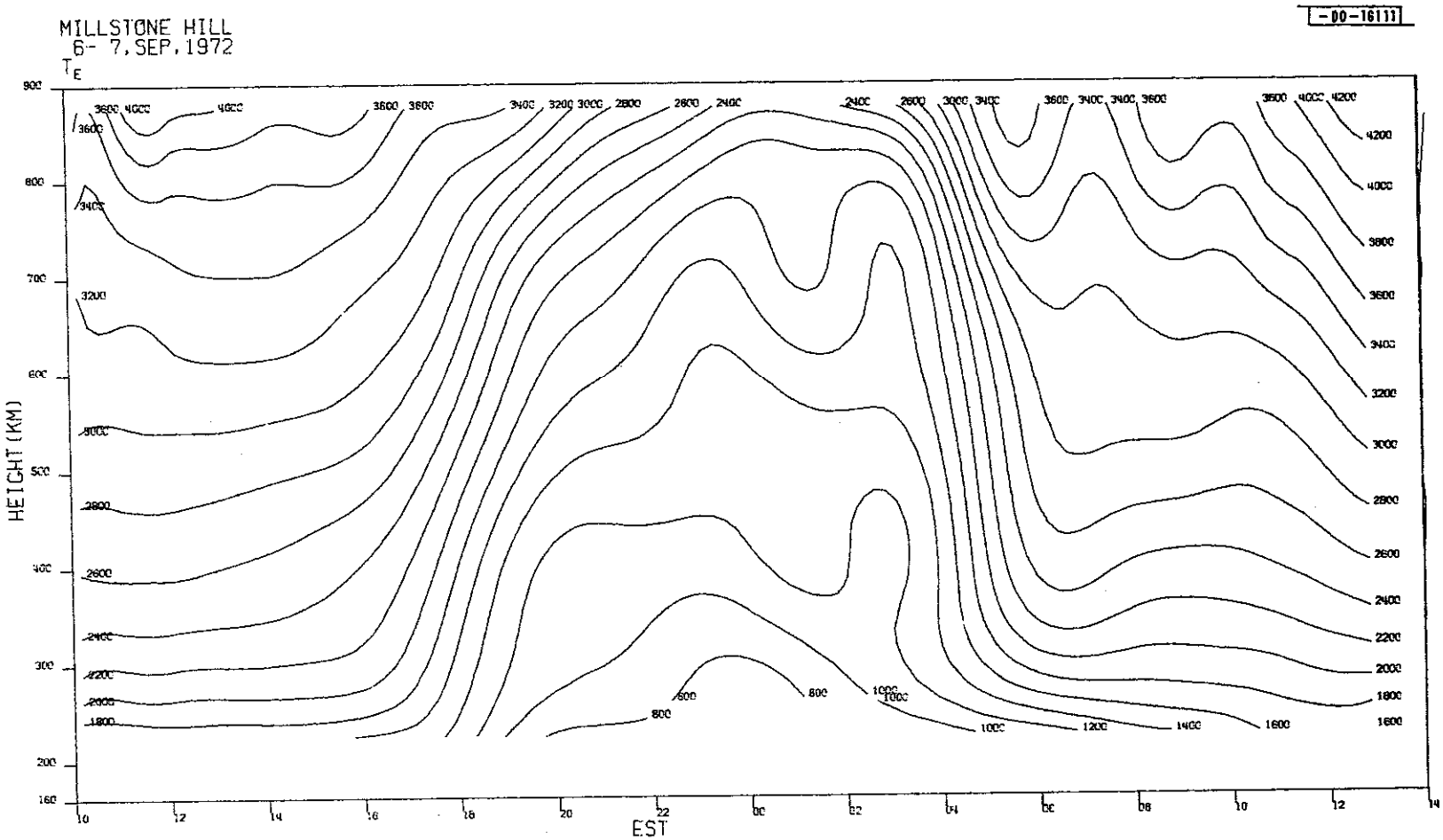

(b) T_e.

Fig.22(a-d). Continued.

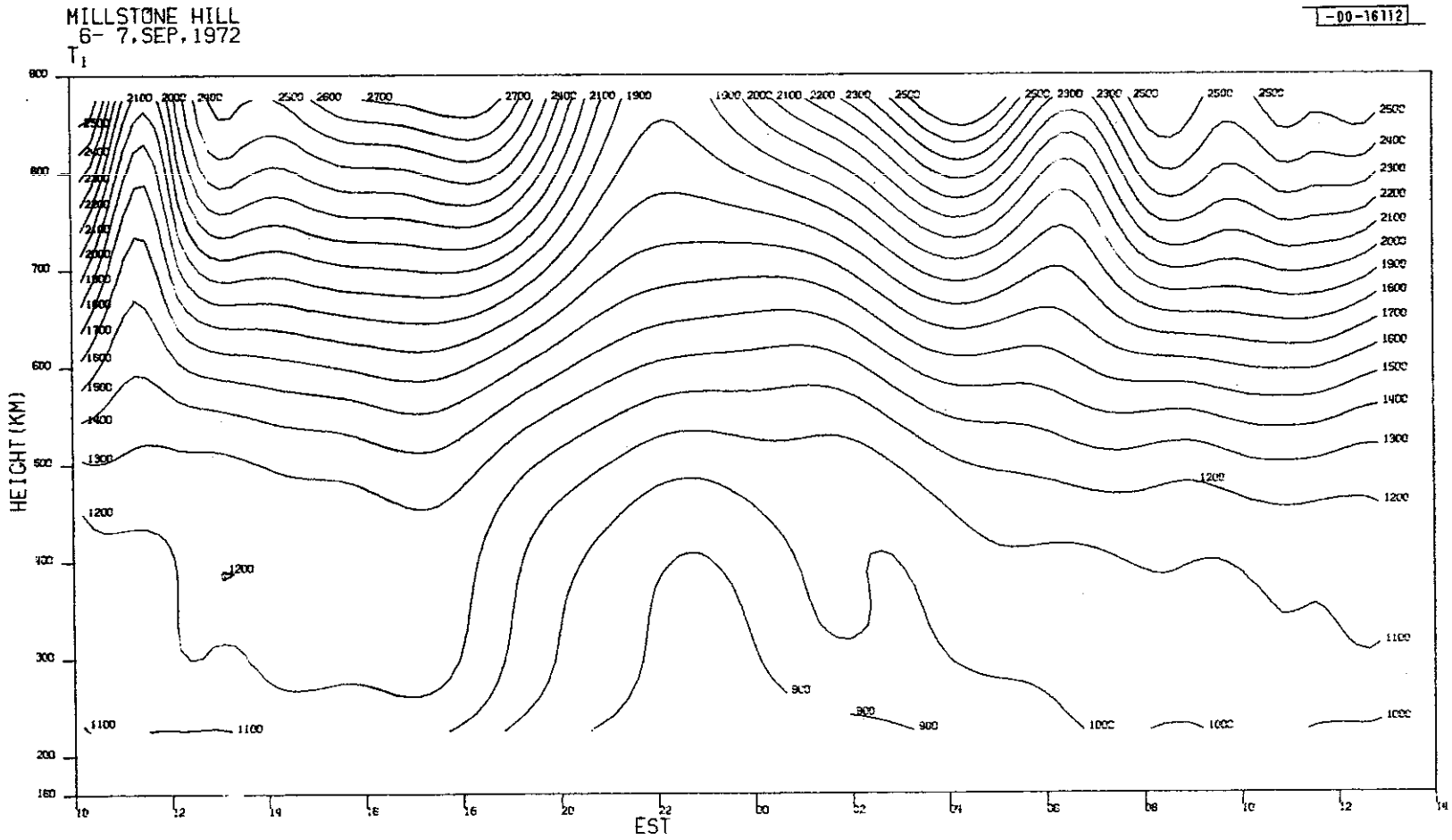

(c) T_i.

Fig.22(a-d). Continued.

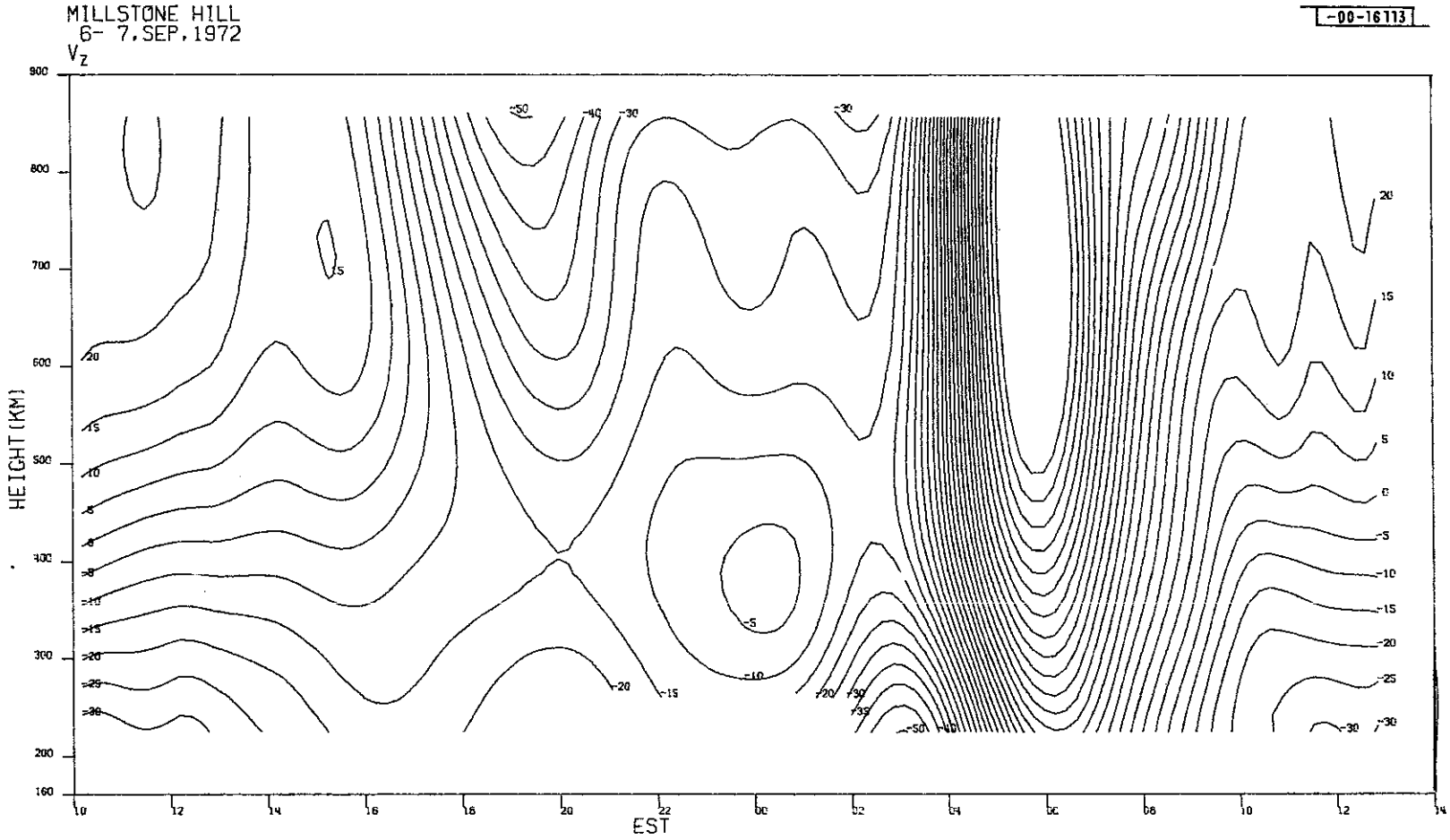

(d) V_z.

Fig.22(a-d). Continued.

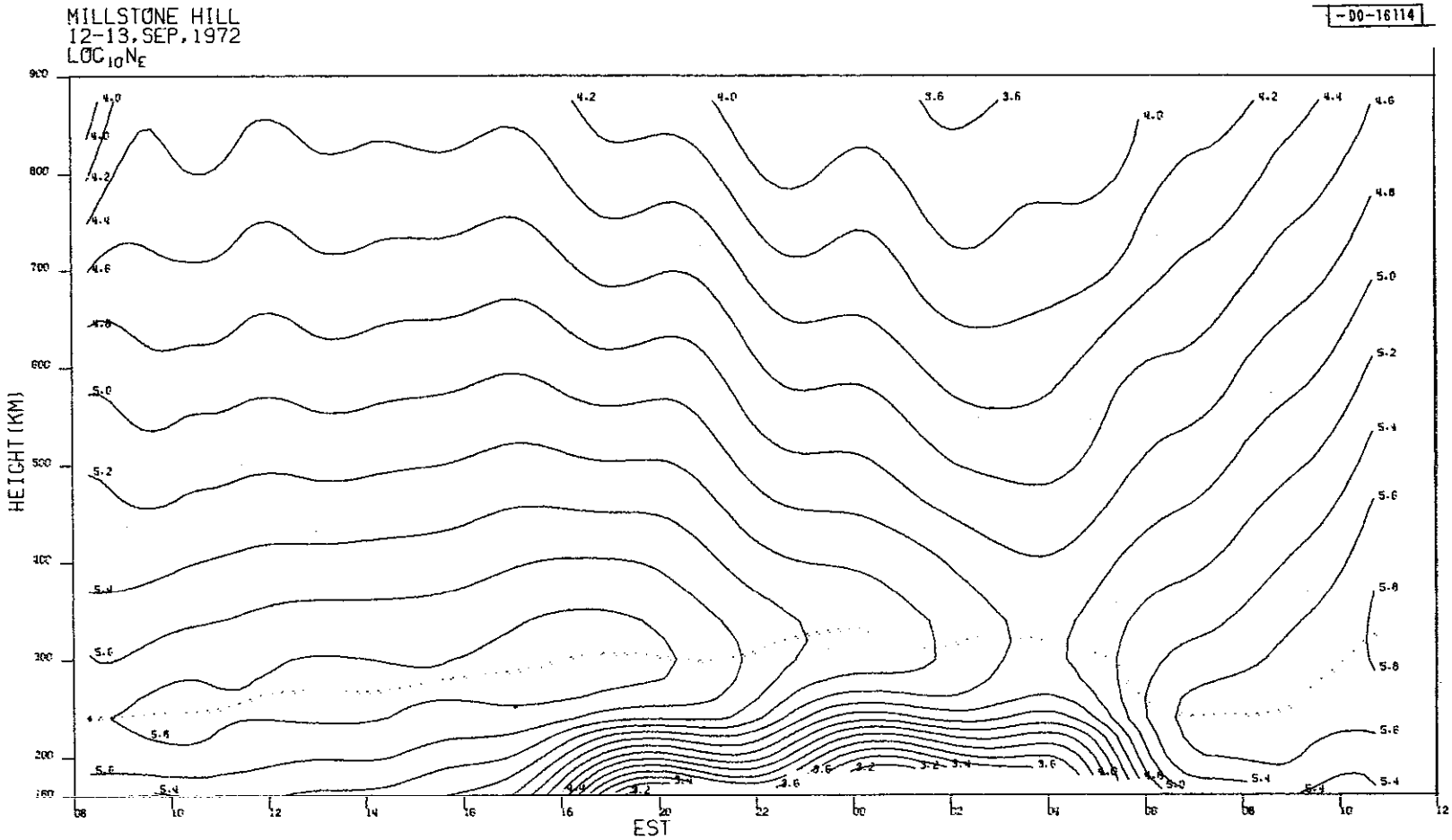

(a) $Log_{10} N_e$.

Fig.23(a-d). Results for 12-13 September 1972.

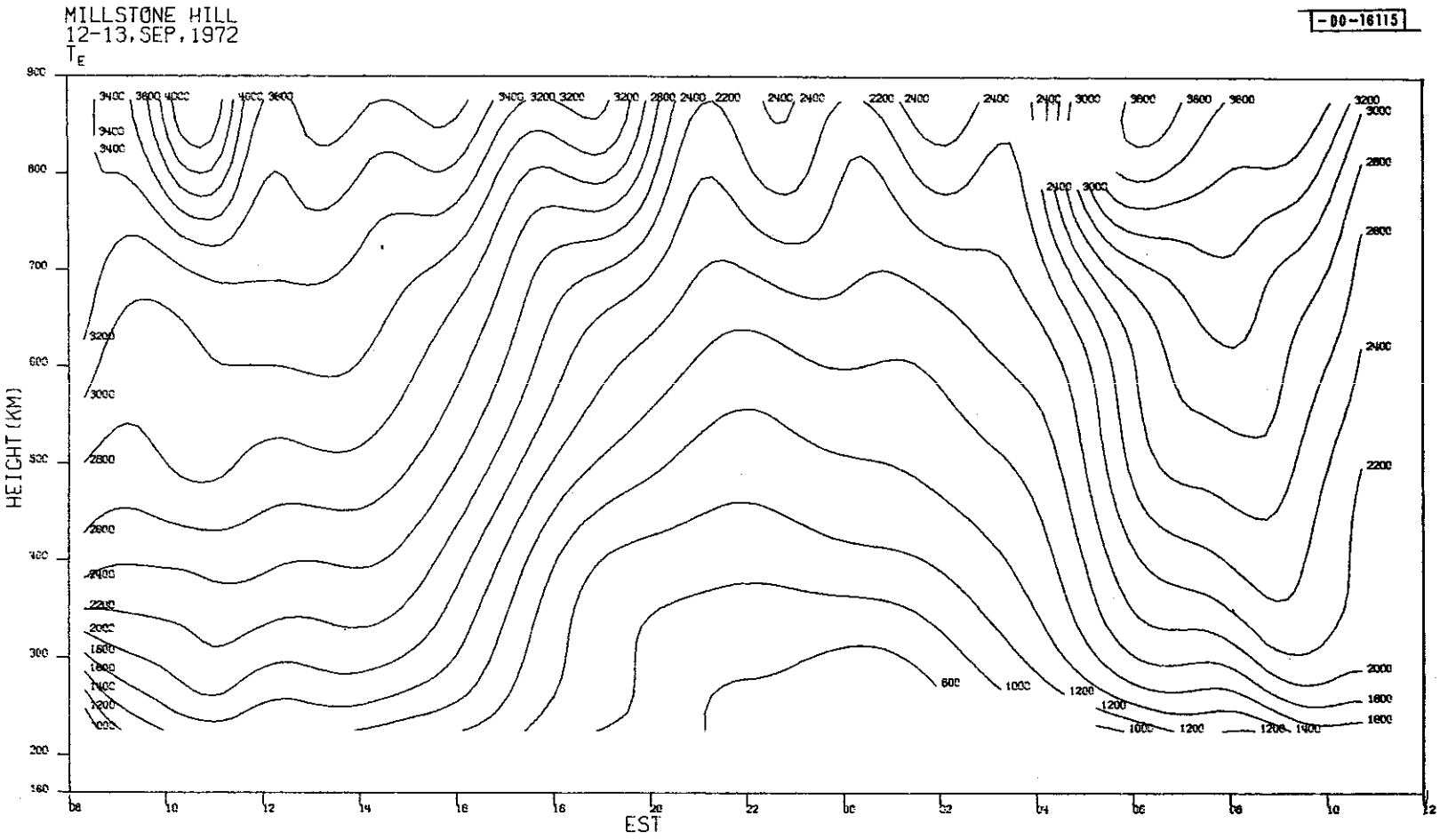

(b) T_e.

Fig.23(a-d). Continued.

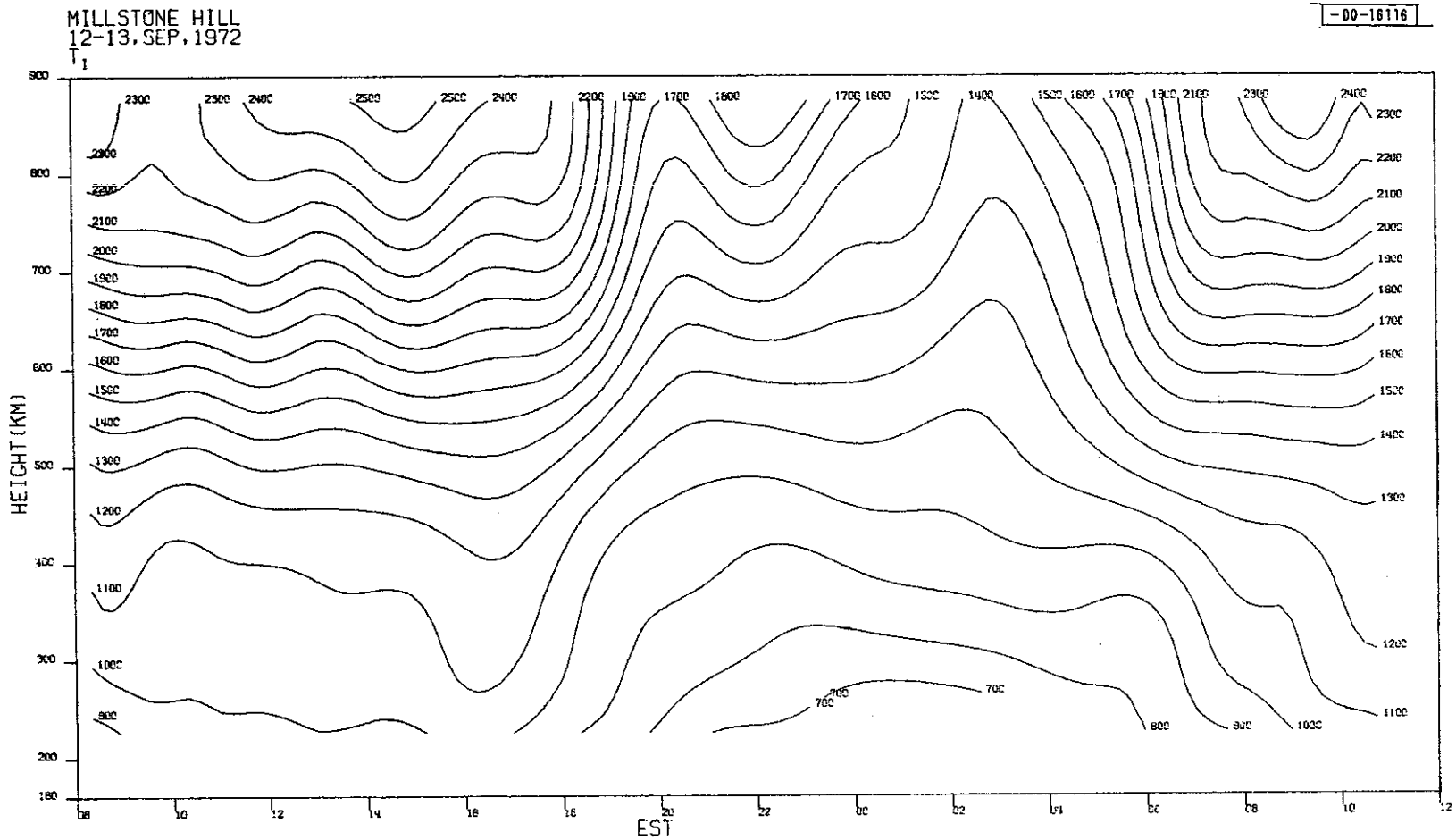

(c) T_i.

Fig.23(a-d). Continued.

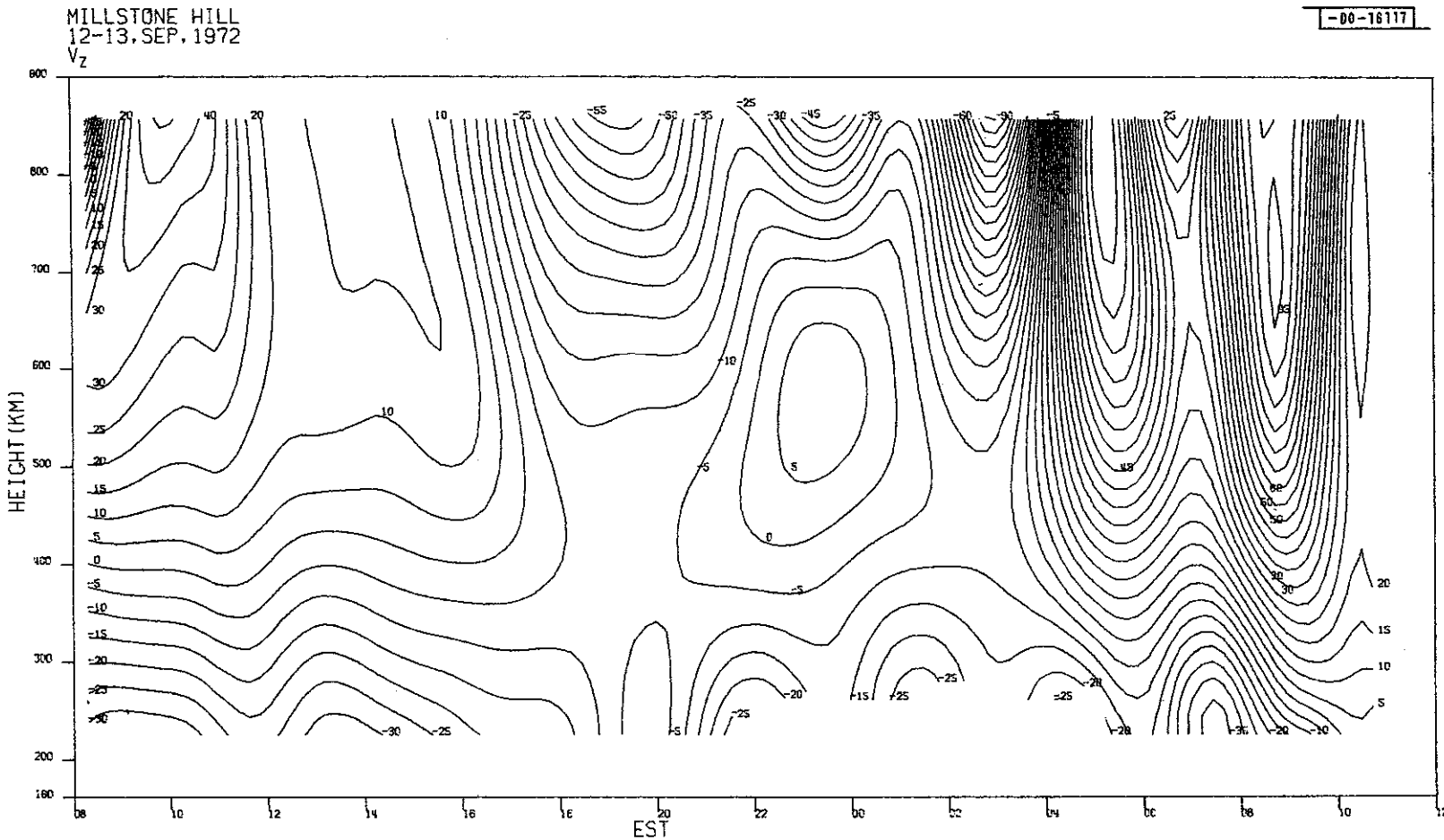

(d) V_z.

Fig.23(a-d). Continued.

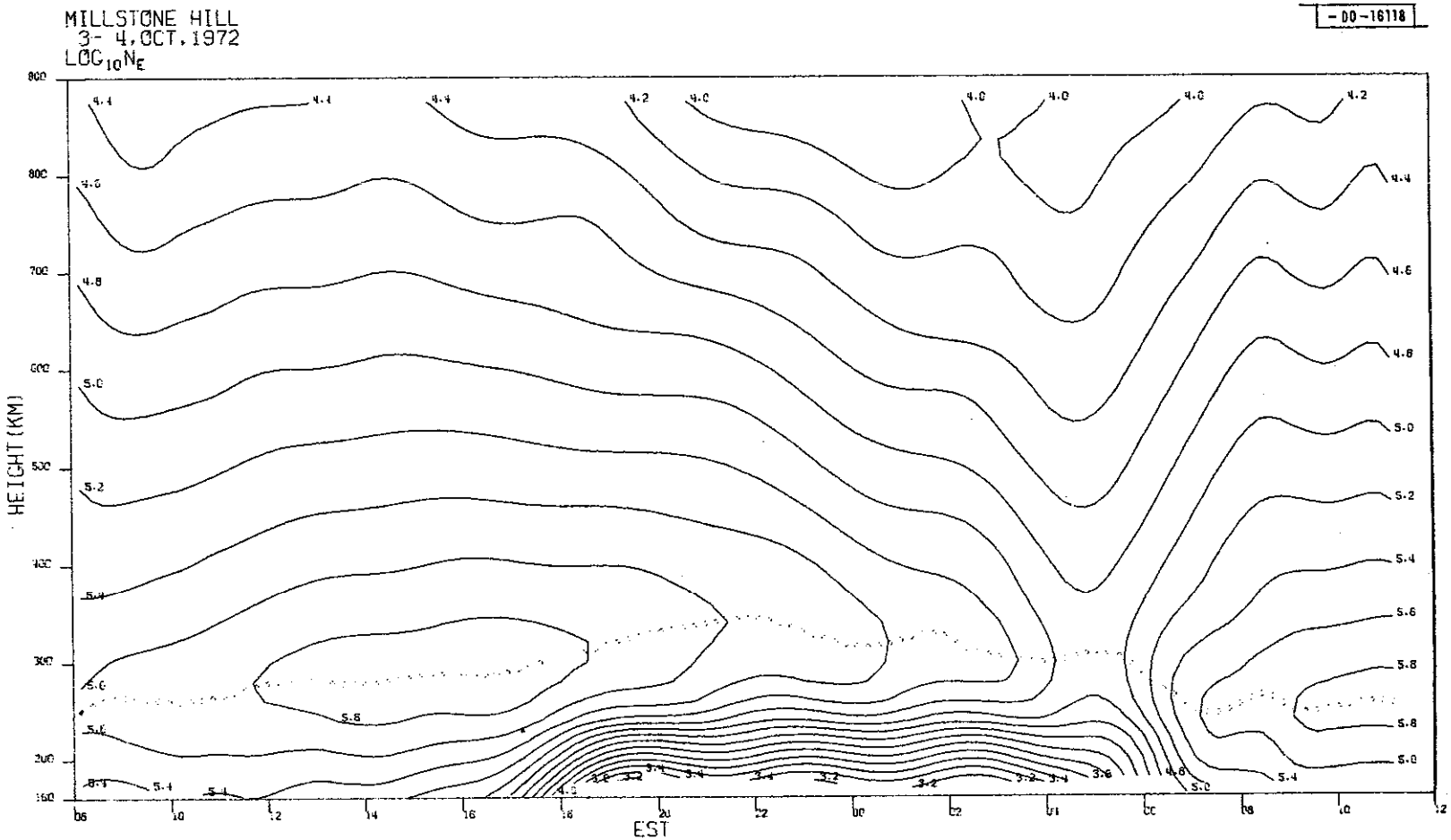

(a) $Log_{10} N_e$.

Fig.24(a-d). Results for 3-4 October 1972.

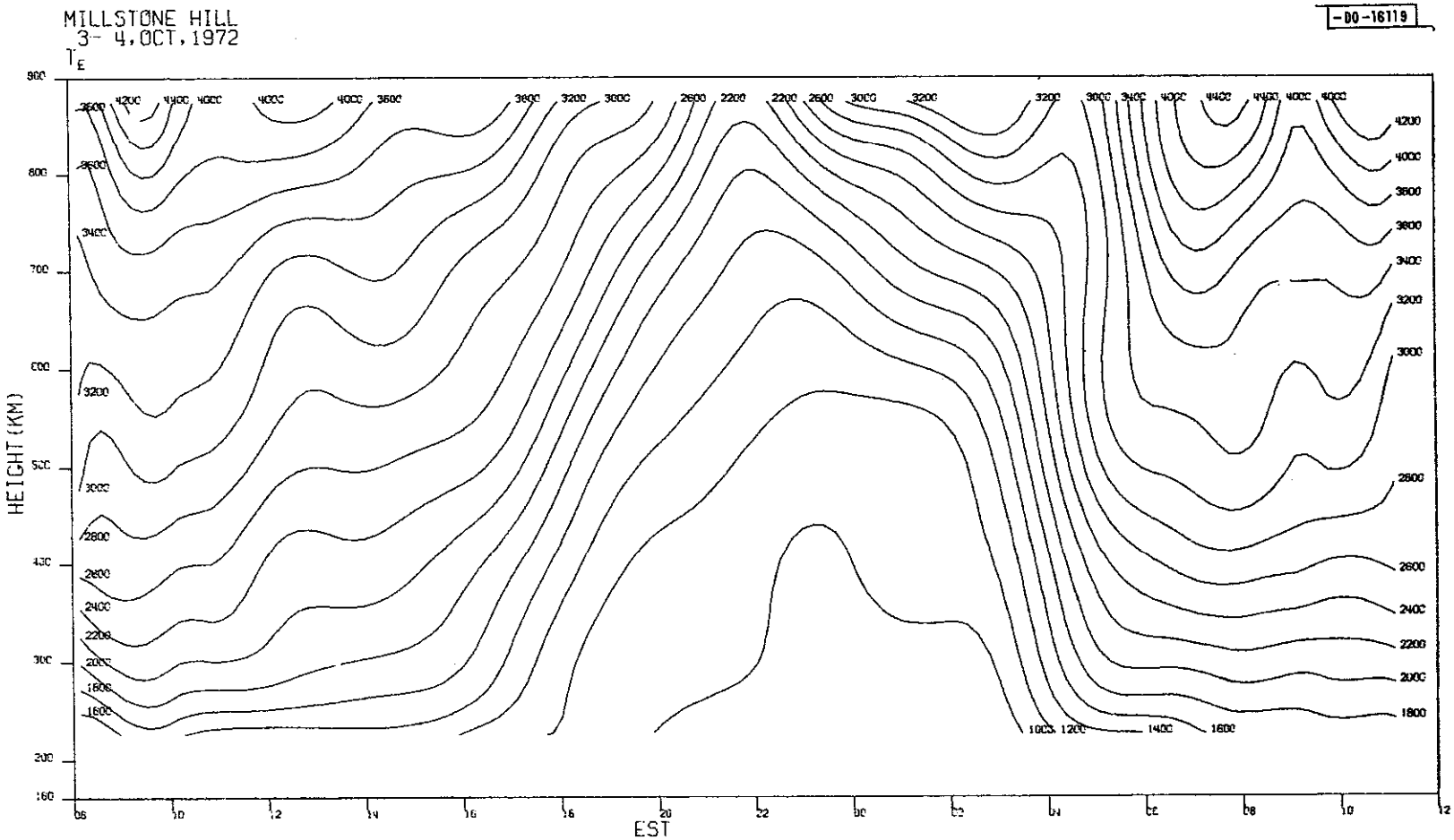

(b) T_e.

Fig.24(a-d). Continued.

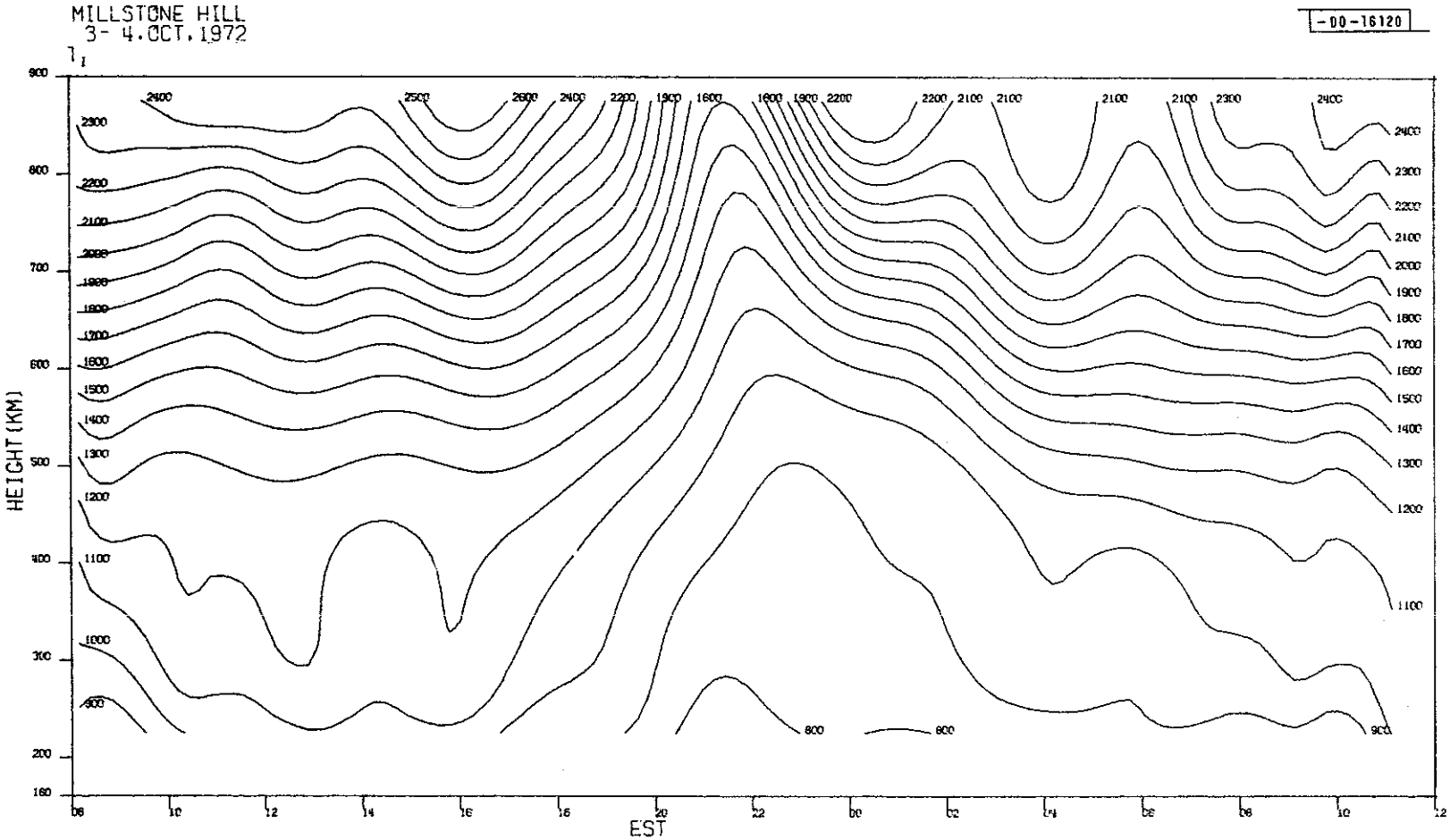

(c) T_i.

Fig.24(a-d). Continued.

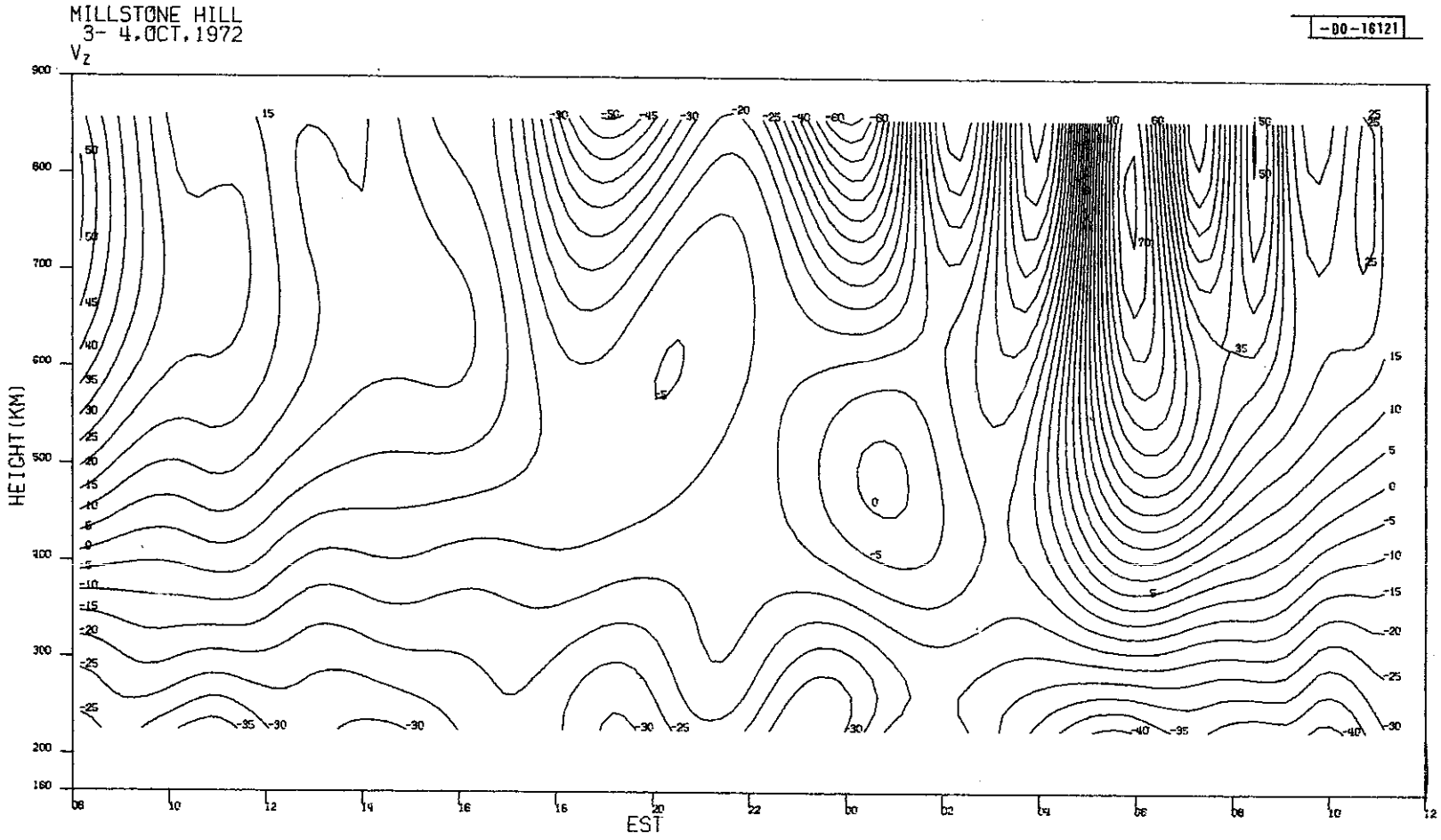

(d) V_z.

Fig.24(a-d). Continued.

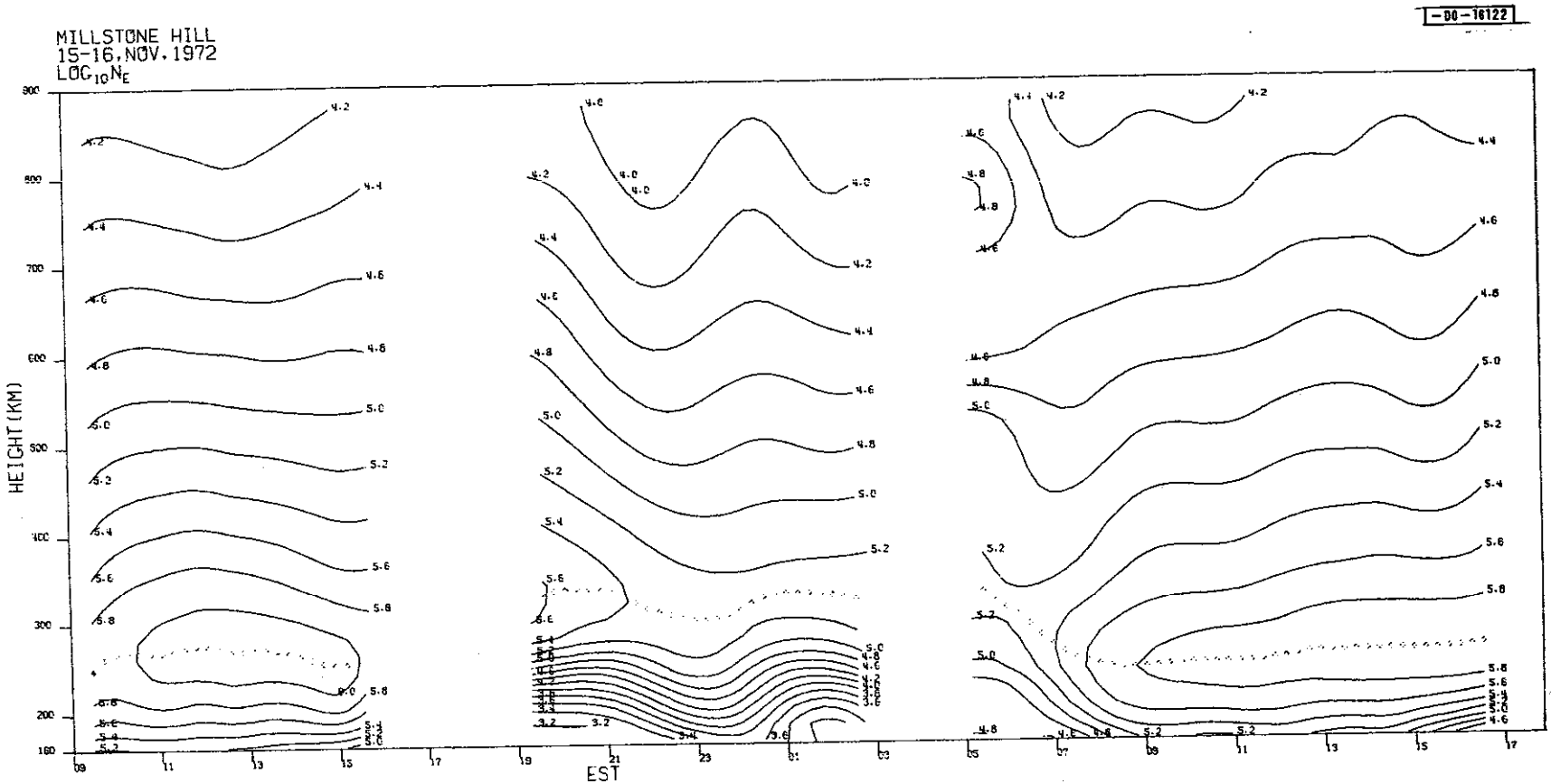

(a) $\mathrm{Log}_{10} N_e$.

Fig.25(a-d). Results for 15-16 November 1972.

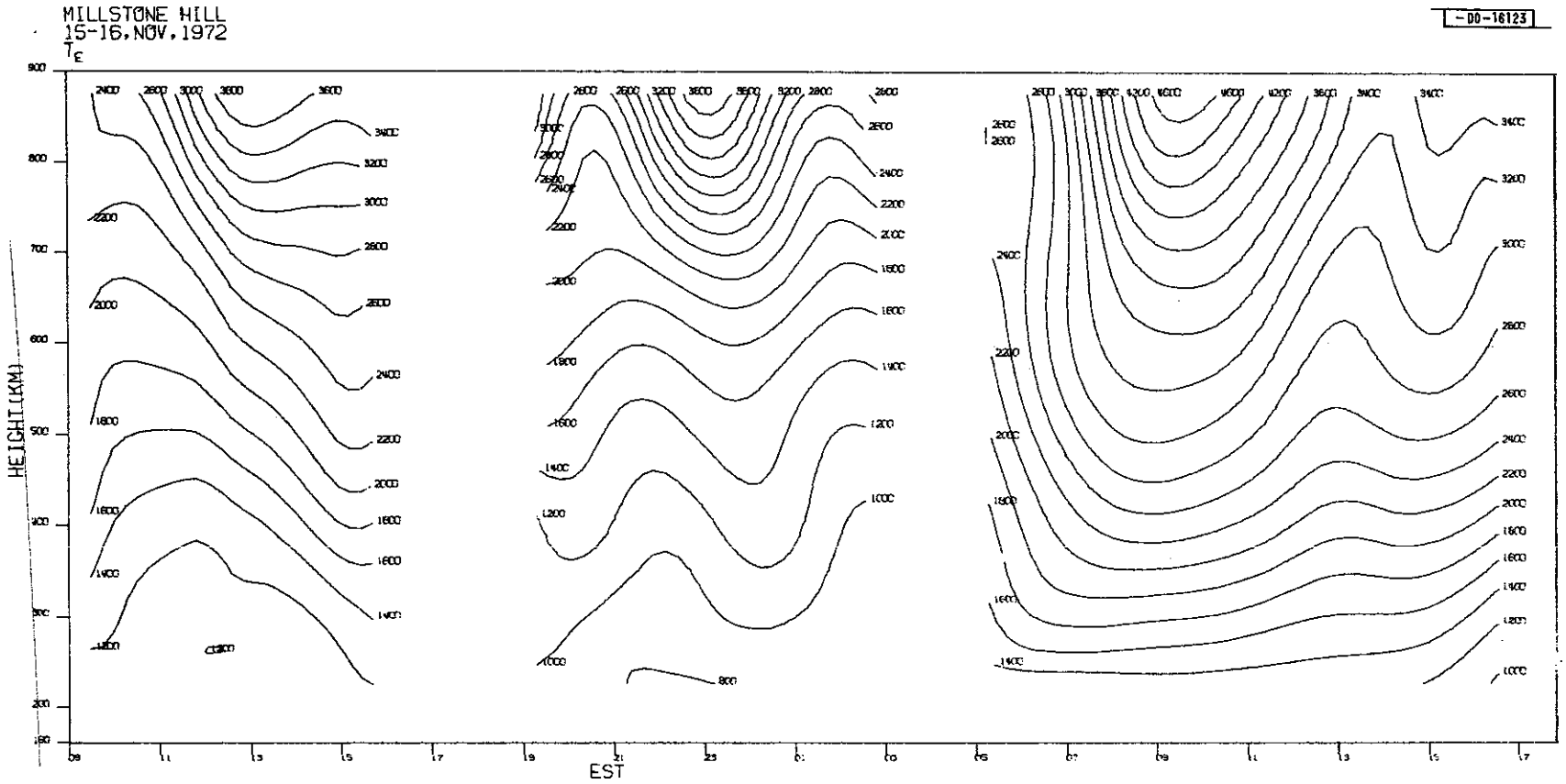

(b) T_e.

Fig.25(a-d). Continued.

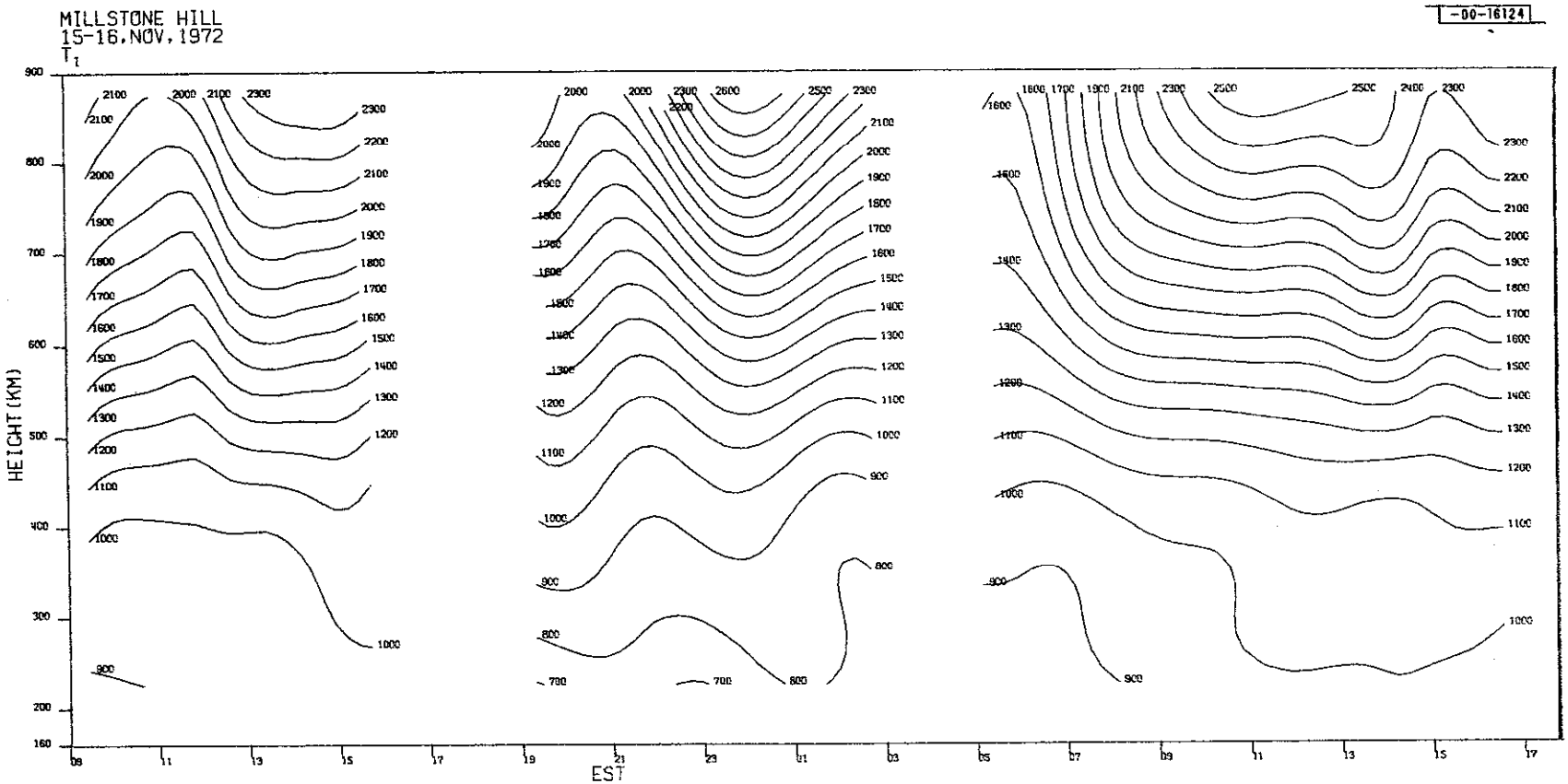

(c) T_i.

Fig.25(a-d). Continued.

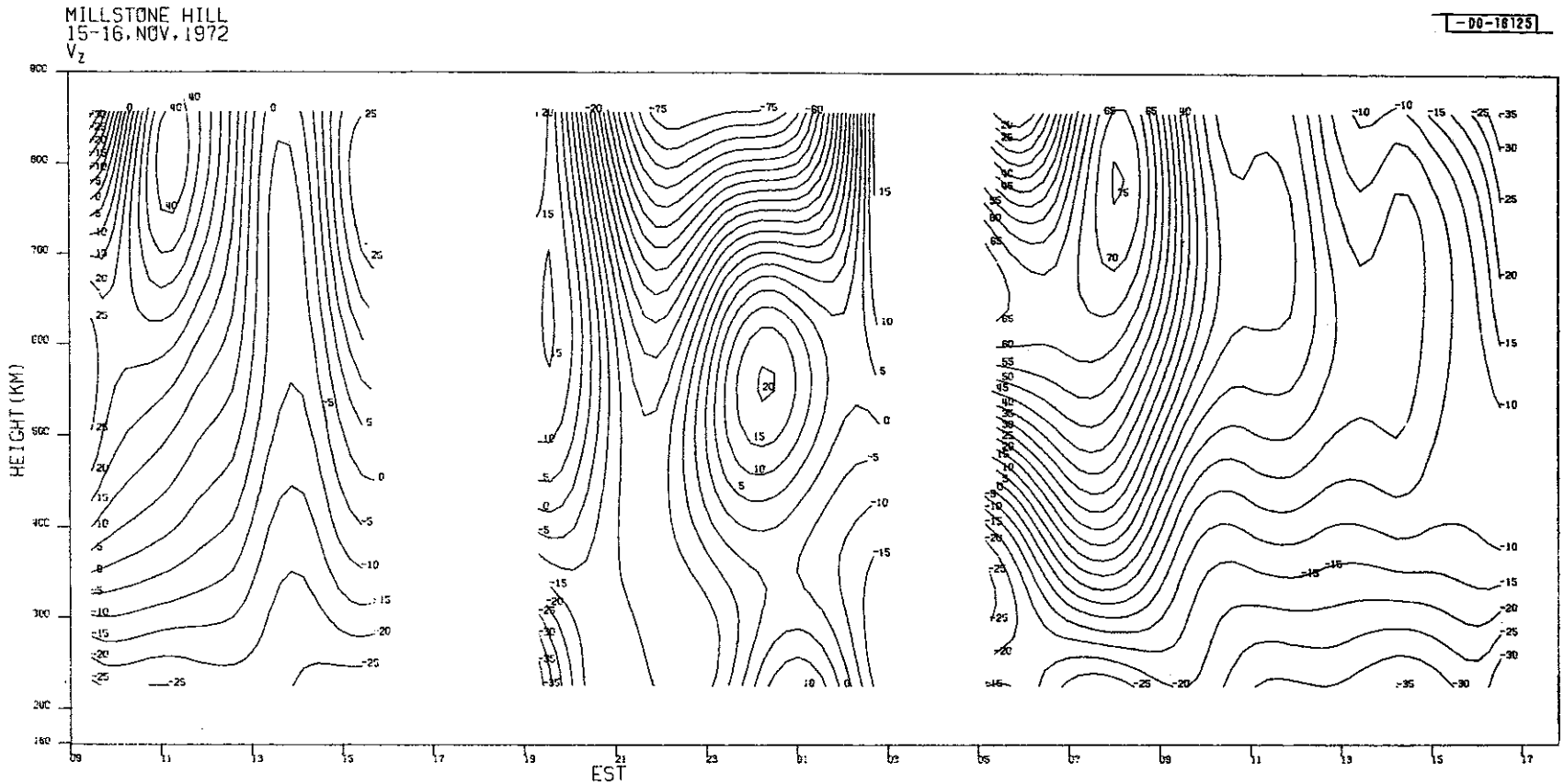

(d) V_z.

Fig.25(a-d). Continued.

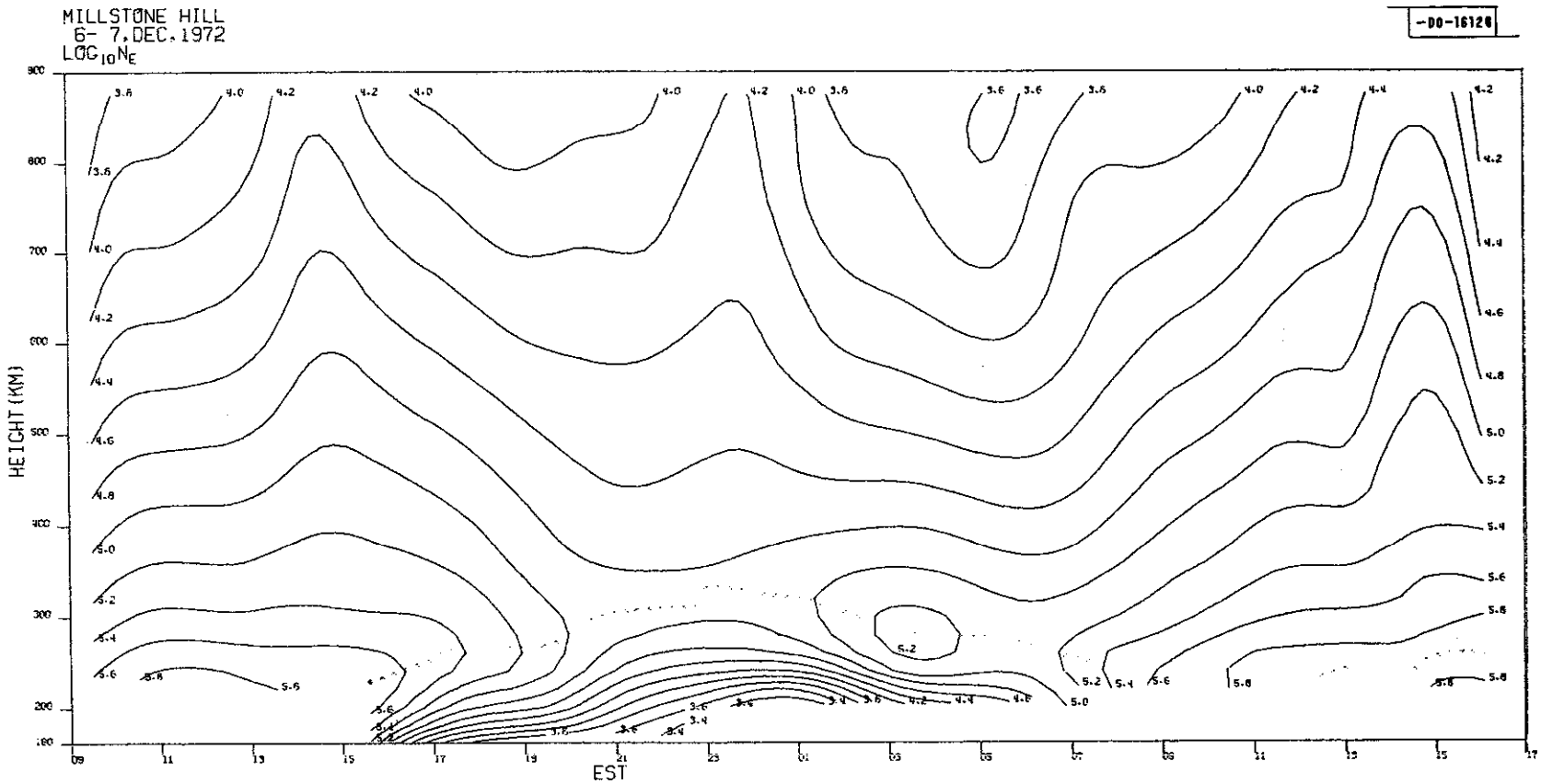

(a) $Log_{10} N_e$.

Fig.26(a-d). Results for 6-7 December 1972.

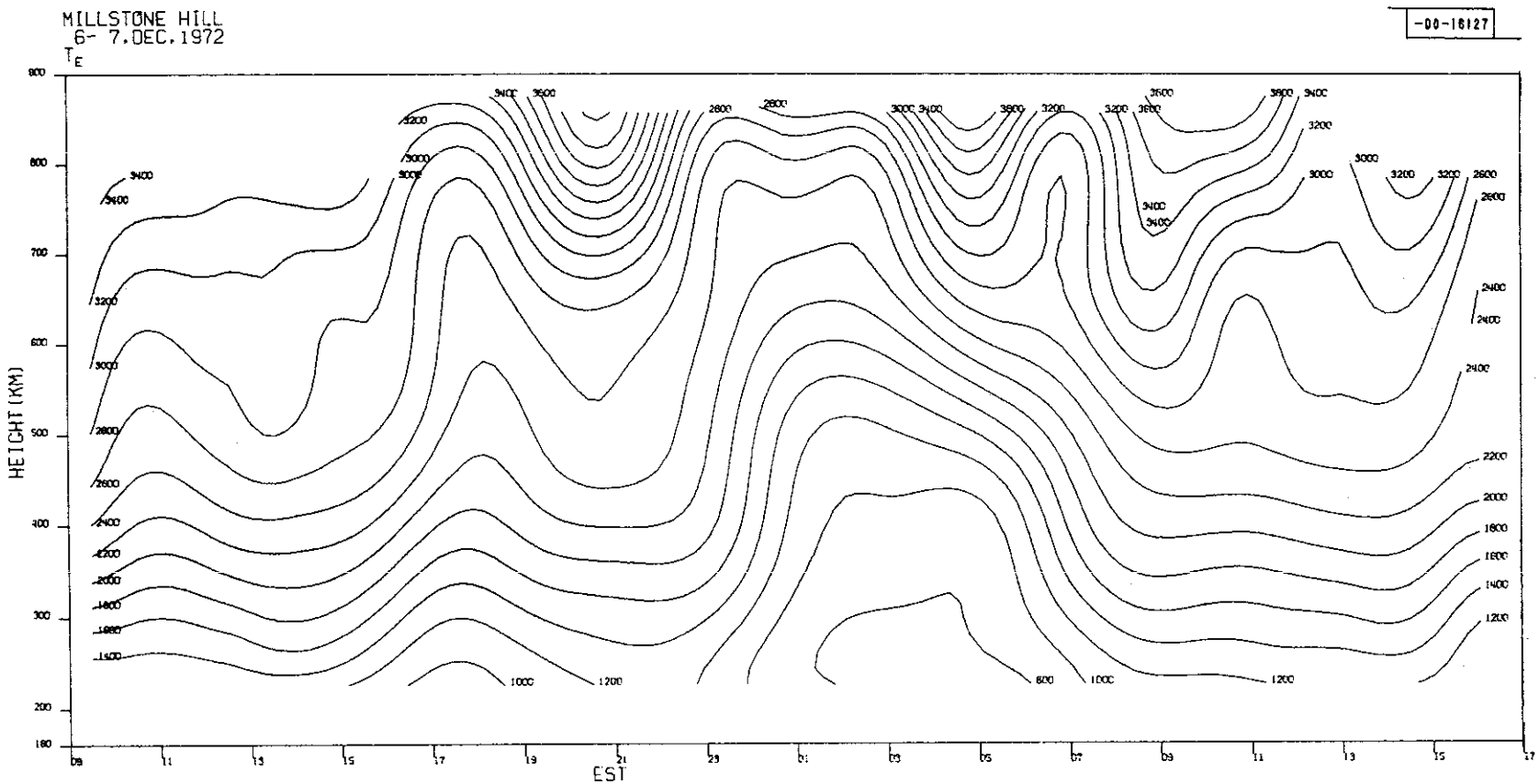

(b) T_e.

Fig.26(a-d). Continued.

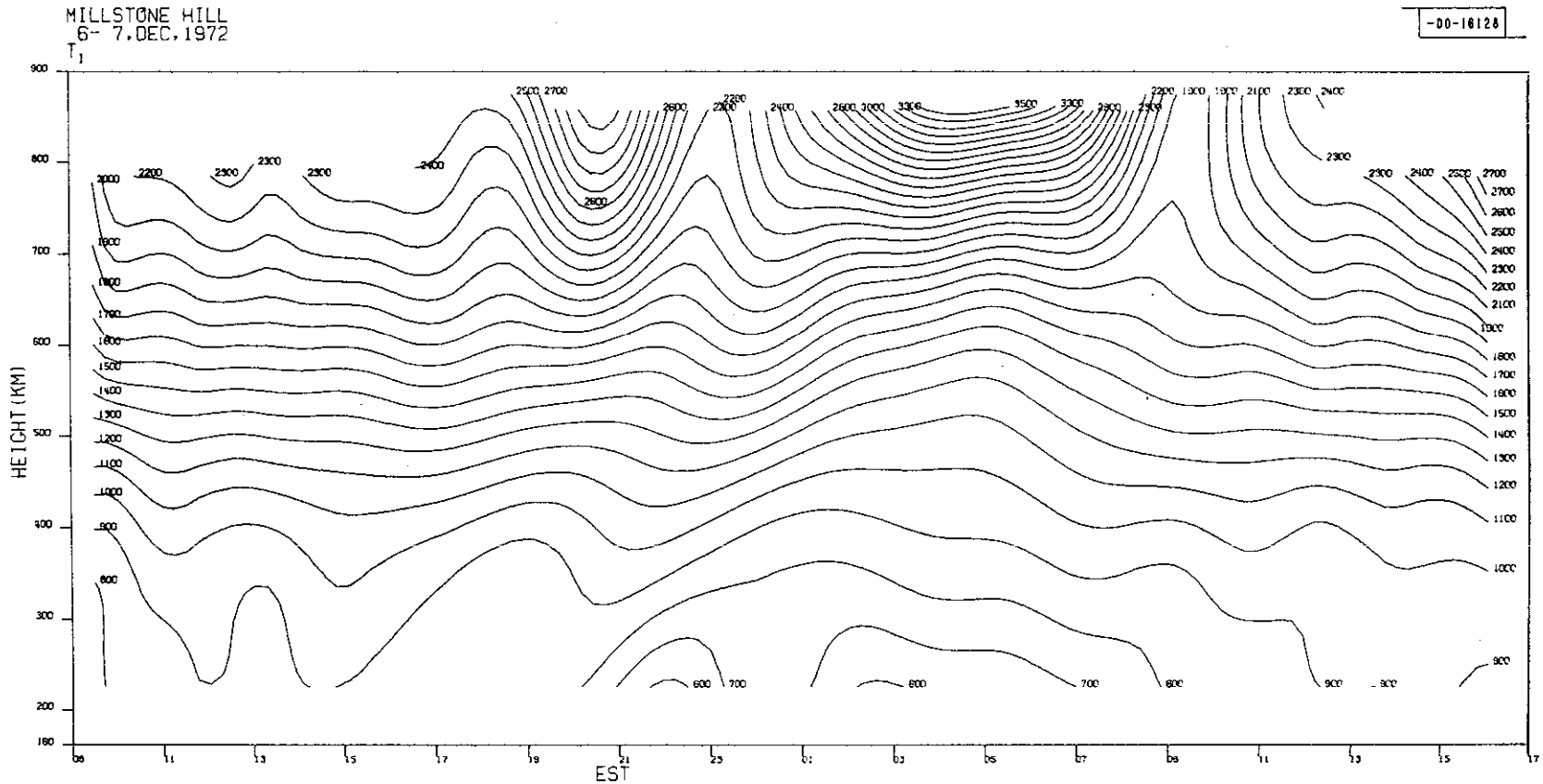

(c) T_i.

Fig.26(a-d). Continued.

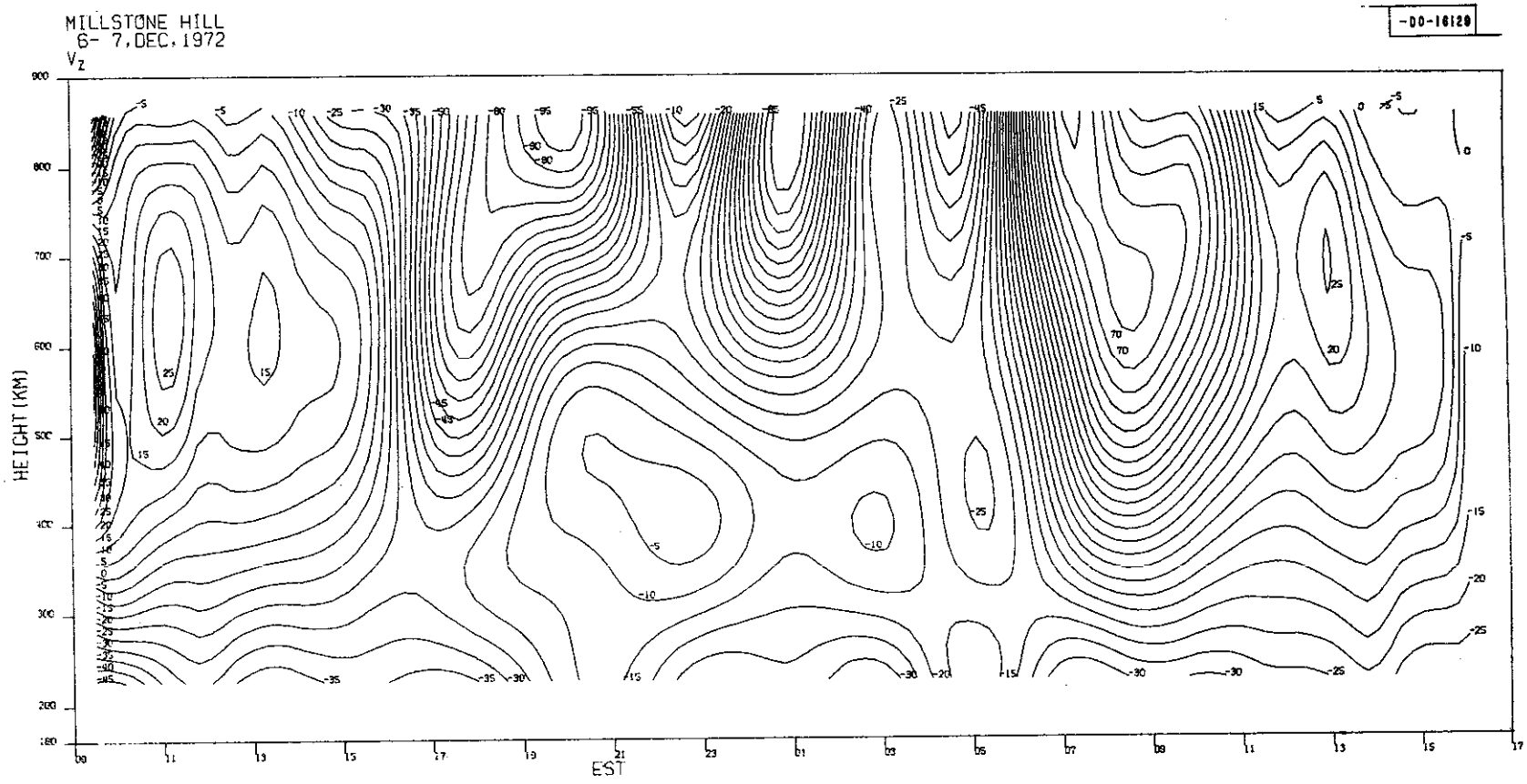

(d) V_z.

Fig.26(a-d). Continued.

The contours of vertical velocity V_z are plotted at intervals of 5 m/sec and have been corrected for the frequency "chirp" introduced by the transmitter.[7] Since the beam is directed at an elevation of 88° due south, the drift component of the plasma that is measured is not precisely vertical, but for most purposes the distinction is unimportant.

Values of the drift observed with the L-band radar usually were very scattered at night and quite unreliable. Accordingly, these measurements have not been included in this report. These data have, however, been employed by Kirchhoff and Carpenter in a study of the diurnal variation of the ionospheric polarization electric field over Millstone and its dependence on magnetic activity.[26]

During 1972, the $F_{10.7}$ solar flux continued to decline as sunspot minimum was approached. Despite this, observations appear to have been made on at least six days that were somewhat disturbed (i.e., with mean Kp given in Table III exceeding 3_o).

B. Quiet Winter Behavior

There is a characteristic quiet-time winter and summer behavior of the ionosphere over Millstone that has been discussed in many previous reports.[5-9] In winter, the electron density exhibits a pronounced diurnal variation with the daytime densities near $h_{max}F2$ exceeding the nighttime densities by a factor of 10 and exceeding the midday density in summer also. As sunspot minimum is approached, this seasonal variation becomes less pronounced. In addition, the F-layer is formed lower in altitude as the neutral atmosphere density of all levels of the thermosphere is reduced. Both of these trends can be detected in the results presented here from a study of Figs. 9(a), 15(a), 18(a), 19(a), 24(a), and 26(a).

One interesting feature, discussed in a number of previous papers[3,6,27] and reviewed in Ref. 7, is the increase in N_{max} that occurs over Millstone during many quiet winter nights. This feature is evident in Figs. 7(a) and 26(a). Typically, N_{max} declines during the evening and reaches a minimum a little after midnight. The density then may remain constant for many hours or increase reaching a peak between 0200 and 0400 local time (LT). Our earliest attempt to explain the phenomenon[27] was to invoke a downward flux of ionization from the magnetosphere. We sought to explain the timing of the increase by noting that the conjugate point to Millstone remains sunlit throughout the winter night and perhaps the heat flux into the tube of force reached its minimum near midnight when the solar zenith distance at the conjugate point reached its maximum. The subsequent cooling of the field tube then caused the flux into the local ionosphere. Subsequent theoretical and experimental work (reviewed in Ref. 7) have shown these ideas to be untenable.

We now believe that the timing of the event can be explained quite simply as a consequence of the diurnal variation of the exospheric temperature. This reaches its minimum at about 0300 LT with the result that the abundance of atomic oxygen in the thermosphere is at a minimum, while that of neutral hydrogen is at a maximum. This is just the condition necessary to cause the charge exchange reaction from H^+ to O to proceed most rapidly, thereby ensuring that the protonospheric flux is downward and large. We discuss this further in Sec. V-B.

C. Disturbed Winter Behavior

At midlatitudes, magnetic storm effects tend to be less pronounced in winter than summer (see, for example, Prölss[28]) and this is thought to indicate that the composition changes in the neutral atmosphere resulting from the storm-induced changes in the thermospheric wind system

are more pronounced in the summer than the winter hemisphere. We have suggested that this arises because the auroral heat deposited during the storm is greater in the summer hemisphere, because the prevailing ionospheric electron densities are larger and this leads to a larger joule heating.[29] At all events, large storm-associated depressions of the daytime electron density are uncommon at Millstone in winter and the most obvious manifestations of disturbed activity tend to be the presence of large TIDs and/or the anomalous behavior of N_e, T_e or V_z at night.

A very large oscillation in h_{max} and electron density between midnight and 0600 LT is evident in Fig. 6(a) that appears to be the result of a long-period TID. There are corresponding oscillations (of appropriate sign) in the electron temperature and vertical velocity. Similar behavior, albeit less pronounced, was evident on 23-24 February [Fig. 8(a)] and 3-4 October [Fig. 24(a)].

Other recognizable features of disturbed nighttime behavior include: (1) enhanced E-region densities (presumably produced by precipitating particles) and (2) enhanced electron F-region temperatures which may be produced by particle precipitation or large heat fluxes from the plasmasphere resulting from the decay of ring-current particles. There seem to have been no instances when overhead particle precipitation was observed at Millstone during 1972. However, there was a large nocturnal increase in electron temperature observed on 24 February [Fig. 8(b)]. It is tempting to attribute this to protospheric heating, since there appears to be no E-region density increase. The oscillation of h_{max} especially between 0600 and 1000 LT is most unusual and probably indicative of large electric field effects. Unfortunately, a clear-cut association is not possible on the basis of the data presented here, and it is possible that the temperature increase is a predawn effect associated with conjugate sunrise. Comparing Figs. 8(b) and (d), it is evident that the temperature increase caused a very large expansion of the layer above $h_{max}F2$ of the type normally seen at local sunrise.

The results for the other disturbed winter day (15-16 November) contain several gaps, making it difficult to draw firm conclusions on possible nocturnal temperature increases, but no obvious ones appeared during the periods for which good measurements are available.

Large perturbations in the height of the layer peak have been noted previously[7] on disturbed winter nights and, following the work of Park[30] and Park and Meng,[31] usually have been attributed to the presence of substorm electric fields. While such is often the case, we recently have recognized that long-lived lifting of the layer centered on about 0100 LT probably has a different origin. A particularly striking example was observed on 23-24 March [Fig. 10(a)]. Based upon observations of 6300-Å airglow, Hernandez and Roble[32] and others have found that there often are large equatorward winds on magnetically disturbed nights near midnight. These strong winds appear to be caused, in part, by the acceleration provided to the air as it crosses the polar cap by the rapid electric field-induced motion of the ions (at speeds of several hundred meters/second) and, in part, by heat deposited along the auroral oval which expands the air in the polar cap region. Since neutral winds can be derived from the incoherent scatter results presented here,[9] these disturbed nighttime cases are of special interest and are the subject of a separate study.

D. Quiet Summer Behavior

In summer time, the electron density at levels near $h_{max}F2$ is lower than in winter during the daytime by an amount that increases at sunspot maximum. It now is recognized that this

reflects a change in the composition of the neutral air at these levels introduced by horizontal transport of atomic oxygen from the summer-to-winter hemisphere.[7,9]

The diurnal variation differs also in that the largest electron density is encountered near sunset and not near midday. The electron temperature exhibits a much larger diurnal variation at Millstone in summer than winter, as then conjugate heating is absent at night. The switch from "winter" to "summer" behavior is quite rapid, occurring within a week or two of equinox. In the present data set, 26-27 April (Fig. 11) is the first day to exhibit the quiet summer behavior and 12-13 September (Fig. 23) the last.

We earlier attempted to account for the evening increase in N_{max} in terms of the contraction of the layer (or collapse) that occurs when the electron temperature decreases at sunset.[11] Subsequent observations of vertical ion drifts[33] confirmed that there are indeed large downward drifts of the ions above $h_{max}F2$ at sunset as a consequence of the cooling of the layer. These lead to downward fluxes through 650 km at sunset of the order 5×10^8 ions/cm^2 (Ref. 7).

An alternative explanation for the phenomenon put forth by Kohl and King[34] and Kohl et al.[35] is that it is caused by the reversal of the meridional component of the neutral wind. During the daytime, the wind blows poleward tending to drive the layer (along the magnetic field direction) to lower altitudes where the recombination rates are higher. At night, the situation is reversed and this accounts for the smallness in the diurnal variation of the F-layer, especially in summer when the night is short. Kohl and King[34] and Kohl et al.[35] proposed that the wind direction reversed earlier in winter than summer and experimental results supporting this were obtained using incoherent scatter observations by Vasseur.[36] Figure 27 illustrates this effect in results for the neutral air winds obtained from Millstone.

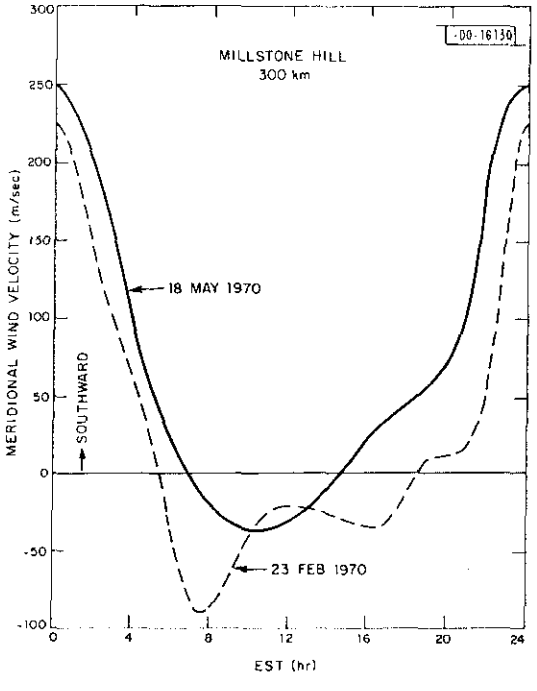

Fig. 27. Estimates of the meridional wind velocity at 300 km derived from incoherent scatter results showing the earlier reversal from northward to southward winds in the afternoon in summer (J.E. Salah, private communication).

The role of neutral air winds in generating an evening increase has been confirmed by the detection of a magnetic declination effect in the size of the increase[37,38] and computer simulation studies.[39] At this juncture, it appears that, while both effects may play a role, that of the winds is the more important.

E. Disturbed Summer Behavior

Owing to the shortness of the night at F-region heights in summer, disturbed behavior resulting from particle precipitation, electric fields or heat fluxes is less often observed than in winter. The most striking feature is a depression of the F2-region peak density sometimes to values below that of the F1. This behavior is thought to be caused by an increase in the rate of migration of atomic oxygen out of the summer hemisphere. Only one day (30-31 May) was disturbed significantly and the densities on this day were [Fig. 14(a)] below normal [cf. Figs. 13(a) or 15(a)]. In addition, h_{max} exhibited an oscillatory behavior between about 1500 and 0300 LT with associated oscillations of V_z suggesting the presence of large-scale TIDs.

While these large-scale TIDs tend to be associated with magnetic activity, this is not always the case. There appears to have been a fairly pronounced TID on 9-10 May (Fig. 12) during a period for which the average value of the Kp index was only 2+. Similar findings were reported in Ref. 9.

IV. RESULTS FOR H^+ DENSITIES AND FLUXES

A. General

The signal spectra of the reflections over the altitude interval 450 to 1125 km, approximately, are measured at intervals of 75 km using a pulse that yields a height resolution of 150 km. Normally, these spectra are analyzed to yield estimates of T_e and T_i assuming that O^+ is the only ion present. It also is possible to reanalyze these spectra to yield estimates of the H^+ percentage as well as T_e and T_i. The computer program employed for this was written by J. L. Massa[40] and modified subsequently by R. Julian. Unfortunately, the program is slow, owing to the large search that must be undertaken, and thus far this has limited the number of days that could be examined.

Early attempts to use this program were for data gathered in 1969, i.e., close to sunspot maximum.[18,19] Subsequently, the program was used to reduce data gathered in 1972 and 1973, i.e., nearer sunspot minimum. We believe that the results are of great interest since they allow conclusions to be drawn concerning the proton fluxes between the ionosphere and magnetosphere over Millstone.

In this section, we discuss the data reduction to obtain estimates of H^+/N_e from incoherent scatter results, report values obtained for eleven of the days listed in Table III, and discuss the implications of these results on the nighttime protonospheric fluxes. This last topic represents a major advance on a previous study[19] whose conclusions were not thought to be very reliable.

B. Data Reduction

The program employed to determine the H^+ concentration is run separately from the ANALYSIS and INSCON programs used to generate the results described in Sec. III. To date, it has been used only to examine the C-mode spectrum results recorded on the original data tape. The program is required to search for the best fit between the measured spectrum and the theoretical

spectrum describing the scattering from an H^+/O^+ ion mixture. To do this, a search is conducted in a library of calculated autocorrelation functions for the one that most closely resembles the Fourier transform of the measured spectrum. The matching of correlation functions rather than spectra facilitates the calculation of the instrumental effects (below). The library is calculated separately and the resulting functions are stored on the drum of the XDS 9300 computer. Unfortunately, there are four variables in all, viz: H^+/N_e, T_e, T_i, and the variable α^2, where

$$\alpha^2 = \left(\frac{4\pi D_e}{\lambda}\right)^2 \tag{1}$$

in which

$$D_e = 6.9\sqrt{\frac{T_e}{N_e}} \quad \text{cm} \tag{2}$$

is the electron Debye length when N_e is in electrons/cm^3. For Millstone (where λ = 68.18 cm)

$$\alpha^2 = 1.62\left(\frac{T_e}{N_e}\right) \quad {}^\circ\text{K cm}^3 \quad . \tag{3}$$

The dependence upon T_i can be eliminated for the purpose of computing the library of correlation functions, since it controls the scale of the time axis only, and not the shape of the function.

As shown by Moorcroft,[41] it becomes difficult to solve for the H^+/N_e ratio as $\alpha^2 \rightarrow 1.0$. Accordingly, the present library of spectra has been computed over a range of cases that includes:

T_e/T_i = 0.8 to 3.0 in 0.2 steps

H^+/N_e = 0.0 to 0.4 in 0.1 steps

α^2 = 0.0, 0.01, 0.025, 0.04, 0.057, 0.074, 0.09, 0.17, 0.25, 0.33, 0.41, 0.49, 0.60

T_i = 800°K .

These theoretical autocorrelation functions are computed for points 10 μsec apart and scaled in delay (by parabolic interpolation) in order to match the actual ion temperature at each iteration performed during the best fit search.

The limited range of H^+/N_e ratios was chosen after an analysis of the 1969 results[18,19,40] showed that at the greatest altitude for which it was thought that reliable estimates could be obtained (825-km nominal height), the H^+ percentage rarely if ever exceeded 40 percent. Subsequent analysis of days in 1972 and 1973 showed that nearer sunspot minimum, this rule was increasingly violated at high altitudes on winter nights. Accordingly, it is believed that the program probably does not yield reliable results for those altitudes where the H^+ abundance exceeds 50 percent. Despite this limitation, useful conclusions can be drawn and no attempt has been made to recompute the library to include cases for H^+ percentage greater than 40 percent.

To allow for instrumental effects on the observations, each experimental spectrum is corrected for the effect of gating the transmitter and sampling the output of a receiver containing a bank of matched filters. This causes the Doppler-broadened power spectrum of the medium $W(\omega)$ to be convolved with a function

$$j(x) = \frac{2}{\pi T x^2}\left[1 - \frac{\sin(xT)}{xT}\right] \tag{4}$$

where $x = \omega - \omega'$ in which ω' is the angular frequency at which the power is observed and T is the pulse length (1 msec). To remove this effect, the experimental spectra are Fourier transformed and the result is divided by the Fourier transform of Eq. (4) namely,

$$j(\tau) = \left[1 - \frac{|\tau|}{T}\right]^2 \tag{5}$$

which is simply a triangular weight function. Since Eq. (5) tends to zero at $\tau \rightarrow T$, it is important to limit the range of τ values over which a match is sought between the measured and theoretical autocorrelation functions.[40]

A second instrumental effect is the limited range of frequencies sampled by the filter bank (±11.5 kHz). This imposes a further weighting of the measured spectra. This cannot be removed and hence it was necessary to weight the theoretical autocorrelation functions to reproduce the same effect. This was accomplished by interpolating the calculated autocorrelation functions (at 10-μsec intervals) by parabolic interpolation to achieve points every 5 μsec. This function then was Fourier transformed, weighted over the frequency range of filter bank by a weight w(f).

$$w(f) = 1 \quad -12 \leqslant f \leqslant +12 \text{ kHz}$$

$$= 0 \quad \text{elsewhere}$$

and then transformed back to an autocorrelation function. The use of points every 5 μsec was deemed necessary to avoid aliasing when the ion temperature becomes much larger than the nominal value of 800°K, causing the time interval between the points of the function to be reduced.[40]

The computer search involves selecting an initial best guess of T_i, T_e/T_i, H^+/N_e, and α^2. Various approaches to selecting this initial best guess have been tried such as using the results from the previous lower height. However, it seems best to use the results of the ANALYSIS reduction for T_e and T_i and set $H^+/N_e = 0$. The value of α^2 can be calculated [via Eq. (3)] and in selecting the appropriate value of N_e from the ANALYSIS profile, allowance is made for the difference (~25 km) between the nominal and weighted mean height to be associated with each spectrum. Having obtained this estimate (e.g., α_1^2), a search is conducted for a match between the measured (corrected) autocorrelation function and any of the set calculated for the value of α^2 closest to α_1^2. The selected autocorrelation function is expanded to first order in a Taylor's expansion to allow calculation in the intervals between H^+/N_e and T_e/T_i grid points and a linear least squares fit is performed to minimize the weighted sum of the differences between the measured (corrected) autocorrelation function and the theoretical one. This is carried out at seven points spaced at τ = 41.66 μsec (1000/24 μsec) apart. The weights are chosen to reflect the variation of signal-to-noise ratio in the measurements.[40] This process is repeated to optimize the estimate of T_i.

After a solution has been obtained, the revised value of T_e is used in Eq. (3) to recalculate α^2. If the value so obtained (e.g., α_2^2) now is closer to another set within the library, the search is conducted again. The entire process is stopped after 15 iterations or whenever α_n^2 has not changed sufficiently to alter the best library set to use. Values of α^2 greater than 0.6 are encountered and for these cases, $\alpha^2 = 0.6$ library is used, and the results are flagged on the printout.

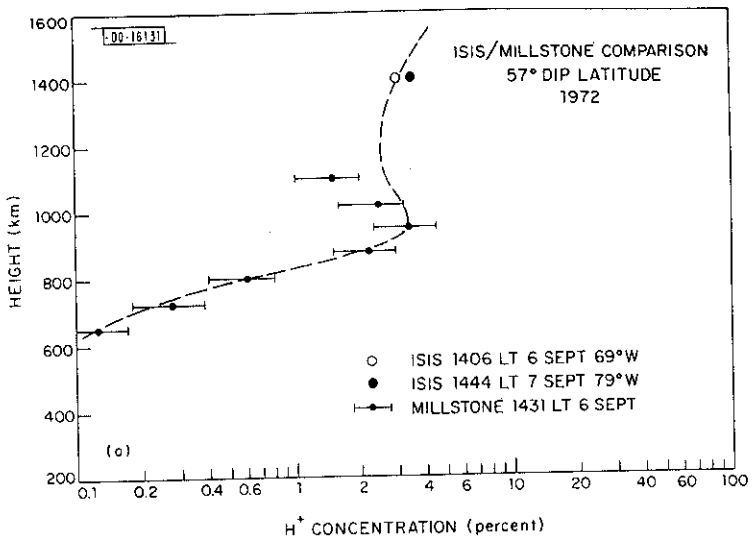

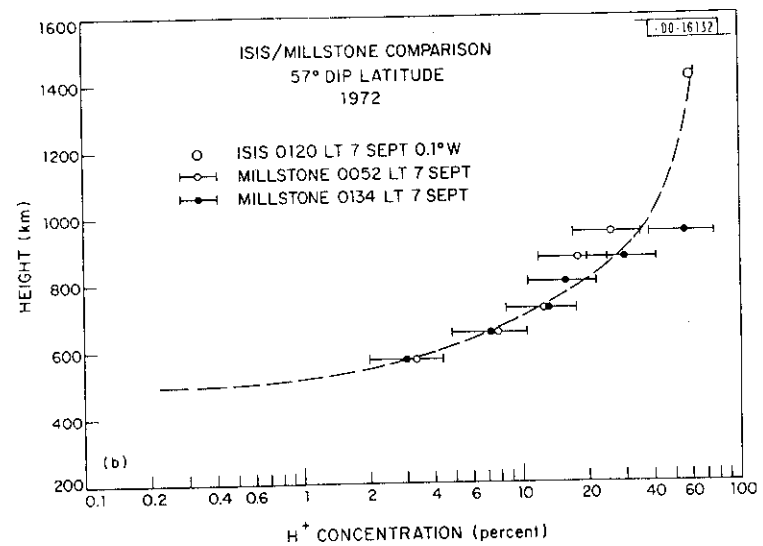

Fig.28. Comparisons of the percentage abundance of H^+ ions at the dip latitude of 57° made by Millstone Hill and the ISIS satellite (J.H. Hoffman, private communication). The broken curve is merely intended to suggest that the two data sets can be connected by a reasonable continuous variation. (a) Daytime and (b) nighttime.

C. Accuracy

It is difficult to assign an experimental accuracy to the H^+ percentage values based solely on an analysis of the accuracy of the experimental spectrum measurements. Some confidence in the incoherent scatter values can be gained by examining them for consistency both with respect to altitude and time. The "drifts" data [6-9] are particularly useful for such analyses. It is found that some fraction of the estimates are outside the range of likely values, and these points also are associated with improbable values of T_e, T_i, and/or T_e/T_i suggesting that a poor solution (i.e., the fit between the theoretical and experimental spectra) has been found. It is thought that these usually are cases where the experimental spectra simply are too noisy to provide reliable results and/or suffer from one or more particularly bad points. Eliminating such cases, it typically is found that the root-mean-square scatter of successive estimates of H^+/N_e at a given height is of the order of ±30 percent.

Comparison has been made with H^+/N_e ratios measured using the mass spectrometer on *ISIS II at 1400-km altitude*[42] on a few occasions in 1972 when there was a pass of the satellite to the east or west of Millstone while the radar also was in operation (John Hoffman, private communication). Since there usually was a significant difference in the longitudes of the satellite and Millstone, the two data sets were compared by selecting the value for the percentage of H^+ provided by the satellite as it crossed the dip latitude (57°) of Millstone Hill. The Millstone values at the same local time then were chosen and an attempt made to combine the two into a single plot. Examples are provided in Figs. 28(a-b), where the broken curves are intended simply to suggest that it is possible to connect the two data sets by a reasonable and continuous curve. The incoherent scatter measurement error bars in this plot have been set equal to ±30 percent.

The ISIS results provided estimates of H^+, He^+, and O^+ and appear to show that for the dip latitude of Millstone, He^+ always remains a minor ion so that its neglect in the interpretation of the incoherent scatter results can be justified – at least as a first approximation.

D. Results

For the present study, eleven days in 1972 were analyzed. They were:

25-26 January	12-13 July
23-24 February	7-8 August
9-10 May	6-7 September
30-31 May	15-16 November
13-14 June	6-7 December
30 June – 1 July	

The diurnal variation of H^+ percentage at the highest altitude for which reliable estimates could be obtained (usually 825-km nominal altitude for which the effective weighted height of the pulse lies near 800 km) is shown in Figs. 29(a-k). Where the density at this height exceeded 50 percent, results for the next lowest height are given.

The diurnal variation of the H^+ percentage concentration at a single altitude for four days in 1969 were published previously.[18,19] A marked difference in abundance appeared to exist between summer and winter days with the latter exhibiting higher abundances. This difference was attributed to the annual variation in the mean exospheric temperature.[43] During the daytime, the H^+ percentage at 800 km was found to be quite small – usually <1 percent. Beginning

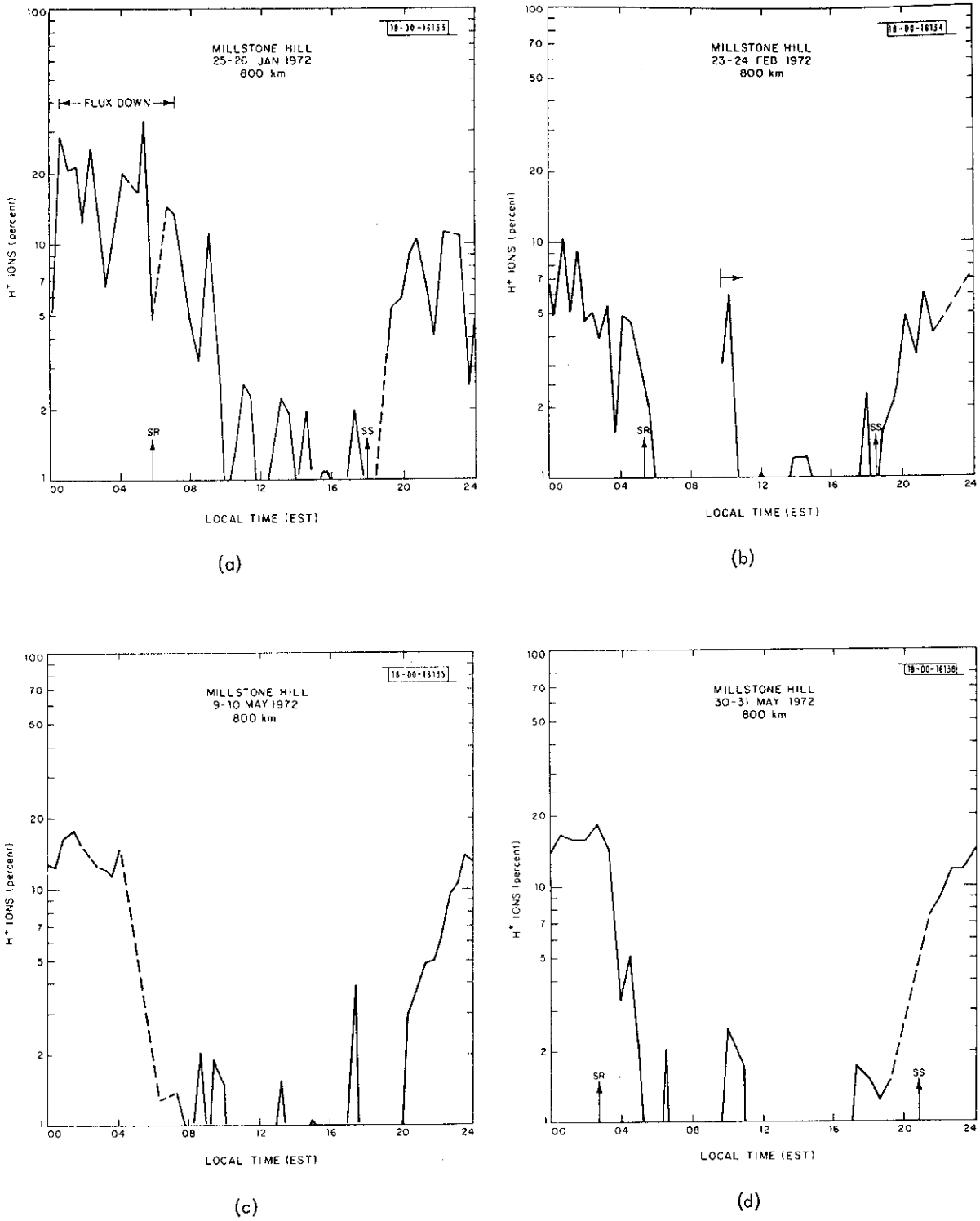

Fig.29(a-k). Estimates of the percentage of H^+ ions over Millstone Hill vs local time in 1972.

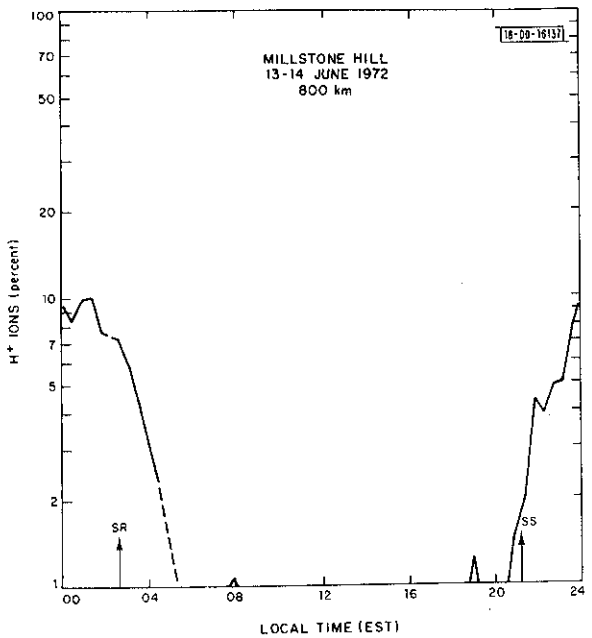

(e)

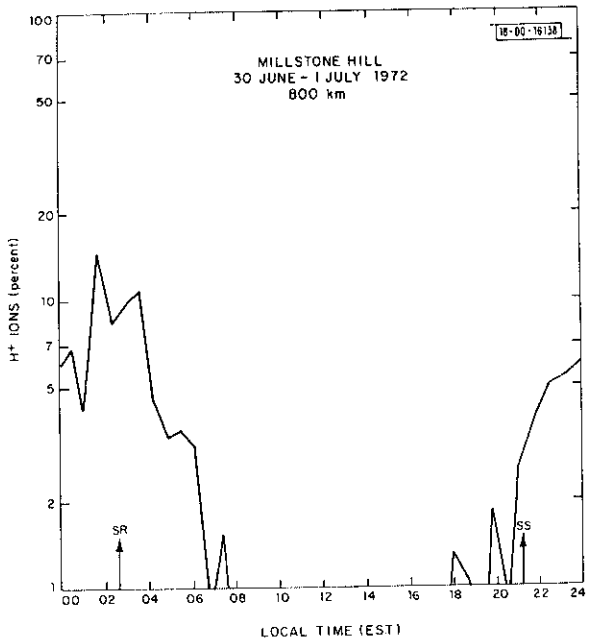

(f)

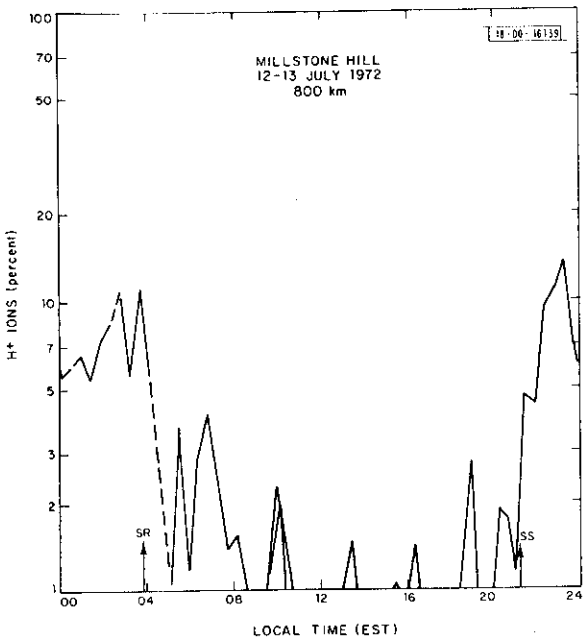

(g)

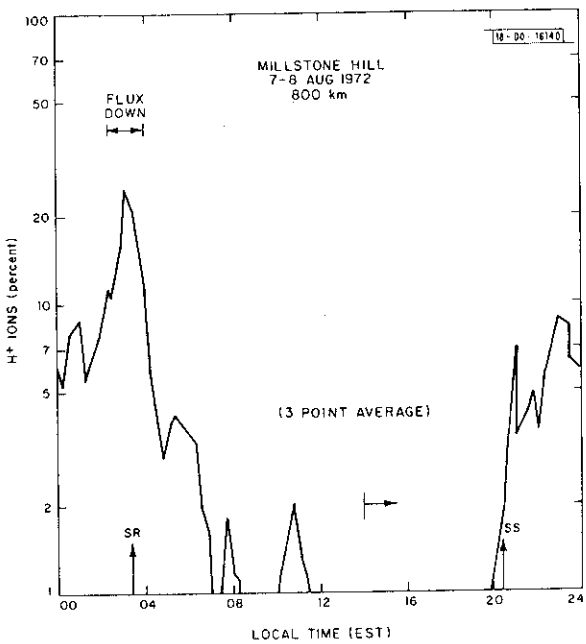

(h)

Fig.29(a-k). Continued.

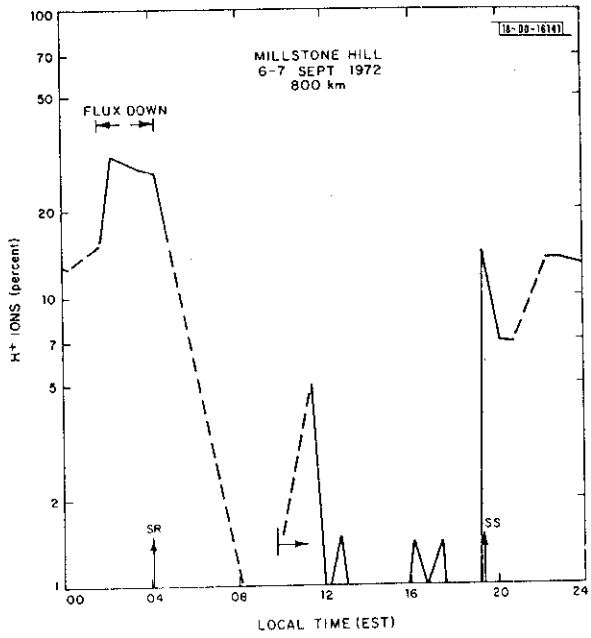

(i)

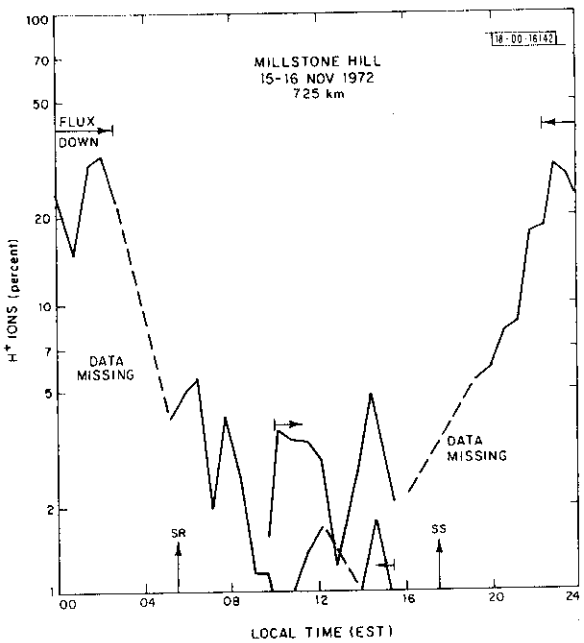

(j)

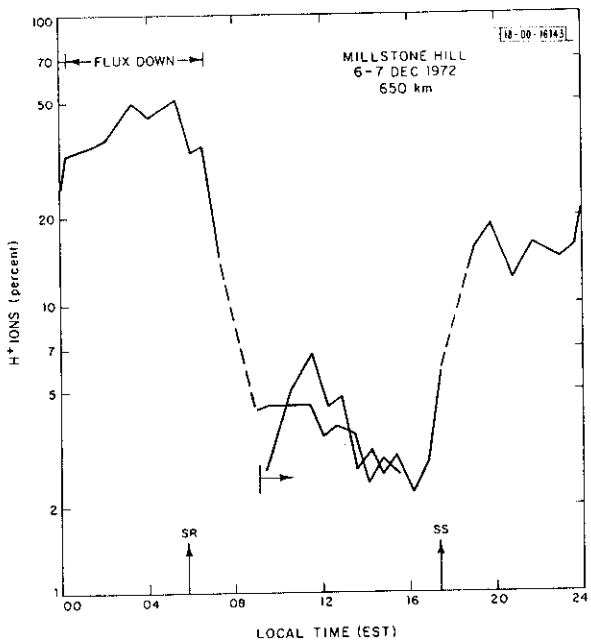

(k)

Fig.29(a-k). Continued.

just before midnight, it usually increased, reaching a maximum just before ionospheric sunrise. During 1969, this peak value typically was ≤10 percent in summer and in the range 10 to 30 percent in winter at 800 km. These small values of H^+ percentage made it difficult to construct vertical profiles of H^+ density and tended to suggest that at this phase of the sunspot cycle, the H^+ flux at Millstone was upward both by day and by night except for perhaps a few hours prior to sunrise on some winter nights.

In an effort to test this conclusion, additional days in 1972 and 1973 were analyzed, with the expectation that the lower exospheric temperatures then prevailing would cause the H^+ abundance to be larger.[44,45] This expectation was borne out as indicated in Figs. 29(a-k), which provide examples of the winter and summer behavior in 1972.

It is clear that as sunspot minimum is approached, larger amounts of H^+ can be detected over Millstone at 800-km altitude. In 1972, the H^+ concentration found in summer remained small throughout the night and hence it appears that the flux was still upward at all times. By contrast, in winter, a period when the flux is downward clearly can be identified that persists between midnight and ionospheric sunrise (Sec. F).

E. H^+ Concentration Profiles

By combining the percentage of H^+ estimates with the electron density profile (deduced separately), it is possible to construct a profile of H^+ vs altitude. Figure 30 provides such a

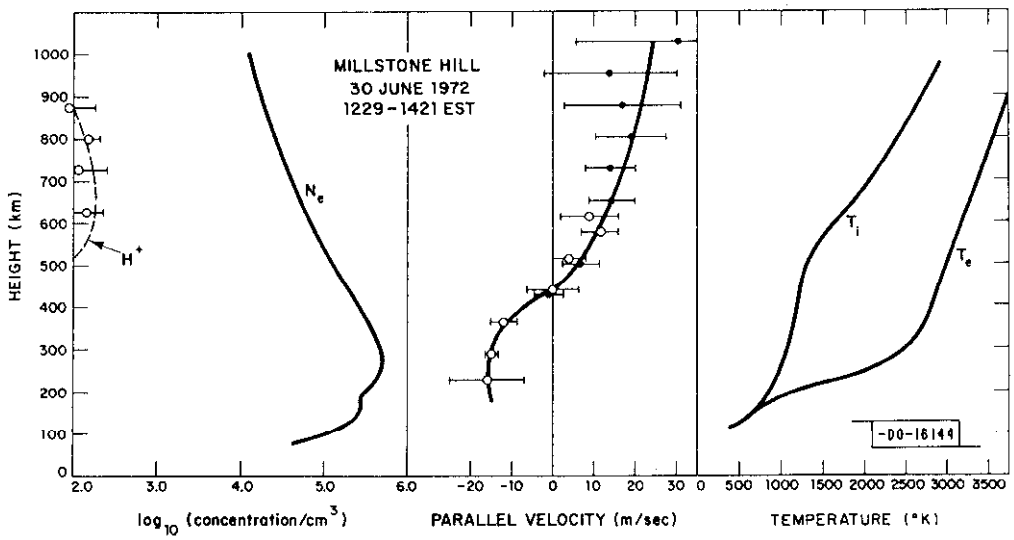

Fig.30. Example of the daytime altitude variations of N_e, $N(H^+)$, O^+ ion velocity, T_i, and T_e observed over Millstone Hill in 1972.

plot constructed using data gathered over a 2-hour interval near noon on 30 June 1972. In these measurements, the plasma drift in the N-S magnetic meridian plane was measured using the smaller L-band steerable radar system, allowing the ion velocity to be resolved into components along and perpendicular to the magnetic field. In Fig. 30, the parallel component is plotted and exhibits the usual transition from downward to upward O^+ flux above about 500 km. Also shown in Fig. 30 are the electron and ion temperatures. Where plotted, the error bars indicate the root-mean-square scatter of the points gathered at each altitude over the 2-hour interval.

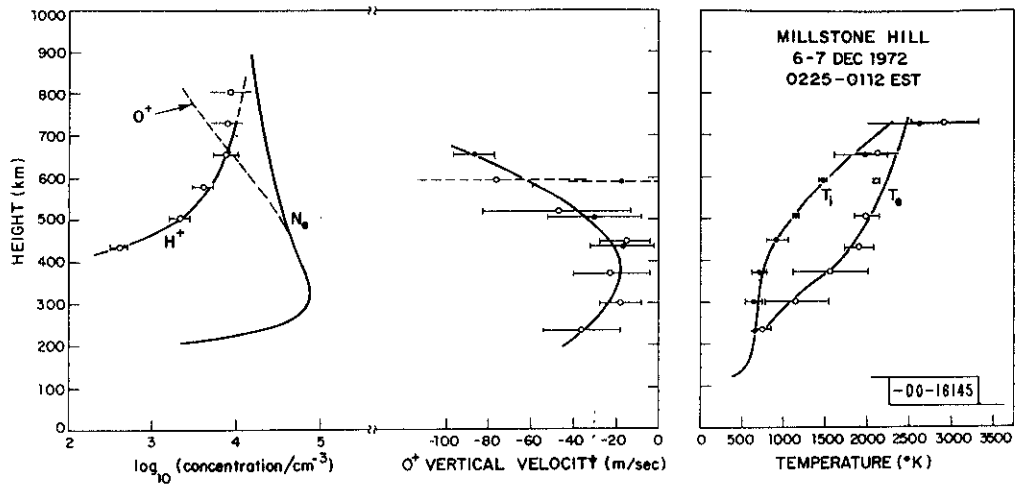

(a) Winter.

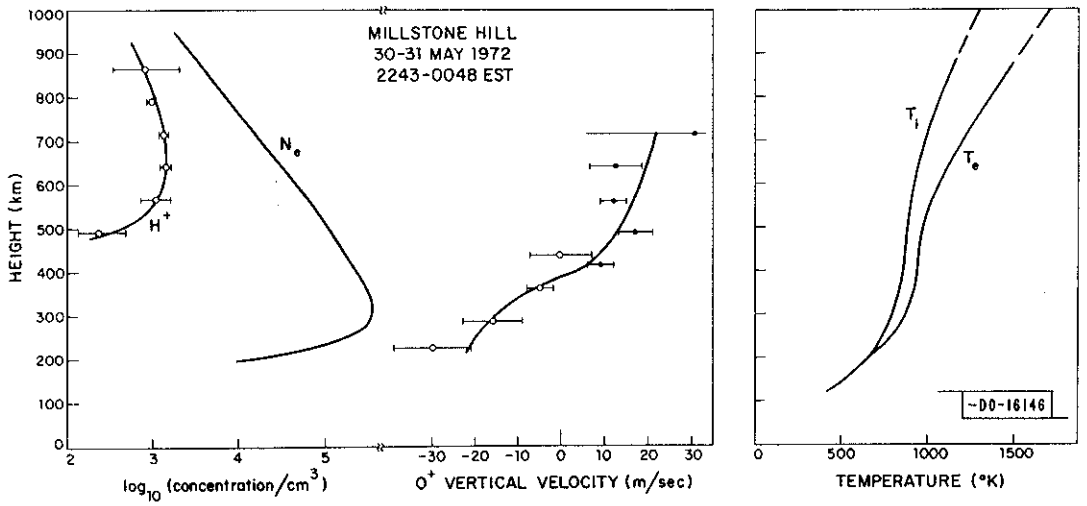

(b) Summer.

Fig.31(a-b). Examples of the nighttime altitude variations of N_e, $N(H^+)$, O^+ ion velocity, T_i, and T_e observed over Millstone Hill when the H^+ flux appeared to be large.

The H^+ profile exhibits a peak value near 600 to 700 km that is a characteristic of the variation expected when the flux is upward and close to its limiting value (cf. Sec. F). This behavior appears to prevail over Millstone during the daytime in all seasons and over most of the sunspot cycle. (We have not examined yet the behavior at exactly sunspot minimum.) In sum, it seems that whenever the flux is upward (as it always is in the daytime), it is close to its limiting value.

Examples of the behavior found at night are shown in Figs. 31(a-b). The results plotted in Fig. 31(a) are typical of winter night conditions. The H^+/O^+ transition altitude on this occasion appears to be near 650 km, and hence the H^+ flux is almost certainly downward, albeit with a value that cannot reliably be estimated from the H^+ abundance curve alone.

Some idea of the arriving flux can be gathered from the O^+ vertical velocity results. In this instance, the velocity is not constant at all altitudes as would be expected if the layer simply were descending. Instead, the values between 400 and 600 km suggest that there is a downward flux of O^+ ions of 2.1×10^8 ions/cm^2/sec that is independent of altitude. The constancy of the flux implies that these ions were created by charge exchange with H^+ ions at some greater height. Some contribution to this value may be caused by any descent of the layer, but probably this will be small. Thus, the arriving H^+ flux at this time appears to have a value of approximately 2×10^8 ions/cm^2/sec.

In Fig. 31(b), we show an example of the summer night behavior. In this case, the H^+ concentration exhibits a peak near 650 km and then declines suggesting that the flux is upward. This conclusion is supported by the O^+ vertical velocity results which show that above about 400 km, the O^+ flux is positive with a value of about 1.2×10^8 ions/cm^2/sec. This would appear to be a lower limit on the H^+ flux escaping as the layer as the whole appears to be descending (based on the velocity measurements obtained near the layer peak). If it is assumed that the velocity observed near the layer peak is the best estimate of the downward velocity of the layer as a whole, then the escape flux must be $\sim 2 \times 10^8$ ions/cm^2/sec. This case seems quite similar to the behavior predicted by Bailey et al.[46] from their time-dependent model for 2300 LT in March 1970, although the escape flux then was considerably smaller.

If the layer is decaying rapidly, then the O^+ flux may everywhere be downward, even though the H^+ flux is upward.[46] In this case, the O^+ velocity observed by the radar will everywhere be negative. This is the more usual situation encountered at Millstone, and is illustrated in Fig. 32.

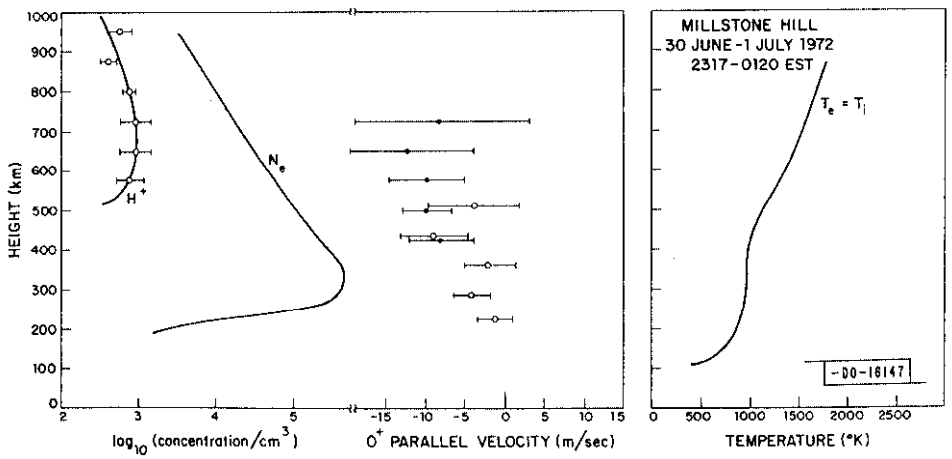

Fig.32. More usual example of the nighttime altitude variations of N_e, $N(H^+)$, O^+ ion velocity, T_i, and T_e observed in summer. Here the H^+ flux is thought to be weak (see text).

It usually is impossible to secure useful oblique-incidence drift measurements using the L-band radar at night and hence the observed vertical velocity cannot be resolved into components parallel and perpendicular to the field line. The observed vertical velocity then must be assumed to be caused entirely by drifts parallel to the field line, and at night the scatter in these measurements also becomes large when the signals are weak. Thus, if the H^+ escape flux is small, it may be difficult to infer its value from the vertical O^+ flux estimates obtained at Millstone. Nevertheless, it usually can be established whether the flux indeed is upward (Sec. F).

F. H^+ Fluxes

Protons are created in the F-region by the charge-exchange reaction

$$O^+ + H \rightleftharpoons H^+ + O \qquad (6)$$

where the forward and reverse reaction rates may be found in Banks et al.[47] H^+ ions are created [via Eq. (6)] in the daytime and diffuse upward within the flux tube in an effort to establish a diffusive equilibrium distribution of their own. The upward H^+ flux is limited by the fact that the ions are created chiefly at altitudes just above the F2 peak (i.e., where the O^+ concentration is large) and then must diffuse some considerable distance through the neutral atomic oxygen with a finite likelihood of being converted back to O^+ [via the reverse reaction Eq. (6)]. This leads to the concept of a limiting escape flux[48,49] which is the maximum possible upward flux that can be sustained for a given H^+ production rate.

In the region where H^+ is a minor ion, its concentration can be found by solving the coupled equations of continuity and momentum for O^+ and H^+ and allowing for diffusion under the influence of thermal gradients.[50] Figure 33 illustrates the essential features of such calculations; it is evident that the H^+ concentration is quite sensitive to the value of the flux when this is upward. In Fig. 33, the limiting or critical escape flux $\overline{G}_p$ is 1.45×10^7 ions/cm^2/sec and curves of H^+ concentration are shown for values of upward flux G_p = 1.0, 0.9, 0.6, 0, −1.0, and −3.0 times

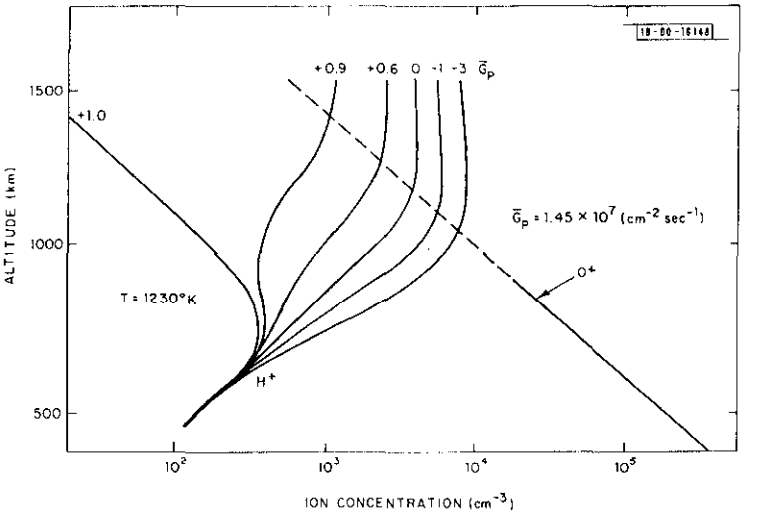

Fig. 33. Idealized curves of H^+ and O^+ concentration for various values of the H^+ flux. Here the O^+ flux is zero and $\overline{G}_p$ is the critical escape flux for H^+ (after Geisler[49]).

this amount. It can be seen that for zero or downward fluxes, the H^+ concentration initially is found to increase approximately as fast as the O^+ ion density decreases – until the transition altitude [$N(O^+) = N(H^+)$] is reached. For significant positive fluxes, however, the H^+ density increases less rapidly, thereby raising the transition altitude considerably. As the escape flux approaches the limiting value, the H^+ concentration may exhibit a peak in the upper part of the F-region and remain a minor ion throughout the region accessible to observations from Millstone Hill ($\leq$1000 km).

The curves of Fig. 33 were constructed for an isothermal ionosphere[49] ($T_n = T_i = T_e$ = 1230°K) and realistic altitude variations of the temperatures ($T_e \geq T_i \geq T_n$ during the daytime) will modify the distribution somewhat – tending to increase the transition altitude. However, the role of the temperature distribution is less important than the magnitude of the flux, whenever this is both positive and close to its limiting value. Use can be made of this feature to attempt to identify periods when the flux over Millstone Hill is upward.

From Fig. 33 and other more realistic calculations conducted by Banks and Kockarts,[51] Narasinga Rao and Jain,[52] and others, it appears that a practical guide to the identification of intervals when the flux is large and downward is to search for periods when the transition altitude <1000 km, and therefore in view of the radar. In practice, the most reliable H^+ (percent) values at Millstone appear to be obtained near 800 km, i.e., about one scale height below 1000 km. Thus, the actual test for large downward flux has been to find periods when the H^+ abundance at 800 km > 20 percent. Where good results are obtained at higher altitudes, they appear to support this rule.

From an inspection of the H^+ vs altitude and time variations, we have attempted to find the times over which large arriving fluxes appear to be present. These are listed in Table IV, which includes results obtained for 1969 and 1973. It is clear that periods of downward flux are confined to winter nights near sunspot maximum, but are encountered on summer nights near sunspot minimum (albeit for shorter periods, as a rule, than in winter). They always end shortly after ionospheric sunrise, and appear to begin earlier as sunspot minimum is approached.

V. DISCUSSION OF THE RESULTS FOR H^+ DENSITIES AND FLUXES

A. Comparison with Previous Experimental Findings

Previously, efforts to measure the concentrations of light ions in the upper part of the F-layer and infer the presence of exchange fluxes have been made from incoherent scatter observations at Arecibo (e.g., Ho and Moorcroft[53]), from in situ ion mass spectrometer measurements[42,54-58] and from topside electron density profiles.[59-60]

The in situ results have identified a region of very low light ion concentration that commences at high latitudes and extends over the polar cap (the so-called "light ion trough"). This phenomenon has been attributed to the continuous escape of H^+ ions at high latitudes at values close to the critical flux along open field lines (sometimes called the polar-wind). Banks and Doupnik[59] have shown from topside sounder records that the region of rapid escape extends inside the plasmasphere in the morning sector.

Ho and Moorcroft[53] have inferred the existence of very large escape fluxes ($\geq 10^9$ ions/cm^2/sec) over Arecibo. While these values seem overly large in the light of later evidence, the diurnal variation they observed on one day is interesting as the flux was seen to be upward between 2000 and 2400 LT and large and downward near sunrise. Unfortunately, the time resolution of their measurements was poor and results were presented for only a single day.

TABLE IV

PERIODS WHEN THERE APPEAR TO BE LARGE H^+ ARRIVING FLUXES

Year	Date	Begins	Ends	Comment
1969	5- 6 February	–	–	No data above 800 km
	12-13 February	0200	0630	
	9-10 April	–	–	
	23-24 April	–	–	No data above 800 km
	9-10 July	–	–	No data above 800 km
	23-24 September	–	–	No data above 800 km
	20-21 November	0200	0600	
1972	25-26 January	0200	0700	
	23-24 February	–	–	
	9-10 May	–	–	
	30-31 May	–	–	
	13-14 June	–	–	
	30 June – 1 July	–	–	
	12-13 July	–	–	
	7- 8 August	0300	0400	
	6- 7 September	0200	0400	
	15-16 November	2200	0300	
	6- 7 December	0000	0700	
1973	2- 3 January	0200	0600	
	13-14 February	0000	0530	
	22-23 May	–	–	
	18-19 July	2300	0400	
	14-15 August	0200	0400	
	16-17 October	0000	0600	
	13-14 November	0000	0700	

The most extensive study undertaken to date of the light ion distribution appears to be that of Titheridge,[60] who examined 60,000 topside electron density profiles gathered with Alouette I near solar minimum. By fitting theoretical profiles to these, Titheridge has been able to identify the transition altitude [$N(H^+) = N(O^+)$] as a function of local time and latitude. The transition heights observed then were compared with those calculated from charge-equilibrium considerations (i.e., ignoring the presence of fluxes). Titheridge concluded that, within the plasmasphere, the fluxes are downward throughout the night in winter, but in summer become downward only briefly around sunrise. These results are summarized in Fig. 34 and are in reasonable agreement with those reported here. They imply that for much of the night, there is a loss of ionization from the flux tube only in the winter hemisphere as illustrated in Fig. 35. The flux in summer hemisphere is upward tending to sustain the tube content. This allows the flux tube to provide ionization that serves to maintain the winter night ionosphere without incurring large day-to-night changes in tube content.

The Millstone observations suggest that there is a continuous variation of the flux behavior with sunspot cycle. Downward fluxes appear for longer intervals on winter nights as sunspot minimum is approached. On summer nights, the fluxes are upward throughout the night at sunspot maximum, but periods of downward flux are encountered prior to sunrise as sunspot minimum is approached. Large day-to-day variations also occur, presumably in response to changes in exospheric temperature and O^+ density.

Using the ESRO-4 satellite measurements of H^+ abundances during the northern hemisphere summer of 1973, Raitt and Dorling[58] also have come to the conclusion that the flux remains upward at the magnetic latitude of Millstone ($\Lambda = 57°$) at night. They were, however, unable to detect any period when the flux became downward (except at lower latitudes).

B. Control of the Diurnal Variations

Titheridge[60] concluded that the diurnal variations of the fluxes (and hence O^+/H^+ transition heights) are caused primarily by the production and loss of O^+ in the ionosphere. We suggest, however, that variations in the abundance of neutral atomic hydrogen and oxygen jointly exert comparable or greater control.

When the pressure variations in the topside plasma are changing only slowly, the direction of the H^+ flux will depend primarily on the direction of the reaction Eq. (6), i.e., on whether H^+ ions are being created or lost in the F-region.[61] The expectation of upward daytime fluxes and downward nighttime fluxes, thus presupposes that the O^+ variations dominate and that during each day, the protons lost during the previous night are replenished. The finding of upward fluxes at night demonstrates that this cannot always be true. Under conditions of charge-exchange equilibrium, the H^+ ion abundance would be given by Eq. (6). The temporal variation of H^+ ions then will be given by

$$\frac{1}{N(H^+)} \frac{\partial N(H^+)}{\partial t} \approx \left[\frac{1}{N(H)} \frac{\partial N(H)}{\partial t} + \frac{1}{N(O^+)} \frac{\partial N(O^+)}{\partial t} - \frac{1}{N(O)} \frac{\partial N(O)}{\partial t} \right] \tag{7}$$

i.e., the relative variation of H^+ with time is controlled by the relative variation in the other three constituents, when variations in the temperature ratio T_n/T_i (which are small) are neglected. It follows that in order to generate an upward flux at night, the percentage <u>increase</u> in H together with the percentage <u>decrease</u> in O per unit time must exceed the percentage decrease in O^+ per unit time.

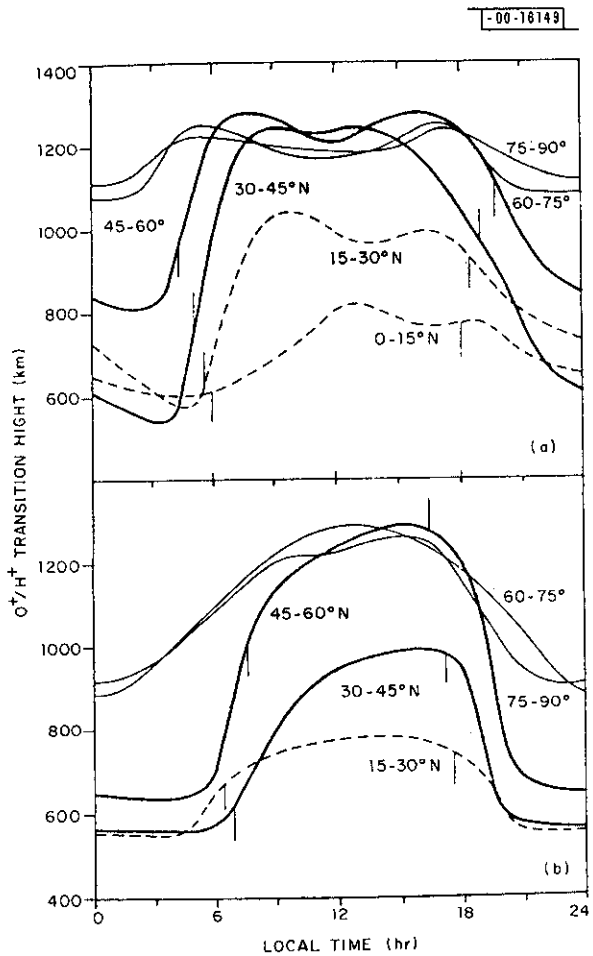

Fig.34. Observed $O^+ - H^+$ transition heights at midlatitudes derived by Titheridge[60] in 1976 from topside sounder profiles: (a) summer and (b) winter. Broken lines show the altitudes computed assuming no vertical fluxes. Where the observed heights exceed those computed, the flux is presumed to be upward.

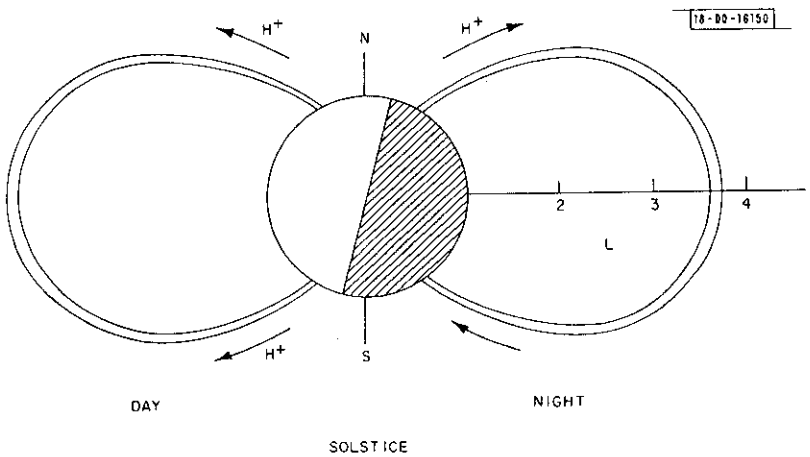

Fig.35. Directions of the H^+ fluxes over most parts of the day and night at solstice (northern summer).

The diurnal variation of O^+ is measured directly in our experiments, while that for atomic oxygen can be inferred quite reliably from models of the upper atmosphere (such as the MSIS model[62]) that are based upon in situ mass-spectrometer measurements. It is possible, therefore, to estimate the abundance of neutral hydrogen from incoherent scatter observations of the H^+ percentage at the level where charge-exchange equilibrium [Eq. (6)] prevails, and such measurements have been made in France (Derieux et al.[63]). This same experiment can be carried out using in situ ion mass-spectrometer measurements of H^+ and O^+ abundances[64-67] and this approach probably has provided the most reliable estimates of neutral hydrogen to date. Additional measurements of neutral hydrogen abundance have been made via satellite observations of the UV Lyman-α airglow intensity.[68-72]

The hydrogen concentration derived from in situ measurements of $N(H^+)$, $N(O^+)$ and N(O), considering charge-exchange equilibrium, exhibits an approximately sinusoidal variation with a maximum at ~0400 LT and a minimum near ~1700 LT, with about a 3:1 diurnal variation (Fig. 36). This variation is in marked contrast to that inferred from some of the Lyman-α airglow measurements, which over the interval 0100 to 0900 LT indicate a predawn depression in N(H) followed by a rapid increase at sunrise. It is possible that the airglow measurements are contaminated in some way by effects at high latitudes, as the simple sinusoidal variation seems more consistent with theory.[73,74]

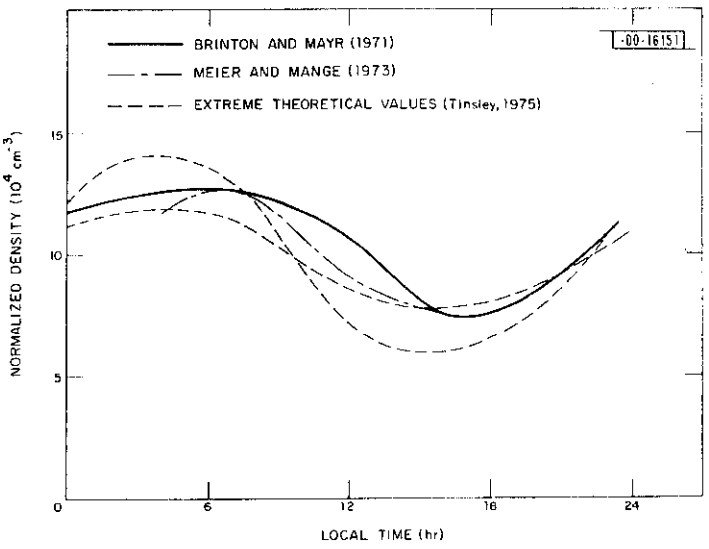

Fig. 36. Diurnal variation of neutral hydrogen according to several sources.[64,70,74]

The diurnal variation of neutral hydrogen has been the subject of a number of recent theoretical studies.[63,73-76] It appears that a 3:1 variation is larger than expected as a result of temperature changes alone, and may reflect the influence on the distribution brought about by charge-exchange with O^+ and thermospheric neutral winds.

According to the MSIS model,[62] O and H have comparable diurnal amplitude variations at altitudes (400 to 500 km) where charge-exchange equilibrium would be expected to prevail, but are almost in antiphase. These variations appear to be sufficient to force Eq. (6) to proceed to the right causing upward fluxes throughout most of the night in summer.

In the MSIS model, N(H) reaches its maximum near 0400 LT while N(O) reaches its minimum near 0200 LT. Thus, following about 0300 LT, the O and H variations always will act in concert with that of O^+ to cause the flux to be downward. In midsummer, sunrise occurs near 0300 and hence there may be only a short period when the flux can be expected to be downward, but in winter when sunrise is later, there always should be a period of downward flux.

These findings serve to explain why the downward flux from the magnetosphere reaches its maximum well after midnight, and hence the timing of the increase in the winter night ionosphere discussed in Sec. III-B.

C. Comparison with Theoretical Models

A number of authors have investigated the coupling between the ionosphere and protonosphere from theoretical considerations. In the most comprehensive treatments, the ionosphere-protonosphere has been modeled as a single unit whose time-dependent behavior has been simulated.[40,46,61,77-80] To avoid a complete solution for the behavior of the F-layer (i.e., including production, loss, winds, and electric fields), it is convenient to adopt a lower boundary for the region to be simulated near 400 km where charge-exchange equilibrium between H^+ and O^+ can be assumed to prevail. One then may appeal to incoherent scatter measurements to establish the O^+ density and temperature at the boundary and the variation of the temperature along the field line. For this reason, a number of the above studies have been carried out to simulate the behavior along the Millstone field (L = 3.2).

The need to adopt an upper boundary condition has forced many authors to treat only the equinox condition when (it is assumed) behavior along the two halves of the field line are identical and there are no interhemispheric fluxes. In the case of Millstone, this condition might never apply totally as the conjugate point (70.7°S, 78.9°W) lies at a very high southerly latitude, where the ionospheric conditions may differ considerably.

In the study conducted by Marubashi and Grebowsky,[61] an attempt was made to avoid this difficulty by adopting additional boundary conditions at 3000 km altitude. The flux through this level was set equal to the rate of change of tube content above, assuming that the distribution is governed by static diffusive equilibrium. These calculations were conducted for sunspot maximum conditions (March 1970) and showed that upward fluxes of $\sim 5\text{-}7 \times 10^7$ ions/cm^2/sec are to be expected during the daytime, i.e., in agreement with the observations we have reported previously.[18] Marubashi and Grebowsky[61] concluded that the nighttime flux becomes downward at sunset and increases in magnitude to a peak of $\sim 1.5 \times 10^8$ ions/cm^2/sec just prior to sunrise. In these calculations, the atomic oxygen abundance at 500 km was taken from the CIRA 1972 model and the diurnal variation of neutral hydrogen was modeled on the results of Brinton and Mayr.[64] These variations, however, were not large enough to offset the diurnal variation in O^+ and thereby maintain the flux upward in the evening hours. This suggests that the competing effects of the variations in O^+, O, and H at the lower boundary make it quite difficult to model the coupling between the ionosphere and protonosphere unless very precise values are available. In contrast to that study, Bailey et al.[46] have found that upward fluxes of H^+ can persist into the evening hours at Millstone based upon calculations employing different lower boundary values.

ACKNOWLEDGMENTS

We are grateful to R. H. Wand, W. A. Reid, L. B. Hanson and others at the Millstone Hill observatory who assisted with the gathering of the data reported here, and to R. Julian and Mrs. Alice Freeman who helped with the data reduction. Dr. J. H. Hoffman kindly provided the ISIS data shown in Figs. 28(a-b), and helpful comments on Sec. IV were provided by Professor R. J. Moffett. The work was supported by the Atmospheric Science Section of the National Science Foundation under Grant No. ATM 75-22193.

REFERENCES

1. J. V. Evans, "Ionospheric Backscatter Observations at Millstone Hill," Technical Report 374, Lincoln Laboratory, M. I. T. (22 January 1965), DDC AD-616607.
2. _____, "Millstone Hill Thomson Scatter Results for 1964," Technical Report 430, Lincoln Laboratory, M. I. T. (15 November 1967), DDC AD-668436.
3. _____, "Millstone Hill Thomson Scatter Results for 1965," Technical Report 474, Lincoln Laboratory, M. I. T. (18 December 1969), DDC AD-707501.
4. _____, "Millstone Hill Thomson Scatter Results for 1966," Technical Report 481, Lincoln Laboratory, M. I. T. (15 December 1970), DDC AD-725742.
5. _____, "Millstone Hill Thomson Scatter Results for 1967," Technical Report 482, Lincoln Laboratory, M. I. T. (22 July 1971), DDC AD-735727.
6. _____, "Millstone Hill Thomson Scatter Results for 1968," Technical Report 499, Lincoln Laboratory, M. I. T. (23 January 1973), DDC AD-767251/2.
7. _____, "Millstone Hill Thomson Scatter Results for 1969," Technical Report 513, Lincoln Laboratory, M. I. T. (23 July 1974), DDC AD-A008505/0.
8. J. V. Evans and J. M. Holt, "Millstone Hill Thomson Scatter Results for 1970," Technical Report 522, Lincoln Laboratory, M. I. T. (11 May 1976).
9. J. V. Evans, B. A. Emery, and J. M. Holt, "Millstone Hill Thomson Scatter Results for 1971," Technical Report 528, Lincoln Laboratory, M. I. T. (24 March 1978).
10. J. V. Evans, Planet. Space Sci. 13, 1031 (1965), DDC AD-616607.
11. _____, J. Geophys. Res. 70, 1175 (1965), DDC AD-614310.
12. _____, Planet. Space Sci. 15, 1387 (1967).
13. _____, Planet. Space Sci. 18, 1225 (1970), DDC AD-716056.
14. _____, J. Atmos. Terr. Phys. 32, 1629 (1970), DDC AD-716057.
15. _____, J. Geophys. Res. 75, 4803 and 4815 (1970), DDC AD-714447 and DDC AD-714446, respectively.
16. _____, Planet. Space Sci. 21, 763 (1973), DDC AD-772137/6.
17. _____, J. Atmos. Terr. Phys. 35, 593 (1973), DDC AD-771877/8.
18. _____, Planet. Space Sci. 23, 1461 (1975).
19. _____, Planet. Space Sci. 23, 1611 (1975).
20. J. V. Evans, R. F. Julian, and W. A. Reid, "Incoherent Scatter Measurements of F-Region Density, Temperatures, and Vertical Velocity at Millstone Hill," Technical Report 477, Lincoln Laboratory, M. I. T. (6 February 1970), DDC AD-706863.
21. G. W. Armistead, J. V. Evans, and W. A. Reid, Radio Sci. 7, 153 (1972).

22. W. L. Oliver, J. E. Salah, R. H. Wand, and J. V. Evans, "Incoherent Scatter Measurements of E- and F-Region Density, Temperatures, and Collision Frequency at Millstone Hill," Technical Report 531, Lincoln Laboratory, M. I. T. (in preparation).

23. J. E. Salah, R. H. Wand, and J. V. Evans, Radio Sci. 10, 347 (1975).

24. J. C. Ghiloni, editor, "Millstone Hill Radar Propagation Study: Instrumentation," Technical Report 507, Lincoln Laboratory, M. I. T. (20 September 1973), DDC AD-775140.

25. K. Bibl and B. W. Reinsich, Radio Sci. 13, 519 (1978).

26. V. W. J. H. Kirchhoff and L. A. Carpenter, J. Geophys. Res. 81, 2737 (1976).

27. J. V. Evans, J. Geophys. Res. 70, 4331 (1965).

28. G. W. Prölss, J. Geophys. Res. 82, 1635 (1977).

29. J. V. Evans, "Thermospheric Properties as Deduced from Incoherent Scatter Measurements," paper presented to COSPAR Meeting, Innsbruck, Austria (June 1978).

30. C. G. Park, J. Geophys. Res. 76, 4650 (1971).

31. C. G. Park and C. I. Meng, J. Geophys. Res. 76, 8326 (1971) and 78, 3828 (1973).

32. G. Hernandez and R. G. Roble, J. Geophys. Res. 81, 5173 (1976).

33. J. V. Evans, Radio Sci. 6, 609 (1971), DDC AD-731927.

34. H. Kohl and J. W. King, J. Atmos. Terr. Phys. 29, 1045 (1967).

35. H. Kohl, J. W. King, and D. Eccles, J. Atmos. Terr. Phys. 30, 1733 (1968).

36. G. Vasseur, J. Atmos. Terr. Phys. 31, 397 (1969).

37. M. D. Papagiannis and H. Mullaney, J. Atmos. Terr. Phys. 33, 451 (1971).

38. D. Eccles, J. W. King, and H. Kohl, J. Atmos. Terr. Phys. 33, 1371 (1971).

39. D. Eccles and J. D. Burge, J. Atmos. Terr. Phys. 35, 1927 (1973).

40. J. L. Massa, "Theoretical and Experimental Studies of the Ionization Exchange Between the Ionosphere and Plasmasphere," PhD Thesis, University of Michigan, Ann Arbor, Michigan (1974).

41. D. R. Moorcroft, J. Geophys. Res. 69, 955 (1964).

42. J. H. Hoffman, W. H. Dodson, C. R. Lippincott, and H. D. Hammick, J. Geophys. Res. 79, 4246 (1974).

43. J. E. Salah, J. V. Evans, D. Alcayde, and P. Bauer, Ann. Geophys. 32, 97 (1976).

44. G. Kockarts and M. Nicolet, Ann. Geophys. 18, 269 (1962).

45. _____, Ann. Geophys. 19, 370 (1963).

46. G. J. Bailey, R. J. Moffett, and J. A. Murphy, J. Atmos. Terr. Phys. 39, 105 (1977).

47. P. M. Banks, A. F. Nagy, and W. I. Axford, Planet. Space Sci. 19, 1053 (1971).

48. W. B. Hanson and T. N. L. Patterson, Planet. Space Sci. 12, 979 (1964).

49. J. E. Geisler, J. Geophys. Res. 72, 81 (1967).

50. R. W. Schunk and J. C. G. Walker, Planet. Space Sci. 17, 535 (1970).

51. P. M. Banks and G. Kockarts, Aeronomy Part B (Academic Press, New York, 1973).

52. B. C. Narasinga Rao and V. C. Jain, Ind. J. Radio and Space Phys. 3, 284 (1974).

53. M. C. Ho and D. R. Moorcroft, Planet. Space Sci. 19, 1431 and 1441 (1971).

54. H. A. Taylor, Jr., Planet. Space Sci. 20, 1593 (1972).

55. _____, J. Geophys. Res. 78, 315 (1973).

56. H. A. Taylor, Jr. and W. J. Walsh, J. Geophys. Res. 77, 6716 (1972).

57. J. M. Grebowsky, A. J. Chen, and H. A. Taylor, Jr., J. Geophys. Res. 81, 690 (1976).

58. W. J. Raitt and E. B. Dorling, J. Atmos. Terr. Phys. 38, 1077 (1976).

59. P. M. Banks and J. R. Doupnik, Planet. Space Sci. 22, 79 (1974).

60. J. E. Titheridge, Planet. Space Sci. 24, 229 (1976).

61. K. Marubashi and J. M. Grebowsky, J. Geophys. Res. 81, 1700 (1976).

62. A. E. Hedin, C. A. Reber, G. P. Newton, N. W. Spencer, H. C. Brinton, H. G. Mayr, and W. E. Potter, J. Geophys. Res. 82, 2148 (1977).

63. A. Derieux, P. Bauer, and A. Lejeune, Ann. Geophys. 31, 447 (1975).

64. H. C. Brinton and H. G. Mayr, J. Geophys. Res. 76, 6198 (1971).

65. _____, Space Res. 12, 751 (1972).

66. H. C. Brinton, H. G. Mayr, and W. E. Potter, Geophys. Res. Lett. 2, 389 (1975).

67. E. L. Breig, W. B. Hanson, J. H. Hoffman, and D. C. Kayser, J. Geophys. Res. 81, 2677 (1976).

68. A. Vidal-Madjar, J. E. Blamont, and B. Phissamy, J. Geophys. Res. 78, 1115 (1973) and 79, 233 (1974).

69. J. L. Bertaux, J. Geophys. Res. 80, 639 (1975); also J. Atmos. Terr. Phys. 38, 821 (1976).

70. P. R. Meier and P. Mange, Planet. Space Sci. 21, 309 (1973).

71. G. E. Thomas and D. E. Anderson, Jr., Planet. Space Sci. 24, 303 (1976).

72. C. Emerich, S. Cazes, and J. E. Blamont, J. Geophys. Res. 81, 6103 (1976).

73. B. A. Tinsley, Planet. Space Sci. 21, 686 (1973).

74. _____, J. Geophys. Res. 80, 626 (1975).

75. L. Wallace and D. F. Strobel, Planet. Space Sci. 20, 521 (1972).

76. J. A. Quessette, Ann. Geophys. 30, 375 (1974).

77. A. F. Nagy and P. M. Banks, J. Geophys. Res. 77, 4277 (1972).

78. H. G. Mayr, E. G. Fontheim, L. H. Brace, H. C. Brinton, and H. A. Taylor, Jr., J. Atmos. Terr. Phys. 34, 1659 (1972).

79. R. J. Moffett and J. A. Murphy, Planet. Space Sci. 21, 43 (1973).

80. J. A. Murphy, G. J. Bailey, and R. J. Moffett, J. Atmos. Terr. Phys. 38, 351 (1976).

APPENDIX

INSCON SUMMARY

1 JANUARY 1979

INSCON SUMMARY. 01, JAN, 1979

DATE	TYPE		START (EST)	END (EST)	TEST VALUE	KDAT	FIT NO.
25-26,JAN,1972	DENSITY	RETIAS	1242	1248	.52706E 01	101	720250
25-26,JAN,1972	ELECTRON TEMPERATURE	RETIAS	1242	1248	-.94533E 03	203	720250
25-26,JAN,1972	ION TEMPERATURE	RETIAS	1242	1248	-.72797E 03	303	720250
25-26,JAN,1972	VERTICAL ION DRIFT	RETIAS	1242	1248	-.25701E 03	1001	720250
25-26,JAN,1972	ELECTRON TEMPERATURE	RETIAS	1242	1248	-.94558E 03	293	720250
25-26,JAN,1972	ION TEMPERATURE	RETIAS	1242	1248	-.72802E 03	393	720250
25-26,JAN,1972	VERTICAL ION DRIFT	RETIAS	1242	1248	-.25710E 03	1091	720250
26-27,JAN,1972	DENSITY	L/UHF	1155	1440	.52775E 01	101	720260
26-27,JAN,1972	ELECTRON TEMPERATURE	L/UHF	1155	1440	-.89529E 03	203	720260
26-27,JAN,1972	ION TEMPERATURE	L/UHF	1155	1440	-.70040E 03	303	720260
26-27,JAN,1972	VERTICAL ION DRIFT	L/UHF	1155	1440	-.26046E 03	1001	720260
26-27,JAN,1972	ELECTRON TEMPERATURE	L/UHF	1155	1440	-.89560E 03	293	720260
26-27,JAN,1972	ION TEMPERATURE	L/UHF	1155	1440	-.69959E 03	393	720260
26-27,JAN,1972	VERTICAL ION DRIFT	L/UHF	1155	1440	-.26027E 03	1091	720260
23-24,FEB,1972	DENSITY	RETIAS	0947	1153	.53322E 01	101	720540
23-24,FEB,1972	ELECTRON TEMPERATURE	RETIAS	0947	1153	-.97605E 03	203	720540
23-24,FEB,1972	ION TEMPERATURE	RETIAS	0947	1153	-.71946E 03	303	720540
23-24,FEB,1972	VERTICAL ION DRIFT	RETIAS	0947	1153	-.24834E 03	1001	720540
23-24,FEB,1972	ELECTRON TEMPERATURE	RETIAS	0947	1153	-.97630E 03	293	720540
23-24,FEB,1972	ION TEMPERATURE	RETIAS	0947	1153	-.71948E 03	393	720540
23-24,FEB,1972	VERTICAL ION DRIFT	RETIAS	0947	1153	-.24863E 03	1091	720540
06-07,MAR,1972	DENSITY	STATS	1816	0631	-.38059E 01	101	720660
06-07,MAR,1972	ELECTRON TEMPERATURE	STATS	1816	0631	-.78291E 03	203	720660
06-07,MAR,1972	ION TEMPERATURE	STATS	1816	0631	-.71730E 03	303	720660
06-07,MAR,1972	VERTICAL ION DRIFT	STATS	1816	0631	-.23727E 03	1001	720660
09-10,MAR,1972	DENSITY	RETIAS	0957	1141	.54056E 01	101	720690
09-10,MAR,1972	ELECTRON TEMPERATURE	RETIAS	0957	1141	-.78232E 03	203	720690
09-10,MAR,1972	ION TEMPERATURE	RETIAS	0957	1141	-.74757E 03	303	720690
09-10,MAR,1972	VERTICAL ION DRIFT	RETIAS	0957	1141	-.22471E 03	1001	720690
09-10,MAR,1972	ELECTRON TEMPERATURE	RETIAS	0957	1141	-.78250E 03	293	720690
09-10,MAR,1972	ION TEMPERATURE	RETIAS	0957	1141	-.74550E 03	393	720690
09-10,MAR,1972	VERTICAL ION DRIFT	RETIAS	0957	1141	-.22469E 03	1091	720690
17-18,MAR,1972	DENSITY	STATS	1720	2341	-.44876E 01	101	720770
17-18,MAR,1972	ELECTRON TEMPERATURE	STATS	1720	2341	-.88782E 03	203	720770
17-18,MAR,1972	ION TEMPERATURE	STATS	1720	2341	-.75744E 03	303	720770
17-18,MAR,1972	VERTICAL ION DRIFT	STATS	1720	2341	-.25864E 03	1001	720770
17-18,MAR,1972	ELECTRON TEMPERATURE	STATS	1720	2341	-.88419E 03	293	720770
17-18,MAR,1972	ION TEMPERATURE	STATS	1720	2341	-.75663E 03	393	720770
17-18,MAR,1972	VERTICAL ION DRIFT	STATS	1720	2341	-.25893E 03	1091	720770

DATE	TYPE		START (EST)	END (EST)	TEST VALUE	KDAT	FIT NO.
23-24,MAR,1972	DENSITY	L/UHF	1619	1610	.50609E 01	101	720830
23-24,MAR,1972	ELECTRON TEMPERATURE	L/UHF	1619	1610	-.90862E 03	203	720830
23-24,MAR,1972	ION TEMPERATURE	L/UHF	1619	1610	-.74096E 03	303	720830
23-24,MAR,1972	VERTICAL ION DRIFT	L/UHF	1619	1610	-.26377E 03	1001	720830
23-24,MAR,1972	ELECTRON TEMPERATURE	L/UHF	1619	1610	-.90832E 03	293	720830
23-24,MAR,1972	ION TEMPERATURE	L/UHF	1619	1610	-.74021E 03	393	720830
23-24,MAR,1972	VERTICAL ION DRIFT	L/UHF	1619	1610	-.26416E 03	1091	720830
13-14,APR,1972	DENSITY	STATS	2111	0559	-.30205E 01	101	721040
13-14,APR,1972	ELECTRON TEMPERATURE	STATS	2111	0559	-.69928E 03	203	721040
13-14,APR,1972	ION TEMPERATURE	STATS	2111	0559	-.65812E 03	303	721040
13-14,APR,1972	VERTICAL ION DRIFT	STATS	2111	0559	-.25724E 03	1001	721040
13-14,APR,1972	ELECTRON TEMPERATURE	STATS	2111	0559	-.69700E 03	293	721040
13-14,APR,1972	ION TEMPERATURE	STATS	2111	0559	-.65660E 03	393	721040
13-14,APR,1972	VERTICAL ION DRIFT	STATS	2111	0559	-.25702E 03	1091	721040
26-27,APR,1972	DENSITY	RETIAS	1604	1701	.57314E 01	101	721170
26-27,APR,1972	ELECTRON TEMPERATURE	RETIAS	1604	1701	-.10056E 04	203	721170
26-27,APR,1972	ION TEMPERATURE	RETIAS	1604	1701	-.73898E 03	303	721170
26-27,APR,1972	VERTICAL ION DRIFT	RETIAS	1604	1701	-.27774E 03	1001	721170
26-27,APR,1972	ELECTRON TEMPERATURE	RETIAS	1604	1701	-.10049E 04	293	721170
26-27,APR,1972	ION TEMPERATURE	RETIAS	1604	1701	-.73778E 03	393	721170
26-27,APR,1972	VERTICAL ION DRIFT	RETIAS	1604	1701	-.27782E 03	1091	721170
09-10,MAY,1972	DENSITY	RETIAS	1231	1314	.54065E 01	101	721300
09-10,MAY,1972	ELECTRON TEMPERATURE	RETIAS	1231	1314	-.11293E 04	203	721300
09-10,MAY,1972	ION TEMPERATURE	RETIAS	1231	1314	-.76517E 03	303	721300
09-10,MAY,1972	VERTICAL ION DRIFT	RETIAS	1231	1314	-.28894E 03	1001	721300
09-10,MAY,1972	ELECTRON TEMPERATURE	RETIAS	1231	1314	-.11291E 04	293	721300
09-10,MAY,1972	ION TEMPERATURE	RETIAS	1231	1314	-.76424E 03	393	721300
09-10,MAY,1972	VERTICAL ION DRIFT	RETIAS	1231	1314	-.28904E 03	1091	721300
25-26,MAY,1972	DENSITY	STATS	1136	1303	.53280E 01	101	721460
25-26,MAY,1972	ELECTRON TEMPERATURE	STATS	1136	1303	-.11286E 04	203	721460
25-26,MAY,1972	ION TEMPERATURE	STATS	1136	1303	-.73123E 03	303	721460
25-26,MAY,1972	VERTICAL ION DRIFT	STATS	1136	1303	-.29003E 03	1001	721460
25-26,MAY,1972	ELECTRON TEMPERATURE	STATS	1136	1303	-.11322E 04	293	721460
25-26,MAY,1972	ION TEMPERATURE	STATS	1136	1303	-.73194E 03	393	721460
25-26,MAY,1972	VERTICAL ION DRIFT	STATS	1136	1303	-.28994E 03	1091	721460
30-31,MAY,1972	DENSITY	L/UHF	0922	1015	-.53907E 01	101	721510
30-31,MAY,1972	ELECTRON TEMPERATURE	L/UHF	0922	1015	-.10966E 04	203	721510
30-31,MAY,1972	ION TEMPERATURE	L/UHF	0922	1015	-.70211E 03	303	721510
30-31,MAY,1972	VERTICAL ION DRIFT	L/UHF	0922	1015	-.27415E 03	1001	721510
30-31,MAY,1972	ELECTRON TEMPERATURE	L/UHF	0922	1015	-.10962E 04	293	721510
30-31,MAY,1972	ION TEMPERATURE	L/UHF	0922	1015	-.69988E 03	393	721510
30-31,MAY,1972	VERTICAL ION DRIFT	L/UHF	0922	1015	-.27410E 03	1091	721510
08-09,JUN,1972	DENSITY	STATS	1023	1714	-.54471E 01	101	721600
08-09,JUN,1972	ELECTRON TEMPERATURE	STATS	1023	1714	-.10252E 04	203	721600
08-09,JUN,1972	ION TEMPERATURE	STATS	1023	1714	-.73511E 03	303	721600

INSCON SUMMARY. 01, JAN, 1979 (Continued)

DATE	TYPE		START (EST)	END (EST)	TEST VALUE	KDAT	FIT NO.
08-09,JUN,1972	VERTICAL ION DRIFT	STATS	1023	1714	-.23595E 03	1001	721600
08-09,JUN,1972	ELECTRON TEMPERATURE	STATS	1023	1714	-.10252E 04	293	721600
08-09,JUN,1972	ION TEMPERATURE	STATS	1023	1714	-.73346E 03	393	721600
08-09,JUN,1972	VERTICAL ION DRIFT	STATS	1023	1714	-.23606E 03	1091	721600
13-14,JUN,1972	DENSITY	RETIAS	0914	1056	-.54611E 01	101	721650
13-14,JUN,1972	ELECTRON TEMPERATURE	RETIAS	0914	1056	-.89208E 03	203	721650
13-14,JUN,1972	ION TEMPERATURE	RETIAS	0914	1056	-.70065E 03	303	721650
13-14,JUN,1972	VERTICAL ION DRIFT	RETIAS	0914	1056	-.28107E 03	1001	721650
13-14,JUN,1972	ELECTRON TEMPERATURE	RETIAS	0914	1056	-.89161E 03	293	721660
13-14,JUN,1972	ION TEMPERATURE	RETIAS	0914	1056	-.69914E 03	393	721660
13-14,JUN,1972	VERTICAL ION DRIFT	RETIAS	0914	1056	-.28095E 03	1091	721660
28-29,JUN,1972	DENSITY	L/UHF	1036	0505	-.53018E 01	101	721800
28-29,JUN,1972	ELECTRON TEMPERATURE	L/UHF	1036	0505	-.11319E 04	203	721800
28-29,JUN,1972	ION TEMPERATURE	L/UHF	1036	0505	-.70268E 03	303	721800
28-29,JUN,1972	VERTICAL ION DRIFT	L/UHF	1036	0505	-.31155E 03	1001	721800
28-29,JUN,1972	ELECTRON TEMPERATURE	L/UHF	1036	0505	-.11308E 04	293	721800
28-29,JUN,1972	ION TEMPERATURE	L/UHF	1036	0505	-.70051E 03	393	721800
28-29,JUN,1972	VERTICAL ION DRIFT	L/UHF	1036	0505	-.31152E 03	1091	721800
30JUN-01JUL,1972	DENSITY	L/UHF	1148	1203	.54613E 01	101	721820
30JUN-01JUL,1972	ELECTRON TEMPERATURE	L/UHF	1148	1203	-.11674E 04	203	721820
30JUN-01JUL,1972	ION TEMPERATURE	L/UHF	1148	1203	-.72147E 03	303	721820
30JUN-01JUL,1972	VERTICAL ION DRIFT	L/UHF	1148	1203	-.27917E 03	1001	721820
30JUN-01JUL,1972	ELECTRON TEMPERATURE	L/UHF	1148	1203	-.11671E 04	293	721820
30JUN-01JUL,1972	ION TEMPERATURE	L/UHF	1148	1203	-.72129E 03	393	721820
30JUN-01JUL,1972	VERTICAL ION DRIFT	L/UHF	1148	1203	-.27919E 03	1091	721820
10-11,JUL,1972	DENSITY	RETIAS	1208	1921	-.54054E 01	101	721910
10-11,JUL,1972	ELECTRON TEMPERATURE	RETIAS	1208	1921	-.11509E 04	203	721910
10-11,JUL,1972	ION TEMPERATURE	RETIAS	1208	1921	-.73532E 03	303	721910
10-11,JUL,1972	VERTICAL ION DRIFT	RETIAS	1208	1921	-.27354E 03	1001	721910
10-11,JUL,1972	ELECTRON TEMPERATURE	RETIAS	1208	1921	-.11542E 04	293	721910
10-11,JUL,1972	ION TEMPERATURE	RETIAS	1208	1921	-.73510E 03	393	721910
10-11,JUL,1972	VERTICAL ION DRIFT	RETIAS	1208	1921	-.27230E 03	1091	721910
12-13,JUL,1972	DENSITY	RETIAS	0840	1034	-.52426E 01	101	721940
12-13,JUL,1972	ELECTRON TEMPERATURE	RETIAS	0840	1034	-.98585E 03	203	721940
12-13,JUL,1972	ION TEMPERATURE	RETIAS	0840	1034	-.62273E 03	303	721940
12-13,JUL,1972	ELECTRON TEMPERATURE	RETIAS	0840	1034	-.98077E 03	293	721940
12-13,JUL,1972	ION TEMPERATURE	RETIAS	0840	1034	-.61538E 03	393	721940
26-27,JUL,1972	DENSITY	L/UHF	1029	1409	-.54304E 01	101	722080
26-27,JUL,1972	ELECTRON TEMPERATURE	L/UHF	1029	1409	-.11483E 04	203	722080
26-27,JUL,1972	ION TEMPERATURE	L/UHF	1029	1409	-.72707E 03	303	722080
26-27,JUL,1972	VERTICAL ION DRIFT	L/UHF	1029	1409	-.27342E 03	1001	722080
26-27,JUL,1972	ELECTRON TEMPERATURE	L/UHF	1029	1409	-.11477E 04	293	722080
26-27,JUL,1972	ION TEMPERATURE	L/UHF	1029	1409	-.72617E 03	393	722080
26-27,JUL,1972	VERTICAL ION DRIFT	L/UHF	1029	1409	-.27354E 03	1091	722080
07-08,AUG,1972	DENSITY	RETIAS	0929	1106	-.53095E 01	101	722200

DATE	TYPE		START (EST)	END (EST)	TEST VALUE	KDAT	FIT NO.
07-08,AUG,1972	ELECTRON TEMPERATURE	RETIAS	0929	1106	-.11237E 04	203	722200
07-08,AUG,1972	ION TEMPERATURE	RETIAS	0929	1106	-.74026E 03	303	722200
07-08,AUG,1972	VERTICAL ION DRIFT	RETIAS	0929	1106	-.26739E 03	1001	722200
07-08,AUG,1972	ELECTRON TEMPERATURE	RETIAS	0929	1106	-.11233E 04	293	722200
07-08,AUG,1972	ION TEMPERATURE	RETIAS	0929	1106	-.73890E 03	393	722200
07-08,AUG,1972	VERTICAL ION DRIFT	RETIAS	0929	1106	-.26764E 03	1091	722200
06-07,SEP,1972	DENSITY	L/UHF	1011	1251	.53781E 01	101	722500
06-07,SEP,1972	ELECTRON TEMPERATURE	L/UHF	1011	1251	-.11305E 04	203	722500
06-07,SEP,1972	ION TEMPERATURE	L/UHF	1011	1251	-.74688E 03	303	722500
06-07,SEP,1972	VERTICAL ION DRIFT	L/UHF	1011	1251	-.25270E 03	1001	722500
06-07,SEP,1972	ELECTRON TEMPERATURE	L/UHF	1011	1251	-.11299E 04	293	722500
06-07,SEP,1972	ION TEMPERATURE	L/UHF	1011	1251	-.74661E 03	393	722500
06-07,SEP,1972	VERTICAL ION DRIFT	L/UHF	1011	1251	-.25286E 03	1091	722500
12-13,SEP,1972	DENSITY	RETIAS	0819	1043	-.53976E 01	101	722560
12-13,SEP,1972	ELECTRON TEMPERATURE	RETIAS	0819	1043	-.78833E 03	203	722560
12-13,SEP,1972	ION TEMPERATURE	RETIAS	0819	1043	-.69589E 03	303	722560
12-13,SEP,1972	VERTICAL ION DRIFT	RETIAS	0819	1043	-.25305E 03	1001	722560
12-13,SEP,1972	ELECTRON TEMPERATURE	RETIAS	0819	1043	-.78830E 03	293	722560
12-13,SEP,1972	ION TEMPERATURE	RETIAS	0819	1043	-.69261E 03	393	722560
12-13,SEP,1972	VERTICAL ION DRIFT	RETIAS	0819	1043	-.25295E 03	1091	722560
03-04,OCT,1972	DENSITY	RETIAS	0809	1108	-.53208E 01	101	722770
03-04,OCT,1972	ELECTRON TEMPERATURE	RETIAS	0809	1108	-.10054E 04	203	722770
03-04,OCT,1972	ION TEMPERATURE	RETIAS	0809	1108	-.74985E 03	303	722770
03-04,OCT,1972	VERTICAL ION DRIFT	RETIAS	0809	1108	-.32869E 03	1001	722770
03-04,OCT,1972	ELECTRON TEMPERATURE	RETIAS	0809	1108	-.10051E 04	293	722770
03-04,OCT,1972	ION TEMPERATURE	RETIAS	0809	1108	-.74835E 03	393	722770
03-04,OCT,1972	VERTICAL ION DRIFT	RETIAS	0809	1108	-.32397E 03	1091	722770
15-16,NOV,1972	DENSITY	L/UHF	0928	1632	.49251E 01	101	723200
15-16,NOV,1972	ELECTRON TEMPERATURE	L/UHF	0928	1632	-.77187E 03	203	723200
15-16,NOV,1972	ION TEMPERATURE	L/UHF	0928	1632	-.62382E 03	303	723200
15-16,NOV,1972	VERTICAL ION DRIFT	L/UHF	0928	1632	-.25933E 03	1001	723200
15-16,NOV,1972	ELECTRON TEMPERATURE	L/UHF	0928	1632	.28773E 03	293	723200
15-16,NOV,1972	ION TEMPERATURE	L/UHF	0928	1632	-.62418E 03	393	723200
15-16,NOV,1972	VERTICAL ION DRIFT	L/UHF	0928	1632	-.25965E 03	1091	723200
06-07,DEC,1972	DENSITY	L/UHF	0929	1603	-.58992E 01	101	723410
06-07,DEC,1972	ELECTRON TEMPERATURE	L/UHF	0929	1603	-.88118E 03	203	723410
06-07,DEC,1972	ION TEMPERATURE	L/UHF	0929	1603	-.54083E 03	303	723410
06-07,DEC,1972	VERTICAL ION DRIFT	L/UHF	0929	1603	-.22533E 03	1001	723410
06-07,DEC,1972	ELECTRON TEMPERATURE	L/UHF	0929	1603	-.88085E 03	293	723410
06-07,DEC,1972	ION TEMPERATURE	L/UHF	0929	1603	.54324E 03	393	723410
06-07,DEC,1972	VERTICAL ION DRIFT	L/UHF	0929	1603	.30370E 03	1091	723410

☆U.S. GOVERNMENT PRINTING OFFICE: 1979 — A-1173/28

BIBLIOGRAPHIC DATA SHEET	1. Report No.	3. Recipient's Accession No.
4. Title and Subtitle Millstone Hill Thomson Scatter Results for 1972		5. Report Date 18 September 1978 6.
7. Author(s) John V. Evans and John M. Holt		8. Performing Organization Rept. No. Technical Report 530
9. Performing Organization Name and Address Lincoln Laboratory, M. I. T. P.O. Box 73 Lexington, MA 02173		10. Project/Task/Work Unit No. 11. Contract/Grant No. ATM 75-22193
12. Sponsoring Organization Name and Address National Science Foundation Atmospheric Science Section Washington, DC 20550		13. Type of Report & Period Covered Technical Report 14.

15. Supplementary Notes

16. Abstracts

During 1972, the vertically directed incoherent scatter radar at Millstone Hill (42.6°N, 71.5°W) was employed to measure electron density, electron and ion temperatures, and vertical ion velocity in the F-region over periods of 24 hours, one or two times per month. The observations spanned the height interval 200 to 900 km, approximately, and achieved a time resolution of about 30 minutes. This report presents the results of these measurements in a set of contour diagrams.

For a number of the days, the spectra of the signals gathered at altitudes between 450 and 1125 km have been the subject of further analysis in an effort to determine the percentage of H^+ ions present over Millstone. The results suggest that H^+ ions are escaping from the F-region to the magnetosphere at a value close to the theoretical limiting flux during the daytime in all seasons. At night the flux becomes downward commencing near midnight in winter, but may remain upward throughout the night in summer.

17. Key Words and Document Analysis. 17a. Descriptors

Millstone radar
F-region
diurnal variations
electron density
ionospheric scatter
seasonal variations
temperature effects
magnetosphere
proton flux

17b. Identifiers/Open-Ended Terms

17c. COSATI Field/Group

18. Availability Statement	19.. Security Class (This Report) UNCLASSIFIED	21. No. of Pages 132
	20. Security C[illegible] Page UNCL	

FORM NTIS-35 (REV. 10-73) ENDORSED BY ANSI AND UNESCO. THIS FORM MAY BE RE